

SART

LECTURE NOTES

Stellar Atmospheres & Radiative Transfer

Author:

Prof. dr. Alex DE KOTER

Affiliation:

Astronomical Institute “Anton Pannekoek”
University of Amsterdam
P.O. Box 94249, 1090 GE Amsterdam

&

Astronomical Institute Utrecht,
Utrecht University
P.O. Box 8000, 3508 TA Utrecht

Contents

1	Introduction	6
1.1	Radiation as probe and as constituent	6
1.2	About these lecture notes	7
1.3	Literature	8
2	The spectra of stars	11
2.1	Spectral classification	11
2.2	Special stellar spectra	15
2.3	Special binary spectra	24
2.4	Nebulae	25
2.5	Supernovae	26
2.6	The continuum energy distribution of stars	28
3	Characterizing the radiation field	35
3.1	Coordinate systems	35
3.2	Specific intensity	37
3.3	Mean intensity	39
3.4	Flux	41
3.5	Radiation pressure	45
3.6	Eddington factors	46
4	The equation of transfer	50
4.1	Absorption, emission, and scattering processes	50
4.2	General form of the equation of transfer	54
4.3	Optical depth and the source function	56
4.4	Formal solution of the equation of transfer	59
4.5	Moments of the transfer equation	60
4.6	Simple examples of transfer problems	61
5	Numerical methods for solving the equation of transfer	72
5.1	Short characteristics	73
5.2	Feautrier method	76

6 Radiation and matter	80
6.1 Introduction	80
6.2 Thermodynamic equilibrium	81
6.3 Planck function	83
6.4 Laws describing the material medium in TE	86
6.5 The TE equation of state for an ionized gas	90
6.6 Temperature definitions	95
6.7 Approximations in describing the interaction of matter and radiation	99
7 Discrete processes	102
7.1 From a macroscopic toward a microscopic description	103
7.2 Einstein relations	107
7.3 Relation between Einstein coefficients and η_ν^ℓ and χ_ν^ℓ	107
8 Continuum processes	112
8.1 Bound-free transitions	112
8.2 Free-free transitions	117
8.3 H ⁻ absorption	118
8.4 Elastic scattering by electrons	120
8.5 Comparison of the main sources of extinction	122
9 Conservation laws	125
9.1 Continuity equation	125
9.2 Momentum equation	128
9.3 Energy equation	134
9.4 Convection	136
10 Grey atmosphere in radiative equilibrium	141
10.1 Description of the grey atmosphere	141
10.2 Constructing the grey atmosphere	144
10.3 Mean extinction coefficients	146
11 LTE atmosphere in hydrostatic and radiative equilibrium	149
11.1 Constructing the LTE atmosphere	149
11.2 Obtaining the temperature structure	152
11.3 Kurucz models	156
12 Spectral lines	167
12.1 Describing the line profile	167
12.2 Line broadening	170
12.3 Rotational broadening	179
12.4 Curve of growth	183

13 Scattering	189
13.1 Continuum scattering	190
13.2 Line scattering in a two-level atom	193
14 NLTE mechanisms and models	201
14.1 LTE versus NLTE	201
14.2 Photo- and collisional ionization in a low density medium	203
14.3 Excitations in a low density medium	205
14.4 Fluorescence	208
14.5 The NLTE behavior of hydrogen in O stars	210
15 The sun	215
15.1 Introduction	215
15.2 General information about the sun	215
15.3 Solar spectrum	224
15.4 Solar activity	225
16 Stellar winds	233
16.1 Historical introduction	234
16.2 P Cygni profiles	235
16.3 The determination of mass loss from H α	241
16.4 The determination of mass loss from radio measurements	243
17 H II regions	247
17.1 Historical introduction	247
17.2 The primary radiation mechanism in nebulae	249
17.3 Ionization equilibrium and the Strömgren sphere	249
17.4 The emission measure as a density diagnostic	254
17.5 The equation of state of nebular hydrogen gas	255
17.6 Free-free radio continuum emission as a temperature diagnostic	257
17.7 Collisional excitation of meta-stable levels and forbidden line emission	260
18 ISM and IGM	267
18.1 Introduction	267
18.2 Continuum extinction by interstellar dust	270
18.3 Dust in and in-between galaxies	275

1

Introduction

In the vast majority of cases radiation is the only information we have from distant astronomical objects. Almost all knowledge we have gathered about the stars, the interstellar medium, galaxies, et cetera, is derived from analysis of this radiation. It is therefore of considerable importance to study the physics of the creation and transport of radiation in these objects, and to develop reliable methods that allow to decode the information about such systems that is contained in their spectra.

If we construct a model of the problem of interest and predict the corresponding spectral energy distribution, we can make quantitative statements about the physical state of the object that is observed, if we compare our predictions with the measurements. In this way we may learn about properties such as temperature, density, chemical composition, magnetic fields, velocities, geometry, mass, mass loss, luminosity, and distance.

1.1 Radiation as probe and as constituent

In the astrophysical context, radiation has a conspicuously dualistic character. On the one hand it carries the information that we use to derive the physical state of a medium, i.e. it serves as a probe of this medium. On the other hand it is, in many cases, an important constituent of this medium, i.e. it in fact determines the structure of the medium itself.

The best known example of such an astrophysical medium is the stellar atmosphere. In the outermost layers of a star photons escape to the surrounding space, taking away energy. This energy is often transported from the stellar centre to the edge by photons, and photons therefore in part determine the temperature, and – because of radiation pressure – density of the atmospheric layers. If radiation pressure is intense, photons may drive a stellar wind through which matter is lost to space. Coded in the spectral lines and the continuum energy distribution, that both originate in the stellar atmosphere, is information on the local conditions. This illustrates the dualistic nature of radiation.

In the past decades impressive progress has been made in the quantitative analysis of stellar atmospheres. Several reasons for this may be identified: *i*) the unprecedented increase in the quality of ground- and space-based observations; *ii*) the development of extremely fast and efficient numerical methods; and *iii*) an ever increasing computer power. The theory of stellar atmospheres has reached such a high level of sophistication that it can be used as a methodological handbook for the study of other astrophysical systems where radiation has the above mentioned dualistic nature. Examples of such systems are the circumstellar medium, accretion disks, H II regions, and the interstellar and intergalactic medium.

In these lectures we focus on the physics of the creation and transport of radiation, and on methods that help us decode spectral information. We primarily discuss stellar atmospheres, however a few chapters are devoted to other astrophysical objects.

Exercise 1.1

- a) Give a number of astrophysical information carriers other than electromagnetic radiation.
- b) Think of types of observations and areas of astronomical research where knowledge of the creation and transport of radiation is *not* important.

1.2 About these lecture notes

In chapter 2 we discuss the spectra of stars and their classification. This classification is done primarily on the basis of spectral line properties, but may also be done using broadband color indices. The calibration of the spectral types, luminosity classes and color indices in terms of effective temperature, gravity and chemical composition is done using models of stellar atmospheres. Several chapters are devoted to discussing the basic physics of stellar atmospheres as well as methods used to construct model atmospheres.

In chapter 3 we introduce the macroscopic quantities that characterize the radiation field; in chapter 4 the equation that describes the transfer of radiation is derived. This 4th chapter also discusses simple analytical solutions of the radiation transfer equation. Numerical solutions are treated in (the optional) chapter 5. The coupling between the radiation field and the material medium is discussed in chapter 6. We will invest time to study types of equilibrium between radiation and matter. In thermodynamic equilibrium (TE) the state of the gas is fully described by the equations of Boltzmann and Saha. The Saha equilibrium specifies the ionization as a function of temperature and density of the medium. This provides a relatively simple, but already quite successful way to classify a stellar spectrum (see § 6.5). In TE the radiation field is described by the Planck function. This is a 0th order description of the emerging radiation field of a star, and could, at least in principle, be used to calibrate color indices (see § 6.6). However, a real stellar spectrum is more complex and shows appreciable deviations

from that of a Planck curve. A meaningful calibration therefore requires more sophisticated models.

The transfer of radiation is dependent on the sources of extinction χ_ν and of emission η_ν in the medium. In chapters 7 and 8 we make the link between these macroscopic quantities and the microscopic processes that cause extinction and emission.

Starting with chapter 9 we focus on the modeling of stellar atmospheres. We start out with a discussion of the conservation of mass, momentum, and energy. In essence, the problem of stellar atmospheres is to solve the equation of radiation transfer for a suitable equilibrium between radiation and matter, subject to the conservation constraints given above.

In chapter 10 we discuss the grey atmosphere. This relatively simple model provides important insight in the role of the energy equation. A widely used model to describe the stellar atmosphere assumes that the gas is in local thermodynamic equilibrium (LTE) and that hydrostatic and radiative equilibrium hold. This type of model is treated in chapter 11. Next, the processes that determine the shape and strength of spectral lines are reviewed. These need to be included in our models if the aim is to construct a representation of the atmosphere that may be compared to observations. Chapter 13 focusses on the process of scattering, arguably the most fundamental *physical* complication inherent to solving the model atmosphere problem. In some cases, the assumptions that make up LTE break down in the stellar atmosphere. In that case non-LTE models are needed to describe the medium. Aspects of non-LTE physics & models are discussed in chapter 14.

The sun is such a special star that we devote a separate chapter to it. In the final chapters we “move away from the stellar surface”. We successively discuss stellar winds, nebulae, and the interstellar and intergalactic medium.

1.3 Literature

No books fully cover what is presented in these lecture notes. However, we follow parts of:

- Mihalas: *Stellar Atmospheres*, 2nd edition. W.H. Freeman and Company, New York, 1978. Standard work, including a detailed description of the basic physics of stellar atmospheres.
- Rybicki and Lightman: *Radiative Processes in Astrophysics*. Excellent standard book. Treats parts of the basic physics in more detail than is done in these lecture notes.
- Pradhan & Nahar: *Atomic Astrophysics and Spectroscopy*, 1st edition. Cambridge University Press, 2011. Excellent overview of atomic structure and processes relevant for radiative transfer.

- Gray: *Observation and Analysis of Stellar Photospheres*. Excellent book. More simple than these lectures, however interesting because of the emphasis on instrumentation and observing techniques in optical spectroscopy.
- Gray & Corbally: *Stellar Spectral Classification*. Very useful book. Discusses the spectral classification method, but unfortunately does not provide an overview of spectral calibration.
- Rutten: *Opwekking en Transport van Straling*. Second year lecture notes of the University of Utrecht (in Dutch). Very clear and conceptual discussions. Though at a lower level, it is used as the main guide to write several chapters of these lecture notes.
- Rutten: *Radiative Transfer in Stellar Atmospheres*. Doctoral lectures at the University of Utrecht. Almost encyclopedic approach, though less conceptual than his second year lectures. Available through internet. Comparable level.
- Hubeny: In: *Stellar Atmospheres: Theory and Observations*. Excellent discussion of modern techniques in radiation transfer.
- Osterbrock & Ferland: *Astrophysics of Gaseous Nebulae and Active Galactic Nuclei*. University Science Books, California, 2006, Second Edition. Standard textbook on the physics of nebulae and AGNs. Beautifully written.
- Aller: *Physics of Thermal Gaseous Nebulae*. Standard work on the physics of nebulae with many useful tables. Well written though printed in an horrific font.
- Lamers & Cassinelli: *Introduction to Stellar Winds*. Standard work on the theory of stellar winds. Clear, very didactic approach.
- Aller: *The Atmospheres of the Sun and Stars*. Somewhat outdated, though very readable book on the physics of stellar spectra and stellar atmospheres with a good introduction on atomic and molecular line formation.
- Hearnshaw: *The analysis of starlight*. Very readable book on the history of stellar spectroscopy.

Prof. dr. Alex de Koter

Astronomical Institute 'Anton Pannekoek'
University of Amsterdam
P.O. Box 94249, 1090 GE Amsterdam

and

Astronomical Institute
Utrecht University
Princetonplein 5, 3584 CC Utrecht

Summer 2012.

2

The spectra of stars

The history of astronomical spectroscopy reaches back for less than two centuries. In this introductory chapter we first give a short (and therefore incomplete) summary of this history. We then discuss the spectra of stars and their classification.

2.1 Spectral classification

In 1802 William Wollaston (1766–1828) found that the spectrum of the sun contained dark stripes (spectral lines), which he interpreted as natural separations between colors. From 1814 on the maker of lenses Joseph von Fraunhofer (1787–1826) studied these lines in detail,

which he labeled with the letters A to K (a notation which in part is still in use today). He hoped to be able to use these dark stripes as markers of wavelengths for the development of optical instruments. Fraunhofer also observed the spectra of stars, and noticed large differences in color and stripe pattern. In the yellow and orange part of the spectrum of Sirius and Castor he could not detect lines at all, however, in the green-blue part he found three strong lines. The spectra of Pollux and Capella were very similar to that of Venus (i.e. to that of the sun). The spectrum of Betelgeuse did not look like that of the sun at all, though Fraunhofer thought he saw the D-line.



Figure 2.1: *Fraunhofer*

Later, others described the spectral differences between stars as recognized by Fraunhofer in more detail. These differences

were used to classify stars. The first systematic classification is from father Angelo Secchi (1818–1878), who founded a Jesuit observatory in the city of Rome in the mid of the nineteenth century. In 1867 he published a catalogue of 314 stars subdivided in four types. In 1890 at Harvard Observatory a large program to classify stars was initiated by Edward Charles Pickering (1846–1919), leading to the Henri Draper Memorial Catalogue, which contained the spectra of 10 351 stars. These spectra were recorded on photographic objective-prism plates,

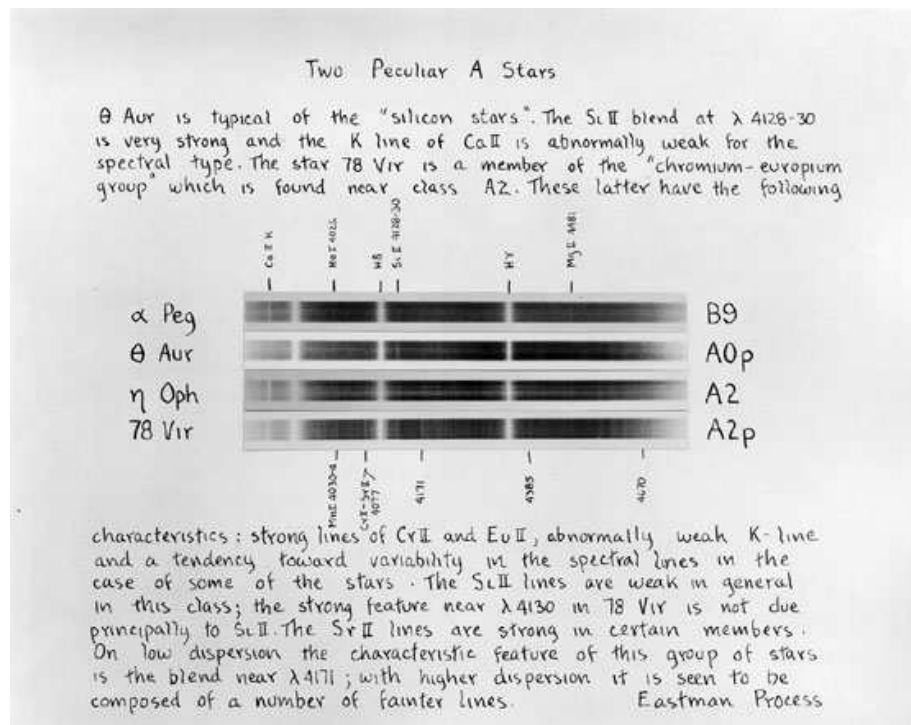


Figure 2.2: Discussion of the peculiar A-type stars by Morgan, Keenan & Kellman in their "Atlas of stellar spectra, with an outline of spectral classification" (1943), which is at the basis of the MK classification scheme.

and were classified by means of visual inspection. The estimated ratio between the strengths of spectral lines determined their spectral class.

The spectral classes were denoted by the capital letters A through P (later some of these letters disappeared as labels of spectral type). Besides this large scale classification project more detailed studies were done, from which emerged that some stars needed an extra label to properly describe their spectra. For this, small letters were used. Some examples of this are: *e*, in case emission lines are present, especially those of the Balmer series; *c*, in case the spectral lines were unusually sharp; *f*, in case of emission in the He II λ 4686 and N III λ 4640 lines. The latter may occur in the spectra of O-type stars.

The great importance of a precise classification became clear with, among others, the discovery by Ejnar Hertzsprung (1873–1967)¹ in 1905 that the proper motion of early-type stars that carried the label *c* was much smaller than that of normal stars of the same spectral class, having comparable apparent magnitudes. Hertzsprung concluded that *c*-stars of equal apparent magnitude were much more distant than normal stars, and therefore intrinsically much

¹Born in Denmark, Hertzsprung worked at Leiden Observatory from 1919 to 1944, the last nine years as director.

brighter. We now know that these *c*-stars are giants and supergiants. The sharpness of their spectral lines is linked to a much lower density of their atmospheres, which results in less "pressure broadening" of these lines (see chapter 12).

On an even larger scale, the spectra of almost a quarter of a million stars were classified at Harvard from 1911 to 1916. This work, by Annie Jump Cannon (1863–1941) and assistants, culminated in the new version of the Henri Draper Catalogue, in which 225 300 stars were included. In this monumental catalogue the spectral classes were indicated by capital letters, followed by a number (0 to 9) for a possible finer subdivision. The original series A through P was thinned out, and ended up in the non-alphabetic order we use today²:



This enormous industry was purely morphological. The idea was that the classification reflected the evolution of stars, hence the terms "early-" and "late"-type stars. Even after Hertzsprung in 1908 and, independently, Henry Norris Russell (1877–1957) in 1913 presented their diagram of absolute magnitude versus spectral type, the true meaning of the spectral types remained unclear. Only after Pannekoek realized the implications of pressure broadening; Saha derived the equations for ionization equilibrium, and Fowler and Milne coupled the colors of stars to differences in ionization, things became clear.

The spectral sequence is one of stellar surface temperature. As we will see later in these lectures it is temperature that determines the ionization and excitation properties of the outer layers of a star, where the spectral lines are formed. The degree of ionization of an element depends also on the density of the medium. This forms the basis of the luminosity classification of stars, first proposed by William Sydney Adams (1876–1956) in 1914, and later refined by many others, and which, after calibration, can be used for "spectroscopic parallax" determination. In its present form the luminosity-classification divides stars in types I, II, III, IV, and V (see figure 2.3). A more refined devision can be made using the letters a, ab, and b (class Ia being the most luminous).

Todays standard for the classification of stellar spectra is that defined by Morgan, Keenan, and Kellman in the forties, and later revised by Morgan and Keenan (MK), and which is based on spectra of standard stars. The earliest spectral type in this system is O3 (O0..O2 are not in use); the latest type is M8.³ Of all stars brighter than magnitude 8, for which the Henri Draper Catalogue is still complete, 99.95% can be classified in this way. An overview of the MK classification scheme is given in table 2.1. Roughly the classification works as follows.

²Mnemonics to remember the spectral order are, for the ladies: O Be A Fine Guy, Kiss Me; and for the gentlemen: Only Boys Accepting Feminism Get Kissed Meaningfully.

³More recently also the types O2 and M8.5, 9, and 9.5 have been introduced.

Table 2.1: An overview of the Morgan and Keenan (MK) spectral classification scheme, and of a number of the additions made to this system. For extremely cool objects, such as very cool stars, brown dwarfs, and planets with gaseous atmospheres the types L and T have been added. For giants with peculiar abundance patterns the types S, R, N, and C are used.

MK spectral class	Class characteristics
O	Hot stars with He II absorption
B	He I absorption; H developing later
A	Very strong H, decreasing later; Ca II increasing
F	Ca II stronger; H weaker; metals developing
G	Ca II strong; Fe and other metals strong; H weaker
K	Strong metallic lines; CH and CN bands developing
M	Very red, TiO bands developing strongly
L	Weakening VO and TiO bands, stronger alkaline and H ₂ O absorption
T	Appearance of strong CH ₄ bands in near-IR
Additional spectral classes	Class characteristics
S	Strong bands of ZrO and YO, LaO present, TiO weak compared to M stars, strong CN bands though not as strong as in C stars
R (or C)	Strong bands of CN and CO instead of TiO in class M
N (or C)	Swan bands of C ₂ , Na I (D), Ca I λ 4227, for the rest similar to R
Other characteristics sometimes included with MK types	
e	emission lines when not expected, e.g. Be
f	certain O type emission line stars
p	peculiar spectrum, e.g. anomalous line strengths or nebular (diffuse) lines
n	broad lines
s	sharp lines
c	especially sharp lines, characteristic of supergiants
k	interstellar lines present
m	metallic line star
v	variable lines
MK luminosity class	
I	supergiants
Ia ⁺ or Ia-0	extreme supergiants
Ia	luminous supergiants
Iab	normal supergiants
Ib	underluminous supergiants
II	bright giants
III	giants
IV	subgiants
V	dwarfs (main sequence)

O- and *B-type stars* are principally classified on the basis of lines of hydrogen and of neutral and singly ionized helium. In addition lines of several ionization stages of heavier elements, such as Si, are used. *A-type stars* are difficult to classify, as in this group of stars the Balmer series lines reach their maximum strength, and most lines of other elements are relatively weak. One uses the K-line of Ca II, which rapidly increases in strength from B8 to F0, as the prime criterion. *F0 to early M-type stars* show the following changes: In general the F-type stars show the absorption lines of heavy elements. These lines become stronger toward later spectral type. From type F toward later types the Balmer series lines become weaker, and are no longer conspicuous in K- and M-type spectra. Classification of F- to K-type spectra is based on Balmer lines, the lines of Fe I, Ca I, Ca II, and the G-band at ca. 4300 Å (a superposition of lines of the CH molecule and of a number of heavy elements, which Fraunhofer referred to with the letter G). *M-type stars* are characterized by the presence of molecular TiO bands, which rapidly increase in strength toward later types.

The luminosity of a star is inversely proportional to its surface gravity, which sets the absolute scale of the pressure structure – and by that the density in the region in which the spectral lines are formed (see § 9.2). In early-type stars the wings of hydrogen lines are sensitive to atmospheric pressure. These lines (notably those of the Balmer series, such as H α , H β , H γ and H δ) are therefore used to determine the luminosity class of O, B, A, and F-type stars.

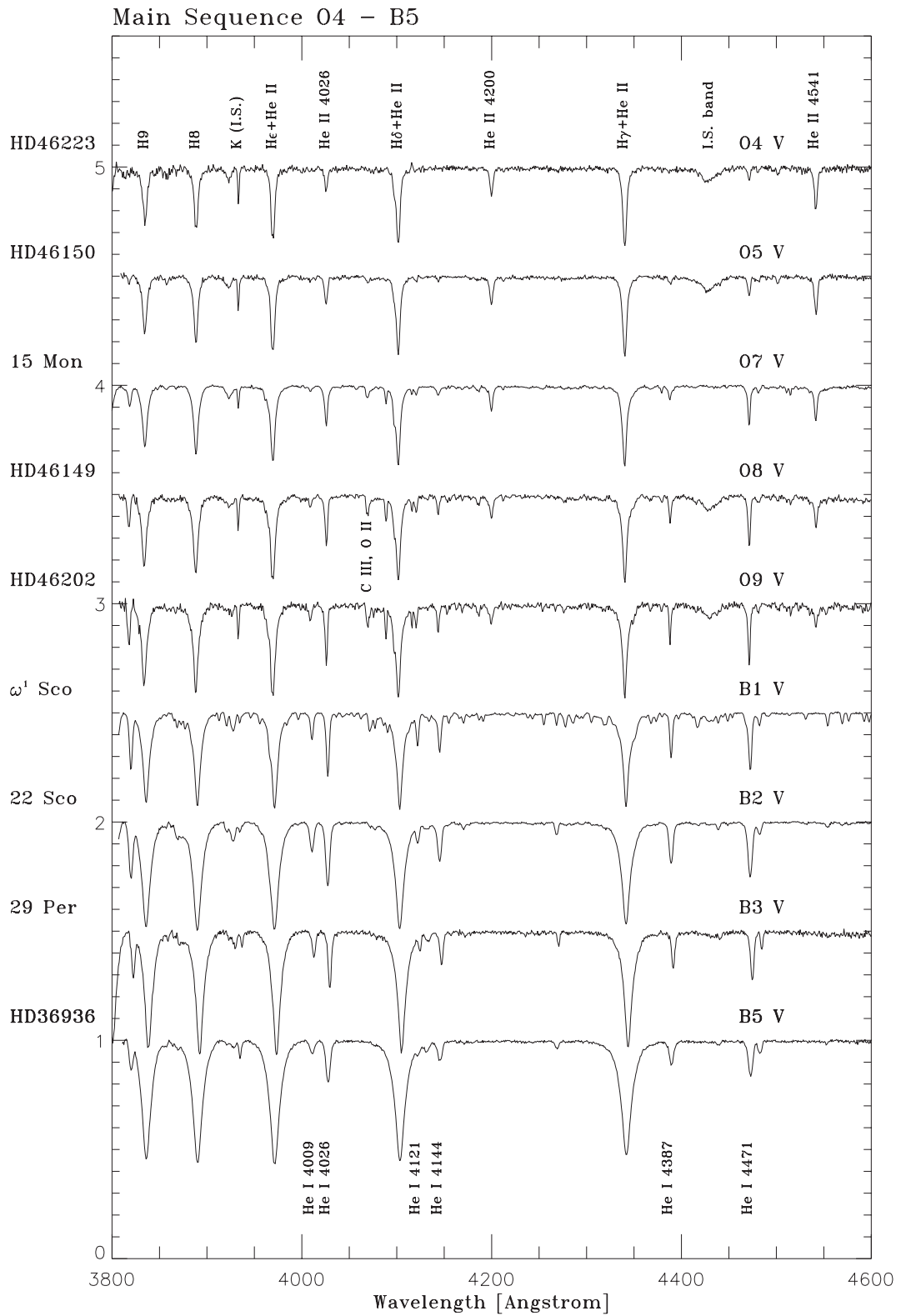
The calibration of spectral type, luminosity class and color indices (which will be discussed in § 2.6) in terms of temperature and density of the medium – expressed in terms of *effective temperature* T_{eff} and *gravity* $\log g$ – is done using model atmospheres, which will be discussed later on in these lectures.

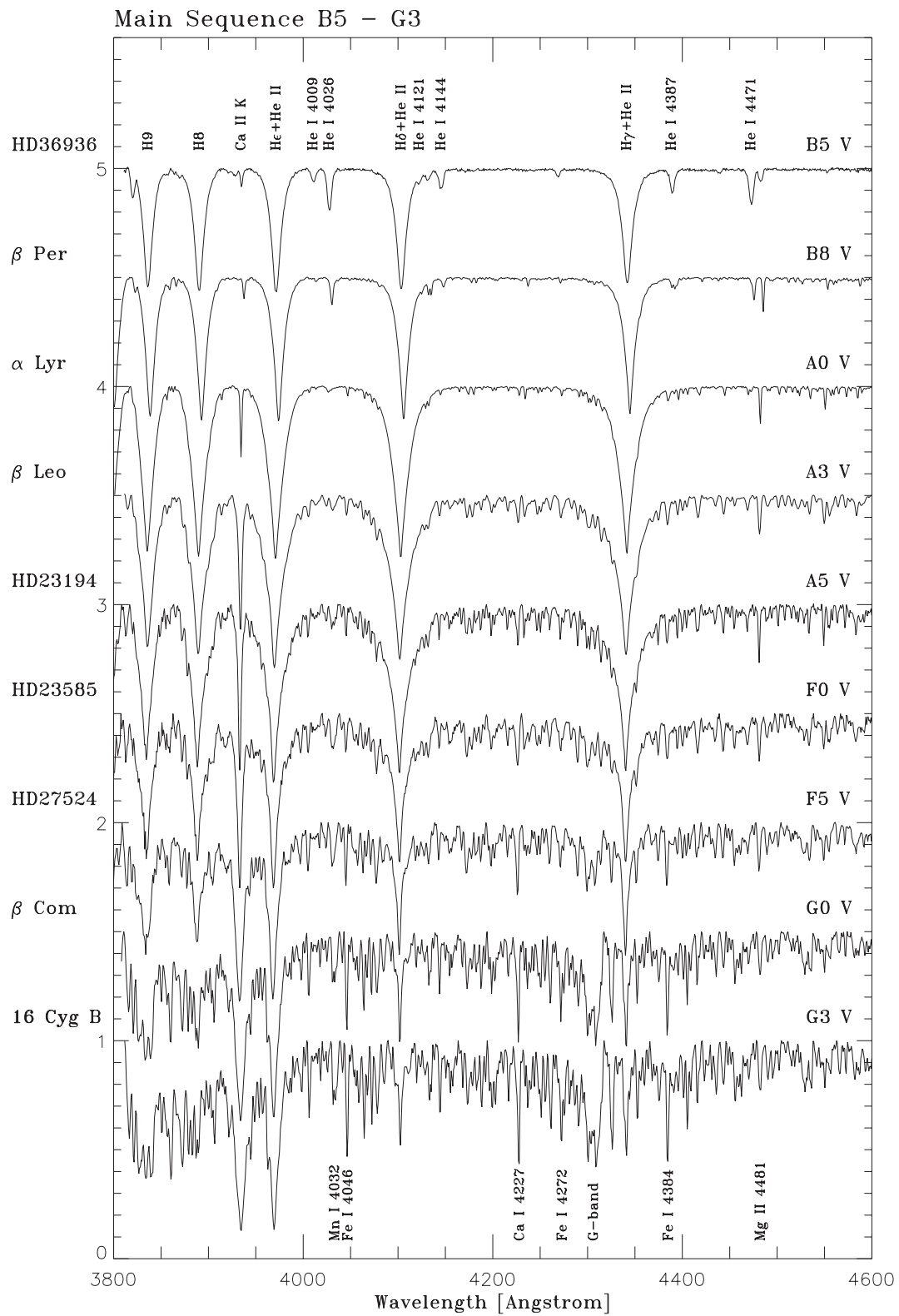
2.2 Special stellar spectra

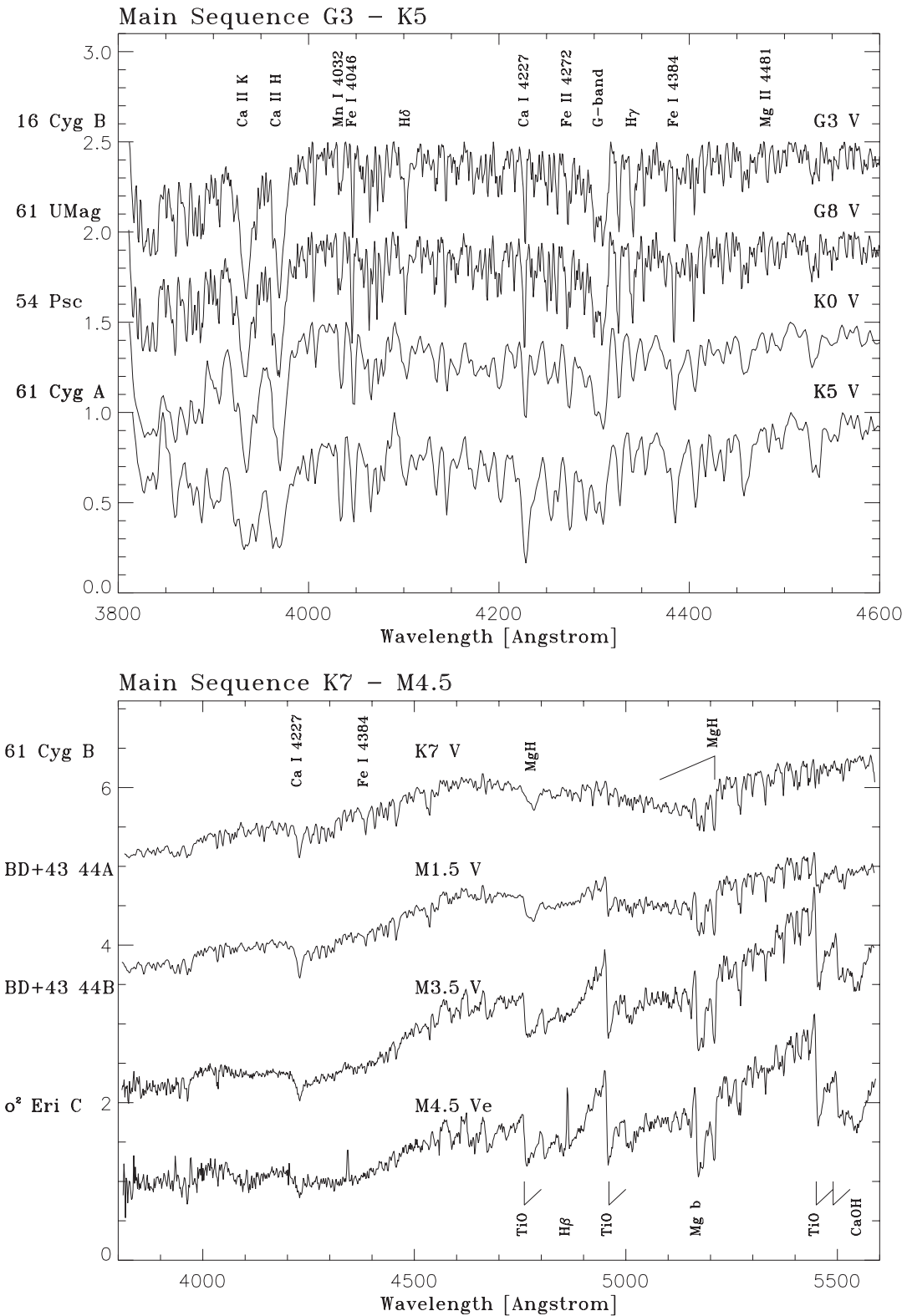
The vast majority of stars emit spectra that are well classified using the method we have just described. There are however stars of which the spectra show special characteristics. We will give a brief description of a few of such objects.

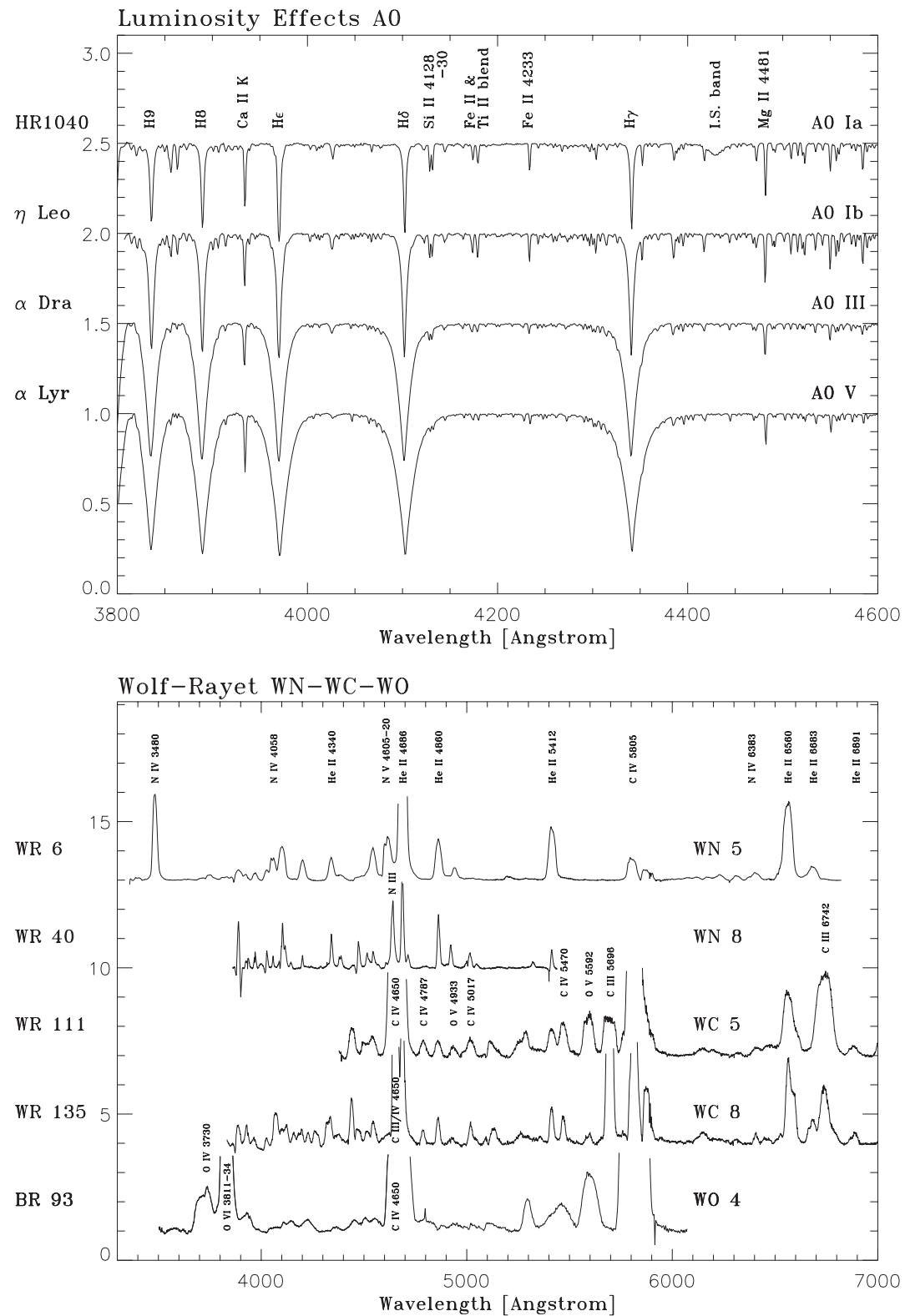
Be-stars

The spectra of some B- (and also O-) type stars show emission lines of, notably, the Balmer series (discrete transitions between the first and higher excited stages of neutral hydrogen). H α is the strongest; the emission strength decreases toward higher members of the Balmer series. These stars are called B-emission (Be) stars. Be stars constitute about 15% of all B stars. In some Be stars the Be phenomenon is transient, i.e. it may be present for some time, then disappear for a while. It has been established that the rotation velocities of Be stars are on average significantly higher than that of normal B stars. Whether all B stars show the Be phenomenon during some part of their main sequence evolution is currently being









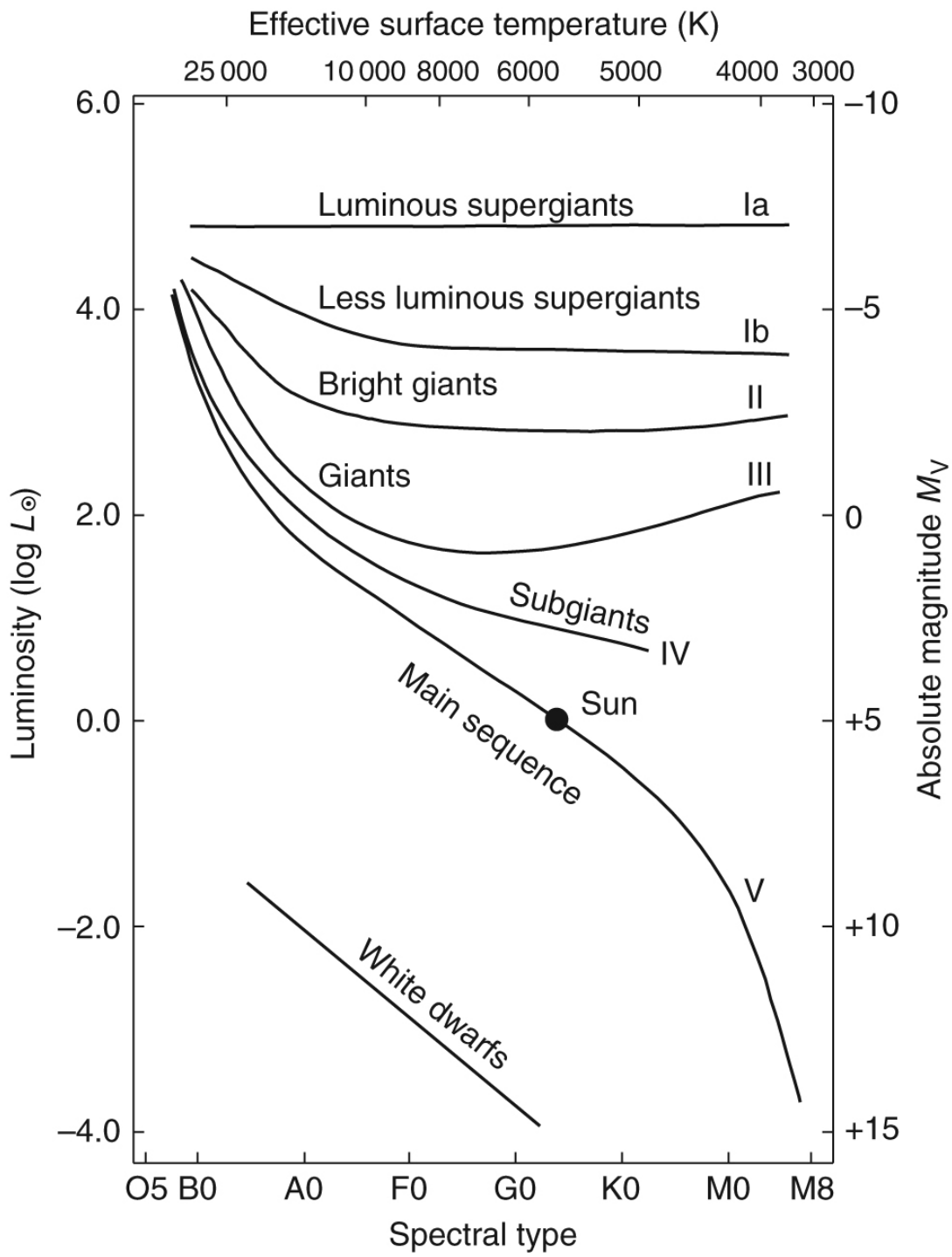


Figure 2.3: Hertzsprung-Russell diagram showing the stellar spectral types and luminosity classes. Note the large span in luminosity of the supergiants, illustrating the need for a sub-classification in Ia⁺ (not shown), Ia, Iab (not shown) and Ib. Source: Pradhan & Nahar, Atomic Astrophysics and Spectroscopy.

investigated. The near break-up velocities of Be stars apparently allows these stars to eject material, mainly in the equatorial regions. Line emission of this disk like distribution of gas dominates the profile shape of the strong Balmer lines. A second characteristic of most Be stars is that they show an excess in their infrared brightness.

Wolf-Rayet stars

This type of stellar spectrum was first discovered by the French astronomers Charles Wolf (1827–1918) and Georges Rayet (1839–1906), in 1867, and is characterized by broad emission lines of highly ionized elements, superposed on a very "hot" continuum spectrum. The lines are formed in a dense, optically thick outflow or stellar wind and reflect the high mass loss of the star.

The temperatures of Wolf-Rayet (WR) stars are in the range of that of O-type stars. The mass loss rates are in the order of 10^{-5} to $10^{-4} M_{\odot}\text{yr}^{-1}$. Because of the extreme character of their spectra they can not be classified using the MK scheme. They have an independent classification scheme consisting of three types. Depending of the presence of strong lines of ionized nitrogen, carbon, or oxygen one refers to them as WN-, WC- and WO stars, respectively. These are further subdivided in the spectral sequences WN2–11, WC4–9 and WO1–4, depending on the ionization-excitation conditions and the density in the outflowing atmosphere.

The *VIIth catalogue of galactic Wolf-Rayet stars* (van der Hucht 2000) contains 227 galactic WR stars; more than 100 are known in the Magellanic Clouds. The WR stars represent the last phase in the evolution of very massive stars (i.e. stars with an initial mass $\gtrsim 25M_{\odot}$). In absolute terms they are young stars ($\sim 5 - 10$ Myr). During the WR phase these stars end their lives in a supernova explosion.

In a completely different category of stars WR spectra have also been observed, i.e. in some of the (\sim solar mass) central stars of planetary nebulae.

Stars with P Cygni profiles

Resonance lines of abundant ions in the ultraviolet part of the spectra of O- and B-type stars often show P Cygni type profiles. Such line profiles consist of a blue shifted absorption component and a symmetric emission component. They are the result of a spherical stellar wind in which material is ejected from the star with a high velocity (on the order of 10^3 km sec^{-1}). In the part of the wind that is seen in projection in front of the stellar disk, and in which the flow accelerates over a large interval in velocity (causing a shift in wavelength), the blue shifted absorption is formed. The emission originates from those parts of the outflow that are seen next to the stellar disk, and that give rise to a symmetric profile centered on the rest wavelength of the line (see chapter 16).

Luminous Blue Variable stars

There is a small group of stars, so called *Luminous Blue Variable stars* (LBVs), which not only show P Cygni type lines in the ultraviolet but also in the optical spectrum, e.g. in H α . The widths of the lines in terms of velocity is typically a few hundred km sec $^{-1}$. The best known member of this group of stars is the star P Cygni itself (in which the profiles were discovered for the first time). LBVs represent a phase in the evolution of massive stars that is between the main sequence (when they are O-type stars) and the Wolf-Rayet phase. During the LBV phase the stars are strongly variable in both photometric and spectroscopic properties. They may show variations in visual magnitude of up to 1 to 2 magnitudes on timescales of years to decades. During their quiescent visual minimum phases they are B supergiants. In periods of maximum visual brightness they are A- to F-type supergiants.

On an estimated timescale of millennia they may "erupt" increasing their brightness by more than three magnitudes. During such eruptions they expel their outer layers.

Carbon stars

These are very cool stars of which the spectrum is dominated by absorption bands of molecules that contain carbon. Important molecules are C₂, CH, and CN.

Whether a cool star has an M- or a C-type spectrum does not depend on its temperature, but on the number ratio of carbon and oxygen O atoms. The reason is the exceptional stability of the CO molecule, which binds all available C and O atoms. When the star is oxygen rich, i.e. when the oxygen abundance is higher than that of carbon, a surplus of oxygen atoms will remain after the formation of carbon monoxide to form molecules such as TiO. In this case we observe an M-type spectrum. Reversely, when a star is carbon rich, a surplus of carbon atoms will remain to form carbon compounds such as the ones mentioned above. This yields a C-type spectrum.

If the C/O ratio is ~ 1 the spectral properties are intermediate between M- and C-type. These stars are often referred to as of S-type.

The atmospheric C/O number ratio of evolved stars of low or intermediate mass (more precisely, those that are on the asymptotic giant branch in the Hertzsprung-Russell diagram or HRD) may change over time when carbon, produced in thermonuclear reactions in the stellar interior, reaches the surface layers by means of convective motions. The turnover of an M-type star into a C-type star takes only a very short time ($< 10^4$ year).

Peculiar stars

The chemically anomalous or "peculiar" stars form a group that in the HRD is located along the main sequence, from about spectral type B5 to F2. In total about 15% of all main sequence stars is situated in this spectral interval. They are roughly subdivided in two groups, the

peculiar A (Ap) stars, and the metal line A (Am) stars. They deviate from other stars in that they show strong lines of very specific elements. Examples are the Hg-Mn stars and the Si-Cr-Eu stars. For these stars atmospheric abundances of the elements mentioned can be enhanced up to a factor 10^3 relative to normal values.

These deviations are thought to be the result of the exceptional stability of the atmosphere, in which a combination of gravitational forces and selective radiation pressure on spectral lines causes a differential diffusion of elements, such that some show preference to "float" to the surface. The exceptional stability of the atmosphere is most probably linked to the absence of: *i*) a convection zone that penetrates to layers close to the surface, which explains the absence of peculiar stars later than type F2; *ii*) strong mass loss, which explains the absence of peculiar stars earlier than type B2. The atmospheric stability of peculiar stars is also illustrated by, for instance, a systematically lower X-ray luminosity of A-type main sequence stars compared to that of dwarfs of neighboring spectral types.

Magnetic fields and rotation (or the lack of it) also play a role in determining which elements show high surface abundances. Most Am stars, to give an example, are part of close binary systems in which the two components slow each other down by tidal action. The Hg-Mn stars are also slow rotators; in addition this subgroup of the B-type stars has markedly weak magnetic fields.

Brown dwarfs and Jupiter-like planets

The masses of brown dwarfs are too low to allow thermonuclear burning of hydrogen in their cores. Deuterium is fused during the contraction phase. Lithium however always remains present (and it is therefore the detection of Li that is used to identify these dim objects as brown dwarfs). Very low mass stars and brown dwarfs are probably the most common objects in our Milky Way. The spectra of these cool objects are dominated by molecular absorption bands of H₂, CO, H₂O and metal oxides. The later types also show absorption bands of condensed (solid state) materials. In ultra cool objects (with spectral type L and effective temperatures $T_{\text{eff}} \lesssim 2\,200$ K) Ti and V is locked up in solid state particles causing the TiO and VO molecular bands to disappear. Even cooler, Jupiter-like objects with masses less than $\simeq 13 M_J$ do not even burn deuterium. If the spectra of such objects show strong CH₄ bands then $T_{\text{eff}} \lesssim 1\,300$ K and spectral type T is used to characterize them. Brown dwarfs differ from Jupiter-like objects, as are presently being discovered around nearby stars, in their genesis. For example, the bulk of the discovered L dwarfs is "free floating", i.e. they exist as individual objects in space, contrary to (exo)-planets.

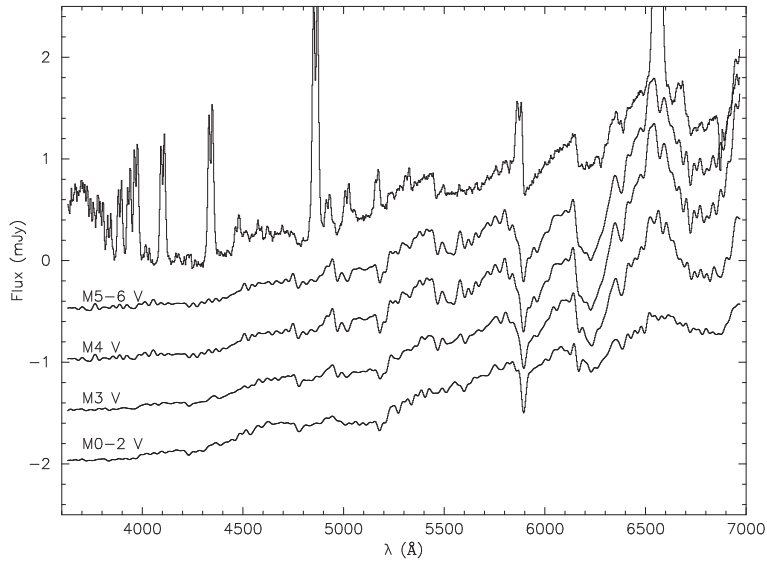


Figure 2.4: Spectrum of the cataclysmic variable IP Pegasi (top) together with four spectra of M-type stars. IP Peg is a system with a low mass transfer rate. The spectrum shows a hybrid nature in-between that of the “blue” spectrum of the accretion disk around the white dwarf and the “red” spectrum of its M3V companion. Clearly visible in emission are the lines of the Balmer series of hydrogen and the He I $\lambda 5875$ line. These are formed in the optically thin outer regions of the rotating disk. This can be deduced, for instance, from the fact that they are double peaked. The M3V companion reveals itself e.g. by the strong molecular bands of TiO.

2.3 Special binary spectra

It is estimated that about 40%-60% of all stars is part of a binary or multiple star system. We briefly discuss the spectra of two special types of binaries.

Cataclysmic variables

Cataclysmic variables (CVs) are close binary stars in which a low mass star (which in the HRD is usually located close to the main sequence) transfers mass to a white dwarf. This mass transfer proceeds through an accretion disk, in which material spirals in, in almost Keplerian orbits, toward the white dwarf. In most cases the disk dominates the optical light of the binary system. The spectral characteristics of CVs sensitively depend on the rate of mass transfer. If this is low (of the order of $10^{-10} M_{\odot}$ per year, e.g. in dwarf novae in quiescence) one sees strong emission lines, notably those of the Balmer series (see figure 2.4), superimposed on a blue continuum. These lines originate from a large optically thin regime in the outer parts of the disk. When the mass transfer rate is high (of the order of $10^{-8} M_{\odot}$ per year) the continuum emission increases relative to that of the lines (the outer parts of the disk become

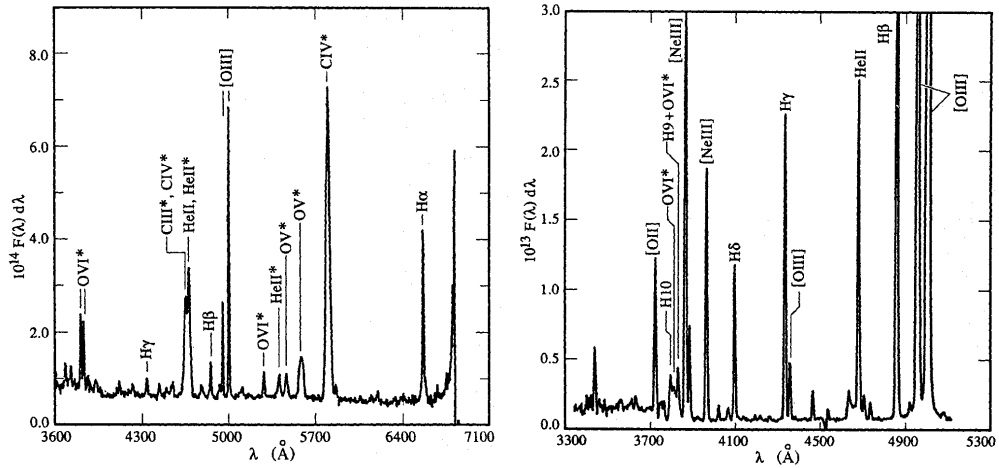


Figure 2.5: Spectra of the Planetary nebulae NGC 1501 (left) and IC 1297 (right) in visible light. Planetary nebulae are characterized by strong emission lines and a (very) weak continuum. The strongest nebular lines in PN spectra are often those of the forbidden $[O\text{ III}]\lambda 4959$ en 5007 transitions. The lines that have the superscript * are from the central star (in both cases $T_{\text{eff}} \sim 80\,000$ K); the nebulae have an electron temperature $T_e \sim 10\,000$ K. Source: Stanghellini, Kaler, & Shaw 1994, A&A 291, 604.

optically thick). In some cases the lines disappear (e.g. during a dwarf nova eruption).

Low-mass X-ray binaries

These systems are similar to CVs, except that the compact object is a neutron star or a black hole i.s.o. a white dwarf. The optical spectra of low-mass X-ray binaries (LMXB) show a blue continuum (corresponding to a temperature of 30 000 K or higher), on which superposed are a number of weak emission lines. The most important of these lines are Balmer series transitions, He II $\lambda 4686$, and C III/N III $\lambda 4640$ -50. The spectra originate in the accretion disk around the compact star, where x-ray radiation from the compact object is being converted in optical and ultraviolet photons (so called x-ray heating or “reprocessing”).

2.4 Nebulae

Planetary nebulae

Diffuse objects that can not be resolved in stars are referred to as nebulae. It may be clear that in many cases this definition says more about the spatial resolution of the instrument that is used than about the nature of the observed object. Planetary nebulae were termed as such by Frederick William Herschel (1738–1822), who saw them with his telescope and thought

they looked somewhat like the disks of planets. The first spectrum of a planetary nebula was recorded in 1864 by William Huggins (1824–1910). Huggins discovered that a single emission line seemed responsible for the light. At higher spectral resolution this single line could be resolved in three individual lines, of which $H\beta$ is one.

Planetary nebula contain a central star. The nebula is ejected by this star. Planetary nebula represent a short (of the order of 10^4 year) period near the end of the lives of low mass stars, after evolving of the asymptotic giant branch but before reaching the white dwarf stage. The spectra of planetary nebulae are dominated by line emission; continuum emission is relatively weak. The nebula lights up because it is illuminated by Lyman continuum photons from the very hot (30 000 to $\sim 150 000$ K) central star, which ionizes the nebular gas. After recombination a line cascade occurs (e.g. in the Balmer series) giving rise to the emission lines. Planetary nebulae also show forbidden line emission. This radiation originates from metastable levels, which as a result of the extremely low densities in nebulae are no longer depopulated by collisional processes. Figure 2.5 shows two examples. We will discuss the line formation in gaseous nebulae at a conceptual level in more detail in chapter 14. Further quantitative elaborations will be given in chapter 17.

Nebulae around massive stars

Massive stars may also be surrounded by nebulae. These may form from material ejected by the star, typically in evolutionary phases characterized by a high mass loss in a stellar wind. Nebulae are observed around for instance LBV and Wolf-Rayet stars and red supergiants. The nebular spectra of LBVs en WRs are dominated by recombination lines, just as in the case of planetary nebulae. In the infrared one often observes the thermal emission of solid state material (or dust), that may condense in the stellar outflow or in the nebular environment.

2.5 Supernovae

Supernovae (SNe) are stellar explosions during which the luminosity of a star reaches $10^9 - 10^{10} L_\odot$ at maximum, remaining bright for several months afterwards. SNe have been historically classified into Type I (those that show no hydrogen lines) and Type II (those that do). A more detailed subdivision, summarized in Figure 2.6, is as follows:

Type Ia

The main spectral features are the lack of H lines and the presence of strong Si II lines around maximum brightness. After several months, lines of Fe and Co appear in the spectra. Type Ia supernovae are caused by the thermonuclear explosion of a CO white dwarf that reaches the Chandrasekhar limit by mass accretion in a binary system. The white dwarf is completely

destroyed in the explosion and no compact stellar remnant is left behind. They are (on average) the most luminous of all supernova types and their lightcurves (see Fig. 2.7) form a rather homogeneous group (see top Fig 2.8), which makes them of great interest as cosmological probes.

Type II, Ib and Ic

The spectra of Type II supernovae (see bottom Fig. 2.8) are dominated by H lines, while lines of Ca, O and Mg are also present. SNe II correspond to the explosion of massive stars. They form the main class of explosions associated with the core collapse of massive stars that have hydrogen-rich envelopes (red supergiants if $M \gtrsim 8M_{\odot}$). Type II supernovae show a variety of lightcurve shapes (see Fig. 2.7), on the basis of which they are often sub-classified into Type II-P (showing, after an initial rapid rise and decline in brightness, a long 'plateau' phase of almost constant luminosity lasting 2–3 months, before a slow exponential decay) and Type II-L (which lack the plateau phase). In addition, one distinguishes Type IIb, in which the spectral signatures change from Type II to Type Ib (see below); and Type IIn, showing narrow emission lines on top of broad emission lines, which are interpreted as resulting from heavy mass loss prior to the explosion. The light curves of II-P and II-L supernovae have been well modeled with the explosion of red-supergiant stars (though also the blue supergiant progenitor of SN1987A has type II-P). Progenitors of Type IIb supernovae may have been red-supergiants with an unusually thin hydrogen-rich envelope. Some indications point to Type IIn supernovae progenitors being Luminous Blue Variables, or stars that experienced an LBV phase not too long before the explosion.

Type Ib supernovae have strong He lines in their spectra, which are lacking in Type Ic supernovae. Both types show a lack of hydrogen, and strong lines of O, Ca and Mg are present. Type Ib and Ic supernovae are also associated with core collapse of massive stars, more specifically to those that have lost their H-envelopes prior to explosion. Their progenitors are Wolf-Rayet stars that result from the evolution of stars initially more massive than about $25 M_{\odot}$.

Main type	Type I			Type II	
hydrogen	no H lines			H lines dominate	
other lines	Si II $\lambda 6150$		no Si		
			He I $\lambda 5876$	weak He	
lightcurve				plateau, then linear	linear
Sub type	Ia	Ib	Ic	II-P	II-L

Figure 2.6: Overview of the classification scheme of supernova spectra. The SNIa are characterized by a deep absorption through around $\lambda 6150 \text{ \AA}$ produced by blueshifted Si II $\lambda\lambda 6347, 6371$ (collectively called $\lambda 6355$).

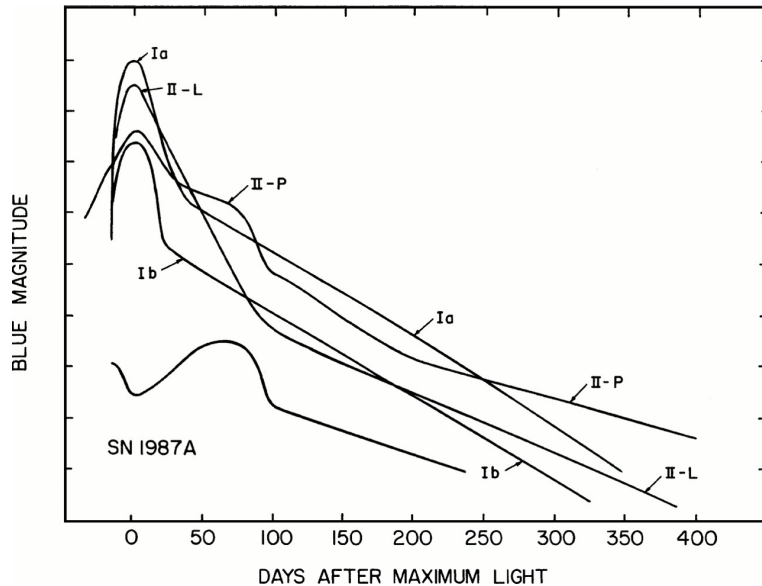


Figure 2.7: Schematic supernova lightcurves. Typical maximum B -band magnitudes are -19.5 for SNe Ia, -17.6 for SNe Ib, Ic and II-L, and -17.0 for SNe II-P. The lightcurves of SNe Ic resemble those of SNe Ib. Figure from Filippenko 1997.

(see section 2.2). A subclass of very bright Type Ic supernovae, known as hypernovae, may be associated with gamma-ray bursts.

2.6 The continuum energy distribution of stars

Connected to the changes in relative line strengths that are observed along the spectral sequence, and which are caused by changes in the ionization and excitation conditions in the stellar atmospheres, is a change in the continuum energy distribution of the emitted light.

A library of optical spectra obtained with the VLT/UVES instrument of hundreds of stars has been published by Bagnulo et al. (2003, Messenger 114, 10). The spectra cover the wavelength range from 3040 to 10400 Å (save for a few narrow wavelength gaps) and have a spectral resolving power (see eq. 12.3) of about 80 000. For most of the spectra, the typical signal-to-noise ratio in the V band is between 300 and 500. All this implies that both the individual spectral lines and continuum energy distribution are clearly visible. The spectra can be obtained and/or visualized using the UVES POP archives, for which the URL is www.eso.org/sci/observing/tools/uvespop.html.

These changes in the spectral energy distribution can be measured by one or more *color indices*. The best known are the $B-V$ and $U-B$ indices introduced by Johnson & Morgan

(1953). The central wavelengths of U , B , and V broad-band filters, as defined by Johnson, are at 3600, 4400, and 5500 Å, respectively. The typical filter width is about 1000 Å. Their transmission efficiency as a function of wavelength is given in figure 2.9. It is customary to define the index in such a way that the magnitude in the long wavelength filter is subtracted from that in the short wavelength filter, such that an increase in the color index signifies a "redder" spectrum. The run of the $B-V$ and $U-B$ indices (in the Johnson system) with spectral type and luminosity class is shown in figure 2.11 and in table A.1.

The $B-V$ color index is a relative measure of the temperature of the star in the Paschen continuum (see figure 6.4); the $U-B$ color index is primarily a measure of the extend of the Balmer jump, which in addition to temperature is also somewhat dependent on density. If one plans to use these indices to determine the spectral type and luminosity class of a star it is important to realize that extinction in the interstellar medium – as a result of the interaction of star light with "interstellar dust" – can affect the intrinsic continuum energy distribution (see § 18.2). The importance of extinction increases with decreasing wavelength and therefore also has an effect on the color indices. Interstellar extinction is typically important for stars at relatively large distances in the plane of the Milky Way and for stars in star forming regions. For nearby stars (say $d \lesssim 100$ pc) interstellar extinction is negligible. Spectral lines do not suffer from interstellar extinction as they cover only a very small wavelength band, such that one may ignore the wavelength dependence of the extinction. Often stellar spectra show absorption lines that originate from extinction of star light passing through interstellar gas.

The jungle of photometric systems

For different reasons no universal photometric system exists. Johnson (1966, ARA&A 4, p193), who measured the photometric magnitudes of a large number of stars in ten different filters, lost his filter set before he could measure the filter transmissions. Later, others tried to design filters with properties that best recovered the colors of the stars measured by Johnson – but no one has succeeded in getting a perfect match. One should also realize that the quantum efficiency of the detector and the optical efficiency of the lenses in the telescope may differ for each observatory, as, obviously, will the atmospheric transmission. Especially in the near- and mid-infrared the atmospheric transmission is a problem. Figure 2.10 shows the measured atmospheric transmission on mount Mauna Kea, Hawaii, where the UKIRT infrared telescope is located. Note that the near-infrared filters are designed to make optimal use of relatively transparent "windows" in the earth atmosphere.

Filter properties and calibration constants C_m for a few often used filter systems are given in table 2.2. Usually, the (arbitrary) constants have been chosen such that they provide fixed values for the magnitudes of a set of standard stars. Using C_m one may obtain the measured flux, f_m , corresponding to the observed or *apparent magnitude* m , from

$$\log f_m = -0.4 m + C_m \quad (2.1)$$

The measured flux and the calibration constant have dimensions $\text{erg cm}^{-2} \text{ sec}^{-1} \text{ Hz}^{-1}$. If, for

	λ_o	Johnson system			UKIRT system			ESO system				
		$\Delta\lambda$	C_m	Johnson	Land.-B.	λ_o	C_m	UKIRT	λ_o	$\Delta\lambda$	C_m	
U	0.36	400	-19.726	-19.764		U	0.36	-19.73				
B	0.44	1000	-19.353	-19.348		B	0.43	-19.36				
V	0.55	800	-19.436	-19.436		V	0.54	-19.42				
R	0.70	2100	-19.556	-19.556		R	0.70	-19.54				
I	0.90	2200	-19.614	-19.650		I _s	0.80	-19.60				
						I _j	0.90	-19.65				
J	1.25	3000	-19.752	-19.802		J	1.25	-19.82	J	1.20	2000	-19.786
						H	1.65	-20.01	H	1.65	3000	-19.963
K	2.20	6000	-20.201			K	2.20	-20.21	K	2.20	4000	-20.177
	2.22	—		-20.200								
L	3.40	9000	-20.509			L	3.45	-20.54	L	3.80	7000	-20.558
	3.60	—		-20.562		L'	3.80	-20.62				
M	5.00	11000	-20.745	-20.807		M	4.80	-20.82	M	4.70	5000	-20.785
							7.80	-21.21				
							8.70	-21.31				
							9.80	-21.41				
N	10.20	60000	-21.367			N	10.1	-21.43	N	10.30	52000	-21.367
	10.60	—		-21.413			10.3	-21.46	N ₁	8.30	8500	-21.292
							11.6	-21.55	N ₂	9.40	16500	-21.444
							12.5	-21.65	N ₃	12.00	37000	-21.658
						Q	20.0	-21.02	Q ₀	17.40	56000	—
									Q ₁	19.60		-22.081
									Q ₁	30.50		-22.432

Table 2.2: Properties of the optical and infrared filters of three common systems. The central wavelength λ_o is in micron; the full width of the filter $\Delta\lambda$ is measured at half the maximum filter transmission and is given in Å. The calibration constant C_m of filter m has dimensions $\text{erg cm}^{-2} \text{ sec}^{-1} \text{ hz}^{-1}$. Johnson system: see Johnson (1966, ARA&A 4, p193), Landolt-Börnstein (1982). UKIRT system: see UKIRT users manual. ESO system: see Koornneef (1983, A&A 128, p84) for JHKLM, Echtein et al. (19XX, A&AL 85, L1) for NQ.

instance, we would be considering the Johnson V filter, the above equation would tell us that for a star with $V = 0$ the measured flux is $10^{-19.436} = 3.66 \times 10^{-20} \text{ erg cm}^{-2} \text{ sec}^{-1} \text{ hz}^{-1}$.

The measured flux is related to the true flux distribution of the star at the distance of the earth, $\mathcal{F}_\nu(d)$, where d is the distance to the star, as

$$f_m = \frac{\int_0^\infty \mathcal{F}_\nu(d) S_m(\nu) d\nu}{\int_0^\infty S_m(\nu) d\nu} \quad (2.2)$$

where S_m = (filter transmission) \otimes (detector quantum efficiency) \otimes (optical efficiency) \otimes (atmospheric transmission) is the *response function*. Defining $\int_0^\infty S_m(\nu) d\nu \equiv S_m^\circ$, yields for the apparent magnitude

$$m = -2.5 \log \int_0^\infty \mathcal{F}_\nu(d) S_m(\nu) d\nu + 2.5 (C_m + \log S_m^\circ). \quad (2.3)$$

Exercise 2.1

We have classified the spectrum of a star as M2 III and have measured its visual magnitude: $V = 1.63$ magn. We assume that in the line-of-sight towards the star there is no

interstellar extinction at visual wavelengths: $A_V = 0$ magn. Use the equation for the distance modulus

$$m - M = 5 \log d - 5 + A_\lambda, \quad (2.4)$$

where m is the apparent magnitude, M the absolute magnitude, d the distance in parsec, and A_λ the interstellar extinction (see also eq. 18.2), as well as table A.1 to determine its distance. This procedure of distance determination is known as spectroscopic parallax method.

Exercise 2.2

Consider the two stars whose properties have been described below. The symbols in the table have their usual meaning.

Star	V	$B-V$	M_V	T_{eff}	Spectral Class	BC
Betelgeuse	0.45	1.50	-0.60	3370	M2 Ib	-1.62
Gliese 887	7.35	1.48	9.76	3520	M2 V	-1.89

How much larger in radius is Betelgeuse than Gliese 887?

Exercise 2.3

The top panel of Figure 2.11 shows a plot of the color-color diagram in which $U-B$ is plotted as a function $B-V$. Explain why the $U-B$ color shows a local maximum at about spectral type F5.

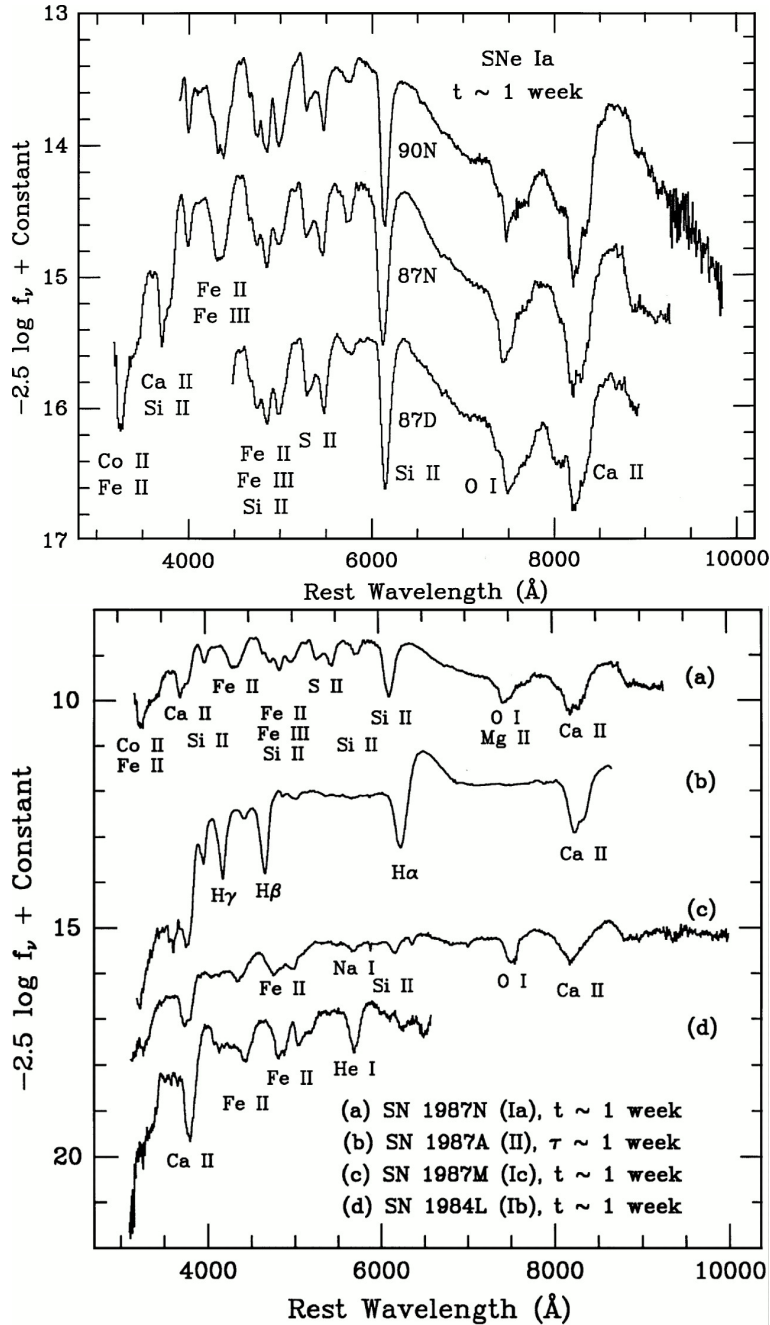


Figure 2.8: Top: Examples of supernova spectra of type Ia, approximately 1 week after maximum brightness. Note the strong Si II $\lambda 6150$ line and the overall homogeneous nature of these spectra. The parent galaxies are as follows: SN 1990N (NGC 4639); SN 1987N (NGC 7606), and SN 1987D (MCG+00-32-01). Bottom: Examples of supernova spectra of the four major types and subtypes. The variable t and τ represent time after observed B-band maximum and time after core collapse, respectively. The parent galaxies are as follows: SN 1987N (NGC 7606); SN 1987A (LMC); SN 1987M (NGC 2715), and SN 1984L (NGC 991). Figures from Filippenko (1997).

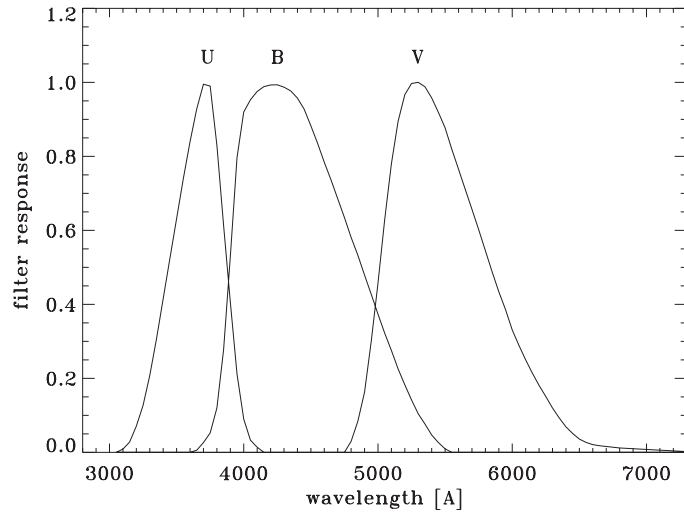


Figure 2.9: Normalized filter transmission functions for the U , B , and V filters in the Johnson system. The central wavelengths of these filters are 3600, 4400, and 5500 \AA , respectively.

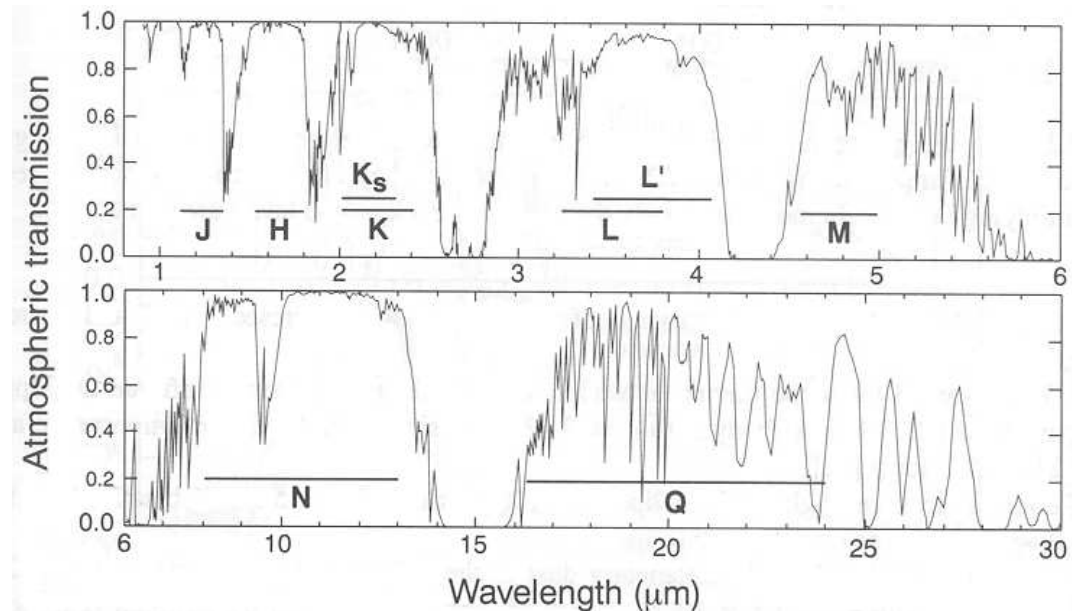


Figure 2.10: The atmospheric transmission from 9000 \AA to 30 μm measured at the summit of maunt Mauna Kea, Hawaii (Height: 4.2 km; zenith angle 30°, i.e. air mass 1.15). The near-infrared photometric filters are represented by horizontal lines. Note that filter magnitudes are affected by the transmission properties of the earth atmosphere.

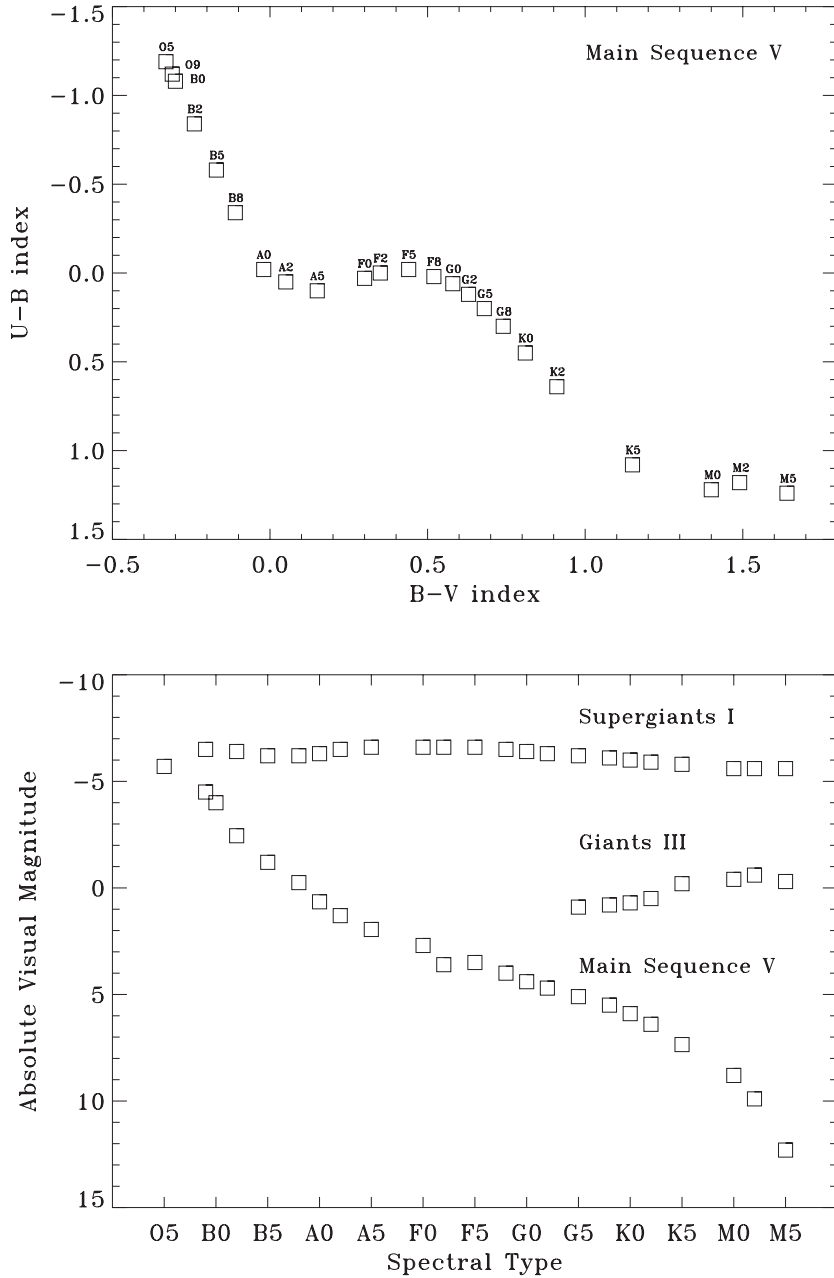


Figure 2.11: Top: The color indices $U-B$ and $B-V$ as a function of spectral type and luminosity class. Bottom: The absolute visual magnitude versus spectral type, i.e. the Hertzsprung-Russell diagram.

3

Characterizing the radiation field

In this chapter we give the basic definitions that characterize the radiation field. We start out with a short discussion of the two geometries that will be used frequently throughout these lecture notes.

3.1 Coordinate systems

Plane parallel layers

Throughout these lectures we will almost exclusively concentrate on one dimensional problems in either a geometry of plane parallel layers or of spherical shells (see figure 3.1).

In a geometry of plane parallel homogeneous layers we use a Cartesian coordinate system, such that $\mathbf{r} = (x, y, z)$ and z denotes the direction normal to the planar layers. In case of homogeneous layers *axial symmetry* will hold, such that all quantities relevant in describing the state of the medium depend on z only. They are constant in the x and y directions, therefore all gradients $\partial/\partial x$ and $\partial/\partial y$ will be zero. For a beam entering the medium at a polar angle θ between the normal direction and the beam direction, we will frequently use the variable $\mu = \cos \theta$.

The atmospheres of most stars are well described using a plane parallel geometry. This may seem surprising. However, taking the sun as an example, one should realize that the thickness of the solar atmosphere (where the spectral lines in the visible part of the solar spectrum originate) is only some 500 km whereas the radius of the sun is about 700 000 km. The curvature of the solar atmosphere is therefore negligible. For some stars the assumption of plane parallel layers can not be justified. For example, if the star has a stellar wind (see § 16) the strongest lines may form over a radial extend of ~ 10 stellar radii. In that case we must assume a geometry of spherical shells.

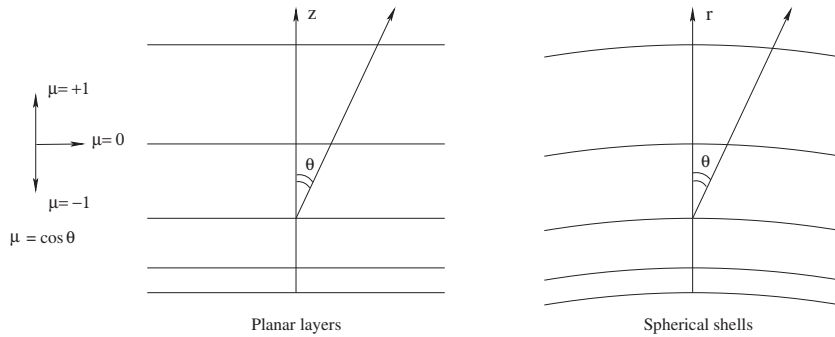


Figure 3.1: Diagram showing the geometry of plane parallel layers and of spherical shells.

Spherical shells

In a spherical coordinate system the spatial point \mathbf{r} is described using the coordinates (r, Θ, Φ) . If we assume that the shells are homogeneous, *spherical symmetry* will hold. All quantities describing the medium will only depend on the radial coordinate r . At the position \mathbf{r} we specify the direction of a beam using the polar and azimuthal angles (θ, ϕ) . The angle θ is that between the radial direction and the beam direction, and we will frequently replace it by $\mu = \cos \theta$. As spherical symmetry implies axial symmetry, all azimuthal gradients $\partial/\partial\phi$ are zero.

Vector calculus in a geometry of planar layers or spherical shells

As a reminder we list some formulas from vector calculus used in these lecture notes to describe planar layers and spherical shells.

CARTESIAN COORDINATES ($\mathbf{x}, \mathbf{y}, \mathbf{z}$)

$$\text{A vector field} \quad \mathbf{A} = (A_x, A_y, A_z) = A_x \mathbf{x} + A_y \mathbf{y} + A_z \mathbf{z}$$

$$\text{Gradient} \quad \nabla f = \left(\frac{\partial f}{\partial x}, \frac{\partial f}{\partial y}, \frac{\partial f}{\partial z} \right) = \frac{\partial f}{\partial x} \mathbf{x} + \frac{\partial f}{\partial y} \mathbf{y} + \frac{\partial f}{\partial z} \mathbf{z}$$

$$\text{Divergence} \quad \nabla \cdot \mathbf{A} = \frac{\partial A_x}{\partial x} + \frac{\partial A_y}{\partial y} + \frac{\partial A_z}{\partial z}$$

$$\text{Differential displacement} \quad d\mathbf{s} = dx \mathbf{x} + dy \mathbf{y} + dz \mathbf{z}$$

$$\text{Differential volume} \quad dV = dx dy dz$$

SPHERICAL COORDINATES (\mathbf{r}, θ, ϕ)

$$\text{A vector field} \quad \mathbf{A} = (A_r, A_\theta, A_\phi) = A_r \mathbf{r} + A_\theta \boldsymbol{\theta} + A_\phi \boldsymbol{\phi}$$

$$\text{Gradient} \quad \nabla f = \left(\frac{\partial f}{\partial r}, \frac{\partial f}{\partial \theta}, \frac{\partial f}{\partial \phi} \right) = \frac{\partial f}{\partial r} \mathbf{r} + \frac{1}{r} \frac{\partial f}{\partial \theta} \boldsymbol{\theta} + \frac{1}{r \sin \theta} \frac{\partial f}{\partial \phi} \boldsymbol{\phi}$$

$$\text{Divergence} \quad \nabla \cdot \mathbf{A} = \frac{1}{r^2} \frac{\partial(r^2 A_r)}{\partial r} + \frac{1}{r \sin \theta} \frac{\partial(A_\theta \sin \theta)}{\partial \theta} + \frac{1}{r \sin \theta} \frac{\partial A_\phi}{\partial \phi}$$

$$\text{Differential displacement} \quad d\mathbf{s} = dr \mathbf{r} + rd\theta \boldsymbol{\theta} + r \sin \theta d\phi \boldsymbol{\phi}$$

$$\text{Differential volume} \quad dV = r^2 \sin \theta dr d\theta d\phi$$

3.2 Specific intensity

The *specific intensity* or *surface brightness* I_ν at position \mathbf{r} and time t , traveling in direction \mathbf{n} , is defined such that the amount of energy transported by radiation of frequencies $(\nu, \nu + d\nu)$ across an element of area dS into a solid angle $d\omega$ in a time interval dt is

$$\begin{aligned} \delta E_\nu &= I_\nu(\mathbf{r}, \mathbf{n}, t) \mathbf{n} \cdot d\mathbf{S} d\omega d\nu dt \\ &= I_\nu(\mathbf{r}, \mathbf{n}, t) \cos \theta dS d\omega d\nu dt \end{aligned} \quad (3.1)$$

where θ is the angle between the direction of the beam and the normal to the surface, i.e. $\mathbf{n} \cdot d\mathbf{S} = \mathbf{n} \cdot s dS = \cos \theta dS$ (see figure 3.2). The dimensions of I_ν are $\text{erg cm}^{-2} \text{ sec}^{-1} \text{ Hz}^{-1} \text{ sr}^{-1}$. From a macroscopic point of view, the specific intensity provides a complete description of the (unpolarized) radiation field.

Formally it would be better to refer to $I_\nu(\mathbf{r}, \mathbf{n}, t)$ as the *surface brightness*, however we will opt for the term *specific intensity*. By default we will drop an explicit reference to the position, time and direction for which the specific intensity is given and will suffice with I_ν . If the specific intensity is given as a function of wavelength, we will use I_λ . These quantities can be converted into each other if one realizes that

$$|I_\nu d\nu| = |I_\lambda d\lambda| \quad (3.2)$$

Using $\nu = c/\lambda$ yields: $I_\lambda = c/\lambda^2 I_\nu$.

The frequency integrated or *total specific intensity* is

$$I \equiv \int_0^\infty I_\nu d\nu = \int_0^\infty I_\lambda d\lambda \quad (3.3)$$

The invariance of I_ν

The specific intensity is defined such that it is independent of distance if there are no sources or sinks of radiation along the direction of the beam. This implies that the value for the intensity

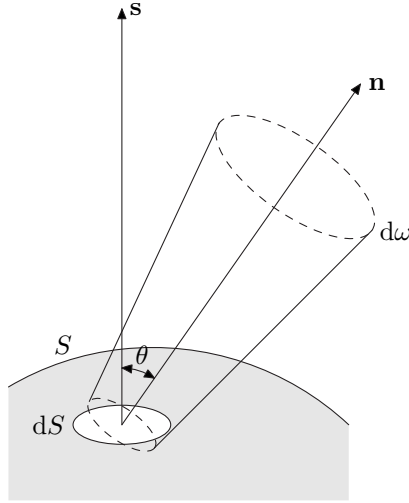


Figure 3.2: Definition of the specific intensity as a beam of radiation into a solid angle $d\omega$, across a surface dS oriented in direction s . The vector n is the direction of propagation of the beam which is at an angle θ with s .

at the source location can be obtained by measuring the amount of energy per unit time and per frequency interval that hits a detector (with known efficiency) per unit detector surface, when the solid angle subtended by the source is known. To be able to measure the specific intensity it is therefore required that the source is spatially resolved.

In other words: if we use our telescope to observe a fragment of an extended source somewhere in the sky (for instance a nebula, a galaxy, a planet, or the sun), then the intensity that we derive from the amount of energy that reaches our detector, per unit frequency and time, is the same as that is emitted by the fragment in our direction.

We can understand this property by considering a beam of radiation that passes through a surface element dS at position \mathbf{r} , as well as through an element dS' at position \mathbf{r}' (see figure 3.3). The amount of energy passing through both areas is

$$\delta E_\nu = I_\nu \cos \theta dS d\omega d\nu dt = I'_\nu \cos \theta' dS' d\omega' d\nu dt. \quad (3.4)$$

where $d\omega$ is the solid angle subtended by dS' as seen from position \mathbf{r} , and $d\omega'$ is the solid angle subtended by dS as seen from \mathbf{r}' . As the distance between \mathbf{r} and \mathbf{r}' is equal to d , it follows from $d\omega = 4\pi \cos \theta' dS'/4\pi d^2$, and $d\omega' = 4\pi \cos \theta dS/4\pi d^2$, that $I_\nu = I'_\nu$.

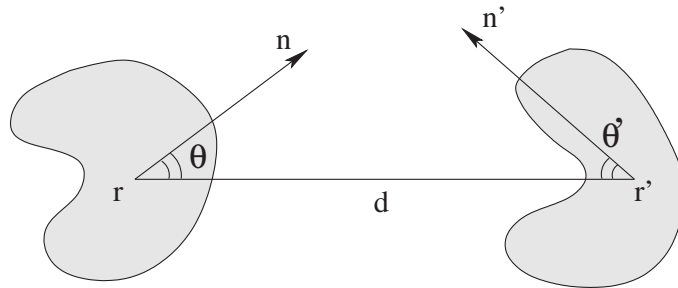


Figure 3.3: Illustration of the proof of invariance of the specific intensity. The points \mathbf{r} and \mathbf{r}' are separated by a distance d . Area dS subtends a solid angle $d\omega'$ seen from position \mathbf{r}' , and the area dS' subtends $d\omega$ at \mathbf{r} . \mathbf{n} and \mathbf{n}' are unit vectors normal to dS and dS' .

3.3 Mean intensity

The mean specific intensity or *mean intensity* averaged over all directions is

$$J_\nu(\mathbf{r}, t) = \frac{1}{4\pi} \oint I_\nu(\mathbf{r}, \mathbf{n}, t) d\omega \quad (3.5)$$

The mean intensity is the zero-order moment of the specific intensity and has dimensions $\text{erg cm}^{-2} \text{ sec}^{-1} \text{ Hz}^{-1}$. In spherical coordinates $d\omega = \sin \theta d\theta d\phi = -d\mu d\phi$ (see figure 3.4). The total solid angle Ω therefore is

$$\Omega = \oint d\omega = \int_0^{2\pi} \int_0^\pi \sin \theta d\theta d\phi = 2\pi \int_{-1}^{+1} d\mu = 4\pi \quad (3.6)$$

This explains the normalization factor 4π in (3.5). We may therefore rewrite (3.5) as

$$\begin{aligned} J_\nu &= \frac{1}{4\pi} \int_0^{2\pi} \int_0^\pi I_\nu \sin \theta d\theta d\phi \\ &= \frac{1}{2} \int_{-1}^{+1} I_\nu d\mu \end{aligned} \quad (3.7)$$

The mean intensity is e.g. used in the description of processes such as photoexcitation and photoionization, which only depend on the number of photons at some position at some time and do not depend on the direction of origin of these photons. For an isotropic radiation field $J_\nu = I_\nu$.

The frequency integrated or *total mean intensity* is

$$J \equiv \int_0^\infty J_\nu d\nu \quad (3.8)$$

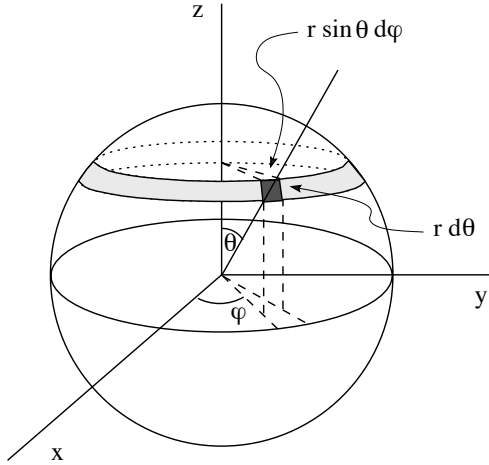


Figure 3.4: The infinitesimal solid angle $d\omega$ expressed in spherical coordinates. The area O of a sphere of radius r in the interval $(\theta, \theta + d\theta)$ and $(\phi, \phi + d\phi)$ is $O = r^2 \sin \theta d\theta d\phi = r^2 d\omega$, so that $d\omega = \sin \theta d\theta d\phi$. The total solid angle is 4π steradians.

Geometrical dilution

Consider a spherical star that emits an isotropic radiation field $I_\nu(\theta, \phi) = I_\nu$ from its surface at R_* . We are interested in the mean intensity above the stellar surface, i.e. at $r > R_*$. Figure 3.5 shows the directions from which the point r receives the stellar intensity I_ν . For the mean intensity in this point we find

$$J_\nu(r) = \frac{1}{2} \int_{\mu_*}^1 I_\nu d\mu = \frac{1}{2}(1 - \mu_*) I_\nu \equiv W(r) I_\nu \quad (3.9)$$

where $\mu_* = [1 - (R_*/r)^2]^{1/2}$ is the grazing angle that just hits the stellar rim (seen from r) and

$$W(r) = \frac{1}{2} \left\{ 1 - \left[1 - \left(\frac{R_*}{r} \right)^2 \right]^{1/2} \right\} \quad (3.10)$$

The factor W is called *geometrical dilution* and denotes the fraction of the total solid angle subtended by a star of radius R_* seen from a point in the sky at distance r . If $r = R_*$ one finds $W = 1/2$. This is easy to understand as an observer on the stellar surface sees half of the sky filled by the star. At very large distances, i.e. $r \gg R_*$, one may approximate the dilution factor by $W(r) \simeq 1/4(R_*/r)^2$. This also is easy to grasp: at large distances one sees the stellar disk, therefore $W(r) = \pi R_*^2 / 4\pi r^2$.

Energy density of radiation

In order to obtain the energy density u_ν of the radiation field (dimensions $\text{ergs cm}^{-3} \text{ Hz}^{-1}$) we determine the amount of radiation energy E_ν that is contained in an elementary volume

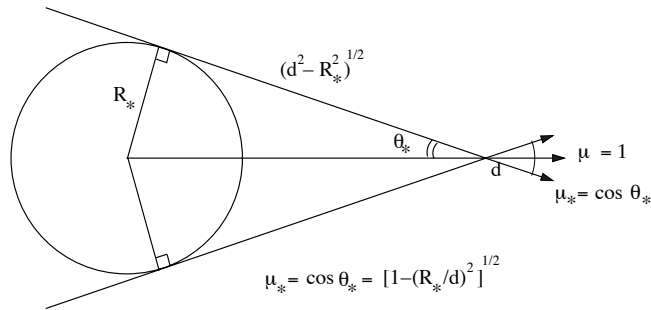


Figure 3.5: Geometry showing the directions from which a point d receives the stellar intensity I_ν .

V , such that $u_\nu = E_\nu/V$.

The amount of energy in a beam of solid angle $d\omega$ passing through a surface element dS of this volume is given by eq. (3.1). We are only interested in those photons in the beam that are actually inside V . Say the path length of these photons through V is l , then they will be inside of the elementary volume during a time $dt = l/c$. The part of the volume in which the photons are located is $dV = ldS \cos \theta$, where θ is the angle between the direction of the beam and the normal to the surface element dS . The energy in this part of the volume provided by the beam is therefore $\delta E_\nu = c^{-1} I_\nu(\mathbf{r}, \mathbf{n}, t) d\omega d\nu dV$. Integrating over all of the volume, one finds for the total energy in V in the frequency band $d\nu$

$$E_\nu(\mathbf{r}, t) d\nu = \frac{1}{c} \left[\int_V \left\{ \oint I_\nu(\mathbf{r}, \mathbf{n}, t) d\omega \right\} dV \right] d\nu \quad (3.11)$$

As the volume V is chosen so small that it is elementary, i.e. I_ν is independent of position within V , we may evaluate the integrals independently. We find for the monochromatic energy density

$$u_\nu(\mathbf{r}, t) = \frac{1}{c} \oint I_\nu(\mathbf{r}, \mathbf{n}, t) d\omega = \frac{4\pi}{c} J_\nu(\mathbf{r}, t) \quad (3.12)$$

The frequency integrated total energy density is

$$u = \int_0^\infty u_\nu d\nu \quad (3.13)$$

3.4 Flux

We define the flux of radiation $\mathcal{F}_\nu(\mathbf{r}, t)$ as a vector quantity such that $\mathcal{F}_\nu \cdot d\mathbf{S}$ gives the net rate of radiant energy flow across the arbitrarily oriented surface $d\mathbf{S} = s dS$ per unit time and frequency interval. The flux can be derived from the specific intensity. In the definition of the specific intensity (3.1) it so happens that $\delta E_\nu/d\omega d\nu dt$ is the contribution to the flux from the

beam of radiation into solid angle $d\omega$ propagating in the direction \mathbf{n} . To obtain the net flux of radiation we only need to integrate over all solid angles

$$\begin{aligned}\mathcal{F}_\nu(\mathbf{r}, t) \cdot d\mathbf{S} &= \oint \frac{\delta E_\nu}{d\omega d\nu dt} d\omega \\ \text{consequently} \\ \mathcal{F}_\nu(\mathbf{r}, t) &= \oint I_\nu(\mathbf{r}, \mathbf{n}, t) \mathbf{n} d\omega\end{aligned}\quad (3.14)$$

The flux has dimensions $\text{erg cm}^{-2} \text{ sec}^{-1} \text{ hz}^{-1}$. One may therefore also think of the flux being the power per unit surface per unit frequency bandwidth (which a radio astronomer would likely find more appealing). In infrared and radio astronomy the flux is often given in units of jansky (symbol: Jy): $10^{-23} \text{ erg cm}^{-2} \text{ sec}^{-1} \text{ hz}^{-1} \equiv 1 \text{ Jy}$.

In a plan parallel medium only the flux in the z direction $\mathcal{F}_z = \oint I_\nu(\mathbf{r}, \mathbf{n}, t) n_z d\omega \neq 0$. Symmetry arguments show that in the x and y directions the flux $\mathcal{F}_x = \mathcal{F}_y = 0$. As in this case only the z component of the flux is relevant one usually denotes this flux vector component as "the" flux. It follows that

$$\begin{aligned}\mathcal{F}_\nu(z, t) &= \int_0^{2\pi} \int_0^\pi I_\nu \cos \theta \sin \theta d\theta d\phi \\ &= 2\pi \int_{-1}^{+1} I_\nu(z, \mu, t) \mu d\mu\end{aligned}\quad (3.15)$$

Again: $\mathcal{F}_\nu(z, t)$ is the net flow of radiant energy, per second per frequency interval, that passes through a surface of 1 cm^2 that at position z is oriented normal to the z -direction. It is a *net* flow of energy as the perspective factor $\mu = \cos \theta$ (measuring the effective surface) counts inward directed contributions ($-1 \leq \mu \leq 0$) negative. We may write

$$\begin{aligned}\mathcal{F}_\nu(z, t) &= 2\pi \int_0^{+1} I_\nu(z, \mu, t) \mu d\mu - 2\pi \int_0^{-1} I_\nu(z, \mu, t) \mu d\mu \\ &\equiv \mathcal{F}_\nu^+(z, t) - \mathcal{F}_\nu^-(z, t)\end{aligned}\quad (3.16)$$

where the outward directed flux \mathcal{F}_ν^+ and the inward directed flux \mathcal{F}_ν^- are both positive. With the "flux of a star" one most often intends to say the outward flux \mathcal{F}_ν^+ crossing 1 cm^2 of the stellar surface.

Two alternative definitions for the flux are also used. These are the *astrophysical flux* $F_\nu \equiv \pi^{-1} \mathcal{F}_\nu$ and the *Eddington flux*

$$H_\nu \equiv \frac{1}{4\pi} \mathcal{F}_\nu = \frac{1}{2} \int_{-1}^{+1} I_\nu \mu d\mu\quad (3.17)$$

which is of a similar form as eq. (3.7) for the mean intensity and is referred to as the first-order moment of the intensity.

The frequency integrated or *total flux* is

$$\mathcal{F} \equiv \int_0^\infty \mathcal{F}_\nu d\nu \equiv \sigma T_{\text{eff}}^4 \quad (3.18)$$

where the last equality already introduces the *effective temperature* T_{eff} (see § 6.6). Integration of the flux over all of the stellar surface results in the *monochromatic luminosity* $L_\nu = 4\pi R_\star^2 \mathcal{F}_\nu(R_\star)$, where R_\star is the stellar radius. Further integration over all frequencies yields the *luminosity* of the star

$$L_\star = \int_0^\infty L_\nu d\nu = 4\pi R_\star^2 \mathcal{F}(R_\star) = 4\pi R_\star^2 \sigma T_{\text{eff}}^4 \quad (3.19)$$

The r^{-2} dependence of the flux

The observational meaning of the flux can be understood in the following way: Consider a constant, isotropically radiating source, e.g. a spherical star with radius R_\star and surface $4\pi R_\star^2$. When we place a concentric spherical surface around this source, with radius d – and if we assume there is no absorption or emission in the space around the source – the total amount of radiation energy passing through the outer surface will be the same as that passing through the stellar surface. Therefore

$$\mathcal{F}_\nu(R_\star) 4\pi R_\star^2 = \mathcal{F}_\nu(d) 4\pi d^2 \quad (3.20)$$

If d is the distance of the source to earth, then $\mathcal{F}_\nu(d)$ is the observed flux, also referred to as the *irradiance* \mathcal{R}_ν . The flux therefore decreases with distance as $\mathcal{F}_\nu(r) \propto r^{-2}$.

At first sight it may seem that this result is in contradiction to the invariance of the specific intensity along the line of sight. This is not so. Again consider a constant, isotropically radiating star with radius R_\star and emerging intensity I_ν . At a point r the intensity is equal to I_ν for all beams that intersect the star, for all other beams it is zero. We then find for the flux in r (see figure 3.5)

$$\mathcal{F}_\nu(r) = 2\pi \int_{\mu_*}^1 I_\nu \mu d\mu = \pi I_\nu (1 - \mu_*^2) = \pi I_\nu \left(\frac{R_\star}{r} \right)^2 \quad (3.21)$$

So we again find the flux to be proportional to r^{-2} . Note that the flux at the surface $\mathcal{F}_\nu(R_\star) = \pi I_\nu$, a result that can also be obtained directly from

$$\mathcal{F}_\nu(R_\star) = 2\pi \int_{\mu_*=0}^1 I_\nu \mu d\mu \equiv \mathcal{F}_\nu^+ = \pi I_\nu \quad (3.22)$$

Reconstruction of the flux using a ray-by-ray description

We formulate the r^{-2} dependence of the flux in yet another way. Assume that the distance d between star and observer is very much larger than the stellar radius, i.e. $d \gg R_\star$, so that all

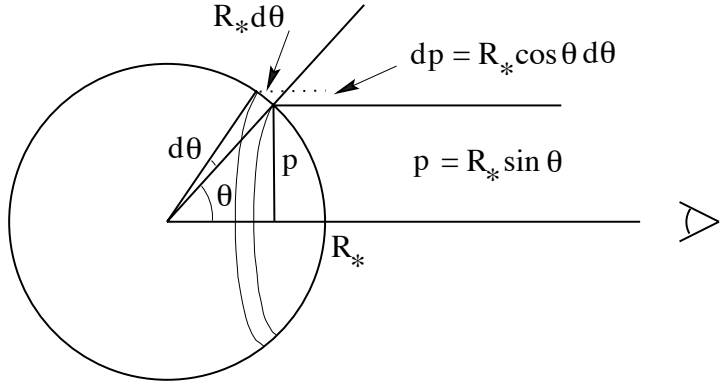


Figure 3.6: Geometry of measurement of stellar flux. The projected annulus on the surface of the star has an area $dS = 2\pi pdp = 2\pi R_* \sin \theta R_* \cos \theta d\theta = -2\pi R_*^2 \mu d\mu$, normal to the line of sight. This area subtends a solid angle $d\omega = dS/d^2$ as seen by the observer at distance d .

rays of light from star to observer may be considered to be parallel. The energy received, per unit area normal to the line of sight, from a differential area on the star is

$$d\mathcal{F}_\nu(d) = I_\nu d\omega, \quad (3.23)$$

where $d\omega$ is the solid angle subtended by the area, seen from the position of the observer. This follows directly from the definition of the flux, eq. (3.14).

We subdivide the stellar surface in differential projected annuli $dS = 2\pi p dp = -2\pi R_*^2 \mu d\mu$, where $\mu = \cos \theta$ as usual (see figure 3.6). The projected distance p to the center of the stellar disk is called *impact parameter*. The solid angle of the area $d\omega = dS/d^2 = -2\pi(R_*/d)^2 \mu d\mu$ as seen by the observer. The radiation emitted from this annulus in the direction of the observer emerged at angle θ ; hence the appropriate value of the specific intensity is $I_\nu(\mu)$. Integrating over the disk, we find

$$\mathcal{F}_\nu(d) = \frac{2\pi}{d^2} \int_0^{R_*} I_\nu(p) p dp = \left(\frac{R_*}{d}\right)^2 2\pi \int_0^1 I_\nu(\mu) \mu d\mu = \left(\frac{R_*}{d}\right)^2 \mathcal{F}_\nu(R_*) \quad (3.24)$$

Once more we see that the flux is proportional to r^{-2} (because the solid angle subtended by the stellar disk decreases with the square of the distance). This way of reconstructing the flux is known as a *ray-by-ray* solution.

Angular diameter

The *angular diameter* of a star is

$$\alpha_* = \frac{2R_*}{d} \quad (3.25)$$

such that the observed flux can also be written as $\mathcal{F}_\nu(d) = (\alpha_*^2/4) \mathcal{F}_\nu(R_*)$. For unresolved objects (such as is the case for almost all stars), we can measure only the flux. If the angular

diameter is known, then the measured flux can be converted to the flux at the stellar surface. Reversely, if we know the value for the stellar surface flux from (other) observed quantities we may determine the angular diameter of the star using the measured flux.

3.5 Radiation pressure

Consider an amount of momentum p_ν transported by the radiation field through an area dS , per unit time per frequency interval.

The photon of frequency ν has a momentum $h\nu/c$ such that the amount of momentum in a beam with energy ∂E_ν is $\partial E_\nu/c$. If we consider the component of the momentum in the direction normal to that of surface dS , then the contribution of the beam is

$$\partial p_\nu dS d\nu dt = \frac{1}{c} \partial E_\nu \cos \theta \quad (3.26)$$

where again θ is the angle between the direction of the beam \mathbf{n} and the direction \mathbf{s} normal to the surface area. If we express the energy in terms of the specific intensity, using eq. (3.1), and if we integrate over all directions we find for the *radiation pressure*.

$$\begin{aligned} p_\nu &= \frac{1}{c} \oint I_\nu(\mathbf{r}, \mathbf{n}, t) \mathbf{n} \mathbf{n} d\omega \\ &= \frac{1}{c} \oint I_\nu \cos^2 \theta d\omega \end{aligned} \quad (3.27)$$

The dimensions of radiation pressure are ergs $\text{cm}^{-3} \text{hz}^{-1}$. For clarity: the one “ $\cos \theta$ ” term determines the effective size of area dS , oriented in the direction \mathbf{s} , for radiation propagating in direction \mathbf{n} ; the other “ $\cos \theta$ ” determines the momentum component in the direction \mathbf{s} .

If axial symmetry is valid

$$p_\nu = \frac{2\pi}{c} \int_{-1}^{+1} I_\nu(z, \mu, t) \mu^2 d\mu = \frac{4\pi}{c} K_\nu \quad (3.28)$$

where

$$K_\nu \equiv \frac{1}{2} \int_{-1}^{+1} I_\nu \mu^2 d\mu \quad (3.29)$$

is the second-order moment of the specific intensity.

Radiation pressure is completely analogous to gas pressure, and is a scalar when the radiation field is isotropic. Radiation only exerts a force when there is a gradient in radiation pressure, analogous to the upward force associated with gas pressure. We will return to this when we discuss hydrostatic equilibrium (see § 9.2).

The total radiation pressure is

$$p_R = \int_0^\infty p_\nu d\nu \quad (3.30)$$

where we have introduced the subscript R to avoid confusion with the gas pressure (see e.g. eq. 6.30).

3.6 Eddington factors

The moment equations (3.7), (3.17) and (3.29) of the radiation field are used to define the so-called *Eddington factors*

$$f_\nu(\mathbf{r}, t) \equiv \frac{K_\nu(\mathbf{r}, t)}{J_\nu(\mathbf{r}, t)} \quad (3.31)$$

and

$$g_\nu(\mathbf{r}, t) \equiv \frac{H_\nu(\mathbf{r}, t)}{J_\nu(\mathbf{r}, t)}. \quad (3.32)$$

The Eddington factors have no dimension and vary within only a very limited range: f_ν typically between 1/3 and 1; and g_ν typically between 0 and 1. In essence both factors are a measure of the amount of anisotropicity that is contained in the radiation field. Is the radiation field completely isotropic then $f_\nu = 1/3$ and $g_\nu = 0$. Is the radiation field sharply peaked then both factors tend toward unity. In § 4.5 we will see that f_ν can be used to seemingly reduce the number of independent variables in a transfer problem; they also provide a means to close a system of moment equations derived from the equation of transfer. The factor g_ν is often used in formulating boundary conditions to the equation of transfer (see § 11.2).

Exercise 3.1

Give the relation between the specific intensity of solar radiation as measured at the position of earth and the flux, mean intensity and irradiation of the solar radiation. Assume that the sun emits an isotropic radiation field of which the specific intensity is I_ν .

Exercise 3.2

At some point in the calculation of the observed stellar flux under the assumption of plane parallel layers one needs to introduce the fact that a star is a sphere. Where is this done?

Exercise 3.3

Consider an infinitely extended flat plate emitting from its surface an isotropic radiation field $I_\nu(\theta, \phi) = I_\nu$. Show that the mean intensity above the surface is given by $J_\nu = 1/2 I_\nu$. Explain this in a simple way.

Exercise 3.4

We take a picture of the lunar disk, which is at distance d and emits an isotropic radiation field with specific intensity I_ν . Our camera has a spatial resolving power $d\omega \ll \pi R_m^2/d^2$ – defined by the pixel size of the ccd – and we find that we need to open the shutter a time t to assure that we have the desired exposure.

- a) If we would now place the moon at twice the original distance, how long should we open the shutter to gain an identical exposure?

We now place the moon at such a distance that the lunar disk subtends a solid angle equal to the spatial resolving power of our camera, i.e. $d\omega = \pi R_m^2/d^2$. The camera is pointed such that the moon falls in a single pixel.

- b) How long should we open the shutter to get an identical exposure?
- c) If now place the moon at twice the distance (than in b), implying we can no longer resolve the lunar disk. All photons that reach the ccd hit the same pixel. What should be the shutter time to get an identical exposure?

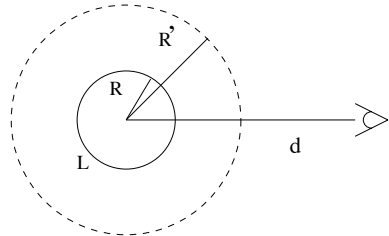
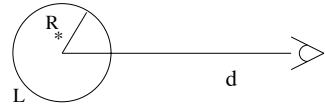
Exercise 3.5

L is a spatially resolved spherical lamp with radius R that is positioned at distance d from an observer and that radiates an isotropic radiation field with specific intensity I_ν .

- a) Give the specific intensity $I_\nu(d)$ and flux $\mathcal{F}_\nu(d)$ as measured by the observer.

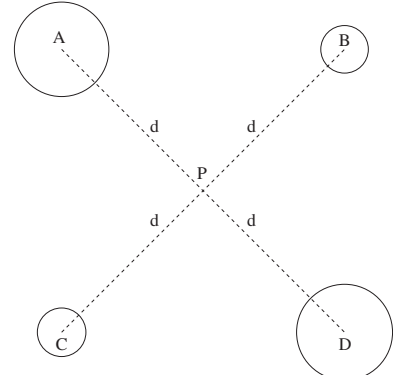
It starts to fog. The light from the lamp is purely scattered with the result that it appears to originate from a spherical surface of radius Rt .

- b) For this new situation, give the specific intensity $I_\nu(d)$ and flux $\mathcal{F}_\nu(d)$ as measured by the observer.

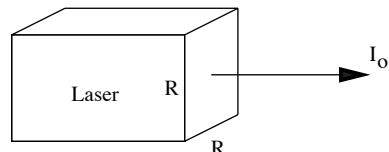
**Exercise 3.6**

Consider a cluster of four stars; each star radiates an isotropic radiation field of which the specific intensity is I_ν . The four stars and the observer are in the same plane. The observer is in the center P of the cluster. The distance from P to each of the four stars is d . The radius of the stars B and C is R ; that of the stars A and D is $2R$.

- a) Give the mean intensity at P .
 b) Give the flux at P .

**Exercise 3.7**

Consider a laser that emits a perfectly parallel beam of light. The radiating surface of the laser is a square of R times R cm. The monochromatic luminosity of the laser is L_ν . We observe the laser from a distance d with a telescope that is large in comparison to the laser and that can spatially resolve the laser.



- a) Give the flux as measured by the observer?

We now place the laser at a distance $3d$ of the telescope. For this new situation:

- b) Give the flux as measured by the observer?
 c) Why are you not asked to give the specific intensity as measured by the observer?

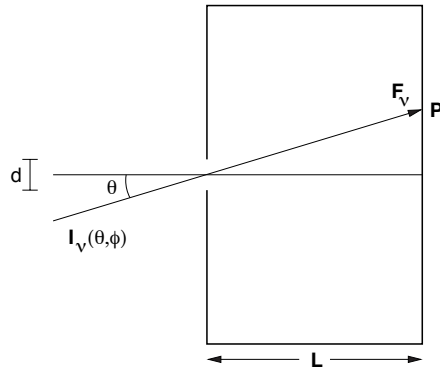
Exercise 3.8

A "pinhole" camera consists of a very small circular hole of diameter d , at distance L from the "film-plane" (see figure). The pinhole is so small that the specific intensity that falls through the pinhole on a square centimeter of the film-plane may be assumed to be constant.

- a) Derive an expression for the solid angle $\Delta\Omega$ that is extended by the pinhole as seen from the position P on the image plane.

The energy received per unit area normal to the line of sight from solid angle $\Delta\Omega$ is given by $d\mathcal{F}_\nu = I_\nu(\theta, \phi)\Delta\Omega$.

- b) Derive an expression for the flux \mathcal{F}_ν at the film plane.



Exercise 3.9

Show that for isotropic radiation $p_\nu = u_\nu/3$. What is the meaning of the factor 1/3?

Exercise 3.10

- a) Deep in the atmosphere the radiation field will be almost isotropic, i.e. $I_\nu(\theta, \phi) = I_\nu$. Show that in this case the Eddington factor $f_\nu = 1/3$.
- b) Far above the stellar surface the radiation field will be strongly peaked in the radial direction, i.e. $I_\nu(\theta, \phi) = I_\nu(\mu, \phi) = I_\nu\delta(\mu - 1)$. Show that in this case the Eddington factor $f_\nu = 1$.

We may conclude that the Eddington factor will not vary much throughout the atmosphere (only by about a factor of three).

4

The equation of transfer

In this chapter we formulate the equation that describes the transfer of radiation through a medium, and we introduce the macroscopic quantities that play a role in this equation. The transfer equation has a formal solution which reflects that the specific intensity at each point in the medium can be determined if the source function S_ν and the optical depth τ_ν are known throughout the medium, or – equivalently – the extinction coefficient χ_ν and the emission coefficient η_ν . We discuss analytical solutions to simple transfer problems.

4.1 Absorption, emission, and scattering processes

Photons traveling through a material medium will experience interactions with the particles that are present: they can be absorbed or scattered. The medium itself may also emit radiation. Here, we give a macroscopic description of these processes. In principle, the nature of the medium is irrelevant. It may be a neutral or (partly) ionized gas, a molecular gas, or a medium of solid state particles. In these lecture notes we are particularly interested in describing atomic gases.

We will make a distinction between “real” absorption and emission processes on the one hand, and scattering processes on the other hand. In a “real” absorption process (for the sake of convenience we will simply refer to this as absorption) energy is removed from the radiation field, and added to the local thermal energy of the medium. In this process photons are really destroyed and we say that the photon has been thermalized. The reverse process is thermal emission, which adds energy from the local thermal pool into the radiation field. The photons that are created in this way are referred to as *thermal* photons. An example of a “real” absorption process is the photo excitation of an electron in an atom or ion, followed by a downward transition in which the energy that is released is added to a free electron that is interacting with the atom or ion. An example of a thermal emission is the reverse process, i.e. a collisional excitation involving a free electron followed by the spontaneous emission of a photon.

In a scattering process the photon essentially only changes direction. So, although the photon is absorbed and emitted, it keeps, as it were, its identity. One distinguishes between *pure* and *non pure* scatterings. In a pure scattering the frequency of the photon changes only slightly. Examples of pure scattering processes are the interaction of photons in a resonance transition (for instance Ly α or C IV $\lambda\lambda 1548,1551$) or the elastic scattering of photons by free electrons (Thomson scattering) or by an atom or molecule (Rayleigh scattering). In a scattering process that is not pure the frequency of the photon is changes significantly. An example of such a process is the in-elastic scattering of photons by free electrons (Compton scattering).

When “real” absorption and emission processes dominate over scattering processes there will be a strong coupling between the local thermodynamic properties of the gas and the properties of the radiation that is generated by it. Concerning scattering processes the situation is different. Here the nature of the emitted radiation will predominantly be determined by the properties of the infalling radiation field. If scatterings dominate, the photons that are present in the local medium typically originate from elsewhere and simply propagate through the local medium without actually being coupled to it in any way. Depending on the origin of the photons the radiation field may be thermal or non-thermal.

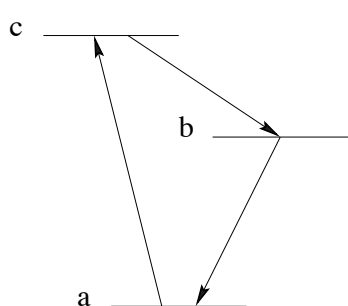


Figure 4.1: Photon conversion

A description in terms of absorption/emission and of scattering has its conceptual limitations. Take for instance an atom that has three bound states, a , b , and c , in order of increasing energy (see figure 4.1). Say that an absorption of a photon brings the atom from state a to c , and that this is followed by the spontaneous emission of a photon bringing the atom in state b , after which the atom returns into state a after again emitting a photon. One can not speak of a “real” absorption/emission as the thermal energy content of the gas did neither increase nor decrease. Also, it is clear that one can not speak of a scattering as the initial photon lost its identity.

Processes in a beam of light

The transfer of radiation along a ray of light – in terms of “real” absorption and emission and pure scattering – is schematically given in figure 4.2. There are two processes that add photons of given frequency to the ray, i.e. “real” emissions and scattering of photons that come in from different directions into the direction of the ray. There are also two processes that remove photons from the ray, i.e. “real” absorptions and scattering of photons out of the direction of the beam.

We will now formulate a quantitative description of these processes.

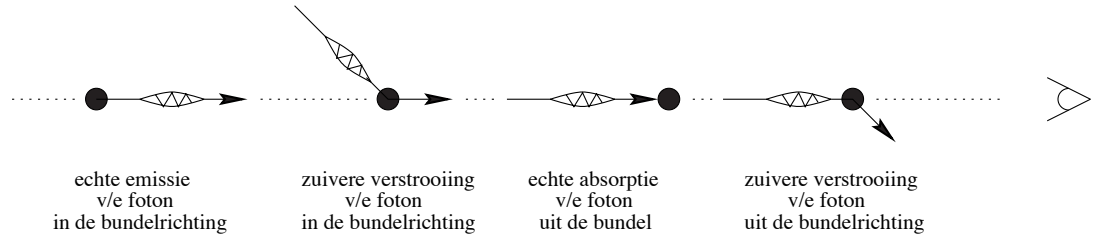


Figure 4.2: Schematic representation of the transfer of radiation along a ray of light.

Let us consider a gas and a radiation field that is described by a specific intensity $I_\nu(s)$ in a given direction. The path-length along the ray is described by s . Let us consider a flat cylinder, of length ds and cross-section dO , perpendicular to s . We describe changes in $I_\nu(s)$ due to absorption and emission processes between s and $s + ds$ as follows

$$\begin{aligned} I_\nu(s + ds) dO d\omega d\nu dt &= I_\nu(s) dO d\omega d\nu dt + dI_\nu(s) dO d\omega d\nu dt \\ \text{or} \\ I_\nu(s + ds) &= I_\nu(s) + dI_\nu(s) \end{aligned} \quad (4.1)$$

Extinction coefficient

If only extinction processes occur along the path-length ds , either as a result of absorption or because of scattering out of the direction of the ray, then the decrease in the specific intensity is proportional to the incident specific intensity, to the path-length ds , and to the properties and number of absorbing/scattering particles. The constant of proportionality is called the extinction coefficient and can be defined in three ways (see eq. 4.5 for an overview).

We will often use the *linear extinction coefficient* χ_ν , which has dimension cm^{-1} , such that

$$dI_\nu(s) = -I_\nu(s) \chi_\nu(s) ds \quad (4.2)$$

This coefficient is defined such that an element of material, of cross-section dO and length ds , removes from a beam with specific intensity $I_\nu(\mathbf{r}, \mathbf{n}, t)$, incident normal to dS and propagating into a solid angle $d\omega$, an amount of energy

$$\delta E_\nu \equiv \chi_\nu(\mathbf{r}, \mathbf{n}, t) I_\nu(\mathbf{r}, \mathbf{n}, t) dO ds d\omega d\nu dt \quad (4.3)$$

within a frequency band $d\nu$ in a time dt . The linear extinction coefficient is sometimes also called the *volume extinction coefficient* as it refers to the total extinction surface in cm^2 , per cm^{-3} ($[\text{cm}^2 \text{ cm}^{-3}] = [\text{cm}^{-1}]$). The value of the extinction coefficient is determined by the properties/state of the medium and is not dependent on the radiation field. However, the latter can have an indirect effect on the properties/state of this medium.

The linear extinction coefficient can be split up in a contribution due to absorption, κ_ν , and due to scattering, σ_ν

$$\chi_\nu(s) = \kappa_\nu(s) + \sigma_\nu(s) \quad (4.4)$$

Here it is implicitly assumed that these processes are independent of each other and that they are additive.

Alternative definitions of the extinction coefficient are

$$\chi_\nu = \chi'_{\nu} \rho = \alpha_\nu n \quad (4.5)$$

Here χ'_{ν} is the *mass extinction coefficient* ($[\text{cm}^2 \text{ gr}^{-1}]$) and ρ the density of the material medium ($[\text{gr cm}^{-3}]$); and α_ν is the extinction coefficient or *cross section* per particle ($[\text{cm}^2]$) and n the number density of particles ($[\text{cm}^{-3}]$) that cause the extinction.

Emission coefficient

If only emission processes occur along the path-length ds , either as a result of thermal emission or because of scattering into the direction of the ray, then the increase in the specific intensity is given by

$$dI_\nu(s) = \eta_\nu(s) ds \quad (4.6)$$

The constant of proportionality is called the *volume emission coefficient* and is defined such that the amount of energy released from an element of material of cross-section dO and length ds , into a solid angle $d\omega$, within a frequency band $d\nu$, in direction \mathbf{n} in a time interval dt , is

$$\delta E_\nu \equiv \eta_\nu(\mathbf{r}, \mathbf{n}, t) dO ds d\omega d\nu dt \quad (4.7)$$

The emission coefficient has dimensions $[\text{erg cm}^{-3} \text{ sec}^{-1} \text{ hz}^{-1} \text{ sr}^{-1}]$. η_ν always depends on the properties of the medium, and in case of scattering from other directions into the ray of light, also on the radiation field. For completeness we mention that in studies of gaseous nebulae it is custom to use the letter j (so j_ν) to denote the emission coefficient (for instance in Osterbrock & Ferland).

An alternative definition of the emission coefficient is

$$\eta_\nu = \eta'_{\nu} \rho \quad (4.8)$$

where η'_{ν} is the *mass emission coefficient* ($[\text{erg gr}^{-1} \text{ sec}^{-1} \text{ hz}^{-1} \text{ sr}^{-1}]$).

— — —

If different extinction/emission processes occur at once they may be added

$$\chi_\nu = \sum_i \chi_{\nu,i} \quad \eta_\nu = \sum_i \eta_{\nu,i} \quad (4.9)$$

The subscript i labels all different processes contributing at frequency ν .

Extinction and emission: the equation of transfer

If both extinction and emission occur along the path-length ds then we may write

$$dI_\nu(s) = [\eta_\nu(s) - I_\nu(s)\chi_\nu(s)] ds \quad (4.10)$$

or

$$\frac{dI_\nu}{ds} = \eta_\nu - \chi_\nu I_\nu \quad (4.11)$$

This is a simple form of the *equation of transfer*.

4.2 General form of the equation of transfer

Now that we know the quantities that describe the macroscopic interaction between radiation and matter, it is relatively simple to give a heuristic derivation of the general form of the equation of transfer. Let us again consider a ray of light of specific intensity I_ν , that is transported in a frequency interval $(\nu, \nu + d\nu)$, passing in a time dt through a volume element of length ds (such that $dt = ds/c$) and cross-section dO oriented normal to the ray in direction \mathbf{n} into solid angle $d\omega$ (eq. 3.1). The difference between the amount of energy that emerges (at position $\mathbf{r} + \Delta\mathbf{r}$ and at time $dt + \Delta t$) and that incident (at \mathbf{r} and t) must equal the amount created by emission from the material in the volume minus the amount absorbed. Therefore, using the definition of specific intensity (eq. 3.1) and of the extinction and emission coefficient it must hold that in order to conserve the total photon energy

$$\begin{aligned} & [I_\nu(\mathbf{r} + \Delta\mathbf{r}, \mathbf{n}, t + \Delta t) - I_\nu(\mathbf{r}, \mathbf{n}, t)] dO d\nu dt d\omega = \\ & [\eta_\nu(\mathbf{r}, \mathbf{n}, t) - \chi_\nu(\mathbf{r}, \mathbf{n}, t) I_\nu(\mathbf{r}, \mathbf{n}, t)] ds dO d\nu dt d\omega \end{aligned} \quad (4.12)$$

The difference in specific intensity at the left hand side of this equation can be written as

$$\begin{aligned} I_\nu(\mathbf{r} + \Delta\mathbf{r}, \mathbf{n}, t + \Delta t) - I_\nu(\mathbf{r}, \mathbf{n}, t) &= \frac{\partial I_\nu}{\partial t} dt + \frac{\partial I_\nu}{\partial s} ds \\ &= \left[\frac{1}{c} \frac{\partial I_\nu}{\partial t} + \frac{\partial I_\nu}{\partial s} \right] ds \end{aligned} \quad (4.13)$$

The general form of the equation of transfer holds for all geometries. To adopt a specific coordinate system one should express the derivatives along the ray of light in terms of the orthogonals in the chosen coordinate system. If ds is an infinitesimal displacement along the direction of the ray then

$$\frac{\partial}{\partial s} = \frac{\partial x}{\partial s} \frac{\partial}{\partial x} + \frac{\partial y}{\partial s} \frac{\partial}{\partial y} + \frac{\partial z}{\partial s} \frac{\partial}{\partial z} = n_x \frac{\partial}{\partial x} + n_y \frac{\partial}{\partial y} + n_z \frac{\partial}{\partial z} = \mathbf{n} \cdot \nabla, \quad (4.14)$$

for a Cartesian coordinate system, where (n_x, n_y, n_z) are the components of the unit vector \mathbf{n} .

For the general form of the equation of transfer we then find

$$\left(\frac{1}{c} \frac{\partial}{\partial t} + \mathbf{n} \cdot \nabla \right) I(\mathbf{r}, \mathbf{n}, \nu, t) = \eta(\mathbf{r}, \mathbf{n}, \nu, t) - \chi(\mathbf{r}, \mathbf{n}, \nu, t)I(\mathbf{r}, \mathbf{n}, \nu, t) \quad (4.15)$$

In these lectures we will assume by default that the medium is time-independent, in which case the partial derivative $\partial/\partial t = 0$. Furthermore, we will focus on solving transfer equations in three special types of geometries. These are: (i) along a line, i.e. a pencil beam; (ii) a medium of homogeneous plan-parallel layers; or (iii) a medium of homogeneous spherical shells.

Along a pencil beam

The equation of transfer along a pencil beam, where s is the coordinate along the beam, is given by eq. (4.11).

Planar layers

If the medium consists of homogeneous plane-parallel layers, such that the properties of this medium are only a function of the z direction, then $n_z = dz/ds = \cos \theta = \mu$ (see figure 3.1). The equation of transfer reduces to

$$\mu \frac{dI_\nu(z, \mu)}{dz} = \eta_\nu(z, \mu) - \chi_\nu(z, \mu)I_\nu(z, \mu) \quad (4.16)$$

Note that in the case $\mu = 1$, i.e. a beam along the z direction, the equation of transfer is equal to eq. (4.11).

Spherical shells

If the medium consists of spherical shells, and θ and ϕ specify the direction of the beam at position r , such that θ is the angle of the beam relative to the local outward normal direction (which is the radial direction) and ϕ is the azimuthal angle, then the specific intensity will be independent of ϕ , i.e. $\partial/\partial\phi = 0$.

An infinitesimal displacement along the beam direction is given by $ds = dr \hat{\mathbf{r}} + rd\theta \hat{\theta}$. The geometry implies (see figure 4.3) that $dr = \cos \theta ds$ and $rd\theta = -\sin \theta ds$. Note that always $d\theta \leq 0$ for any ds ; this explains the minus sign. We find

$$\frac{\partial}{\partial s} = \frac{\partial r}{\partial s} \frac{\partial}{\partial r} + \frac{\partial \theta}{\partial s} \frac{\partial}{\partial \theta} = \cos \theta \frac{\partial}{\partial r} - \frac{1}{r} \sin \theta \frac{\partial}{\partial \theta} = \mu \frac{\partial}{\partial r} + \frac{1}{r} (1 - \mu^2) \frac{\partial}{\partial \mu} \quad (4.17)$$

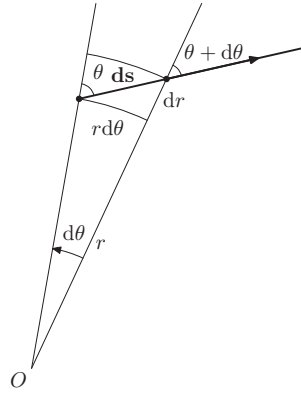


Figure 4.3: Geometric relation among the variable ds and dr and $d\theta$ used in the derivation of the transfer equation in a spherical symmetric medium.

where $\mu = \cos \theta$, such that

$$\frac{\partial}{\partial \theta} = \frac{\partial \mu}{\partial \theta} \frac{\partial}{\partial \mu} = -\sin \theta \frac{\partial}{\partial \mu} \quad (4.18)$$

Using these results the transfer equation for a spherically symmetric medium is

$$\left[\mu \frac{\partial}{\partial r} + \frac{1}{r} (1 - \mu^2) \frac{\partial}{\partial \mu} \right] I_\nu(r, \mu) = \eta_\nu(r, \mu) - \chi_\nu(r, \mu) I_\nu(r, \mu) \quad (4.19)$$

4.3 Optical depth and the source function

Optical depth

Let us introduce an elementary *optical depth interval* $d\tau_\nu$ along a path-length ds , measured along the direction of the ray.

$$d\tau_\nu \equiv \chi_\nu(\mathbf{r}, \mathbf{n}) ds \quad (4.20)$$

This defines the *optical depth* τ_ν which gives the integrated extinction of the material along the line of sight. For a geometrical thickness D the optical depth is

$$\tau_\nu(D) = \int_0^D \chi_\nu(s) ds \quad (4.21)$$

The optical depth is a dimensionless number. The physical meaning of τ_ν is simple. In the absence of emission in the medium the equation of transfer along the beam is given by (see eq. 4.2 and/or 4.11)

$$\frac{dI_\nu}{d\tau_\nu} = -I_\nu \quad (4.22)$$

This yields

$$I_\nu(D) = I_\nu(0)e^{-\tau_\nu(D)} \quad (4.23)$$

and shows that $\tau_\nu(D)$ is the exponential decline parameter that determines what remains of a beam that has passed through a layer of thickness D in which extinction processes occur. How far can photons penetrate in this layer? The chance that an incident photon travels an optical depth $\tau_\nu(s)$ in the layer (for $s < D$) before it is absorbed or scattered is $p(\tau_\nu(s)) = \exp(-\tau_\nu(s))$. As the average of a quantity x that has a probability distribution $p(x)$ is given by

$$\langle x \rangle = \frac{\int_0^\infty x p(x) dx}{\int_0^\infty p(x) dx} \quad (4.24)$$

the *mean optical photon path* of the photon must be

$$\langle \tau_\nu \rangle = \frac{\int_0^\infty \tau_\nu e^{-\tau_\nu} d\tau_\nu}{\int_0^\infty e^{-\tau_\nu} d\tau_\nu} = 1 \quad (4.25)$$

Photons therefore typically travel one optical depth unit before interacting with the medium.

Mean free path of the photon

This result immediately shows what the mean geometrical path ([cm]) of a photon in a homogeneous medium must be, i.e. the path length it can travel before it is absorbed or scattered. This is

$$\ell_\nu = \frac{\langle \tau_\nu \rangle}{\chi_\nu} = \frac{1}{\chi_\nu} = \frac{1}{\chi'_{\nu} \rho} \quad (4.26)$$

and is formally referred to as the photon *mean-free-path*.

Optically thick and optically thin

One of the first questions one should ask himself/herself when trying to understand the transfer of radiation through a medium is whether this medium is *optically thin* or *optically thick* for radiation of given frequency. Optically thin implies that almost all incident photons, as well as almost all photons emitted in the medium, can propagate undisturbed by the medium and escape from it. An optically thin medium therefore describes the limiting case $\tau_\nu \ll 1$. In an optically thick medium $\tau_\nu \gg 1$. This (opposite) limit therefore describes a medium that is almost opaque for photons. Almost all photons in a beam that is incident to a medium that is optically thick will be absorbed or scattered inside the medium. Of all photons that are emitted by the medium only those will contribute to the emerging specific intensity that are emitted at a position and into a direction for which the optical depth to the edge of the medium is $\tau_\nu \sim 1$.

At which optical depth do half of the emitted photons escape? This is from $\tau_\nu = -\ln 0.5 = 0.693 \simeq 2/3$ along the direction of the beam. Relying on ones intuition, this implies that we may expect that the layer in a stellar atmosphere from which the radiation that we observe originates should be at an optical depth $\tau_\nu \simeq 2/3$, measured from outside in (so $\tau_\nu = 0$ is at

the position of the observer). Later on in these lectures we will show that this is indeed the case.

Source function

The *source function* is defined as

$$S_\nu \equiv \frac{\eta_\nu}{\chi_\nu} \quad (4.27)$$

and has dimensions erg cm⁻² sec⁻¹ hz⁻¹ sr⁻¹. It has the same units as the specific intensity, therefore S_ν and I_ν can be added and subtracted (see eq. 4.34). The extinction and emission coefficients are *local* quantities, implying the source function is independent of the adopted geometry.

The meaning of the source function can be understood as follows: The number of photons that is emitted per bandwidth and time interval from an elementary volume of cross-section dO and length ds into all directions is $N_{\text{em}} = (4\pi/h\nu) \eta_\nu dO ds d\nu dt$, where we have assumed that the emission is isotropic. The factor 4π is the result from the integration over all solid angles, and $h\nu$ converts energy to number of photons (see eq. 4.7). From the definition of optical depth, eq. (4.20), it follows that $\eta_\nu ds = (\eta_\nu/\chi_\nu)\chi_\nu ds = S_\nu d\tau_\nu$. So, we may also write for the number of emitted photons

$$N_{\text{em}} = S_\nu d\tau_\nu \frac{4\pi}{h\nu} d\nu dt dO \quad (4.28)$$

In other words, the source function is proportional to the number of photons that is emitted per unit optical depth.

Using an analogous reasoning we may derive the number of photons, coming from all direction, that is absorbed per unit optical depth. Using the definition of the extinction coefficient (eq. 4.3) we find that the number of photons in a ray traveling in direction \mathbf{n} into solid angle $d\omega$ that suffer extinction is given by $dN_{\text{abs}} = \chi_\nu(\mathbf{r}) I_\nu(\mathbf{r}, \mathbf{n}) dO ds d\omega d\nu dt$, where we have assumed that the extinction is isotropic. Integration over all solid angles, again using the definition of the optical depth, gives

$$N_{\text{abs}} = J_\nu d\tau_\nu \frac{4\pi}{h\nu} d\nu dt dO \quad (4.29)$$

— — —

If several extinction/emission processes play a role the total source function is

$$S_\nu \equiv \frac{\eta_\nu}{\chi_\nu} = \frac{\sum_i \eta_{\nu,i}}{\sum_i \chi_{\nu,i}} \quad (4.30)$$

The subscript i labels all different processes contributing at frequency ν (see eq. 4.9).

Let us for a moment get ahead of things such that we can already give the proto-typical form of the source function. In a medium that shows both absorption and scattering processes, Kirchhoff's law (eq.6.3) implies that for the thermal emission $\eta_\nu^{\text{th}} = \kappa_\nu B_\nu$; if we assume isotropic and coherent (i.e. $\nu = \nu l$) continuum scattering, the emission term for scattering is given by $\eta_\nu^{\text{sc}} = \sigma_\nu J_\nu$. For the proto-typical source function we get

$$S_\nu = \frac{\kappa_\nu B_\nu + \sigma_\nu J_\nu}{\kappa_\nu + \sigma_\nu} \quad (4.31)$$

In section 9.3 the proto-typical source function will be discussed in more detail.

The frequency integrated or *total source function* is

$$S \equiv \int_0^\infty S_\nu d\nu \quad (4.32)$$

Exercise 4.1

Suppose that in Sherwood Forest, the average radius of a tree is $R = 1 \text{ m}$ and that the average number of trees per unit area is $\Sigma = 0.005 \text{ m}^{-2}$. When Robin Hood or Little John shoots an arrow, it flies horizontally until it strikes a tree.

- a) What is the mean cross section of a tree in m^2 ?
- b) If Robin Hood shoots an arrow in a random direction, how far, on average, will it travel before it strikes a tree?
- c) If Little John shoots a total of 1000 arrows in random directions, how many, on average, will travel at least 500 m?

Exercise 4.2

Show that for a medium in which no photons are created, destructed or converted, but in which only pure scattering processes occur, the source function is equal to the mean intensity: $S_\nu = J_\nu$.

4.4 Formal solution of the equation of transfer

We define the optical depth scale in a geometry of planar layers such that for z increasing in the direction to the observer, τ_ν is decreasing, i.e.

$$d\tau_\nu(z) = -\chi_\nu(z) dz \quad (4.33)$$

This implies that for an observer at $z = \infty$, the optical depth $\tau_\nu(\infty) = 0$. Adopting this optical depth scale, and using the source function, the planar transfer equation (eq. 4.16) may be written in its standard form

$$\mu \frac{dI_\nu(\tau_\nu, \mu)}{d\tau_\nu} = I_\nu(\tau_\nu, \mu) - S_\nu(\tau_\nu, \mu) \quad (4.34)$$

Note that we measure τ_ν along the z direction. The relation between the optical depth in the μ direction, $\tau_{\nu\mu}$, and that in the z direction (for which $\mu = 1$) is $\tau_{\nu\mu} = \tau_\nu/\mu$.

For known source function S_ν , eq. (4.34) has a formal solution. To find this solution we bring I_ν to the left hand side, divide by μ and multiply both sides by the integrating factor $\exp(-\tau_\nu/\mu)$. This yields

$$\left[\frac{dI_\nu}{d\tau_\nu} - \frac{I_\nu}{\mu} \right] e^{-\tau_\nu/\mu} = \frac{d}{d\tau_\nu}(I_\nu e^{-\tau_\nu/\mu}) = -\frac{S_\nu}{\mu} e^{-\tau_\nu/\mu} \quad (4.35)$$

Integration from τ_1 to τ_2 , and multiplying by $-\exp(\tau_1/\mu)$ results in

$$I_\nu(\tau_1, \mu) = I_\nu(\tau_2, \mu) e^{-(\tau_2 - \tau_1)/\mu} + \int_{\tau_1}^{\tau_2} S_\nu(t_\nu) e^{-(t_\nu - \tau_1)/\mu} \frac{dt_\nu}{\mu} \quad (4.36)$$

This is the formal solution of the equation of transfer. We will discuss the meaning of the two terms in this solution in § 4.6 using some example problems. Before doing so, however, we introduce the first two moments of the transfer equation.

4.5 Moments of the transfer equation

The angular moments (i.e. with respect to μ) of the transfer equation yield results of deep physical significance and great mathematical utility when constructing, for instance, models of stellar atmospheres.

Planar layers

The zero order moment of the equation of transfer in a planar medium can be derived from eq. (4.34)

$$\begin{aligned} \frac{1}{2} \int_{-1}^{+1} \mu \frac{dI_\nu}{d\tau_\nu} d\mu &= \frac{1}{2} \int_{-1}^{+1} I_\nu d\mu - \frac{1}{2} \int_{-1}^{+1} S_\nu d\mu \\ \frac{dH_\nu}{d\tau_\nu} &= J_\nu - S_\nu \end{aligned} \quad (4.37)$$

where we have assumed that the source function is isotropic. For the first order moment we find

$$\begin{aligned}\frac{1}{2} \int_{-1}^{+1} \mu^2 \frac{dI_\nu}{d\tau_\nu} d\mu &= \frac{1}{2} \int_{-1}^{+1} \mu I_\nu d\mu - \frac{1}{2} \int_{-1}^{+1} \mu S_\nu d\mu \\ \frac{dK_\nu}{d\tau_\nu} &= H_\nu\end{aligned}\quad (4.38)$$

as $\int_{-1}^{+1} \mu S_\nu d\mu = 0$ for an isotropic source function. Substituting eq. (4.38) in (4.37) then gives

$$\frac{d^2 K_\nu}{d\tau_\nu^2} = \frac{d^2(f_\nu J_\nu)}{d\tau_\nu^2} = J_\nu - S_\nu \quad (4.39)$$

where we have used the Eddington factor defined in eq. (3.31). If f_ν and S_ν are known, the above equation reduces to a 2nd order differential equation for the mean intensity. A method to solve this type of equation will be discussed in § 5.

Spherical shells

The zero order moment of the equation of tranfer in a spherical symmetric medium can be derived from eq. (4.19)

$$\frac{1}{r^2} \frac{\partial(r^2 H_\nu)}{\partial r} = \eta_\nu - \chi_\nu J_\nu \quad (4.40)$$

where we have assumed that η_ν and χ_ν are isotropic. For the first order moment we find

$$\frac{\partial K_\nu}{\partial r} + \frac{1}{r}(3K_\nu - J_\nu) = \frac{\partial(f_\nu J_\nu)}{\partial r} + \frac{1}{r}(3f_\nu - 1)J_\nu = -\chi_\nu H_\nu \quad (4.41)$$

Similar to the case of a planar geometry, we may combine eq. (4.40) and (4.41) to arrive at a 2nd order differential equation for the mean intensity.

Exercise 4.3

Derive the moment equations (4.40) and (4.41) in case of a spherical symmetric medium.

4.6 Simple examples of transfer problems

We will now solve the equation of transfer for some simple cases.

Radiation from a homogeneous finite slab

Let us consider a homogeneous finite slab. Homogeneity implies that χ_ν and η_ν , therefore also S_ν are constant. If the integrated optical depth in the normal direction of the slab is τ_ν the emerging intensity at $\tau_1 = 0$ is

$$I_\nu(0, \mu) = I_\nu(\tau_\nu, \mu)e^{-\tau_\nu/\mu} + S_\nu [1 - e^{-\tau_\nu/\mu}] \quad (4.42)$$

We concentrate on the normal direction $\mu = 1$ and for convenience drop reference to the angle dependence. This reduces eq. (4.42) to

$$I_\nu(0) = I_\nu(\tau_\nu)e^{-\tau_\nu} + S_\nu [1 - e^{-\tau_\nu}] \quad (4.43)$$

The first term on the right hand side describes the weakening of the radiation that is incident to the far side of the slab (viewed from the direction of the observer). The second term on the right hand side gives the contribution of radiation emitted by the slab itself. Let us analyse the two limiting cases of this solution.

In the optically thin limit ($\tau_\nu \ll 1$, such that $\exp(-\tau_\nu) \simeq 1 - \tau_\nu$) we find

$$I_\nu(0) \simeq I_\nu(\tau_\nu) + (S_\nu - I_\nu(\tau_\nu)) \tau_\nu \quad (4.44)$$

If no radiation is incident at the far side ($I_\nu(\tau_\nu) = 0$) it follows that $I_\nu(0) \simeq S_\nu \tau_\nu$. This is to be expected as in the optically thin case we observe emission from almost all parts of the slab. The emerging radiation therefore must be $I_\nu(0) \simeq \eta_\nu D = S_\nu \chi_\nu D = S_\nu \tau_\nu$, where D is the geometrical thickness of the slab. If no radiation is emitted by the slab itself ($S_\nu = 0$) then $I_\nu(0) \approx I_\nu(\tau_\nu)$, which is obvious – one sees through the slab.

If the slab is optically thick ($\tau_\nu \gg 1$) then

$$I_\nu(0) \simeq S_\nu \quad (4.45)$$

The radiation $I_\nu(\tau_\nu)$ that is incident at the far side does not penetrate through the slab. One only observes the source function in the slab, irrespective of the nature of the extinction. The nature of the medium is only relevant for the source function S_ν .

We rewrite the solution of eq. (4.43) to

$$I_\nu(0) = I_\nu(\tau_\nu) + (S_\nu - I_\nu(\tau_\nu)) [1 - e^{-\tau_\nu}] \quad (4.46)$$

Note that $I_\nu(0) < I_\nu(\tau_\nu)$ if $S_\nu < I_\nu(\tau_\nu)$, and conversely that $I_\nu(0) > I_\nu(\tau_\nu)$ if $S_\nu > I_\nu(\tau_\nu)$ (see figure 4.4). This is an important result. It shows the principle of the formation of absorption *casus quo* emission lines in a plan-parallel atmosphere. Let us identify the incident intensity $I_\nu(\tau_\nu)$ with the intensity that is emitted by the stellar continuum. The homogeneous layer corresponds to the stellar photosphere, i.e. the region in which the spectral lines are formed. Is the line source function $S_\nu < I_\nu(\tau_\nu)$ then an absorption line will form, i.e.

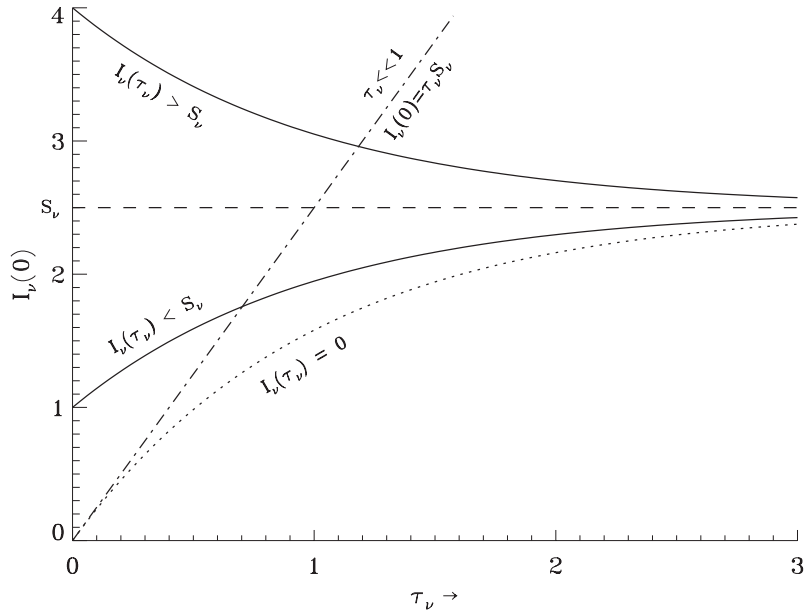


Figure 4.4: The emerging specific intensity $I_\nu(0)$ for a homogeneous finite slab in which the optical depth in the normal direction is τ_ν . The emitted specific intensity approaches the source function S_ν from both sides, and reaches S_ν for a sufficiently large optical depth τ_ν of the slab.

$I_\nu(0) < I_\nu(\tau_\nu)$. Is the line source function $S_\nu > I_\nu(\tau_\nu)$ then an emission line will form, i.e. $I_\nu(0) > I_\nu(\tau_\nu)$. Is the line source function equal to the intensity emitted by the continuum, i.e. $S_\nu = I_\nu(\tau_\nu)$, then no line will form, i.e. $I_\nu(0) = I_\nu(\tau_\nu)$.

Exercise 4.4

Stellar light passes through an interstellar cloud. The continuum specific intensity of the starlight is $I_o = 1$, independent of frequency. Spectral line absorption occurs in the cloud. The optical depth in the spectral line is given by $\tau(x) = \tau_o \phi(x)$, where $\phi(x)$ is a 'bell shaped' function given by Eq. 12.22. The parameter x is a measure of frequency. Use a spreadsheet program to create a graph of the spectrum of the emerging specific intensity I_x in the range $x = [-4.0, +4, 0]$, for $\tau_o = 0.1, 1.0$, and 10 .

Exercise 4.5

- Give the emerging specific intensity, as a function of beam direction μ , for a homogeneous semi-infinite slab.
- Give the specific intensity in a direction $\mu > 0$ inside of a homogeneous, semi-infinite medium.

Exercise 4.6

A radio astronomer states that the radio intensity that she observes from an interstellar cloud of diameter D is given by $I_\nu = \chi_\nu S_\nu D$. Give the five assumptions that she has made.

Radiation from a semi-infinite medium

The assumption of a homogeneous stellar atmosphere is not very realistic. To improve this model, we assume that the medium consists of multiple homogeneous planar layers, i.e. that variations occur in the z direction. As the density increases inward to very high values, the optical depth $\tau_2 \rightarrow \infty$. The emerging intensity ($\tau_1 = 0$) is then given by

$$I_\nu(0, \mu) = \int_0^\infty S_\nu(t_\nu) e^{-t_\nu/\mu} \frac{dt_\nu}{\mu} \quad (4.47)$$

Now let us assume that the source function is a linear function of optical depth, i.e.

$$S_\nu(\tau_\nu) = a_\nu + b_\nu \tau_\nu \quad (4.48)$$

Substitution in eq. (4.47) yields

$$I_\nu(0, \mu) = a_\nu + b_\nu \mu = S_\nu(\tau_\nu = \mu) \quad (4.49)$$

This is known as the *Eddington-Barbier approximation*. It shows that the emerging specific intensity in the outward normal direction ($\mu = 1$) is characterized by the source function at $\tau_\nu = 1$. This does *not* mean that all photons that are observed from this direction originate from the layer where the optical depth $\tau_\nu = 1$. The effective contribution to the integrant $S_\nu \exp(-t_\nu)$ reaches over a broad range in optical depth, from the surface at $\tau_\nu = 0$ down to $\tau_\nu \approx 10$. From all of this part of the semi-infinite atmosphere photons will escape; *together* they are characterized by the value of the source function at $\tau_\nu = 1$.

Exercise 4.7

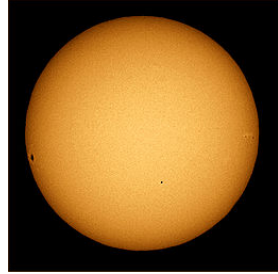
- a) Give the derivation of the Eddington-Barbier approximation.
- b) Give the emerging specific intensity in case $S_\nu(\tau_\nu) = \sum_{n=0}^{\infty} a_{n\nu} \tau_\nu^n$. Remember that

$$\int_0^\infty x^n e^{-x} dx = n! \quad (4.50)$$

Show that one recovers the Eddington-Barbier approximation if $a_{n\nu} = 0 \forall n \geq 2$.

Exercise 4.8

The specific intensity of the solar disk in visual light declines from the center of the disk towards the edge. What does this tell about the variation of the source function as a function of height in the solar atmosphere?

**Exercise 4.9**

Show that if $S_\nu(\tau_\nu) = a_\nu + b_\nu \tau_\nu$, then the emerging flux is given by

$$\mathcal{F}_\nu^+ = \pi S_\nu(\tau_\nu = 2/3) \quad (4.51)$$

Exercise 4.10

We assume a semi-infinite homogeneous stellar atmosphere. The continuum extinction χ^{cont} in the part of the spectrum that we are probing is independent of frequency. The source function is a linear function of optical depth. Using the continuum optical depth as our measuring stick, the source function is $S(\tau^{\text{cont}}) = a + b \tau^{\text{cont}}$. The spectrum contains a spectral line that has a source function that is the same as that of the continuum at every position in the atmosphere. The line extinction coefficient is given by $\chi_x^{\text{line}} = \chi_\circ^{\text{line}} \phi(x)$, where $\phi(x)$ is a 'bell shaped' function given by Eq. 12.22. The parameter x is a measure of frequency. The total optical depth $\tau_x = \tau^{\text{cont}} + \tau_x^{\text{line}}$. As the Eddington-Barbier approximation is valid, the emerging specific intensity in the normal direction is given by $I_x(0) = S(\tau_x = 1)$.

- Show that $\tau_x = 1$ is reached for $\tau^{\text{cont}} = 1/(1 + q)$, where $q = \chi_x^{\text{line}}/\chi^{\text{cont}}$ is the ratio between the line extinction coefficient and continuum extinction coefficient.
- Adopt $\chi_\circ^{\text{line}} = 10$ and $\chi_{\text{circ}}^{\text{cont}} = 1$. Use a spreadsheet program to create a graph of the spectrum of the emerging specific intensity I_x in the range $x = [-4.0, +4.0]$, for $(a, b) = (1.0, 0.0)$, $(0.6, 0.4)$, and $(0.2, 0.8)$. Note that a steeper dependence of the source function with optical depth produces a deeper absorption line.

The formation of spectral lines in a semi-infinite medium

As an example of the results that we have obtained above for the specific intensity in a semi-infinite medium we discuss the formation of spectral lines. A spectral line is always the result

of a discrete (*bound-bound*) transition in an atom or ion, i.e. of a process that occurs in addition to continuous processes that take place at the frequency of interest.

The presence of a spectral lines has two consequences:

- The bound-bound process gives the opportunity for extinction, superposed on the continuous extinction. At the frequency of the spectral line the extinction coefficient of the medium will be larger than at frequencies next to the line.
- The source function associated with the bound-bound process may differ from that of continuous processes at the line frequency.

Together these two effects may cause that the spectral line is observable in the emerging intensity, either in emission or in absorption relative to the continuum background.

We examine the special case that the continuum and line source functions are equal, but may vary (together) with depth in the medium. The effect of the extra line extinction is that the layer of optical depth $\tau_\nu = 1$, which is representative of the emerging photons, is located further out for line frequencies relative to continuum frequencies in the spectrum next to the line. In other words: one can see less deep in the medium at line frequencies as at these frequencies additional bound-bound extinction processes take place. The four panels shown in figure 4.5 illustrate this.

Note that an optically thick medium with identical continuum and line source function will only show a spectral line if the source function changes with depth, such that a different sampling will cause a different specific intensity. In the four panels the source function decreases outward such that spectral lines will *always* show a lower specific intensity compared to the continuum: they will be absorption lines.

The effect of line extinction on the characteristic depth of formation $\tau_\nu = 1$ can be very large as the bound-bound extinction coefficient at line centre is often orders of magnitudes larger than the continuum extinction coefficient. A “strong” spectral line may thus sample the emerging intensity in a geometrically thick layer. This implies that the shape of an observed strong spectral line does not so much reflect the behaviour of the extinction coefficient as a function of frequency, rather it reflects the run of the source function with depth in the atmosphere, sampled by the extinction coefficient. Throughout the line profile it is the depth one views into the atmosphere that is changing, and by that the value of the source function that we see.

The above discussion is not limited to rapid changes of the extinction coefficient in small frequency intervals, as is the case for bound-bound processes. It holds equally well for widely separated frequencies that measure the slow change of the continuum extinction coefficient. Although in this case the assumption that the two source functions are identical is usually not valid, and the extinction coefficients thus measure their own source function.

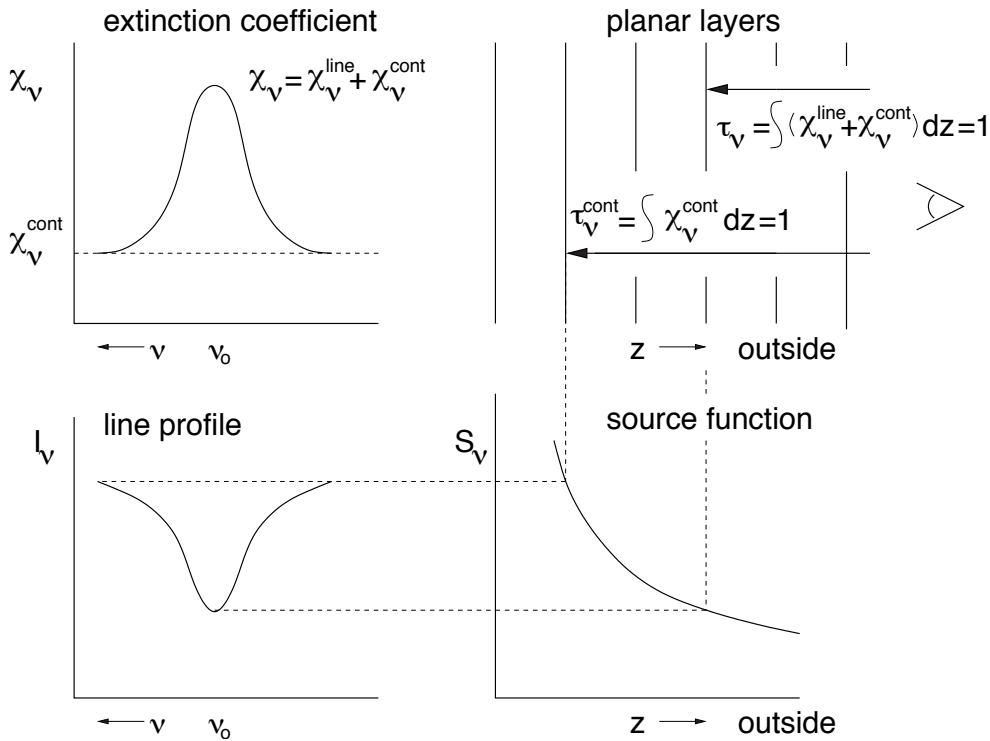


Figure 4.5: Four panels illustrating line formation in a semi-infinite medium consisting of planar layers. The extinction coefficient χ_ν (top left) determines the location of $\tau_\nu = 1$ for each frequency ν (top right). As an example the location of line center is shown. This location defines the value of the source function (bottom right) to which the observed specific intensity will be equal to (bottom left). It is assumed that the continuum and line source function are identical (such that only one curve needs to be plotted in the bottom left panel). Because the source function decreases with increasing distance the spectral line is in absorption.

Exercise 4.11

Make a schematic drawing for the case that the source function increases in the outward direction. What type of spectral line does this give?

Radiation deep inside a semi-infinite medium

The above discussed Eddington-Barbier approximation describes the radiation field close to the surface. Now we will direct our attention to the behaviour of the radiation quantities at great optical depth, $\tau_\nu \gg 1$, i.e. deep inside the medium, far below the surface. Here all characteristic length scales will be larger than the mean free path of the photons, therefore the particles will “see” an almost isotropic radiation field. As large optical depths are reached in regions of high density, collisional processes, i.e. real absorptions and emissions, will dom-

inate over photon scattering processes. Consequently, the properties of the medium will be close to that of thermodynamic equilibrium (see chapter 6) such that LTE is a good approximation. We formulate the source function as a Taylor-McLaurin expansion

$$S_\nu(t_\nu) = \sum_{n=0}^{\infty} \frac{(t_\nu - \tau_\nu)^n}{n!} \left[\frac{d^n S_\nu(t_\nu)}{dt_\nu^n} \right]_{\tau_\nu} \quad (4.52)$$

Substitution in eq. (4.47) (it could be more insightful to use the rightmost term in eq. 4.36) gives for an outward directed beam ($0 \leq \mu \leq 1$)

$$\begin{aligned} I_\nu(\tau_\nu, \mu) &= \sum_{n=0}^{\infty} \frac{1}{n!} \left[\frac{d^n S_\nu(t_\nu)}{dt_\nu^n} \right]_{\tau_\nu} \int_{\tau_\nu}^{\infty} (t_\nu - \tau_\nu)^n e^{-(t_\nu - \tau_\nu)/\mu} dt_\nu / \mu \\ &= \sum_{n=0}^{\infty} \left[\frac{d^n S_\nu(t_\nu)}{dt_\nu^n} \right]_{\tau_\nu} \frac{1}{n!} \int_0^{\infty} x^n e^{-x/\mu} dx / \mu \\ &= \sum_{n=0}^{\infty} \mu^n \left[\frac{d^n S_\nu(t_\nu)}{dt_\nu^n} \right]_{\tau_\nu} = S_\nu(\tau_\nu) + \mu \left. \frac{dS_\nu}{dt_\nu} \right|_{\tau_\nu} + \mu^2 \left. \frac{d^2 S_\nu}{dt_\nu^2} \right|_{\tau_\nu} + \dots \end{aligned} \quad (4.53)$$

where we have made use of eq. (4.50). For an inward directed beam ($-1 \leq \mu \leq 0$) one recovers an identical expression save for correction terms of order $e^{-\tau_\nu}/\mu$. As we consider large optical depths these corrections are unimportant. We may therefore apply the above expression for radiation in all directions; moreover it applies for small optical depths as well, provided that $\mu > 0$.

Using eq. (3.15) we find for the net flux

$$\mathcal{F}_\nu = \sum_{n=0}^{\infty} \frac{4\pi}{2n+3} \left[\frac{d^{2n+1} S_\nu(t_\nu)}{dt_\nu^{2n+1}} \right]_{\tau_\nu} = \frac{4\pi}{3} \left. \frac{dS_\nu}{dt_\nu} \right|_{\tau_\nu} + \frac{4\pi}{5} \left. \frac{d^3 S_\nu}{dt_\nu^3} \right|_{\tau_\nu} + \dots \quad (4.54)$$

To get a rough idea of the rate of convergence of these expansions we make the simple order of magnitude estimate $|d^n S_\nu/d\tau_\nu^n| \sim S_\nu/\tau_\nu^n$, such that the ratio between the differentials $|d^{n+2} S_\nu/d\tau_\nu^{n+2}| / |d^n S_\nu/d\tau_\nu^n| \sim 1/\tau_\nu^2$. This guarantees fast convergence and yields for $\tau_\nu \gg 1$ the following approximations

$$I_\nu(\tau_\nu, \mu) \simeq S_\nu(\tau_\nu) + \mu \left. \frac{dS_\nu}{dt_\nu} \right|_{\tau_\nu} \quad (4.55)$$

$$J_\nu(\tau_\nu) \simeq S_\nu(\tau_\nu) \quad (4.56)$$

$$\mathcal{F}_\nu(\tau_\nu) \simeq \frac{4\pi}{3} \left. \frac{dS_\nu}{dt_\nu} \right|_{\tau_\nu} \quad (4.57)$$

and

$$K_\nu(\tau_\nu) \simeq \frac{1}{3} S_\nu(\tau_\nu) \quad (4.58)$$

where we have also given the end results for the mean intensity J_ν and for the second order moment K_ν for completeness. In the expansion for the specific intensity we also take the first

order term into account because we want to have a non-zero value for the flux. The isotropic component of the mean intensity is determined by the value of the source function. The net flux is determined by the anisotropic component of the source function. This is logical as \mathcal{F}_ν measures the difference between \mathcal{F}_ν^+ and \mathcal{F}_ν^- . For the radial component only $I_\nu^+ \simeq S_\nu + dS_\nu/d\tau_\nu$ and $I_\nu^- \simeq S_\nu - dS_\nu/d\tau_\nu$. The difference (relevant for the net flux) is proportional to $dS_\nu/d\tau_\nu$. This implies that in order to transport radiation outward the source function has to increase inward. In LTE this corresponds to a temperature that increases in the inward direction (see § 6.7).

Note that

$$\lim_{\tau_\nu \rightarrow \infty} \frac{K_\nu(\tau_\nu)}{J_\nu(\tau_\nu)} = \lim_{\tau_\nu \rightarrow \infty} f_\nu(\tau_\nu) = \frac{1}{3} \quad (4.59)$$

a result that we already obtained in § 3.6 for a strictly isotropic radiation field. Equation (4.59) therefore expresses that for ever increasing optical depth the radiation field becomes more and more isotropic. This can also be learned from a simple order of magnitude estimate of the anisotropy of the specific intensity $|dS_\nu/d\tau_\nu|/S_\nu \sim 1/\tau_\nu$, i.e. if τ_ν increases the anisotropy decreases.

Exercise 4.12

Show that eq. (4.53) is also valid for inward directed beams, i.e. for $-1 \leq \mu \leq 0$.

Exercise 4.13

- a) Show that for the mean intensity a Taylor-McLaurin expansion of the source function (eq.4.52) yields

$$J_\nu(\tau_\nu) = \sum_{n=0}^{\infty} \frac{1}{2n+1} \left[\frac{d^{2n} S_\nu(t_\nu)}{dt_\nu^{2n}} \right]_{\tau_\nu} = S_\nu(\tau_\nu) + \frac{1}{3} \left. \frac{d^2 S_\nu}{dt_\nu^2} \right|_{\tau_\nu} + \dots \quad (4.60)$$

- b) Show that the second order moment is given by

$$K_\nu(\tau_\nu) = \sum_{n=0}^{\infty} \frac{1}{2n+3} \left[\frac{d^{2n} S_\nu(t_\nu)}{dt_\nu^{2n}} \right]_{\tau_\nu} = \frac{1}{3} S_\nu(\tau_\nu) + \frac{1}{5} \left. \frac{d^2 S_\nu}{dt_\nu^2} \right|_{\tau_\nu} + \dots \quad (4.61)$$

Exercise 4.14

Consider a spherical homogeneous cloud of small dust particles. The cloud has a mass m and a radius $R = 0.1$ AU (1 AU = 1.5×10^{13} cm). The dust particles have a temperature T and radiate according to the Planck-function. The optical depth τ , as measured from the edge of the cloud to the center, is independent of frequency ('gray').

- a) Give the specific intensity, mean intensity, and flux at the center of the cloud.

The dust particles have a frequency independent ('gray') extinction coefficient $\chi' = 100 \text{ cm}^2/\text{gr}$.

- b) Derive an expression that gives the gray radial optical depth as a function of the basic parameters of the cloud.
- c) What should be the minimum mass of the cloud to assure that the cloud is optically thick (i.e. $\tau \geq 1$)?
- d) If we increase the radius of the cloud by a factor of two, but keep its mass the same, does this lead to a change in the specific intensity at the center (yes/no). Does the mean intensity at the center change (yes/no)? Does the flux at the center change (yes/no)?

The cloud represents the halo of a comet. This halo develops when the comet gets so close to the sun that because of heating small dust particles come off its surface layers. A comet has a typical initial diameter of 10 km and consists of material that has a typical density of 1 gr cm^{-3} .

- e) Will the halo of this comet be optically thick or optically thin?

Diffusion approximation

At large optical depth the properties of the medium approach (local) thermodynamic equilibrium, as discussed above, such that $S_\nu = B_\nu$ (see § 6.2). For the flux this implies (see eq. 4.57)

$$\mathcal{F}_\nu \simeq \frac{4\pi}{3} \frac{\partial B_\nu}{\partial \tau_\nu} = -\frac{4\pi}{3} \frac{1}{\chi_\nu} \frac{\partial B_\nu}{\partial z} = -\frac{4\pi}{3} \frac{1}{\chi_\nu} \frac{\partial B_\nu}{\partial T} \frac{dT}{dz} \quad (4.62)$$

This equation is known as the *diffusion approximation* because of the similarity of the equations to that of (other) diffusion processes that have a form such that the transported flux of a quantity is the product of a diffusion coefficient times the gradient of the quantity itself. The coefficient $(4\pi/3\chi_\nu)dB_\nu/dT$ is also referred to as the *radiative conductivity*.

In those parts of the atmosphere that can not be observed – or more general in the stellar interior – the total flux \mathcal{F} is a much more interesting quantity than is the monochromatic flux \mathcal{F}_ν . If we integrate eq. (4.62) over frequency and introduce the *Roseland mean extinction coefficient* χ_R (dimension cm^{-1}), defined as

$$\frac{1}{\chi_R} \equiv \frac{\int_0^\infty (1/\chi_\nu)(\partial B_\nu/\partial T) d\nu}{\int_0^\infty (\partial B_\nu/\partial T) d\nu} \quad (4.63)$$

we find using (see eq. 6.11)

$$\int_0^\infty \frac{\partial B_\nu}{\partial T} d\nu = \frac{\partial}{\partial T} \int_0^\infty B_\nu d\nu = \frac{\partial B}{\partial T} = \frac{4\sigma}{\pi} T^3 \quad (4.64)$$

for the total flux

$$\mathcal{F} = -\frac{16}{3} \frac{\sigma T^3}{\chi_R} \frac{dT}{dz} \quad (4.65)$$

where $16\sigma T^3/3\chi_R$ is the *effective radiative conductivity*. This equation shows that in LTE a net outward radiative flux is accompanied by an inward increase of the temperature.

The general form of the above diffusion equation is given by

$$\mathcal{F}(\mathbf{r}, t) = \frac{16}{3} \frac{\sigma T^3}{\chi_R} \nabla T = \frac{16}{3} \frac{\sigma T^3}{\chi_R} \left(\frac{\partial T}{\partial x}, \frac{\partial T}{\partial y}, \frac{\partial T}{\partial z} \right) \quad (4.66)$$

A formal derivation of this equation is given in Wehrse, Baschek, & Waldenfels (2000, A&A 359, 780).

We will return to the diffusion approximation in chapter 10.

Exercise 4.15

In section 9.3 we will discuss in more detail that in a planar atmosphere the total flux \mathcal{F} (see 4.65) is constant. The value for the constant is σT_{eff}^4 , see eq. (3.18). Introduce, using eq. (4.33), the Rosseland optical depth $d\tau_{\text{Ross}} = -\chi_R dz$ and show that in the diffusion limit the temperature structure is given by

$$T^4(\tau_{\text{Ross}}) = \frac{3}{4} T_{\text{eff}}^4 \left(\tau_{\text{Ross}} + \frac{2}{3} \right)$$

if one assumes that the diffusion approximation is valid down to $\tau_{\text{Ross}} = 2/3$ and that the temperature T at $\tau_{\text{Ross}} = 2/3$ is equal to T_{eff} .

5

Numerical methods for solving the equation of transfer

In many cases the equation of transfer can not be solved analytically. In this chapter we discuss a number of numerical techniques that allow to compute the formal solution eq. (4.36). "Formal" implies that both S_ν and τ_ν are known functions. In principle, we may simply replace the integral over optical depth by a quadrature sum, such as for instance the *trapezium rule*

$$\int_{x_1}^{x_2} f(x) dx = \Delta x \left[\frac{1}{2} f_1 + \frac{1}{2} f_2 \right] \quad (5.1)$$

where $f(x) = S(x)e^{-x}$. Solving this problem is trivial. In practice, however, this is not the way in which it is done. The reason for it is that this simple numerical quadrature is *a*) inaccurate because of the strongly non-linear (read: exponential) behaviour of the integrant $f(x)$, and *b*) very inefficient in terms of computation speed. The latter is so because the integrant contains an exponential function, which is very "expensive" to compute. In many complex models, especially those aimed at quantitative spectroscopy, the overall computation time is dominated by the time it costs to perform formal solutions (for all frequencies and angles at all grid points). Highly efficient numerical schemes are therefore indispensable.

One may distinguish between two classes of methods, those based on the *i*) integral solution (eq. 4.36), or *ii*) differential solution (eq. 4.34) of the equation of transfer. The latter class can again be divided in a *a*) first-order form, or *b*) a second-order form. The *formal solution using short characteristics* uses the integral solution. We will first discuss this method. Then we will focus on a second-order differential method that is referred to as *Feautrier method*, named after the person that devised this scheme. Until recently the accurate and efficient Feautrier method (which does not feature exponential functions) has been the preferred numerical tool for solving the transfer equation. Presently, there is a renewed interest in the method of short characteristics. This is so because of the relative ease with which this formalism can be implemented in 2D and 3D transfer problems. For both the 1D and multiD-problems there is a recent increasing interest in an ingenuous adaptation of the *discontinuous finite element* method, which is based on the first-order differential form. We will not discuss this last method.

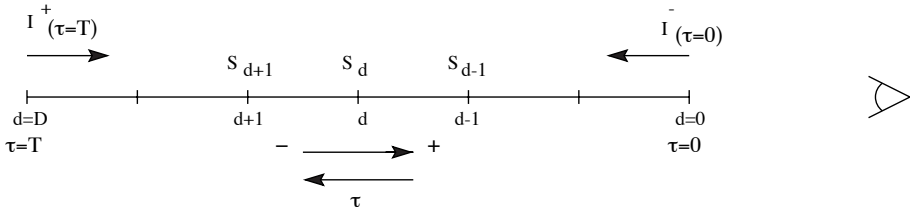


Figure 5.1: Specification of the grid points in our description of the method of short characteristics.

5.1 Short characteristics

The *method of short characteristics* uses the integral solution eq. (4.36) of the equation of transfer. Let us consider a finite slab in planar geometry, through which the total optical depth of the medium in the normal direction is T_ν . Along lines of sight in the outward direction, i.e. for $0 \leq \mu \leq 1$, or, phrased differently, in the direction in which the optical depth decreases, we have

$$I_\nu^+(\tau_\nu, \mu) = I_\nu^+(T_\nu, \mu) e^{-(T_\nu - \tau_\nu)/\mu} + \int_{T_\nu}^{\tau_\nu} S_\nu(t_\nu) e^{-(t_\nu - \tau_\nu)/\mu} \frac{dt_\nu}{\mu} \quad (5.2)$$

where $I_\nu^+(T_\nu, \mu)$ is the incident intensity (in the + direction) at $\tau_\nu = T_\nu$. Similarly, for an inward directed beam, i.e. $-1 \leq \mu \leq 0$, we find using the boundary condition $I_\nu^-(0, \mu)$ that

$$I_\nu^-(\tau_\nu, \mu) = I_\nu^-(0, \mu) e^{\tau_\nu/\mu} + \int_0^{\tau_\nu} S_\nu(t_\nu) e^{-(\tau_\nu - t_\nu)/\mu} \frac{dt_\nu}{(-\mu)} \quad (5.3)$$

Perhaps, intuitively, this last solution may seem somewhat odd. However, realize that μ is negative.

We choose a set of optical depth points $\{\tau_d\}$, $d = 0, \dots, D$ where $\tau_0 = 0$ and $\tau_D = T$. For convenience we drop the frequency subscript. The boundary conditions are given by $I_D^+(\mu, \nu) = I^+(T, \mu, \nu)$ and $I_0^-(\mu, \nu) = I^-(0, \mu, \nu)$. Figure 5.1 illustrates this grid specification.

The above equations provide the solution along beams that pass through the slab at an angle θ , where $\mu = \cos \theta$. We now write the solution in a local form, such that it appears that the specific intensity at point d is only a function of the source function and the boundary conditions $I^+(\tau_{d+1}, \mu, \nu)$ and $I^-(\tau_{d-1}, \mu, \nu)$. This yields

$$I^+(\tau_d, \mu, \nu) = I^+(\tau_{d+1}, \mu, \nu) e^{-\Delta\tau_{d+\frac{1}{2}}} + \Delta I_d^+(S, \mu, \nu) \quad (5.4)$$

and

$$I^-(\tau_d, \mu, \nu) = I^-(\tau_{d-1}, \mu, \nu) e^{-\Delta\tau_{d-\frac{1}{2}}} + \Delta I_d^-(S, \mu, \nu) \quad (5.5)$$

where

$$\Delta\tau_{d+\frac{1}{2}} = (\tau_{d+1} - \tau_d) / |\mu| \quad (5.6)$$

The increase in intensity, ΔI_d^\pm , is the contribution of the source function integrated over the grid interval. We now assume that locally (over the range $\{\tau_{d-1}, \tau_{d+1}\}$) the source function may be written as a parabolic function of the optical depth, i.e.

$$S(\tau) = a + b\tau + c\tau^2 \quad (5.7)$$

Note that if $c = 0$ this expression reduces to the Eddington-Barbier approximation (see § 4.6), which assumes that the source function is linear in each grid interval $\{\tau_d, \tau_{d+1}\}$. Using the adopted behaviour (5.7) we may analytically solve the transfer equation over the relevant grid interval, and we may express this solution as

$$\Delta I_d^\pm = \alpha_d^\pm S_{d-1} + \beta_d^\pm S_d + \gamma_d^\pm S_{d+1} \quad (5.8)$$

After a heroic amount of algebra and integration we find for the parabolic interpolation coefficients

$$\begin{aligned} \alpha_d^- &= e_{0d} + \left[e_{2d} - \left(\Delta\tau_{d+\frac{1}{2}} + 2\Delta\tau_{d-\frac{1}{2}} \right) e_{1d} \right] / \left[\Delta\tau_{d-\frac{1}{2}} \left(\Delta\tau_{d+\frac{1}{2}} + \Delta\tau_{d-\frac{1}{2}} \right) \right] \\ \beta_d^- &= \left[\left(\Delta\tau_{d+\frac{1}{2}} + \Delta\tau_{d-\frac{1}{2}} \right) e_{1d} - e_{2d} \right] / \left[\Delta\tau_{d-\frac{1}{2}} \Delta\tau_{d+\frac{1}{2}} \right] \\ \gamma_d^- &= \left[e_{2d} - \Delta\tau_{d-\frac{1}{2}} e_{1d} \right] / \left[\Delta\tau_{d+\frac{1}{2}} \left(\Delta\tau_{d+\frac{1}{2}} + \Delta\tau_{d-\frac{1}{2}} \right) \right] \\ \alpha_d^+ &= \left[e_{2d+1} - \Delta\tau_{d+\frac{1}{2}} e_{1d+1} \right] / \left[\Delta\tau_{d-\frac{1}{2}} \left(\Delta\tau_{d+\frac{1}{2}} + \Delta\tau_{d-\frac{1}{2}} \right) \right] \\ \beta_d^+ &= \left[\left(\Delta\tau_{d+\frac{1}{2}} + \Delta\tau_{d-\frac{1}{2}} \right) e_{1d+1} - e_{2d+1} \right] / \left[\Delta\tau_{d-\frac{1}{2}} \Delta\tau_{d+\frac{1}{2}} \right] \\ \gamma_d^+ &= e_{0d+1} + \\ &\quad \left[e_{2d+1} - \left(\Delta\tau_{d-\frac{1}{2}} + 2\Delta\tau_{d+\frac{1}{2}} \right) e_{1d+1} \right] / \left[\Delta\tau_{d+\frac{1}{2}} \left(\Delta\tau_{d+\frac{1}{2}} + \Delta\tau_{d-\frac{1}{2}} \right) \right] \end{aligned} \quad (5.9)$$

where

$$\begin{aligned} e_{0d} &= 1 - \exp(-\Delta\tau_{d-\frac{1}{2}}) \\ e_{1d} &= \Delta\tau_{d-\frac{1}{2}} - 1 + \exp(-\Delta\tau_{d-\frac{1}{2}}) = \Delta\tau_{d-\frac{1}{2}} - e_{0d} \\ e_{2d} &= (\Delta\tau_{d-\frac{1}{2}})^2 - 2\Delta\tau_{d-\frac{1}{2}} + 2 - 2\exp(-\Delta\tau_{d-\frac{1}{2}}) = (\Delta\tau_{d-\frac{1}{2}})^2 - 2e_{1d} \end{aligned} \quad (5.10)$$

For a linear source function the interpolation coefficients simplify to

$$\begin{aligned} \alpha_d^- &= e_{0d} - e_{1d}/\Delta\tau_{d-\frac{1}{2}} \\ \beta_d^- &= e_{1d}/\Delta\tau_{d-\frac{1}{2}} \\ \gamma_d^- &= 0 \\ \alpha_d^+ &= 0 \\ \beta_d^+ &= e_{1d+1}/\Delta\tau_{d+\frac{1}{2}} \\ \gamma_d^+ &= e_{0d+1} - e_{1d+1}/\Delta\tau_{d+\frac{1}{2}} \end{aligned} \quad (5.11)$$

Equations (5.4) and (5.5) may now be solved trivially for each angle and frequency. If one opts for second order accuracy, i.e. adopting the parabolic description eq. (5.7) for the source function, one needs to take some special care at the inner boundary for the incoming beam and at the outer boundary for the outgoing beam because α_D^- and β_D^- and β_0^+ and γ_0^+ are not defined (γ_D^- and α_0^+ are both zero). One way out is to assume first order accuracy (i.e. adopt a linear source function) for the above coefficients at $d = D$ and $d = 0$.

The above described technique is called *method of short characteristics* because it reduces the problem of solving the transfer equation to that of a series of analytical solutions over small intervals, where the source function behaves in a characteristic way. Note that the strong non-linear behaviour of the integrant $f(x) = S(x)e^{-x}$ (see eq. 5.1) is no longer a problem because of the analytical integration of the exponential term.

Though these lectures are not concerned with numerical techniques, we do show, for fun, how such a piece of code might look like. The listed routine is for a first order solution of the equation of transfer by means of the method of short characteristics and is programmed in IDL:

```

pro short_characteristics_transfersolver, Src,tau,Int,Int_incident,ND
;
; First order short characteristics transfer solver for outgoing beams
; only, following Olson & Kunasz 1987, JQSRT 38, 325.
;
; INPUT:
;
; Src          - source function grid
; tau          - optical depth grid where tau=0 at the observer
; Int_incident - incident specific intensity at the far side of the
;                 medium (as seen from the observer) for the outgoing
;                 beam. It should have the same units as Src
; ND           - nr of depth points; 0..ND-1 = outer..inner boundary
;
; OUTPUT:
;
; Int          - specific intensity grid for outgoing beam. The
;                 emerging intensity is Int(0)
;
Nill = replicate(0.d0,ND)
Int = Nill & dInt = Nill & dtau_dph = Nill
;
for d = 0,ND-2 do begin
  dtau_dph(d) = tau(d+1)-tau(d)
  e0_dp1      = 1.d0-exp(-dtau_dph(d))
  e1_dp1      = dtau_dph(d)-e0_dp1
  bdp         = e1_dp1/dtau_dph(d)
  cdp         = e0_dp1-e1_dp1/dtau_dph(d)
  dInt(d)     = bdp*Src(d)+cdp*Src(d+1)
endfor
;
Int(ND-1) = Int_incident
for d = ND-2,0,-1 do begin
  Int(d) = Int(d+1)*exp(-dtau_dph(d))+dInt(d)
endfor
;
return

```

end

5.2 Feautrier method

The basis of Feautriers method is *i)* the use of seperate transfer equations for inward and outward directed radiation, and *ii)* the introduction of a symmetric and an anti-symmetric average of the specific intensity. We first rewrite transfer equation eq. (4.34). We limit the beam angles μ to the half space $0 \leq \mu \leq 1$, and, for the moment, drop the standard notation of a subscript ν specifying the frequency dependence. We get

$$\pm\mu \frac{dI(z, \pm\mu, \nu)}{d\tau(z, \nu)} = I(z, \pm\mu, \nu) - S(z, \nu) \quad (5.12)$$

where $I(+\mu)$ and $I(-\mu)$ describe the outward and inward intensity. The symmetric and anti-symmetric average are defined as, respectively

$$u(z, \mu, \nu) = \frac{1}{2} [I(z, +\mu, \nu) + I(z, -\mu, \nu)] \quad (5.13)$$

and

$$v(z, \mu, \nu) = \frac{1}{2} [I(z, +\mu, \nu) - I(z, -\mu, \nu)] \quad (5.14)$$

Note that in a one-dimensional space, u would describe the mean intensity and v the flux. We may obtain a system of two 1st order differential equations by adding the two equations (5.12), i.e.

$$\mu \frac{dv}{d\tau} = u - S \quad (5.15)$$

and subtracting them, i.e.

$$\mu \frac{du}{d\tau} = v \quad (5.16)$$

Substitution of (5.16) in (5.15) yields the 2nd order differential equation

$$\mu^2 \frac{d^2u}{d\tau^2} = u - S \quad (5.17)$$

The boundary conditions are the incoming intensity $I(-\mu) = I_\mu^-$ at the edge $\tau = 0$ and the outgoing intensity $I(+\mu) = I_\mu^+$ at the edge $\tau = \tau_{\max}$. It has been found in many transfer problems that an accurate description of the boundary conditions is essential. The two boundary equations follow from (5.16) and are given by

$$\mu \left. \frac{du}{d\tau} \right|_0 = u(0) - I_\mu^- \quad (5.18)$$

and

$$\mu \left. \frac{du}{d\tau} \right|_{\tau_{\max}} = I_\mu^+ - u(\tau_{\max}) \quad (5.19)$$

— — —

To give an example of what the boundary conditions I_μ^- and I_μ^+ may look like, we use the model atmosphere as an example. In this case the incident intensity at the outer boundary $\tau = 0$ is $I_\mu^- \equiv 0$, such that

$$\mu \frac{du}{d\tau} \Big|_0 = u(0) \quad (5.20)$$

The incoming intensity at the inner boundary $\tau = \tau_{\max}$ of the atmosphere follows from eq. (4.55) and $S_\nu = B_\nu$ (see § 6.2). This yields $I_\mu^+ = B_\nu(\tau_{\max}) + (\chi_\nu^{-1}|dB_\nu/dz|)_{\tau_{\max}}$. For $u(\tau_{\max}, \mu, \nu) = B_\nu(\tau_{\max})$ we then arrive at

$$\mu \frac{du}{d\tau} \Big|_{\tau_{\max}} = \mu \left(\frac{1}{\chi_\nu} \left| \frac{dB_\nu}{dz} \right| \right)_{\tau_{\max}} \quad (5.21)$$

— — —

The next step is to formulate the system of differential equation (5.17), (5.18) and (5.19) as a set of difference equations using the *finite difference method*.

We choose a set of optical depth points $\{\tau_d\}$, $d = 0, \dots, D$ where $\tau_0 < \tau_1 < \dots < \tau_D$; a set of angle points $\{\mu_m\}$, $m = 0, \dots, M$ and a set of frequency points $\{\nu_n\}$, $n = 0, \dots, N$. In this grid notation we may write the symmetric average of the intensity u as $u(z_d, \mu_m, \nu_n) = u_{dmn}$, and the source function as $S(z_d, \nu_n) = S_{dn}$. We apply the central difference approximation for arbitrary stepsize and find for the derivative

$$\frac{du}{d\tau} \Big|_{d+\frac{1}{2}} = \frac{\Delta u_{d+\frac{1}{2}}}{\Delta \tau_{d+\frac{1}{2}}} = \frac{u_{d+1} - u_d}{\tau_{d+1} - \tau_d} \quad (5.22)$$

and for the second derivative

$$\frac{d^2 u}{d\tau^2} \Big|_d = \frac{\frac{du}{d\tau} \Big|_{d+\frac{1}{2}} - \frac{du}{d\tau} \Big|_{d-\frac{1}{2}}}{\frac{1}{2}(\Delta \tau_{d+\frac{1}{2}} + \Delta \tau_{d-\frac{1}{2}})} \quad (5.23)$$

where we have introduced

$$\Delta \tau_{d \pm \frac{1}{2}} = \frac{1}{2} (\chi_{d \pm 1} + \chi_d) |z_{d \pm 1} - z_d| \quad (5.24)$$

and

$$\Delta \tau_d = \frac{1}{2} (\Delta \tau_{d-\frac{1}{2}} + \Delta \tau_{d+\frac{1}{2}}) \quad (5.25)$$

Equiped with these definitions we find for the difference representation of the 2nd order transfer equation (5.17)

$$\begin{aligned} \left(\frac{\mu_m^2}{\Delta \tau_{d-\frac{1}{2}} \Delta \tau_d} \right) u_{d-1} - \frac{\mu_m^2}{\Delta \tau_d} \left(\frac{1}{\Delta \tau_{d-\frac{1}{2}}} + \frac{1}{\Delta \tau_{d+\frac{1}{2}}} \right) u_d + \\ \left(\frac{\mu_m^2}{\Delta \tau_d \Delta \tau_{d+\frac{1}{2}}} \right) u_{d+1} = u_d - S_d \end{aligned} \quad (5.26)$$

This equation is valid at the depth points $d = 2, \dots, D - 1$. At the boundary $\tau = 0$ we have

$$\mu_m \frac{u_1 - u_0}{\Delta\tau_{\frac{1}{2}}} = u_0 - I_m^- \quad (5.27)$$

and at $\tau = \tau_{\max}$

$$\mu_m \frac{u_D - u_{D-1}}{\Delta\tau_{D-\frac{1}{2}}} = I_m^+ - u_D \quad (5.28)$$

Exercise 5.1

- a) Derive the set of difference equations (5.26), (5.27) and (5.28).

The boundary conditions (5.27) and (5.28) are only accurate to within first order. In this exercise we will derive the boundary conditions to within second order precision.

- b) Show by means of a ‘forward’ Taylor series expansion to within second order that the boundary condition (5.27) at $\tau = 0$ can be improved to

$$\mu_m \frac{u_1 - u_0}{\Delta\tau_{\frac{1}{2}}} = u_0 - I_m^- + \frac{\Delta\tau_{\frac{1}{2}}}{2} \frac{(u_0 - S_0)}{\mu_m} \quad (5.29)$$

- c) Show by means of a ‘backward’ Taylor series expansion to within second order that the boundary condition (5.28) at $\tau = \tau_{\max}$ can be improved to

$$\mu_m \frac{u_D - u_{D-1}}{\Delta\tau_{D-\frac{1}{2}}} = I_m^+ - u_D - \frac{\Delta\tau_{D-\frac{1}{2}}}{2} \frac{(u_D - S_D)}{\mu_m} \quad (5.30)$$

Feautrier elimination scheme

The final step in the Feautrier method is to write the set difference equations (5.26), (5.27), and (5.28) as a matrix equation. To that end we introduce the vector \mathbf{u}_d which for given beam angle μ and frequency ν has dimension D . The matrix equation can be expressed as

$$-\mathbf{A}_d \mathbf{u}_{d-1} + \mathbf{B}_d \mathbf{u}_d - \mathbf{C}_d \mathbf{u}_{d+1} = \mathbf{L}_d \quad (5.31)$$

where the $(D \times D)$ matrix \mathbf{A}_d contains only *lower diagonal* terms; \mathbf{B}_d only *diagonal* terms, and \mathbf{C}_d only *upper diagonal* terms. Note that $\mathbf{A}_0 = 0$ and $\mathbf{C}_D = 0$. The right hand side vector \mathbf{L}_d contains source terms. The structure of the system looks as follows

$$\begin{pmatrix} B_0 & -C_0 & & & \\ -A_1 & B_1 & -C_1 & & \\ -A_2 & B_2 & -C_2 & & \\ \dots & \dots & \dots & & \\ & -A_{D-1} & B_{D-1} & -C_{D-1} & \\ & -A_D & B_D & & \end{pmatrix} \begin{pmatrix} u_0 \\ u_1 \\ u_2 \\ \dots \\ u_{D-1} \\ u_D \end{pmatrix} = \begin{pmatrix} L_0 \\ L_1 \\ L_2 \\ \dots \\ L_{D-1} \\ L_D \end{pmatrix} \quad (5.32)$$

The matrix has a tridiagonal structure. One may solve this type of matrix by an efficient forward-backward recursive sweep through the system. We start at $d = 0$, and express the symmetric average u_d in terms of u_{d+1} . If

$$u_d = D_d u_{d+1} + E_d \quad (5.33)$$

then

$$D_d = (B_d - A_d D_{d-1})^{-1} C_d \quad (5.34)$$

and

$$E_d = (B_d - A_d D_{d-1})^{-1} (L_d + A_d E_{d-1}) \quad (5.35)$$

On arrival at $d = D$, where $C_D = 0$, such that $D_D = 0$ we find that $u_D = E_D$. Now that u_D is known we may do a back substitution in (5.33) and recover all values for \mathbf{u}_d . If one is only interested in the emerging intensity at $\tau = 0$, at which in many transfer problems the incident intensity $I_\mu^- = 0$, one could start the recursive sweep at $d = D$ and one would not even require back substitution: $I_0^+ = 2u_0 - I_\mu^-$. A routine for solving tridiagonal systems is given in, for example, Numerical Recipes.

6

Radiation and matter

6.1 Introduction

The most important parameters describing the material medium are the mass density $\rho(\mathbf{r})$ and the temperature $T(\mathbf{r})$. The essential problem in the study of astrophysical media is to understand the interaction between the material medium and the radiation field. The basic quantities mentioned can be determined from the conservation laws of hydrodynamics. The density structure of the medium is determined by the conservation of mass and momentum; the temperature structure follows from the conservation of energy.

The description of the coupling between the gas (and/or dust) and the radiation field can be simplified considerably if the medium and the radiation are in some type of equilibrium.

Types of equilibrium between particles and photons

The most strict form of equilibrium is *thermodynamic equilibrium* (TE). In TE the medium is homogeneous and at rest. There are no gradients. Each process is in a microscopic equilibrium with its reverse process, i.e. all processes are in *detailed balance*. The radiation field is given by the Planck function, which only depends on T , and both the thermal velocity distribution of the particles and the distribution of particles over excitation and ionization states depends only on ρ and T . However, the simple fact that we receive photons of the objects in which we are interested tells us that these media can not be in a state of TE. Because photons escape from these media it must be so that significant gradients are present in the quantities describing the medium.

If we can not assume that the medium may be characterized as a whole with one value for ρ and one value for T , but if we are allowed to describe the state of the material medium *locally* using only the value of $\rho(\mathbf{r})$ and $T(\mathbf{r})$, then we refer to the situation as being in *local thermodynamic equilibrium* (LTE). In LTE all atomic processes are still in detailed balance. However, the radiation field is *not* in equilibrium, but follows from the solution of the equation

of transfer.

In those cases that even LTE is not valid, the medium is (per definition) in a state of *non local thermodynamic equilibrium* (NLTE). This is so when (at least) one microscopic process is not in detailed balance. The population of (at least) two excitation/ionization levels will deviate from their LTE values.

In this chapter we mainly focus on a description of TE.

6.2 Thermodynamic equilibrium

Thermodynamic equilibrium is realized in a cavity that is enclosed by isothermal walls, and that has relaxed to a situation of rest. As photons do not have a mass they can be absorbed and emitted by the walls of the cavity in arbitrary numbers. We expect that the number of photons and the distribution of these photons over frequency will reach an equilibrium state, characterized by the temperature T of the walls. The state of the radiation field (as well as that of the medium; but more about that later) in TE is therefore described by only one variable, the temperature T . This variable is independent of the nature of the walls or of the shape, texture, or size of the container.

The latter we may understand using a thought experiment. We connect the container to a second container of which the isothermal walls are also at the temperature T , and we carefully drill a hole in the containers such that their radiation fields are in contact. We place a filter that only allows through radiation of frequency ν (see figure 6.1). If $I_\nu^1 \neq I_\nu^2$, then an energy flow would occur between both cavities. This would be in contradiction to the second law of thermodynamics (it would allow the possibility of a *perpetuum mobile*). From our experiment we may also conclude that the intensity in the enclosure is isotropic ($I_\nu \neq I_\nu(\mathbf{n})$) and homogeneous ($I_\nu = I_\nu(\mathbf{r})$). Phrased differently

$$I_\nu = I_\nu(T) \equiv B_\nu(T) \quad (6.1)$$

In circa 1860 Gustav Robert Kirchhoff (1824–1887) measured the best approximation of this equilibrium radiation by making a small hole in the side of a closed box. He realized that radiation incident to the enclosure would be absorbed by the box, though perhaps only after very many reflections off the insides of the walls (provided the hole was sufficiently small). The box thus behaves as a perfect *blackbody*, i.e. a body that absorbs radiation of any frequency completely. Such a body is also the *best* possible emitter. The equilibrium radiation that emerges from the hole is therefore referred to as *blackbody radiation*. Max Planck (1858–1947) derived the function that describes the radiation field of a blackbody. We will discuss the shape of this function, after introducing Kirchhoff's law.

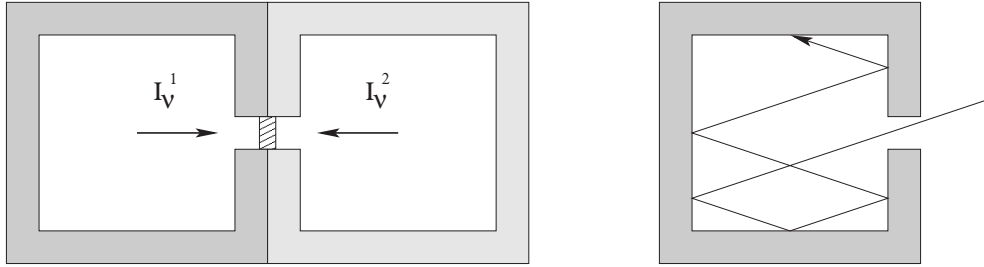


Figure 6.1: *Left panel:* Two isothermal containers of which the walls have identical temperatures. A filter that only allows through radiation of frequency ν is in front of a small hole separating the enclosures. If the system is in equilibrium then the radiation fields in both containers must be identical. *Right panel:* Radiation incident to a small hole in a container will be absorbed by the walls, though perhaps only after many reflections. The radiation emitted by the insides of the walls (so also the radiation that emerges from the hole) will be an excellent approximation of blackbody radiation.

Exercise 6.1

Why is a blackbody the best possible emitter?

Exercise 6.2

- Give the net flux \mathcal{F}_ν in a medium that is in TE and in which the specific intensity is I_ν .
- Do we observe objects in the sky that are in TE?

Kirchhoff's law & the Kirchhoff-Planck relation

In a medium that is in TE there are no gradients, i.e. the specific intensity is homogeneous, isotropic and time independent. In that case eq. (4.11) implies that for all rays, for all frequencies, at all times

$$\eta_\nu = \chi_\nu I_\nu \quad (6.2)$$

This is *Kirchhoff's law*. Combining this law with eq. (6.1) results in

$$\eta_\nu = \chi_\nu B_\nu(T) \quad (6.3)$$

This is the *Kirchhoff-Planck relation*. So, the source function $S_\nu = \eta_\nu / \chi_\nu$ in TE is equal to the Planck function B_ν .

In summary: in TE $I_\nu = B_\nu = S_\nu$. As the radiation field is isotropic, also $I_\nu = J_\nu$.

6.3 Planck function

The Planck function per frequency unit is given by

$$B_\nu(T) = \frac{2h\nu^3}{c^2} \frac{1}{e^{h\nu/kT} - 1} \quad (6.4)$$

where h and k are Planck's constant and Boltzmann's constant respectively. The dimensions of B_ν are $\text{erg cm}^{-2} \text{ s}^{-1} \text{ Hz}^{-1} \text{ sr}^{-1}$. A derivation of the Planck function is for instance given in Rybicki & Lightman. Using the relation

$$|B_\nu(T) d\nu| = |B_\lambda(T) d\lambda| \quad (6.5)$$

we may rewrite the Planck function in wavelength units. We find

$$B_\lambda(T) = \frac{2hc^2}{\lambda^5} \frac{1}{e^{hc/\lambda kT} - 1} \quad (6.6)$$

of which the dimensions are $\text{erg cm}^{-2} \text{ s}^{-1} \text{ cm}^{-1} \text{ sr}^{-1}$.

A series of Planck curves (in frequency unit) is given in figure 6.2. This reveals a number of striking properties of this function: *i*) The maximum of B_ν shifts toward higher frequencies if the temperature increases; *ii*) the Planck curves do not intersect: B_ν increases monotonous with temperature, therefore the frequency integrated or total Planck function will do so too, and *iii*) at frequencies much lower than the peak position $\partial \log B_\nu / \partial \log \nu = 2$.

Let us study the properties of the Planck function in more detail.

Wien's displacement law

Note that if we write $B_\nu(T) = T^3 q^3 \mathcal{B}(q)$, where $q = \nu/T$, that the function $\mathcal{B}(q)$ is a universal function. This proofs that the Planck curves will not intersect. The position of the maximum of the Planck curves follows from *Wien's displacement law*, and can be derived by taking the partial derivative $\partial B_\nu / \partial \nu = 0$. We find

$$h\nu_{\max} = 2.82144 kT \quad \text{or} \quad \frac{\nu_{\max}}{T} = 5.87870 \times 10^{10} \text{ Hz K}^{-1} \quad (6.7)$$

The peak of B_λ is at

$$\lambda_{\max} T = 0.28979 \text{ cm K} \quad (6.8)$$

Note: the maxima of B_ν and B_λ are *not* at the same position in the spectrum.

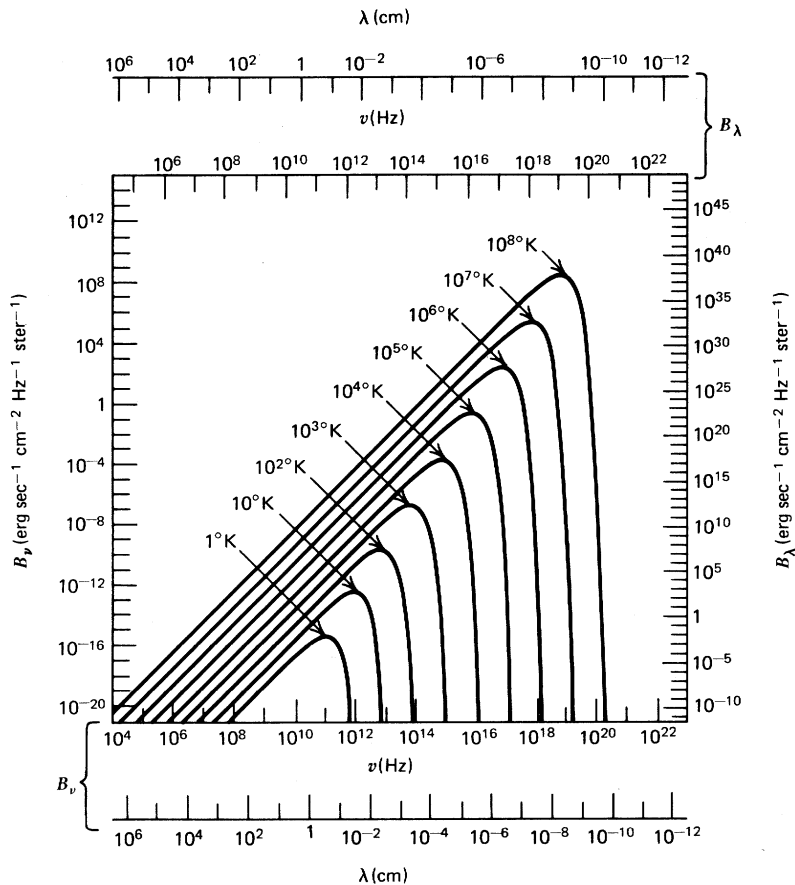


Figure 6.2: The Planck curve B_ν for different temperatures. Note that the peak frequency (Wien's displacement law) and the integral of B_ν (Stefan-Boltzmann's law) increase with temperature.

Rayleigh-Jeans approximation

For frequencies low enough to have $\hbar\nu/kT \ll 1$, the Planck function simplifies to the *Rayleigh-Jeans approximation*

$$B_\nu(T) \simeq \frac{2\nu^2 kT}{c^2} \quad (6.9)$$

This explains the linear parts at the left side of figure 6.2. The Rayleigh-Jeans approximation can almost always be applied in the radio regime.

Wien's approximation

For frequencies high enough to have $h\nu/kT \gg 1$, the Planck function simplifies to *Wien's approximation*

$$B_\nu(T) \simeq \frac{2h\nu^3}{c^2} e^{-h\nu/kT} \quad (6.10)$$

These are the steep parts at the right side of figure 6.2.

Stefan-Boltzmann's law

Integrating over the entire spectrum yields *Stefan-Boltzmann's law*

$$B \equiv \int_0^\infty B_\nu d\nu = \frac{\sigma}{\pi} T^4 \quad (6.11)$$

where

$$\sigma = \frac{2\pi^5 k^4}{15 h^3 c^2} = 5.66961 \times 10^{-5} \text{ erg cm}^{-2} \text{ K}^{-4} \text{ s}^{-1} \quad (6.12)$$

is Stefan-Boltzmann's constant.

Exercise 6.3

- a) Give the derivation of eq. (6.6) using eq. (6.4), and the relation (6.5)
- b) Show that $B_\nu \downarrow 0$ for $T \downarrow 0$, and that $B_\nu \uparrow \infty$ for $T \uparrow \infty \ \forall \nu$.
- c) Derive eq. (6.11) and the constant (6.12), given that

$$\int_0^\infty \frac{x^3}{e^x - 1} dx = \frac{\pi^4}{15} \quad (6.13)$$

Exercise 6.4

- a) The number of photons per cm^3 per Hz in a Planck radiation field is $n(\nu) = u_\nu/h\nu$, where u_ν (see eq. 3.12) is the energy density of the Planck radiation field. Show that the total number of photons per cm^3 in the Planck radiation field

$$n_{\text{tot}} = \frac{16\pi\zeta(3)k^3}{c^3h^3} T^3 \simeq 20 T^3 \quad (6.14)$$

given that

$$\int_0^\infty \frac{x^2}{e^x - 1} dx = 2\zeta(3) \quad (6.15)$$

where $\zeta(3) = 1.202057$ is Apéry's constant.

- b) Compute the mean energy per photon in a Planck radiation field.

6.4 Laws describing the material medium in TE

Maxwellian velocity distribution

The probability, in TE, that a particle of mass m and temperature T has a velocity on the range $(\mathbf{v}, \mathbf{v} + d\mathbf{v})$ is given by the *Maxwellian velocity distribution*

$$f(\mathbf{v}) dv_x dv_y dv_z = \left(\frac{m}{2\pi kT} \right)^{3/2} \exp \left[-m(v_x^2 + v_y^2 + v_z^2)/2kT \right] dv_x dv_y dv_z \quad (6.16)$$

For each component the spread in velocities is thus given by a Gauss distribution. In the x direction for instance

$$f(v_x) dv_x = \frac{1}{\sqrt{\pi}} \left(\frac{m}{2kT} \right)^{1/2} \exp \left[-mv_x^2/2kT \right] dv_x \quad (6.17)$$

The most probable velocity in the x direction is $v_x = 0$. The root-mean-square velocity in this direction is $\langle v_x^2 \rangle^{1/2} = (kT/m)^{1/2}$.

To find the probability distribution in terms of speed v we must integrate over all direction components. We find

$$f(v) dv = \left(\frac{m}{2\pi kT} \right)^{3/2} \exp \left[-mv^2/2kT \right] 4\pi v^2 dv \quad (6.18)$$

The dimensions of $f(v)$ are $\text{cm}^{-1} \text{ sec}$. It is not a Gauss distribution, but shows a “tail” as a result of the v^2 term (see figure 6.3). The most probable velocity in this distribution, i.e. the one for which $f(v)$ reaches a maximum, is $v = (2kT/m)^{1/2}$. The root-mean-square speed is

$$\langle v^2 \rangle^{1/2} = \left(\frac{3kT}{m} \right)^{1/2} = 15.793 \left(\frac{T}{10^4 A} \right)^{1/2} \text{ km s}^{-1} \quad (6.19)$$

where A is the atomic weight (in amu) of the particle.

If the Maxwellian velocity distribution is valid one speaks of *kinetic equilibrium* (KE). In almost all astrophysical media the free electrons are in KE. For this condition to be valid an electron that is ejected from an ion (for instance after a photoionization or a collisional ionization) needs to experience a large number of elastic collisions (usually with other electrons) before it suffers a non-elastic collision with an atom or ion. KE implies that the medium has a unique kinetic *electron temperature* T_e . Atoms and ions also fulfill the Maxwell velocity distribution. Their matching kinetic temperature will be almost identical to T_e if the density is not too low and the temperature is not too high. Only in very rarefied plasmas such as the solar corona, where $T > 10^6 \text{ K}$ and $n_e < 10^5 \text{ cm}^{-3}$, substantial differences between the two may occur.

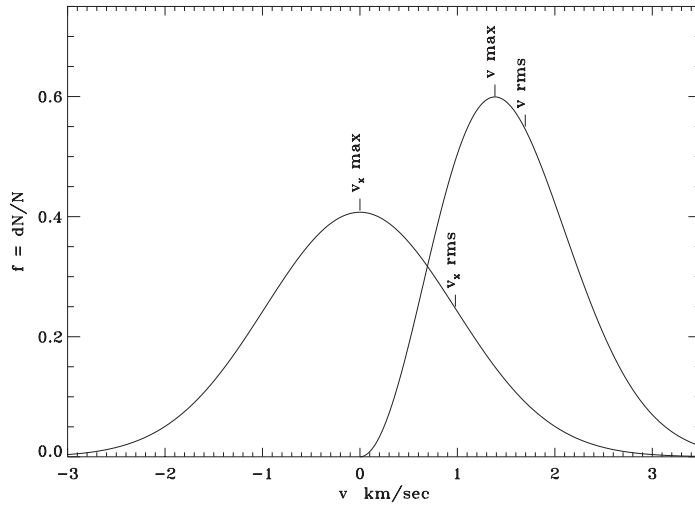


Figure 6.3: The Maxwellian velocity distribution for iron at a temperature of 6 000 K, both in terms of one of the velocity components (for instance the one in the line of sight) and in terms of the absolute velocity v ; v_{\max} indicates the most probable speed, and v_{rms} the root-mean-square velocity.

Exercise 6.5

- a) Derive eq. (6.18) from (6.16).
- b) Show that both distributions are normalized. Remember that

$$\int_{-\infty}^{+\infty} e^{-x^2/a^2} dx = a\sqrt{\pi} \quad \text{and} \quad \int_0^{+\infty} x^2 e^{-x^2/a^2} dx = a^3 \sqrt{\pi}/4 \quad (6.20)$$

- c) Show that the mean particle energy is given by

$$\langle \frac{1}{2}mv^2 \rangle = \frac{3}{2}kT \quad (6.21)$$

if we give that

$$\int_0^{+\infty} x^4 e^{-x^2/a^2} dx = \frac{3}{8}a^5\sqrt{\pi} \quad (6.22)$$

- d) Show that the most probable velocity of eq. (6.17) is given by $v_x = 0$ and of eq. (6.18) by $v = (2kT/m)^{1/2}$.

Boltzmann excitation equation

In TE the number density distribution of atoms, ions, or molecules over all discrete excitation states (the bound energy levels) is given by the *Boltzmann excitation equation*.

$$\frac{n_j}{n_i} = \frac{g_j}{g_i} \exp [-(E_j - E_i)/kT] = \frac{g_j}{g_i} \exp [-h\nu_{ij}/kT] \quad (6.23)$$

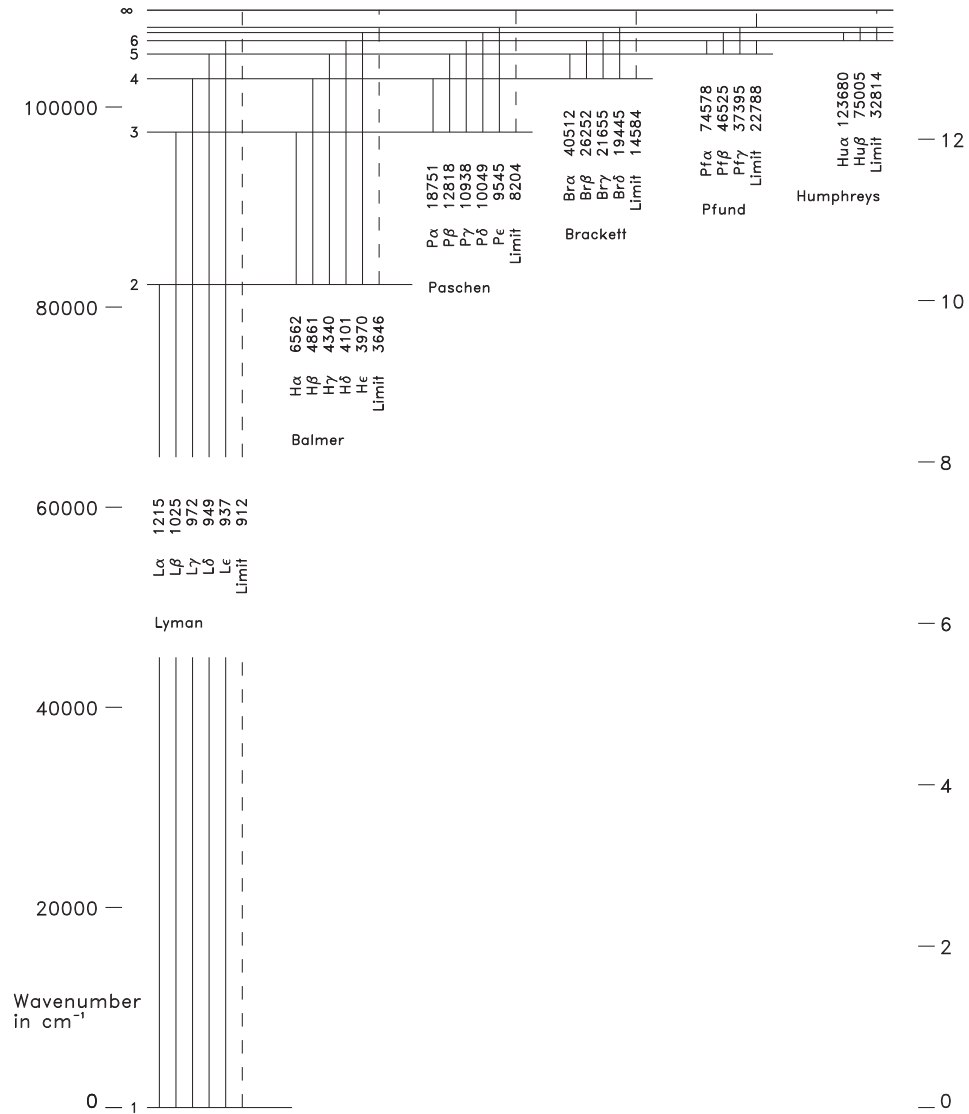


Figure 6.4: Schematic picture of the energy levels or Grotian diagram of hydrogen. See table 7.1 for addiation information.

Here n_i is the number density per cm^3 in level i ; g_i is the *statistical weight*; E_i the *excitation energy* in erg, and $\nu_{ij} = \Delta E_{ij}/h$ the frequency in Hz corresponding to the energy difference $\Delta E_{ij} = E_j - E_i$.

It is customary that within each ionization stage the excitation energy is measured from the

ground state up (see figure 6.4). The ionization energy is also measured per ionization stage from the ground state up. Usually one does not give the energy difference between levels in erg, but in electron volts (eV) or kayser (cm^{-1}). If we adopt the first unit one speaks of *excitation potential*. In this case $E_j[\text{erg}] = 1.602192 \cdot 10^{-12} E_j[\text{eV}]$ and $\Delta E_{ij}[\text{eV}] = 12\,398.54 / \lambda_{ij}[\text{\AA}]$. If we adopt the last unit the wavelength of the transition can trivially be recovered using $\lambda_{ij}[\text{\AA}] = 10^8 / (E_j[\text{cm}^{-1}] - E_i[\text{cm}^{-1}])$.

The Boltzmann equation can also be written as

$$\frac{n_i}{N} = \frac{g_i}{U(T)} \exp[-E_i/kT] \quad (6.24)$$

where $N = \sum_i n_i$ is the sum of populations over all levels, i.e. the total particle density per cm^3 of a given ionization stage, and $U(T)$ is the *partition function* of this ionization stage given by

$$U(T) \equiv \sum_i g_i \exp[-E_i/kT] \quad (6.25)$$

The above two equations are for instance used in traditional curve-of-growth analysis (see § 12.4).

Saha ionization equation

In TE the number density distribution over the ionization stages of an element is given by the *Saha ionization equation*

$$\begin{aligned} \frac{N_I}{N_{I+1}} &= n_e \frac{U_I}{2U_{I+1}} \left(\frac{h^2}{2\pi m_e k T} \right)^{3/2} \exp[E_I/kT] \\ &\equiv n_e \tilde{\Phi}_I(T) \end{aligned} \quad (6.26)$$

where n_e is the electron density per cm^3 and m_e the electron mass; N_I is the particle density of ions in ionization stage I ; U_I is the partition function of this ion; and E_I its ionization energy (in erg), i.e. the minimum energy required to liberate an electron from the ion. The factor 2 in front of the partition function U_{I+1} reflects the statistical weight of the liberated electron, that may have one out of two possible spin orientations.

If the temperature decreases at constant density (such that n_e remains more or less the same) the exponential term in the Saha ionization equation will make that N_I/N_{I+1} goes up, i.e. the medium *recombines*. If the density decreases at constant temperature n_e (more or less proportional to ρ) will decrease and therefore also N_I/N_{I+1} , i.e. the medium *ionizes*.

In many cases the particle density of the ground level $i = 0$ will dominate the particle density of the ion I , i.e. $N_I = \sum n_{i,I} \simeq n_{0,I}$. The Saha equation for ground levels only is given by

$$\frac{n_{0,I}}{n_{0,I+1}} = n_e \frac{g_{0,I}}{2g_{0,I+1}} \left(\frac{h^2}{2\pi m_e k T} \right)^{3/2} \exp[E_I/kT] \quad (6.27)$$

Finally, we may express the particle density n_i in terms of the particle density of the ground level of ion $I + 1$ and the electron density by substitution of eq. (6.23) in (6.27). This gives

$$\begin{aligned} n_{i,I} &= n_{0,I+1} n_e \frac{g_{i,I}}{2g_{0,I+1}} \left(\frac{\hbar^2}{2\pi m_e k T} \right)^{3/2} \exp [(E_I - E_i)/kT] \\ &\equiv n_{0,I+1} n_e \Phi_{iI}(T) \end{aligned} \quad (6.28)$$

This is the *Saha-Boltzmann equation* or *equation of state* (EOS) of a gas in TE or LTE. In the latter case one should use the local values for T and density (see section 6.5). The equation can also be used to *define* LTE particle densities in a NLTE medium, i.e. using the values for $n_{0,I+1}$ and n_e that follow from statistical equilibrium (see eq. 9.15). Deviations from LTE can thus be described by the *NLTE departure coefficient*

$$b_{i,I} \equiv \frac{n_{i,I}}{n_{i,I}^{\text{LTE}}} \quad (6.29)$$

in which $n_{i,I}^{\text{LTE}}$ is given by eq. (6.28). Henceforth we will denote LTE values of the level populations with a superscript * (and not with LTE). However, we will do so only if this is required in the context of the discussion (if not, no superscript is used).

6.5 The TE equation of state for an ionized gas

Using the Saha-Boltzmann relation we may determine for each element the number densities of all ionization stages, and its contribution to the number of free electrons in the plasma. Different elements will have widely different ionization energies; some will be neutral under given conditions, others will be singly or multiply ionized. For increasing temperature the transition from one to the next ionization stage is usually rather abrupt. This yields a sensitive diagnostic for the temperature (structure) of the medium, as it implies that the ratios in line strength of two successive ions (for instance He I & II, or Ca I & II) will rapidly change as a function of temperature (see § 2.1). Fundamental work in this field has been done at the start of the previous century by, among others, Saha, Anton Pannekoek , and Fowler & Milne (see figure 6.5).

In a normal stellar atmosphere hydrogen is by far the most abundant element, followed by helium ($N_{\text{He}}/N_{\text{H}} \sim 0.1$). The heavier elements have far smaller abundances (see table 15.2). In the solar atmosphere, which has a temperature of about 6 000 K, hydrogen is almost completely neutral. Free electrons mainly originate from “metals” such as Na, Mg, Al, Si, Ca, en Fe. At temperatures characteristic for A-type stars (10 000 K) hydrogen starts to ionize and becomes the dominant source of free electrons. At very high temperatures, typically for O- and B-type stars, also helium gets ionized and will contribute noticeably to the electron density.

In this section we will describe how the state of the gas in TE can be determined from the values of the temperature T and the total particle density N , or equivalently, from the total gas pressure p and the electron density n_e .

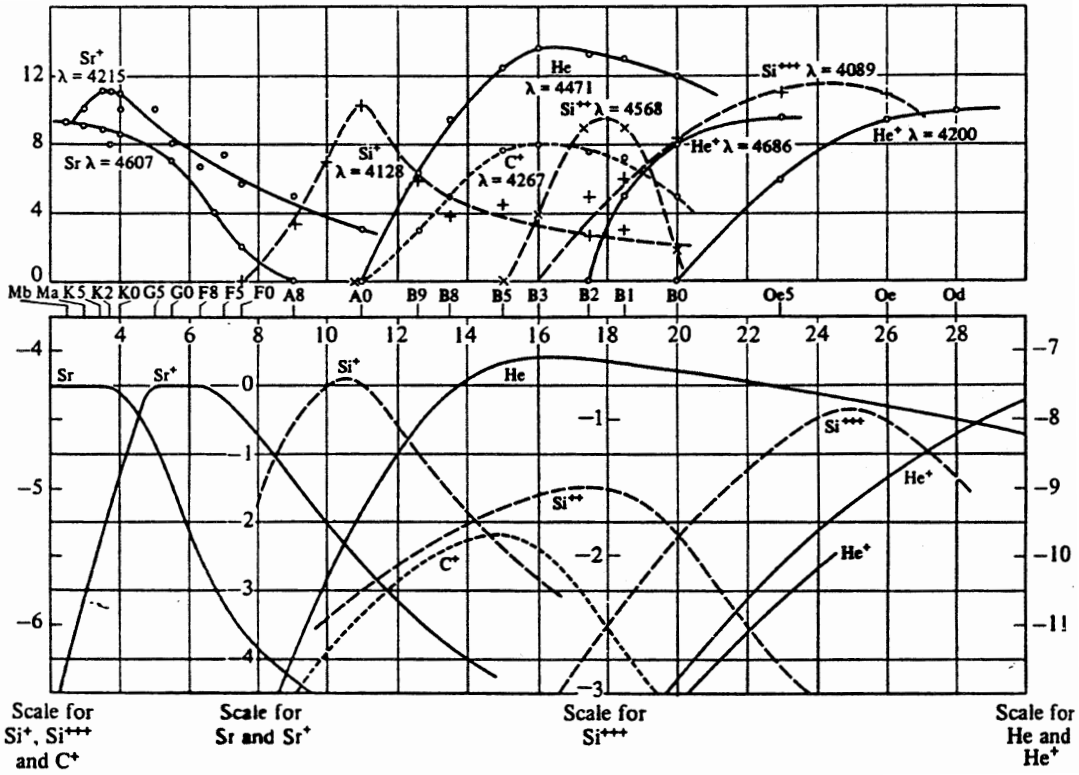


Figure 6.5: The link between the spectral classification and the ionization of a gas in TE. Top: estimates (by eye, from photographic plates) of the strength of representative spectral lines as a function of the heuristically introduced spectral type. Bottom: ionization fractions for $p_e = 131 \text{ dyne cm}^{-2}$. After Payne.

Ideal gas law

As we will show in chapter 9 the total gas pressure is an important quantity in the description of a stellar atmosphere. If we assume that the gas is *ideal*, i.e. that there are no forces at work among the particles themselves – which is in almost all cases a valid assumption – then the gas pressure p and temperature T are related to the total particle number density N in the gas as (see also eq. 9.30)

$$p = NkT \quad (6.30)$$

The total particle number density itself is the sum of all atoms, ions, and free electrons

$$N = N_{\text{atoms}} + N_{\text{ions}} + n_e = N_N + n_e \quad (6.31)$$

where N_N is the number density of nuclei.

Particle and charge conservation

If we define the *abundance* or *number abundance* A_k of a chemical element k as

$$N_k = A_k N_N \quad \text{where} \quad \sum_k A_k \equiv 1 \quad \text{such that} \quad \sum_k N_k = N_N \quad (6.32)$$

then either the last equality of the above equation, or

$$N_k = A_k (N - n_e) \quad (6.33)$$

summarizes the constraint of *particle conservation*.

We will also require that the plasma is electrically neutral. In order for this to hold the total charge of the free electrons must be equal to the total ionic charge, i.e.

$$n_e = \sum_k \sum_{j=1}^{J_k} j N_{jk} = \sum_k N_k \sum_{j=1}^{J_k} j q_{jk}(n_e, T) = (N - n_e) \sum_k A_k \sum_{j=1}^{J_k} j q_{jk}(n_e, T) \quad (6.34)$$

where for each element we start the summation over ionization stages at $j = 1$, as the neutral atom $j = 0$ does not yield any free electrons, and end at the maximum ionization J_k . Note that we have changed the index label of the ionization stages from I to j . Equation (6.34) defines the condition of *charge conservation*. In this condition the *ionization fraction* $q_{jk} \equiv (N_{jk}/N_k)$ gives the fraction of atoms of element k in ionization stage j relative to the total number of atoms of species k .

In TE

$$\begin{aligned} q_{jk} &\equiv (N_{jk}/N_k)^* \\ &= \frac{(N_{jk}/N_{j+1,k})^* \cdots (N_{J-1,k}/N_{Jk})^*}{(N_{0k}/N_{1k})^* \cdots (N_{J-1,k}/N_{Jk})^* + (N_{J-2,k}/N_{J-1,k})^* (N_{J-1,k}/N_{Jk})^* + (N_{J-1,k}/N_{Jk})^* + 1} \\ &= \prod_{l=j}^{J_k-1} \left[n_e \tilde{\Phi}_{lk}(T) \right] / \sum_{m=0}^{J_k} \prod_{l=m}^{J_k-1} \left[n_e \tilde{\Phi}_{lk}(T) \right] \\ &\equiv P_{jk}(n_e, T) / S_k(n_e, T), \quad (j = 1, \dots, J_k) \end{aligned} \quad (6.35)$$

Note that the product term for $l = J_k$, which formally is not defined, is substituted by 1 in both the numerator and denominator. If we know (n_e, T) , we may compute all q_{jk} 's and also, using eq. (6.34), N .

A pure hydrogen gas

For a pure hydrogen gas the system of equations (6.26), (6.33), and (6.34) may be solved analytically to obtain

$$n_e(N, T) = \left[\left(N \tilde{\Phi}_H(T) + 1 \right)^{1/2} - 1 \right] / \tilde{\Phi}_H(T) \quad (6.36)$$

For an increasing density the ionization at constant temperature will decrease as the recombination rate increases as $N^+ n_e$, while the ionization only scales with N^0 (see § 8.1).

General solution for the ionization of a gas in TE

In the general case the problem of determining n_e in a gas in TE, for given values of N and T requires an *iterative linearization procedure*. We will describe this procedure in fair detail because it is a simple example of the approach taken in more complicated problems in stellar atmospheres.

In a multi-dimensional linear perturbation or *Newton-Raphson* method we start with an initial estimate $\mathbf{x}^\circ = (x_1^\circ, \dots, x_n^\circ)$. This is likely not the correct answer to our problem, therefore we assume that the true solution is given by a linear expansion $\mathbf{x} = \mathbf{x}^\circ + \delta\mathbf{x}^\circ$ where $\delta\mathbf{x}^\circ$ is to be determined in such a way as to satisfy exactly the equation at hand. In other words, we if we seek the solution of the problem $f(\mathbf{x}) = 0$, we assume that

$$f(\mathbf{x}^\circ) + \sum_{i=1}^n \frac{\partial f}{\partial x_i} \Big|_{\mathbf{x}^\circ} \delta x_i^\circ = 0 \quad (6.37)$$

Because the equation is nonlinear, we cannot determine the exact value of this $\delta\mathbf{x}^\circ$, but need to start an iteration procedure in which we use $\mathbf{x}^\circ(\text{new}) = \mathbf{x}^\circ(\text{old}) + \delta\mathbf{x}^\circ$ to update the value of $\delta\mathbf{x}^\circ$. The convergence of this procedure is quadratic (if our original estimate lies within the range of convergence) and one can obtain the result to within the desired accuracy quickly.

The only equation we need to solve by linearization is eq. (6.34), where the ionization fractions $q_{jk}(n_e, T)$ are given by (6.35). First order perturbation of both sides gives

$$\begin{aligned} n_e + \delta n_e &\approx (N - n_e^\circ) \tilde{\Sigma}(n_e^\circ, T) + \tilde{\Sigma}(n_e^\circ, T) \left. \frac{\partial(N - n_e)}{\partial n_e} \right|_{n_e^\circ} \delta n_e + (N - n_e^\circ) \left. \frac{\partial \tilde{\Sigma}}{\partial n_e} \right|_{n_e^\circ} \delta n_e \\ &= (N - n_e^\circ - \delta n_e) \tilde{\Sigma}(n_e^\circ, T) + (N - n_e^\circ) \left. \frac{\partial \tilde{\Sigma}}{\partial n_e} \right|_{n_e^\circ} \delta n_e \end{aligned} \quad (6.38)$$

such that

$$\delta n_e \approx \left[(N - n_e^\circ) \tilde{\Sigma} - n_e^\circ \right] \left[1 + \tilde{\Sigma} - (N - n_e^\circ) \left(\partial \tilde{\Sigma} / \partial n_e \right) \right]^{-1} \quad (6.39)$$

where

$$\tilde{\Sigma}(n_e^\circ, T) \equiv \sum_k A_k S_k^{-1}(n_e^\circ, T) \sum_{j=1}^{J_k} j P_{jk}(n_e^\circ, T) \quad (6.40)$$

The derivative $\partial \tilde{\Sigma} / \partial n_e$ can be obtained analytically

$$\frac{\partial \tilde{\Sigma}}{\partial n_e} = \sum_k A_k \left[S_k^{-1} \sum_j^{J_k} j \frac{\partial P_{jk}}{\partial n_e} - S_k^{-2} \frac{\partial S_k}{\partial n_e} \sum_j^{J_k} j P_{jk} \right] \quad (6.41)$$

where $(\partial P_{jk}/\partial n_e)$ and $(\partial S_k/\partial n_e)$ are easily determined if one considers that

$$P_{jk}(n_e, T) \equiv \prod_{l=j}^{J_k-1} [n_e \tilde{\Phi}_{lk}(T)] = n_e^{(J_k-j)} \Pi_{jk}(T) \quad (6.42)$$

and

$$S_k(n_e, T) \equiv \sum_{j=0}^{J_k} P_{jk}(n_e, T) = \sum_{j=0}^{J_k} n_e^{(J_k-j)} \Pi_{jk}(T) \quad (6.43)$$

The derivatives that occur in a linearization procedure can always be determined numerically. However, in quite some cases they can also be derived analytically. The latter is the preferred way to go as experience teaches that this way one has more “control” over the computation.

— — —

Finally, after one has obtained n_e using the above procedure, and, as a by-product all ionization fractions q_{jk} , one may calculate all desired number particle densities from (for instance) Boltzmann equation (6.24). From $N_{jk} = q_{jk} A_k (N - n_e)$ one gets

$$n_{ijk} = \frac{g_{ijk}}{U_{jk}(T)} \exp[-E_{ijk}/kT] q_{jk}(n_e, T) A_k (N - n_e) \quad (6.44)$$

This completes the calculation of the TE equation of state for an ionized gas.

Exercise 6.6

Show that the ideal gas law eq. (6.30) is equivalent to (see also eq. 9.30)

$$p = \frac{\mathcal{R}\rho T}{\mu},$$

where ρ is the density, $\mathcal{R} \equiv k/m_{\text{amu}} = 8.314 \times 10^7 \text{ erg K}^{-1} \text{ mol}^{-1}$ is the gas constant, and μ is the mean mass in atomic mass units m_{amu} of the N (free) particles.

Exercise 6.7

- a) Show that for a pure hydrogen gas in TE the analytical solution of the electron density in terms of N_H and T is given by

$$n_e(N_H, T) = \left[\left(4N_H \tilde{\Phi}_H(T) + 1 \right)^{1/2} - 1 \right] / 2\tilde{\Phi}_H(T), \quad (6.45)$$

where $N_H = N_N = N^0 + N^+ = N - n_e$.

- b) Show that in the general case, i.e. for any atomic gas in TE, the perturbation term δn_e in terms of N_N and T is given by

$$\delta n_e = \left[N_N \tilde{\Sigma} - n_e^\circ \right] \left[1 - N_N \left(\partial \tilde{\Sigma} / \partial n_e \right) \right]^{-1}. \quad (6.46)$$

6.6 Temperature definitions

Based on the above discussions we may define five characteristic temperatures that are often used in astrophysics. The first two are related to the Planck function; the next two to the equations of Boltzmann and Saha, and the final one to the total flux. We conclude with briefly introducing the antenna temperature.

Brightness temperature

The *brightness temperature* T_b is the temperature for which the Planck function, at the frequency at which is measured, reproduces the observed specific intensity

$$I_\nu^{\text{obs}} = B_\nu(T_b) \quad (6.47)$$

The brightness temperature is often used in radio astronomy, where in most cases the Rayleigh-Jeans approximation is valid such that

$$T_b \equiv \frac{h\nu/k}{\ln [1 + 2h\nu^3/c^2 I_\nu^{\text{obs}}]} \simeq \frac{c^2}{2\nu^2 k} I_\nu^{\text{obs}} \quad (6.48)$$

In general T_b will depend on frequency. Only if the source emits a blackbody spectrum T_b will be the same for all frequencies.

If we consider a medium at a constant temperature T that emits according to the Planck function, the solution of the equation of transfer (vgl. 4.43) is

$$T_b(0) = T_b(\tau_\nu) e^{-\tau_\nu} + T [1 - e^{-\tau_\nu}] \quad \forall \frac{h\nu}{kT} \ll 1 \quad (6.49)$$

For large optical depth in the medium the brightness temperature will be equal to the temperature of the material, i.e. $T_b(0) = T$.

Color temperature

The *color temperature* T_c is the temperature for which the Planck function, at the frequency ν_0 at which is measured, reproduces the slope of the observed spectrum

$$\left. \frac{dI_\nu^{\text{obs}}}{d\nu} \right|_{\nu_0} = \left. \frac{dB_\nu(T_c)}{d\nu} \right|_{\nu_0} \quad (6.50)$$

Often the shape of a (part of the) observed stellar spectrum more or less resembles that of a Planck curve. However stars are not spatially resolved (save for the sun and a few nearby supergiants) such that only the flux can be observed. Therefore, flux is what is commonly

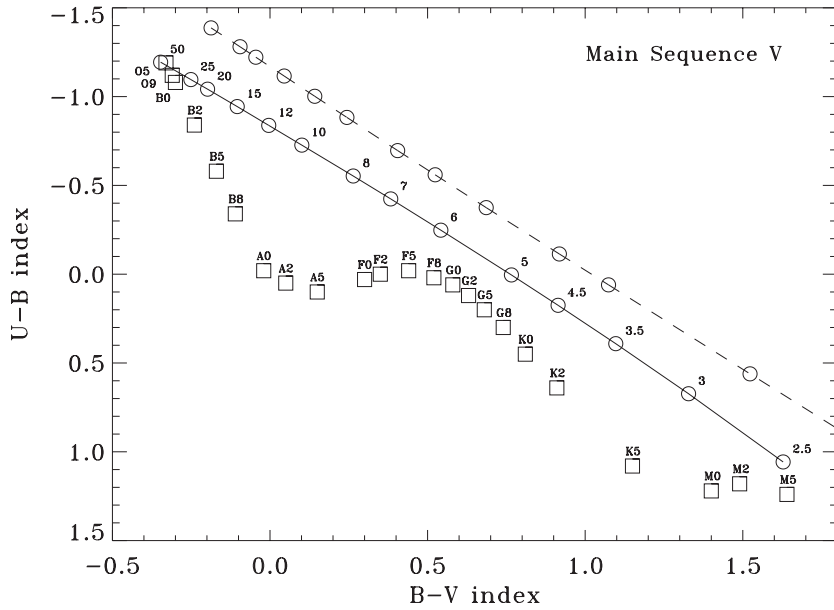


Figure 6.6: Relation between the color indices $U-B$ and $B-V$, assuming the flux distribution of the star is given by the Planck function (solid line). If one does not convolve with the proper response functions, but adopts a peaked profile at the centre wavelength of the filter, one obtains monochromatic values for the color indices (dashed line).

used. In everyday life a number of apparent magnitudes m is measured, as discussed in § 2.6, from which colors are composed. The $B-V$ color, for instance, follows from

$$B-V = -2.5 \log \left[\frac{\int_0^\infty \mathcal{F}_\nu(d) \mathcal{S}_B(\nu) d\nu}{\int_0^\infty \mathcal{F}_\nu(d) \mathcal{S}_V(\nu) d\nu} \right] + 2.5(C_B - C_V) \quad (6.51)$$

where $\mathcal{F}_\nu(d)$ is the stellar flux at the location of the earth, and \mathcal{S}_m has the meaning as given in § 2.6. In figure 6.6 the $U-B$ vs. $B-V$ diagram for the MK spectral types is repeated (see also figure 2.11). Also given is the result of equation 6.51 assuming a Planck curve for the radiation field (solid line). Note that the $U-B$ vs. $B-V$ dependence is almost linear, and that it does not agree very well with the relation given by the MK calibration. The reason for the difference, obviously, is that a real star emits a spectrum that deviates from the Planck curve. Especially the Balmer jump has a strong influence on the U magnitude, therefore on $U-B$.

For a simple estimate of the values of the color indices using the Planck function we assume that the UBV respons functions can be replaced by δ functions at 3600, 4400, and 5500 Å, respectively. Using the constants C_U , C_B , and C_V as given in table 2.2 (Landolt-Börnstein 1982) we get for the colors of the Planck-curves

$$B-V = -2.5 \log \left[\frac{B_B}{B_V} \right] + 0.22 \quad \text{en} \quad U-B = -2.5 \log \left[\frac{B_U}{B_B} \right] - 1.04 \quad (6.52)$$

For this result figure 6.6 also gives the relation between $U-B$ and $B-V$ (dashed line). Because now we did not convolve with the respons functions \mathcal{S}_m the relation differs from the solid line.

Excitation temperature

The excitation temperature is determined by comparison of observed level populations of an atom, ion, or molecule, using the Boltzmann equation (eq 6.23). Obviously, the measured populations need not be in LTE. To conserve a description of the measured population ratios in terms of the Boltzmann equation, we introduce the excitation temperature T_{ext} . This temperature is given by

$$\left(\frac{n_j}{n_i}\right)^{\text{obs}} = \frac{b_j}{b_i} \frac{n_j^*}{n_i^*} = \frac{b_j}{b_i} \frac{g_j}{g_i} \exp[-h\nu_{ij}/kT] \equiv \frac{g_j}{g_i} \exp[-h\nu_{ij}/kT_{\text{ext}}} \quad (6.53)$$

If $b_u/b_l = 1$, such as is the case in LTE, then $T = T_{\text{ext}}$. The excitation temperature can be determined from measurements of the equivalent width of two spectral lines (see e.g. § 12.4). The derived value of the excitation temperature can be rather ambiguous. Even for different line pairs of the same ion the excitation temperatures may differ significantly. Sometimes this is due to uncertainties in the oscillator strength (see § 7.3). More often it is because lines may form in different regions of the atmosphere, where temperatures and/or departures from LTE may be different. The excitation temperatures derived from molecular lines (in cool stellar atmospheres) are usually lower than those found from lines of atomic or ionized gas. This is so because molecular lines typically originate in higher atmospheric layers, where T is relatively low.

Ionization temperature

In analogy to the excitation temperature, the *ionization temperature* is the temperature for which an observed ionization ratio fulfills the Saha equation (eq. 6.26)

$$\left(\frac{N_I}{N_{I+1}}\right)^{\text{obs}} \equiv n_e \frac{U_I}{2U_{I+1}} \left(\frac{h^2}{2\pi m_e k T_{\text{ion}}}\right)^{3/2} \exp[E_I/k T_{\text{ion}}] = n_e \tilde{\Phi}_I(T_{\text{ion}}) \quad (6.54)$$

This temperature can only be determined if the electron density n_e is known. In LTE it holds that $T = T_{\text{ion}}$.

Effective temperature

The *effective temperature* T_{eff} of a source is a measure of the total flux emitted by that source.

$$\mathcal{F}_{\text{source}}^+ = \sigma T_{\text{eff}}^4 \quad (6.55)$$

So, it is the temperature that an isotropic black surface should have such that the total outward directed flux $\mathcal{F}^+ = \pi B = \pi \int_0^\infty B_\nu d\nu$, per cm^2 , is equal to the flux emitted by the source, again per cm^2 .

Antenna temperature

Sub-millimeter and radio astronomers often use the concept of an antenna temperature. The motions of charged particles in a resistor in an electrical circuit cause the resistor to generate noise and to reach a certain temperature. The frequency spectrum of the power of this noise only depends on the temperature of the resistor (and not, for instance, on the material of which the resistor is made). So, by equating the power the antenna is receiving to the temperature of a resistor that is connected to the antenna by power lines one can measure the antenna temperature.

We assume the effective surface of the antenna to be $A_{\text{eff}} \text{ cm}^2$. The definition of the flux (see section 3.4) tells us that we receive a power $P_\nu = \mathcal{F}_\nu A_{\text{eff}}$ from the source. Radio receivers, for instance a dipole antenna, are typically sensitive to only one polarization direction. Therefore, only part of the total power incident to the effective surface is measured. For an unpolarized electromagnetic wave $E(\omega) = E_0 e^{i\omega t}$ the flux scales with the square of the strength of the electrical field. For the mean power of the polarization component $E(\omega) = E_0 \cos \omega$ it then follows that:

$$\langle P_\nu \rangle \propto \langle \cos^2 \omega \rangle = \frac{1}{2\pi} \int_0^{2\pi} \cos^2 \omega d\omega = \frac{1}{2\pi} \left[\frac{\omega}{2} + \frac{1}{4} \sin 2\omega \right]_0^{2\pi} = \frac{1}{2} \quad (6.56)$$

The power absorbed by the antenna is thus given by $P_\nu = 1/2 A_{\text{eff}} \mathcal{F}_\nu$.

For the power that flows through the transmission wire, as well as the noise that is generated in the resistor, one finds analogues to Planck's law¹

$$P_\nu = \frac{h\nu}{e^{h\nu/kT} - 1} \quad (6.57)$$

In the Rayleigh-Jeans limit it follows that $P_\nu = kT$. This is *Nyquist's law*, stating that a resistor at temperature T produces a noise of which the power per unit bandwidth is kT . Equating this to the power that is received from the source leads to an antenna temperature

$$T_A = \frac{\mathcal{F}_\nu A_{\text{eff}}}{2k}. \quad (6.58)$$

This result connects the flux of radiation from the source to an antenna temperature using the effective surface of the telescope.

To establish a relation between the antenna temperature and the physically more relevant brightness temperature we use relation 3.23, where we assume that the solid angle $d\omega$ observed of (part of) the source emits an isotropic radiation field I_ν . This leads to

$$T_A = \frac{A_{\text{eff}}}{\lambda^2} T_b d\omega. \quad (6.59)$$

¹This result follows from a one-dimensional consideration of what leads to the Planck function in three dimensions.

Exercise 6.8

- a) Does the brightness temperature of a radio source depend on its distance?
- b) Can one measure the brightness temperature of a point source (i.e. an object that is not spatially resolved) such as a star? Can one measure T_b for an extended source, such as a nebula, if this source is not in TE?

Exercise 6.9

What requirements have to be fulfilled in order to obtain the stellar temperature from two-color photometry? For which layer of the star would this temperature be representative?

Exercise 6.10

The displacement law of Wien (eq. 6.7) can also be used to derive the temperature of a star. Which characteristic temperature does this give: T_b , T_c or T_{eff} ?

6.7 Approximations in describing the interaction of matter and radiation

Local thermodynamic equilibrium (LTE)

In a medium in LTE the material medium can be described using the equations of Maxwell, Boltzmann and Saha, using the local values of $\rho(\mathbf{r})$ en $T(\mathbf{r})$. However, the radiation field is not in equilibrium, i.e. it may deviate from the Planck function. LTE is an often applied generalization of TE (see chapter 11).

In LTE the assumption of detailed balance in all microscopic processes is still valid (see chapters 7 and 8). An important consequence is that the source function that is ascribed to each process is still given by the Kirchhoff-Planck relation (eq. 6.3), i.e.

$$S_\nu(\mathbf{r}) = B_\nu(T(\mathbf{r})) \quad (6.60)$$

An example of a source function for which this relation holds is the *line source function* S_ν^ℓ that describes the microscopic transition between two bound energy levels (see § 7.3). Also the source functions of bound-free and free-free continuum processes (see chapter 8) are given by Kirchhoff-Planck. In these continuum processes energy is either added to or taken away from the local thermal energy pool of the medium. These source functions are therefore referred

to as *thermal source functions*. A process in LTE that can not be described by eq. (6.60) is that of *scattering*. This is to be expected as the mean intensity $J_\nu(\mathbf{r})$ – the relevant radiation quantity if we assume that the scattering process is isotropic – can deviate from the local emitted thermal radiation field $B_\nu(T(\mathbf{r}))$.

In summary: in LTE

$$n_{ijk} = n_{ijk}(\rho(\mathbf{r}), T(\mathbf{r})) \quad (6.61)$$

and

$$S_\nu^\ell(\mathbf{r}) = B_\nu(T(\mathbf{r})) \quad I_\nu(\mathbf{r}, \mathbf{n}) \neq B_\nu(T(\mathbf{r})) \quad J_\nu(\mathbf{r}) \neq B_\nu(T(\mathbf{r})) \quad \mathcal{F}_\nu(\mathbf{r}) \neq 0 \quad (6.62)$$

The first equality implies that also *complete redistribution* applies (see §§ 7.1 and 7.3).

The essence of LTE is that of the two types of processes that determine the state of the material medium, i.e. the collisionally controlled “true” absorption and emission processes on the one hand and the scattering processes on the other hand, it is the collisional processes that dominate. Phrased differently: the mean-free-path of photons for absorption $\ell_\nu = 1/\kappa_\nu$ is smaller than the mean-free-path for scattering $\ell_\nu = 1/\sigma_\nu$ (see eq. 4.26). According to the assumptions that define LTE the state of the material medium is determined by such a small TE-volume $V(\mathbf{r})$ that the fact that the temperature and density elsewhere in the medium may be different is not noticed by the excitation and ionization state of the gas in $V(\mathbf{r})$. Still, the radiation that is present in this volume does contain information about far away regions. However, the photons in the radiation field that have been created elsewhere and have reached \mathbf{r} directly or through scattering do not bring enough information about these far away places to push the number populations of the energy levels out of equilibrium.

Non-local thermodynamic equilibrium (NLTE)

NLTE is per definition a state that deviates from LTE. In NLTE the state of the particles at position \mathbf{r} is no longer controlled only by the local values of density and temperature but will also depend on the radiation field $J_\nu(\mathbf{r})$, i.e.

$$n_{ijk} = n_{ijk}(\rho(\mathbf{r}), T(\mathbf{r}), J_\nu(\mathbf{r})) \quad (6.63)$$

Departures from LTE typically occur if

- the particle densities are low, such that collisional processes will no longer dominate over scattering processes and photon conversion processes (see § 4.1), and, *in addition*
- the radiation field strongly deviates from the local Planck function, i.e. $J_\nu(\mathbf{r}) \neq B_\nu(T(\mathbf{r}))$.

The exact assumptions that enter in NLTE are not formally defined. Usually it is implied that *statistical equilibrium* is valid (see § 9.1); that the Maxwell velocity distribution holds, and that complete redistribution applies. The level occupation numbers may deviate from the local

Saha-Boltzmann values. The extinction coefficient may differ from the LTE value and the line source function may differ from the Planck function.

Exercise 6.11

Equilibrium	$F_V = 0$	$S_V^{\text{tot}} = B_V$	$S_V^{\text{th}} = B_V$	$S_V^{\text{line}} = B_V$	Maxwell	Saha Boltzmann
TE						
LTE						
NLTE						

Use the table to fill in – with a simple yes or no – whether for each of the three equilibria (TE, LTE, or NLTE) it holds that

- a) the flux is equal to zero;
- b) the total (i.e. continuum + line) source function is equal to the Planck function B_ν ;
- c) the thermal source function is equal to B_ν ;
- d) the line source functions are equal to B_ν ;
- e) the velocity distribution of the free electrons is equal to the Maxwell distribution
- f) the excitation and ionization equilibria are given by the equations of Boltzmann and Saha.

Discrete processes

So far we have given a macroscopic description of emission and extinction processes. In this chapter we focus on a microscopic specification. Between two energy levels five different processes may occur

1. *spontaneous radiative de-excitations*
requires: nothing
2. *radiative excitations*
requires: photon of the right energy
3. *induced radiative de-excitations*
requires: photon of the right energy
4. *collisional excitations*
requires: passing particle with sufficient energy
5. *collisional de-excitations*
requires: passing particle

These processes take place between bound-bound (or bb) transitions as well as between bound-free (or bf) and free-free (or ff) transitions. More general, they occur in any system in which an exchange between internal energy and radiation is possible. So in all systems in which energy states can be defined, either discretely or continuously distributed over energy.

In this chapter we will examine these five processes for the bound-bound transitions between discrete energy levels. There are several types of such discrete states. We will mainly discuss the energy levels in the electron configuration of atoms and ions. Examples of other systems that have energy levels are *i*) shared electron configurations of molecules; *ii*) rotation of atoms in molecules; *iii*) vibration of atoms in molecules; *iv*) vibrations in the lattice structure of solid state particles; and *v*) hadron configurations of atomic nuclei.

The nature of these configurations and the selection rules that apply for them, and that follow from Pauli's exclusion principle for fermions, will not be treated here.

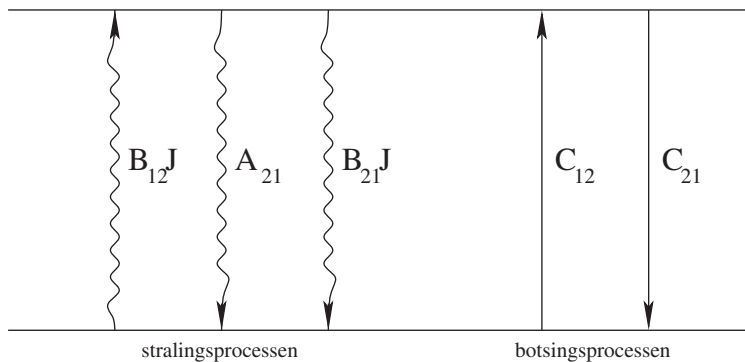


Figure 7.1: Schematic overview of the five possible bound-bound transitions between two energy levels.

7.1 From a macroscopic toward a microscopic description

Spontaneous radiative de-excitation

In a *spontaneous radiative de-excitation* or *spontaneous emission* a particle in an excited energy state u (*upper*) returns spontaneously to a lower energy state l (*lower*) by emitting a photon. The probability for this process to occur is defined by the *Einstein coefficient for spontaneous emission* A_{ul} . The dimension of A_{ul} is sec^{-1} . This transition probability is an atomic parameter and does not depend on the properties of the medium in which the atom or ion is embedded (such as pressure, temperature, or radiation field), but is determined solely by the nature of the transition.

The number of spontaneous de-excitations in $\text{cm}^{-3} \text{ sec}^{-1}$ is given by

$$n_u R_{ul} = n_u A_{ul} \int \psi_\nu d\nu = n_u A_{ul} \quad (7.1)$$

where n_u is the number density of particles in level u in cm^{-3} and ψ_ν de normalized profile function for spontaneous emission (see below for some discussion on the profile function). R_{ul} is the rate for spontaneous de-excitation in sec^{-1} .

Radiative excitation

In a *radiative excitation* or *photoexcitation* a particle in energy state l is excited to a higher energy state u after absorption of a photon. The probability for this process to occur depends on atomic properties, denoted by B_{lu} , as well as on the number of available photons of suitable frequency.

Due to some lack of sharpness of the energy levels, a certain spread in the energy that is required to induce the transition is present. We therefore introduce the *profile function* for excitation ϕ_ν of which the dimension is hz^{-1} , that describes this allowed spread in frequency (see § 12.2). This function is sharply peaked around the central frequency $\nu_{lu} = (E_u - E_l)/h$. The profile function is normalized such that

$$\int_0^\infty \phi(\nu) d\nu \equiv 1 \quad (7.2)$$

The number of radiative excitations in $\text{cm}^{-3} \text{ sec}^{-1}$ is given by

$$n_l R_{lu} = n_l B_{lu} \int \phi_\nu J_\nu d\nu \equiv n_l B_{lu} \bar{J}_{lu} \quad (7.3)$$

where n_l is the number density of particles in level l in cm^{-3} ; B_{lu} is the *Einstein coefficient for extinction* in $\text{erg}^{-1} \text{ cm}^2 \text{ hz}$, and \bar{J}_{lu} is the integral of the mean intensity over the profile function of the transition. Note that the mean intensity is here the relevant radiation quantity: the particles are only interested in the total number of suitable photons, and not in the direction from which these photons arrive.

Induced radiative de-excitation

For Einstein to be able to derive the radiation formula of Planck he introduced a third radiative process, that of *induced de-excitation* or *stimulated emission*. In this process an incident radiation field triggers an emission, such that a particle in an excited state u returns to a lower energy state l .

The number of induced radiative de-excitations in $\text{cm}^{-3} \text{ sec}^{-1}$ is given by

$$n_u R_{ul} = n_u B_{ul} \int \varphi_\nu J_\nu d\nu \equiv n_u B_{ul} \bar{J}_{ul} \quad (7.4)$$

where B_{ul} is the *Einstein coefficient for stimulated emission*, and φ_ν is the profile function for induced de-excitation. In TE ϕ_ν , ψ_ν and φ_ν are identical as in that case detailed balance is valid, which applies for each frequency separately. In less strict circumstances this need not be the case. If, however, there is *no* correlation between the frequency of the incident photon (the one that causes the excitation) and that of the emitted photon (the one that is emitted by the induced de-excitation), then $\phi_\nu = \varphi_\nu (= \psi_\nu)$ therefore $\bar{J}_{lu} = \bar{J}_{ul}$. This situation is known as *complete redistribution* and it is justified if the atoms/ions in a gas are so strongly perturbed by collisions during the excitation/emission process that the excited electrons are randomly redistributed over the substates of the upper level of the transition.

The photons that are emitted in induced radiative de-excitations have the same direction as do the incident photons that trigger the process.

Collisional excitation

In a gas (consisting of atoms, ions, and electrons) of sufficient density a variety of collisions will occur, which may cause excitations and ionization. As soon as the gas is somewhat ionized, collisions of ions with charged particles will dominate over collisions with neutral particles. This is because the Coulomb interaction reaches much further than does the Van der Waals interaction. As a rule electron-ion collisions are much more efficient than are ion-ion collisions. The reason is that the collision rate is proportional to the relative velocity of the colliding particles. In kinetic equilibrium the root-mean-square velocity is proportional to the root of the mass of the particle (see eq. 6.19). Electrons thus move $(m_H A / m_e)^{1/2} \sim 43 A^{1/2}$ times as fast as do ions of atomic weight A .

Even in those parts of the solar atmosphere where the ionization fraction of hydrogen is only $\sim 10^{-5}$ one may assume that the relevant collisional processes are dominated by collisions with free electrons. This is partly so due to contributions of elements that have low ionization energies, such as iron and magnesium. Only in extremely cool stars, collisions with neutral hydrogen atoms may play a role.

The number of *collisional excitations* in $\text{cm}^{-3} \text{ sec}^{-1}$ is given by

$$n_l C_{lu} = n_l n_e \int_{v_o}^{\infty} \sigma_{lu}(v) f(v) v dv \equiv n_l n_e q_{lu}(T) \quad (7.5)$$

where v_o is the threshold velocity (providing the minimum required kinetic energy $E_o = \frac{1}{2}mv_o^2 = h\nu_{lu}$), n_e the electron density per cm^3 , and $\sigma_{lu}(v)$ the electron collision cross-section of the process in cm^2 . In kinetic equilibrium, the velocity distribution $f(v)$ is that according to Maxwell (eq. 6.18). The collision cross-sections are for the most part poorly known. They are determined in experiments or by means of complex quantum mechanical calculations. We give an often used formula based on a dipole approximation, deduced by Van Regemorter

$$q_{lu}(T) \approx p_1 \left(\frac{E_0}{kT} \right)^{p_2} T^{-3/2} e^{-E_0/kT} f_{lu} \quad (7.6)$$

where $p_1 = 2.16$ for atoms and 3.9 for ions, and $p_2 = -1.68$ and -1 for atoms and ions respectively (see e.g. Jefferies). The result is proportional to the oscillator strength f_{lu} of the line transition (see § 7.3), and only applies to allowed transitions. The rates for forbidden transitions (which have very small values of f_{lu}) are usually very poorly known, but most certainly are not as low as implied by Van Regemorter's formula. The term $T^{-3/2} \exp(-E_o/kT)$ finds its origin in the Maxwellian velocity distribution (eq. 6.18); the exponential term dominates the rate, such that it increases rapidly with temperature. For a fixed temperature, the rate increases for decreasing E_0 as a lower threshold for the kinetic energy implies that a larger fraction of the free electrons (distributed according to Maxwell) can participate. This is very relevant for transitions between high lying energy levels, i.e. transitions close to the continuum (see figure 6.4). These have only small level-to-level energies $E_0 = h\nu_{lu}$; which typically correspond to line wavelengths in the infrared or submillimetre. These levels are strongly coupled by collisions.

Collisional de-excitation

The rate of *collisional de-excitations* can be obtained directly from a detailed balance argument. In KE the occupation numbers of the upper and lower level are related according to

$$n_l^* C_{lu} = n_u^* C_{ul} \quad (7.7)$$

In this equilibrium, set by collisions and only dependent on temperature, the ratio $(n_u/n_l)^*$ fulfills the Boltzmann equation (6.23).

The number of collisional de-excitations in $\text{cm}^{-3} \text{ sec}^{-1}$ is then given by

$$n_u C_{ul} = n_u \left(\frac{n_l}{n_u} \right)^* C_{lu} = n_u n_e q_{lu}(T) \frac{g_l}{g_u} e^{+h\nu_{lu}/kT} \quad (7.8)$$

Note that the rate for collisional de-excitations is much less sensitive to the temperature than is that of collisional excitations (the exponential term has dropped out). Roughly one could say that each encounter with an electron suffices to accelerate it, by transferring excitation energy.

Maxwellian averaged collision strength

We provide an alternative expression for the rate of collisional excitations using the *Maxwellian averaged collision strength* Υ , also referred to as the effective collisional strength. It holds that

$$q_{lu}(T) = \frac{8.629 \times 10^{-6}}{g_l T^{1/2}} e^{-E_{lu}/kT} \Upsilon_{lu}(T). \quad (7.9)$$

For the rate of collisional de-excitations it follows that

$$q_{ul}(T) = \frac{g_l}{g_u} e^{+E_{lu}/kT} q_{lu}(T) = \frac{8.629 \times 10^{-6}}{g_u T^{1/2}} \Upsilon_{lu}(T). \quad (7.10)$$

Exercise 7.1

- a) At time $t = 0$ the population of an excited level is $n_u(0)$. How does the population of this level decrease over time if *only* spontaneous emission to a lower level l occurs and the Einstein coefficient of this process is A_{ul} ?
- b) If de-excitations are possible to multiple lower levels the transition probabilities should be added. Show that if $\Gamma_u \equiv \sum_{i < u} A_{ui}$ the *lifetime* (in sec) of the particle in state u is given by

$$\langle t \rangle = \frac{1}{\Gamma_u} \quad (7.11)$$

7.2 Einstein relations

The Einstein coefficients A_{ul} , B_{lu} and B_{ul} can be expressed in each other, assuming that thermodynamic equilibrium is valid.

In TE each specific process is in detailed balance: for each two energy levels the number of radiative excitations equals the number of radiative de-excitations

$$n_l B_{lu} \bar{J}_{lu} = n_u A_{ul} + n_u B_{ul} \bar{J}_{lu} \quad (7.12)$$

If we isolate the profile integrated mean intensity \bar{J}_{lu} , and use that in TE the occupation of the levels is given by Boltzmann (eq. 6.23), then

$$\begin{aligned} \bar{J}_{lu} &= \frac{A_{ul}/B_{ul}}{(n_l/n_u)(B_{lu}/B_{ul}) - 1} \\ &= \frac{A_{ul}/B_{ul}}{(g_l B_{lu}/g_u B_{ul}) e^{h\nu_{lu}/kT} - 1} \end{aligned} \quad (7.13)$$

In TE $J_\nu = B_\nu$. As B_ν is a function that changes very little over the sharply peaked profile function ϕ_ν , we may also assume that $\bar{J}_{lu} = B_{\nu_{lu}}$. To fulfill this equation at each temperature, it must hold that

$$A_{ul} = \frac{2h\nu_{lu}^3}{c^2} B_{ul} \quad \text{and} \quad g_l B_{lu} = g_u B_{ul} \quad (7.14)$$

These are the *Einstein relations*. They connect atomic properties, i.e. properties that are independent of external circumstances. We therefore must conclude that they are universally valid, i.e. also in media that are not in TE, or for cases in which $\bar{J}_{lu} \neq B_{\nu_{lu}}$.

7.3 Relation between Einstein coefficients and η_ν^ℓ and χ_ν^ℓ

The emission coefficient η_ν defines the emitted energy per cm^3 per second per hz per solid angle (see eq. 4.7). We may derive this coefficient for spontaneous emission processes in a simple way. The energy emitted in all directions per cm^3 per second at all frequencies relevant for the transition is $h\nu_{lu} n_u A_{ul}$. To get the emitted energy per hz we need to multiply with the profile function for spontaneous emission ψ_ν (which has dimension hz^{-1}), and, finally, to get the emission per unit solid angle we need to divide by the total solid angle $\Omega = 4\pi$. This yields for the *line emission coefficient*

$$\eta_\nu^\ell = \frac{h\nu_{lu}}{4\pi} n_u A_{ul} \psi_\nu \quad (7.15)$$

Let us now derive an expression for the extinction coefficient χ_ν . The total energy that is absorbed in a volume element dV in a time interval dt by radiative excitation is

$$\begin{aligned}\delta E_\nu^{\text{tot}} &= h\nu_{lu} n_l B_{lu} \bar{J}_{lu} dV dt \\ &= h\nu_{lu} n_l B_{lu} \left[\int \left\{ \frac{1}{4\pi} \oint I_\nu d\omega \right\} \phi_\nu d\nu \right] dV dt\end{aligned}\quad (7.16)$$

where the last equality at the right-hand side follows from eq. (7.4) and (3.5). So, the energy δE_ν that is absorbed in a volume $dV = dO ds$ in a bandwidth $d\nu$ in a time interval dt , from an incident beam of opening angle $d\omega$ and specific intensity I_ν is

$$\delta E_\nu = \frac{h\nu_{lu}}{4\pi} n_l B_{lu} \phi_\nu I_\nu dO ds d\omega d\nu dt \quad (7.17)$$

Using the definition of the extinction coefficient χ_ν (eq. 4.3) we find

$$\chi_\nu^{\text{excitation}} = \frac{h\nu_{lu}}{4\pi} n_l B_{lu} \phi_\nu \quad (7.18)$$

Finally, let us turn to stimulated emissions. Usually this process is not added to that of spontaneous emission, but is treated in terms of a “negative extinction”. The reason is that induced excitation is much more similar to radiative excitation than it is to spontaneous de-excitation. First because – if complete redistribution is valid – it is proportional to \bar{J}_{lu} . Second, the emission is in the same direction as that of the incident radiation by which it is induced (therefore the term “negative extinction”). In fact, radiative excitation and stimulated emission always occur together. We find for the *line extinction coefficient*

$$\chi_\nu^\ell = \frac{h\nu_{lu}}{4\pi} [n_l B_{lu} \phi_\nu - n_u B_{ul} \varphi_\nu] \quad (7.19)$$

Oscillator strength

To quantify the line emission and extinction coefficient we only need one of the Einstein coefficients (which needs to be determined by either measurement or calculation). The others follow from the Einstein relations eq. (7.14). Usually A_{ul} is tabulated. There is a fourth parameter that is used to quantify line strength: the *oscillator strength* f_{lu} .

This parameter is used in the classic description of a spectral line as a damped harmonic oscillator, according to which the extinction coefficient (or cross-section) per particle $\alpha_{lu}(\nu)$ (dimensions cm^2) is given by

$$\alpha_{lu}(\nu) = \frac{\pi e^2}{m_e c} f_{lu} \phi_\nu \quad (7.20)$$

where $(\pi e^2/m_e c) = 0.02654 \text{ cm}^2 \text{ Hz}$ and ϕ_ν is the *Lorentz profile* or *damping profile* of which the dimension is Hz^{-1} . (see § 12.2). The oscillator strength does not feature in the classical theory. A quantum mechanical treatment shows that the transition probabilities for different

Table 7.1: Wavelength λ_{lu} , oscillator strength f_{lu} , and Einstein coefficient A_{ul} for important transitions in hydrogen. See figure 6.4 for the Grotrian diagram

Wavelength in Å								
Series	l	$u=2$	3	4	5	6	7	8
Ly	1	1215.67	1025.72	972.54	949.74	937.80	930.75	926.23
H	2		6562.80	4861.32	4340.46	4101.73	3970.07	3889.05
P	3			18751.0	12818.1	10938.1	10049.4	9545.98
Br	4				40512.0	26252.0	21655.0	19445.6
Pf	5					74578	46525	37395
Hu	6						123680	75005

Oscillator strength								
Series	l	$u=2$	3	4	5	6	7	8
Ly	1	0.4162	0.07910	0.02899	0.01394	0.007799	0.004814	0.003183
H	2		0.6407	0.1193	0.04467	0.02209	0.01270	0.008036
P	3			0.8421	0.1506	0.05584	0.02768	0.01604
Br	4				1.038	0.1793	0.06549	0.03230
Pf	5					1.231	0.2069	0.07448
Hu	6						1.424	0.2340

Einstein coefficient A_{ul} in sec $^{-1}$								
Series	l	$u=2$	3	4	5	6	7	8
Ly	1	$4.699 \cdot 10^8$	$5.575 \cdot 10^7$	$1.278 \cdot 10^7$	$4.125 \cdot 10^6$	$1.644 \cdot 10^6$	$7.568 \cdot 10^5$	$3.869 \cdot 10^5$
H	2		$4.410 \cdot 10^7$	$8.419 \cdot 10^6$	$2.530 \cdot 10^6$	$9.732 \cdot 10^5$	$4.389 \cdot 10^5$	$2.215 \cdot 10^5$
P	3			$8.986 \cdot 10^6$	$2.201 \cdot 10^6$	$7.783 \cdot 10^5$	$3.358 \cdot 10^5$	$1.651 \cdot 10^5$
Br	4				$2.699 \cdot 10^6$	$7.711 \cdot 10^5$	$3.041 \cdot 10^5$	$1.424 \cdot 10^5$
Pf	5					$1.025 \cdot 10^6$	$3.253 \cdot 10^5$	$1.388 \cdot 10^5$
Hu	6						$4.561 \cdot 10^5$	$1.561 \cdot 10^5$

transitions may differ by orders of magnitude. The dimensionless oscillator strength is thus introduced as a correction on the classical value.

The oscillator strength is related to the Einstein coefficient B_{lu} through the total extinction coefficient (or cross-section) per particle

$$\alpha_{lu} \equiv \int_0^\infty \alpha_{lu}(\nu) d\nu = \frac{\pi e^2}{m_e c} f_{lu} = \frac{h\nu_{lu}}{4\pi} B_{lu} \quad (7.21)$$

of which the dimensions are (note!) cm 2 hz. For resonance lines, such as Ly α , a classical oscillator is a good approximation and $f_{lu} \sim 1$. Other observed allowed lines in spectra typically have $10^{-4} \lesssim f_{lu} \lesssim 10^{-1}$. Forbidden transitions have $f_{lu} \lesssim 10^{-6}$. The oscillator strengths of a number of important hydrogen lines are given in table 7.1.

Finally: usually also $g_l f_{lu}$ is tabulated, known as the *gf-value*. In the literature, this quantity is often (erroneously) referred to as the “transition probability”.

Kramers formula

For hydrogen an analytical expression for f_{lu} has been derived by Kramers

$$f_K(l, u) = \frac{32}{3\pi\sqrt{3}} \left(\frac{1}{l^2} - \frac{1}{u^2} \right)^{-3} \left(\frac{1}{l^5 u^3} \right) \quad (7.22)$$

where l and u are the principal quantum numbers of the lower and upper level respectively. The *Kramer formula* is a semi-classical result. A full quantum mechanical derivation results in a correction factor, the bound-bound Gaunt factor g_I , that is of order unity. The oscillator strength is then given by

$$f(l, u) = g_I(l, u) f_K(l, u) \quad (7.23)$$

For the lines of a given spectral series, for instance the Lyman series ($1 \rightarrow u$) or Balmer series ($2 \rightarrow u$), the α -line ($l \rightarrow l + 1$) will have the largest oscillator strength, followed by the β -line ($l \rightarrow l + 2$), *etcetera*. This is reflected in the line strengths, e.g. H α is almost always stronger than is H β , which in turn is stronger than H γ , *etcetera*.

For hydrogenic ions

$$f_{lu} = Z^4 f_{lu}(Z = 1) \quad (7.24)$$

Line source function

The *line source function*, using eq. (7.15) and (7.19), is given by

$$S_\nu^\ell = \frac{\eta_\nu^\ell}{\chi_\nu^\ell} = \frac{n_u A_{ul} \psi_\nu}{n_l B_{lu} \phi_\nu - n_u B_{ul} \varphi_\nu} \quad (7.25)$$

As the Einstein relations do also apply for conditions other than TE, the general form of the line source function (and in fact also of the source function of any arbitrary radiative transition) is

$$S_\nu^\ell = \frac{2h\nu_{lu}^3}{c^2} \frac{1}{(g_u n_l)/(g_l n_u) - 1} \quad (7.26)$$

where we have assumed complete redistribution, i.e. $\phi_\nu = \varphi_\nu = \psi_\nu$. In TE we may apply Boltzmann's law such that $S_\nu^\ell = B_\nu$. This recovers the Kirchhoff-Planck relation (eq. 6.3).

We end this section with two useful relations. The ratio of the number of spontaneous and induced de-excitations in TE is

$$\frac{n_u A_{ul}}{n_u B_{ul} \bar{J}_{lu}} = \frac{2h\nu^3}{c^2 B_\nu} = e^{h\nu/kT} - 1 \quad (7.27)$$

So, if $h\nu/kT \gg 1$ (Wien's approximation) the majority of de-excitations will be spontaneous, and if $h\nu/kT \ll 1$ (Rayleigh-Jeans's approximation) the dominant downward radiative process is induced emission – provided that the populations and radiation field are of the order of what is expected in TE.

The ratio of the number of spontaneous de-excitations and the total radiative de-excitation rate in TE is

$$\frac{n_u A_{ul}}{n_u A_{ul} + n_u B_{ul} \bar{J}_{lu}} = 1 - e^{-h\nu/kT} \quad (7.28)$$

This term is referred to as “the correction factor for stimulated emission”.

Exercise 7.2

- a) Show that in NLTE, assuming complete redistribution, the line extinction coefficient per particle corrected for stimulated emissions is given by

$$\alpha_{lu}^{\text{cse}}(\nu) = \frac{\pi e^2}{m_e c} f_{lu} \left[1 - \frac{n_u g_l}{n_l g_u} \right] \phi_\nu \quad (7.29)$$

- b) Show that in TE and LTE the line extinction coefficient is given by

$$\alpha_{lu}^{\text{cse}}(\nu) = \frac{\pi e^2}{m_e c} f_{lu} \left[1 - e^{-h\nu_{lu}/kT} \right] \phi_\nu \quad (7.30)$$

8

Continuum processes

In this chapter we treat processes that give rise to *continuum* extinction and emission.

8.1 Bound-free transitions

There are also five bound-free processes:

1. *photoionization*
requires: photons of sufficient energy
2. *spontaneous photo-recombination*
requires: free electron that can be captured
3. *stimulated photo-recombination*
requires: free electron that can be captured and a photon to induce the process
4. *collisional ionization*
requires: passing particle with sufficient energy
5. *collisional recombination*
requires: passing particle and a free electron that can be captured

The processes 1 and 4 require an energy (from photon or collision) $E > E_I - E_i = E_o$, where E_i is the energy of the bound level i and E_I is the ionization energy. The relevant extinction coefficient has a threshold value, $\nu_o = E_o/h$ for photoionization, and $v_o = (2E_o/m_e)^{1/2}$ for collisional ionization, below which the process can not take place.

The latter process is a three particle collision and is therefore, as a rule, rare.

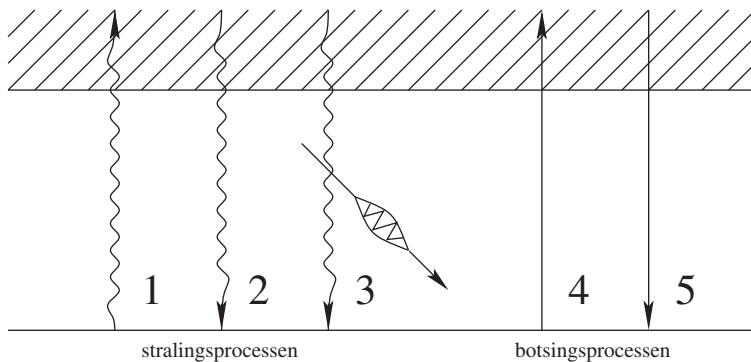


Figure 8.1: Schematic overview of the five possible bound-free processes.

Photoionization

In a *photoionization* a particle in a bound energy state i is ionized to an ionized state κ , through absorption of a photon.

Say, the extinction coefficient for photoionization or *photoionization cross-section* per particle in energy level i is given by $\alpha_{ik}(\nu)$, which has dimension cm^2 . If the energy of a photon is less than what is required to remove the electron from the atom or ion, i.e. $\nu < \nu_o$, then $\alpha_{ik}(\nu) = 0$. The rate of photoionization follows from the product of this cross-section and the number of photons that are available at each frequency $\nu \geq \nu_o$, i.e. $4\pi J_\nu/h\nu$.

From this consideration it follows that the number of photoionizations per second per cm^3 is given by

$$n_i R_{ik} = n_i 4\pi \int_{\nu_o}^{\infty} \alpha_{ik}(\nu) \frac{J_\nu}{h\nu} d\nu \quad (8.1)$$

For hydrogenic ions (H I , He II , Li III , *etcetera*) the extinction coefficient per particle for photoionization (without correction for induced recombinations) from a level of principal quantum number n , for $\nu \geq \nu_o(n, Z)$, is given by

$$\alpha_\nu^{\text{bf}}(n, Z) = \left(\frac{64\pi^4 m_e e^{10}}{3\sqrt{3} ch^6} \right) \frac{Z^4}{n^5} g_{\text{II}}(\nu, n) \nu^{-3} \quad (8.2)$$

where Z is the charge of the ion ($Z = 1$ for hydrogen) and g_{II} is the bound-free Gaunt factor, which close to the ionization edge is ~ 1 . For this type of ion the excitation energy is given by $E(n, Z) = \mathcal{R}Z^2(1 - 1/n^2)$, where \mathcal{R} is the Rydberg constant for hydrogen, such that the edge frequency $\nu_o(n, Z) = (\mathcal{R}Z^2/hn^2)$. Using this relation and substituting constants yields

$$\alpha_\nu^{\text{bf}}(n, Z) = 7.91 \times 10^{-18} \frac{n}{Z^2} g_{\text{II}}(\nu, n) \left(\frac{\nu_o}{\nu} \right)^3 \quad (8.3)$$

The extinction is thus proportional to ν^{-3} for $\nu > \nu_o$. For more complicated ions, that have more valence electrons (for instance Fe I which has an electron shell that is half filled and

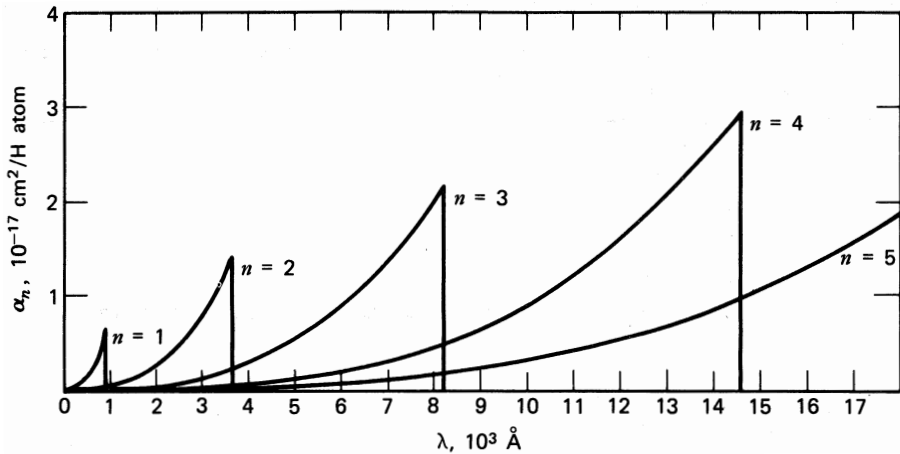


Figure 8.2: The bound-free extinction coefficient per particle for hydrogen atoms, for different principal quantum numbers n . Although $\alpha_{\nu}^{\text{bf}}(n)$ increases with n one should be reminded that the particle number density of excited levels, n_n , usually is a strongly decreasing function of n (see for instance eq. 6.23) such that the behaviour of the linear extinction coefficient as a function of n can be more complex (see for instance fig 8.4).

that provides a multitude of valence electrons and valence cavities), the smooth decline is disrupted by resonances which produce all sorts of peaks in $\alpha_{ik}(\nu)$ that need to be determined in experiments.

Spontaneous recombination

In a *spontaneous recombination* an electron is captured by a particle in an ionized state κ and a photon is emitted that carries with it the recombination energy. We may derive the number of spontaneous recombinations per second per cm^3 using a detailed balance argument.

In TE the number of photoionizations, at each frequency, must be in balance with the number of radiative recombinations. As in this most strict of all equilibria $J_{\nu} = B_{\nu}$, it follows that in TE the total number of radiative recombinations per cm^3 per second is

$$n_{\kappa}^* R_{\kappa i} = n_i^* R_{i\kappa} = n_i^* 4\pi \int_{\nu_0}^{\infty} \alpha_{ik}(\nu) \frac{B_{\nu}}{h\nu} d\nu \quad (8.4)$$

The superscript * indicates that the level occupations are according to the Boltzmann and Saha equilibrium (see for instance eq. 6.28). The total number of radiative recombinations is the sum of spontaneous and induced recombinations, and we may split these two contributions using the correction term for stimulated emission

$$\begin{aligned} n_{\kappa}^* R_{\kappa i} &= n_{\kappa} R_{\kappa i}^{\text{spon}} + n_{\kappa} R_{\kappa i}^{\text{stim}} \\ &= n_i^* 4\pi \left[\int_{\nu_0}^{\infty} \frac{\alpha_{ik}(\nu)}{h\nu} B_{\nu} \left(1 - e^{-h\nu/kT} \right) d\nu + \int_{\nu_0}^{\infty} \frac{\alpha_{ik}(\nu)}{h\nu} B_{\nu} e^{-h\nu/kT} d\nu \right] \end{aligned} \quad (8.5)$$

Using the definition of the Planck function (eq. 6.4) we find for the spontaneous recombinations

$$n_i^* R_{\kappa i}^{\text{spon}} = n_i^* 4\pi \int_{\nu_0}^{\infty} \frac{\alpha_{i\kappa}(\nu)}{h\nu} \frac{2h\nu^3}{c^2} e^{-h\nu/kT} d\nu \quad (8.6)$$

For a spontaneous recombination to occur what is required is a passing free electron that can be captured. What is *not* required is knowledge of possible deviations from TE of the local radiation field. Even if TE (or LTE) is not valid, the rate $R_{\kappa i}^{\text{spon}}$ should still hold per ion, as long as the velocity distribution of the free electrons is according to Maxwell. We therefore only need to rescale eq. (8.6) from the TE ion density to the real ion density n_κ to get a general expression for the number of spontaneous radiative recombinations per cm^3 per second:

$$n_\kappa R_{\kappa i}^{\text{spon}} = n_\kappa \left(\frac{n_i}{n_\kappa} \right)^* 4\pi \int_{\nu_0}^{\infty} \frac{\alpha_{i\kappa}(\nu)}{h\nu} \frac{2h\nu^3}{c^2} e^{-h\nu/kT} d\nu \quad (8.7)$$

This expression states that the emission coefficient for spontaneous recombination, per ion, “feels” the Planck function (which represents the Maxwell velocity distribution) and not the real radiation field. The latter may obviously have caused the ionization into state κ , however, this dependence is locked up in n_κ (and *not* in $R_{\kappa i}^{\text{spon}}$). It may be clear that this recombination process is less “spontaneous” as is a spontaneous de-excitation between two bound levels; after all, the ion needs to wait for a free electron that can be captured. The dependence of $R_{\kappa i}^{\text{spon}}$ on this free electron is hidden in the TE ratio $(n_i/n_\kappa)^*$ and is explicitly given by the Saha-Boltzmann equation (6.28). Substitution yields

$$\begin{aligned} n_\kappa R_{\kappa i}^{\text{spon}} &= n_\kappa n_e \Phi_{i\kappa}(T) 4\pi \int_{\nu_0}^{\infty} \frac{\alpha_{i\kappa}(\nu)}{h\nu} \frac{2h\nu^3}{c^2} e^{-h\nu/kT} d\nu \\ &\equiv n_\kappa n_e \alpha_{i,\kappa-1}^{\text{RR}}(T) \end{aligned} \quad (8.8)$$

where $\alpha_{i,\kappa-1}^{\text{RR}}(T)$ is the *recombination coefficient* in cm^3 per second into level i of ion $\kappa - 1$. This function decreases with increasing temperature, as it is more difficult for an ion to capture a faster moving electron (see e.g. table 17.1). Equation (8.8) shows that the number of spontaneous recombinations scales with the product $n_\kappa n_e$, as expected. The recombination coefficient does not account for stimulated recombinations. The reason is that these are in most cases unimportant compared to the spontaneous recombinations (see for instance eq. 8.5 for the case $J_\nu = B_\nu$ and realize that ν_0 usually is quite large).

Stimulated recombination

The same argument as applies to the process of spontaneous recombination also holds for *stimulated recombinations* or *induced recombinations*. In TE the number of stimulated recombinations per cm^3 per second is (see eq. 8.5)

$$n_\kappa^* R_{\kappa i}^{\text{stim}} = n_i^* 4\pi \int_{\nu_0}^{\infty} \frac{\alpha_{i\kappa}(\nu)}{h\nu} B_\nu e^{-h\nu/kT} d\nu \quad (8.9)$$

Rescaling of the TE ion density n_κ^* to the real ion density n_κ , and substituting the TE radiation field B_ν for the real radiation field J_ν , yields

$$n_\kappa R_{\kappa i}^{\text{stim}} = n_\kappa \left(\frac{n_i}{n_\kappa} \right)^* 4\pi \int_{\nu_0}^{\infty} \frac{\alpha_{i\kappa}(\nu)}{h\nu} J_\nu e^{-h\nu/kT} d\nu \quad (8.10)$$

The end result for the *total number of radiative recombinations*, per cm³ per second, therefore is

$$n_\kappa R_{\kappa,i} = n_\kappa \left(\frac{n_i}{n_\kappa} \right)^* 4\pi \int_{\nu_0}^{\infty} \frac{\alpha_{i\kappa}(\nu)}{h\nu} \left[\frac{2h\nu^3}{c^2} + J_\nu \right] e^{-h\nu/kT} d\nu \quad (8.11)$$

Collisional ionization

The number of *collisional ionizations* per cm³ per second follows from eq. (7.5), where the threshold velocity v_0 now corresponds to the minimum energy $E_0 = \frac{1}{2}mv_0^2 = h\nu_0$ of the electron needed for collisional ionization. We get

$$n_i C_{i\kappa} = n_i n_e \int_{v_0}^{\infty} \sigma_{i\kappa}(v) f(v) v dv \equiv n_i n_e q_{i\kappa}(T) \quad (8.12)$$

For general remarks concerning the collisional process we refer to § 7.1. Here we only give the approximate formula for $q_{i\kappa}(T)$ based on a dipole approximation, derived by Van Regemorter,

$$q_{i\kappa}(T) \approx 2.7 \zeta \left(\frac{E_0}{kT} \right)^{-2} T^{-3/2} e^{-E_0/kT} \quad (8.13)$$

where ζ is the number of electrons in the outer shell.

Collisional recombination

The rate of collisional recombinations can also be obtained using a detailed balance argument. In KE

$$n_i^* C_{i\kappa} = n_\kappa^* C_{\kappa i} \quad (8.14)$$

such that the number of collisional recombinations per cm³ per second is

$$n_\kappa C_{\kappa i} = n_\kappa \left(\frac{n_i}{n_\kappa} \right)^* C_{i\kappa} = n_\kappa n_e^2 \Phi_{i\kappa}(T) q_{i\kappa}(T) \quad (8.15)$$

The equation shows clearly that this is a three particle process, i.e. the process scales as $n_i n_e^2$. The rate of collisional recombinations is much less sensitive to temperature as is that of collisional ionizations, because, similar to collisional processes between bound energy levels (see § 7.1), the exponential term drops out. Collisional recombinations are more likely to occur for energy levels high up in the atom/ion because of the low threshold energy E_0 .

Collisional coupling of high levels with the continuum

The collisional coupling between high lying levels and the continuum is even stronger than that between two bound energy levels close to the ionization edge (see § 7.1). This is so because $q_{ik}(T)$ for given temperature increases more rapidly with decreasing E_0 as does q_{lu} (see eq. 7.6). If the electron density decreases, for instance high up in the atmosphere or in a stellar wind, spontaneous recombinations and spontaneous de-excitations will win over collisional recombination for an increasing number of levels. Consequently, these levels will cascade or “rain down” into the ground level. However, for levels that are extremely high up the collisional processes will continue to dominate and therefore the populations will remain in LTE (relative to the continuum) and will be given by eq. (6.28). We will return to this situation in § 17.5, when we discuss the state of gas in nebulae, i.e. in media with extremely low particle densities.

Exercise 8.1

Give an expression for the total linear extinction coefficient for bound-free processes, χ_ν^{bf} , in a pure hydrogen gas in LTE.

8.2 Free-free transitions

Radiation that is the result of the negative (see below) acceleration of a charge in the Coulomb field of another charge is known as *free-free radiation*. In a dipole approximation free-free radiation only occurs if the two particles are not identical. So, it does not happen for electron-electron or ion-ion interactions, as in those cases the dipole moment $\mathbf{d} \equiv \sum q_i \mathbf{r}_i$ is proportional to the center of mass $\sum m_i \mathbf{r}_i$, which is a conserved quantity. This causes the emitted power, given by Larmor’s law

$$P = \frac{2\ddot{d}^2}{3c^3} \quad (8.16)$$

to be zero. In electron-ion interactions the electrons are the prime radiators as the relative acceleration $\ddot{\mathbf{r}}$ is inversely proportional to the mass of the particles, while the charges are typically about equal. Free-free radiation is also referred to as *bremsstrahlung*. Bremsstrahlung is the German for ‘braking radiation’, since the emitting electron-ion pair are being braked rather than accelerated.

We give, without derivation, the result for the free-free extinction coefficient χ_ν^{ff} per cm for particles of element k in ionization state j

$$\chi_\nu^{\text{ff}} = \frac{4e^6}{3hc} \left(\frac{2\pi}{3km_e^3} \right)^{1/2} \bar{g}_{\text{III}}(\nu, T) \frac{Z_{jk}^2}{T^{1/2}\nu^3} n_e N_{jk} \left(1 - e^{-h\nu/kT} \right) \quad (8.17)$$

where \bar{g}_{III} is the velocity mean for the Gaunt factor of free-free processes, which gives the quantum mechanical correction to the classic result; \bar{g}_{III} is dimensionless and of order unity (but see eq. 16.29 for its behavior in the radio regime). N_{jk} is the density of ions of charge Z_{jk} . For H II and He II, $Z_{jk} = 1$; for He III, $Z_{jk} = 2$. Evaluation of all constants yields a cgs value 3.692×10^8 .

In TE the free-free source function is given by the Planck function $B_\nu(T)$. This is also true if TE is not valid, provided that the velocity distribution of the particles is given by the Maxwell equation, because in free-free processes kinetic and radiative energy is exchanged fully. In each free-free emission a photon is created out of the “thermal pool of particles” that has no prior knowledge about anything; likewise, in a free-free absorption all information about the absorbed photon will be lost. In other words: a free-free process is a *pure* collisional process.

In the Wien approximation ($h\nu/kT \gg 1$) the correction term for stimulated emissions may be neglected. One is left with

$$\chi_\nu^{\text{ff}} = 3.692 \times 10^8 \bar{g}_{\text{III}}(\nu, T) \frac{Z_{jk}^2}{T^{1/2}\nu^3} n_e N_{jk} \quad (8.18)$$

i.e. $\chi_\nu^{\text{ff}} \propto \nu^{-3}$. In the Rayleigh-Jeans regime ($h\nu/kT \ll 1$)

$$\chi_\nu^{\text{ff}} = 1.772 \times 10^{-2} \bar{g}_{\text{III}}(\nu, T) \frac{Z_{jk}^2}{T^{3/2}\nu^2} n_e N_{jk} \quad (8.19)$$

which shows a frequency dependence $\chi_\nu^{\text{ff}} \propto \nu^{-2}\lambda^2$.

Exercise 8.2

Show that the free-free emission coefficient is given by

$$\eta_\nu^{\text{ff}} = \frac{8e^6}{3c^3} \left(\frac{2\pi}{3k m_e^3} \right)^{1/2} \bar{g}_{\text{III}}(\nu, T) \frac{Z_{jk}^2}{T^{1/2}} n_e N_{jk} e^{-h\nu/kT} \quad (8.20)$$

8.3 H⁻ absorption

Hydrogen, because of its large polarizability, can form a negative ion consisting of a proton and two electrons. The H⁻ or hydride ion has a single bound state with a binding energy of 0.754 eV. The wavelength corresponding to this energy is 16444 Å. Therefore, it has no lines, only bound-free and free-free transitions. For bound-free processes



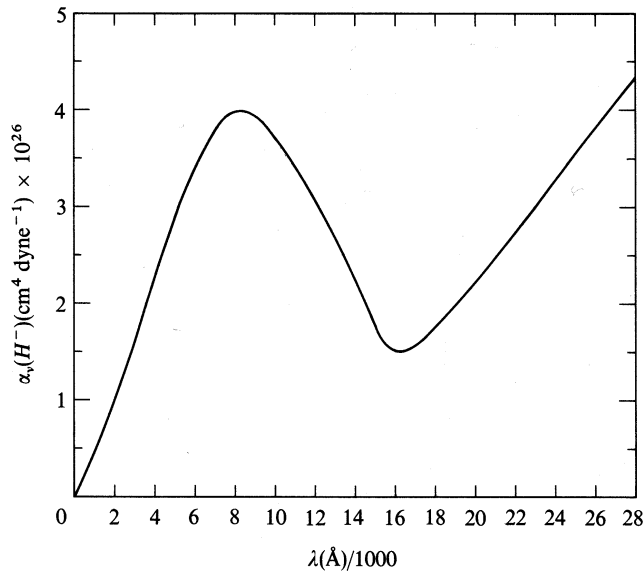
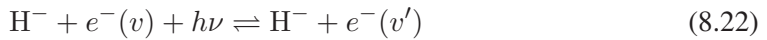


Figure 8.3: Extinction coefficient (in 10^{26} cm^2) of the H⁻ ion, per neutral H atom and per unit of electron pressure $p_e = n_e kT$. The bound-free extinction has a maximum at $\sim 8000 \text{ \AA}$. The free-free extinction is proportional to λ^2 . The sum shows a maximum at 8500 \AA and a minimum at $1.6 \mu\text{m}$. From Mihalas (1978).

where $1/2 m_e v^2 = h\nu - 0.754 \text{ eV}$. For free-free processes



where $1/2 m_e v'^2 = h\nu + 1/2 m_e v^2$. The bound-free continuum does not have a sharp ionization edge at $\lambda_o = 16444 \text{ \AA}$, but a broad peak at lower wavelength reaching a maximum at $\sim 8500 \text{ \AA}$ (see figure 8.3).

Because of its low binding energy H⁻ can only exist in relatively cool stars (up to stars slightly hotter than the sun). In the photosphere of the sun and in that of cooler stars the H⁻ processes are the dominant source of visual and infrared extinction. The extra electrons are supplied by elements such as Na, Mg, Al, Si, Ca, and Fe, that are relatively abundant and have a much lower ionization energy than hydrogen (see also § 6.5). In extremely cool stars H⁻ will no longer be the dominant source of extinction because of a lack of free electrons.

The identification of H⁻ as the most important source of extinction in cool stars by Pannekoek in 1935 and Wildt in 1939 was viewed as a fundamental breakthrough. To illustrate this: Eddington, in his book “The internal constitution of the stars” in 1926 saw the unknown extinction and the (at that time) also unknown internal source of energy of the stars as the *only* remaining problems in the physics of stars!

In TE (or LTE) the number of H⁻ ions is given by the Saha equation (6.26). Usually one formulates this using an explicit reference to the electron pressure $p_e = n_e kT$, such that

$N_{\text{H}^-} = N_{\text{H}} p_{\text{e}} \check{\Phi}(T)$. This yields for the H^- extinction

$$\chi_{\nu}^*(\text{H}^-) = \alpha_{\nu}^{\text{bf}}(\text{H}^-) N_{\text{H}} p_{\text{e}} \check{\Phi}(T) \left[1 - e^{-h\nu/kT} \right] \quad (8.23)$$

where $\alpha_{\nu}^{\text{bf}}(\text{H}^-)$ is the extinction coefficient per cm^2 . For the free-free extinction $\alpha_{\nu}^{\text{ff}}(\text{H}^-)$ a similar expression can be given. Fitting formulas for $\alpha_{\nu}^{\text{bf}}(\text{H}^-)$ and $\alpha_{\nu}^{\text{ff}}(\text{H}^-)$ are discussed in, for instance, Gray.

Exercise 8.3

The bound-free peak in figure 8.3 behaves all but hydrogen like, while it is does concern hydrogen. Why is this so?

8.4 Elastic scattering by electrons

We discuss the scattering of radiation by free and bound electrons in non-relativistic media, such that the scattering is elastic, implying the frequency and energy remain unchanged and only changes in direction occur.

We do not discuss extinction or emission due to electrons being accelerated in a magnetic field, i.e. cyclotron radiation (in case the electrons have non-relativistic velocities) and synchrotron radiation (in case the electrons do have relativistic velocities).

Thomson scattering

In the limit of low photon energy, i.e. $h\nu \ll m_{\text{e}}c^2$, the scattering by *free electrons* of low energy will be *elastic* or *coherent*. This process is referred to as *Thomson scattering*. For high photon energies Compton shifts will occur because of the change of momentum and energy between photon and electron. If the scattering by free electrons involves high energy electrons one needs to apply relativistic corrections; this process is referred to as inverse Compton scattering. We will only concentrate on Thomson scattering.

The extinction coefficient per free electron is given by

$$\sigma_{\text{T}} = \frac{8\pi e^4}{3m_{\text{e}}^2 c^4} = 6.65 \times 10^{-25} \text{ cm}^2 \quad (8.24)$$

and is independent of the frequency of the incident radiation. The result can be obtained using a classical description in which the electron is viewed as a free particle that vibrates (without being damped) in a passing electromagnetic wave.

The linear extinction coefficient is given by

$$\chi^e = \sigma_T n_e \quad (8.25)$$

where n_e is the electron density. Note that no subscript ν is given, as the process is independent of frequency. Thomson scattering is the dominant source of continuous extinction in the atmospheres of early-type stars where hydrogen is almost fully ionized. The much larger value of the bound-free extinction, that is of the order of 10^{-17} cm^2 per particle (see eq. 8.3) usually wins from scattering by free electrons if hydrogen is only partly ionized.

Specifying the mass fraction of hydrogen in a gas by X , and the ionization fraction of hydrogen by q , we find for the contribution of hydrogen to the mass extinction coefficient by Thomson scattering

$$\sigma'_e(H) = \frac{\sigma_T}{m_H} X q = 0.40 X q \quad \text{cm}^2/\text{gr} \quad (8.26)$$

where m_H is the mass of the hydrogen atom. For a gas of solar abundances $X = 0.747$. If in this gas hydrogen is fully ionized ($q = 1$) we find $\sigma'_e(H) = 0.30 \text{ cm}^2/\text{gr}$.

Rayleigh scattering

Photons can also be scattered by *bound electrons* in for instance an atom or molecule. In the classic picture this bound electron will have a resonance frequency that is equal to the eigen frequency ν_{lu} of a harmonically bound electron. In the limit in which the frequency of the incident radiation $\nu \ll \nu_{lu}$, we have Rayleigh scattering. In this process the extinction coefficient per valance electron per resonance line is given by

$$\sigma(\omega) = \sigma_T f_{lu} \frac{\omega^4}{(\omega_{lu}^2 - \omega^2)^2} \simeq \sigma_T f_{lu} \left(\frac{\omega}{\omega_{lu}} \right)^4 = \sigma_T f_{lu} \left(\frac{\nu}{\nu_{lu}} \right)^4 \quad (8.27)$$

where the oscillator strength gives the quantum mechanical correction of the resonance strength compared to the classic value, and the angular frequency $\omega = 2\pi\nu$.

The ratio between the extinction coefficient per particle for Rayleigh and Thomson scattering is $\sigma(\omega)/\sigma_T \simeq f_{lu}(\omega/\omega_{lu})^4 \ll 1$. Rayleigh scattering can only be a significant contribution to the total extinction coefficient if the medium contains only very few free electrons, and if other sources of extinction do not spoil things. This is the case in G- and K-type stars, and specifically those of population III. The latter have very low abundances of metals, which are the most important donors of free electrons in G and K stars (see § 6.5). This implies that H⁻ as a source of extinction is relatively unimportant. In G- and K-type stars hydrogen is almost completely in the ground state. The resonance frequencies of the Lyman series lines (i.e. those originating from the ground level) are in the ultraviolet part of the spectrum, such that photons in the visual part of the spectrum can interact with these transitions through the Rayleigh scattering mechanism. In the very low temperature M stars molecular Rayleigh scattering will dominate because hydrogen, the most abundant element, is mainly present in the form of H₂.

(The extinction coefficient of Rayleigh scattering per H₂ molecule is comparable to that of atomic hydrogen).

Rayleigh scattering by molecules is important in the earth atmosphere and causes the sky to have a blue color and the setting sun to become redder. In the visible spectral range, from 4000 Å (violet) to 8000 Å (red), the extinction coefficient of Rayleigh scattering increases by a factor $2^4 = 16$. Therefore, blue photons will experience significantly more scattering than do red photons. The probability that blue light is scattered out of the sun-eye direction is thus much larger than for red light. At sunset, when the column depth in the line-of-sight becomes large, this effect causes the sun to become redder. Scattered blue photons that originally traveled in a direction that would not reach our eyes have a larger probability of being scattered into a line-of-sight that reaches our eyes. The effect is that the observer sees blue photons from arbitrary directions. This explains the blue color of the sky.

Exercise 8.4

Show that if the mass fraction of helium in a gas is Y ; $q_{\text{He II}}$ is the ionization fraction of He II; and $q_{\text{He III}}$ is the ionization fraction of He III, that the contribution of helium to the mass extinction coefficient of Thomson scattering is

$$\sigma'_e(\text{He}) = 0.10 Y (q_{\text{He II}} + 2q_{\text{He III}}) \quad (8.28)$$

For a gas of solar abundances $Y = 0.236$.

Exercise 8.5

Does the light of the blue sky contain spectral lines? If so, what is the origin of these spectral lines?

Exercise 8.6

Why does the sun turn red at sunset?

8.5 Comparison of the main sources of extinction

Figure 8.4 shows the relative importance of continuous extinction by H I, H⁻, and He⁻ in the photosphere of three types of dwarf stars, as a function of wavelength. The contribution of Thomson scattering is not given as for these three cases it is negligibly small (the stars are too cool to have large numbers of free electrons). We first make an estimate to show that this is so.

The extinction coefficient given on the vertical axis (in units of 10^{26} cm^2) is measured per neutral hydrogen atom for an arbitrary excitation state (distributed according to Boltzmann), and normalized to the electron pressure. The latter is done because free-free and H^- extinction scale with p_e (see §§ 8.2 and 8.3 respectively). The linear extinction coefficient follows from the values given in figure 8.4, which we will call $\kappa_0(\nu)$, via $\chi_\nu = 10^{-26} \kappa_0(\nu) N_0 p_e \text{ cm}^{-1}$. In the unit of κ_0 the extinction by Thomson scattering is $10^{26} \sigma_T n_e / N_0 p_e = (66.5/p_e) n_e / N_0$. The value of the electron pressure, as given in the three panels, is of the order $10^2\text{-}10^3 \text{ dyn cm}^{-2}$. If we assume a pure hydrogen gas, the ratio $n_e/N_0 = N_+/N_0$ is derived immediately from the Saha ionization equation 6.26. As hydrogen is almost completely neutral in the three examples, this ratio $\ll 1$. This shows that the extinction coefficient of Thomson scattering in the unit applied in the figure $\ll 1$, i.e. it is negligible compared to the other sources of extinction.

The top panel in figure 8.4 shows the extinction in a model of a solar-type dwarf (an early-G star). The absorption is dominated by H^- (compare with figure 8.3). The bound-free absorption by hydrogen is significantly larger in the Balmer continuum compared to the Paschen continuum, whereas the cross-section for ionization α_ν^{bf} (eq. 8.3 and figure 8.2) shows an increase with excitation level. The reason is in the temperature dependence of the level population numbers of the excited states: there are much less H-atoms in level $n=3$ (Paschen) compared to atoms in level $n=2$ (Balmer).

The mid panel is for a late-A dwarf. The bound-free and free-free contributions of neutral hydrogen are the most important. Of these two the relative importance of free-free extinction increases for increasing wavelength as in the optical and near-infrared $\chi_\nu^{\text{ff}} \propto \lambda^3$ (see eq. 8.17). This explains the increase of the H-absorption with wavelength. The negative hydrogen ion still adds somewhat to the total extinction.

The bottom panel shows the extinction for a late-B dwarf. The H^- -ion is no longer contributing in any significant way. The absorption is dominated by hydrogen. In the optical the bound-free transitions dominate, while in the near-infrared free-free processes are the most important.

Other sources of extinction

Figure 8.4 does not show the extinction behaviour at ultraviolet wavelengths. In this part of the spectrum the situation is more complex as also bound-free extinction of heavy elements (such as Mg, Al, Si, and C) start to play a role. For the hot O- and early B-type stars the bound-free edges of helium are an important source of absorption in the ultraviolet. The He I continuum starts at 504 Å; that of He II at 228 Å.

Stars cooler than the sun feature several molecular ions, such as H_2^- , CN^- , C_2^- and H_2O^- which contribute strongly to the continuous extinction. Also Rayleigh scattering by hydrogen atoms and H_2 molecules plays a role. For the extremely cool M-type stars molecular bands, notably those of TiO, are strong sources of continuous absorption (see chapter 2).

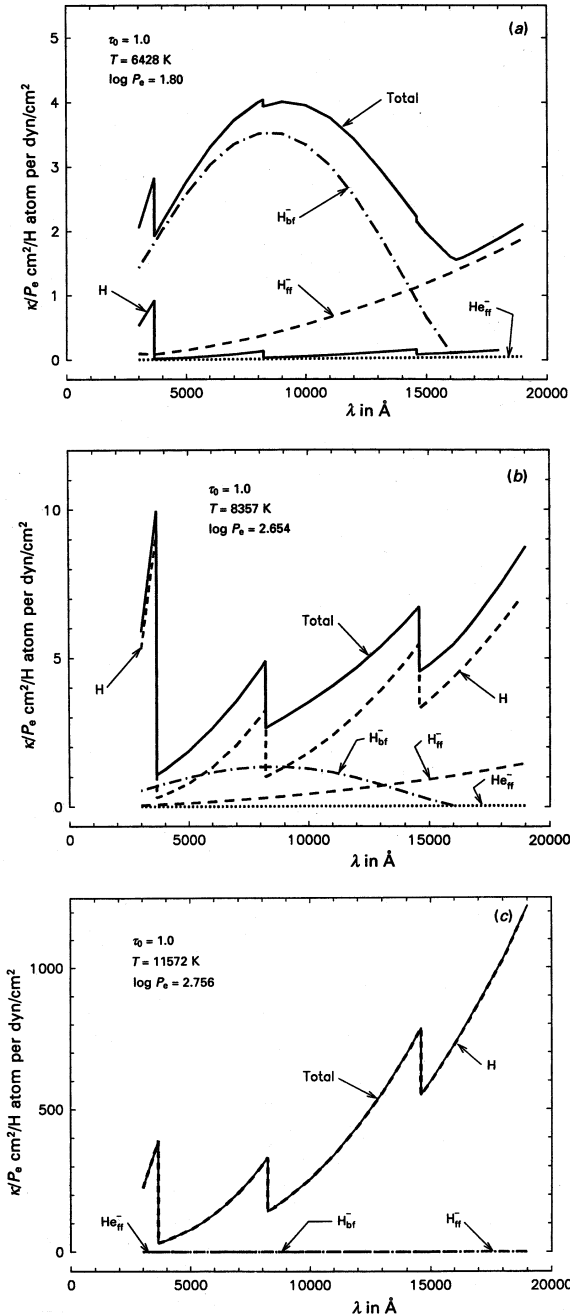


Figure 8.4: The extinction coefficient (in 10^{-26} cm^2 ; note that the scaling by a factor 10^{+26} is not indicated on the vertical axis) for hydrogen and helium for different continuum processes, per neutral hydrogen atom and per unit electron pressure measured at an optical depth $\tau_0 = 1$ for continuum radiation at a wavelength of 5000 \AA . Panel (a) is for a sun-like dwarf; (b) for a late-A dwarf, and (c) for a late-B dwarf. From Gray (1992).

9

Conservation laws

In this chapter we discuss the conservation laws of mass, momentum and energy, which are faithfully fulfilled by stellar atmospheres. In essence the model atmosphere problem consists of solving the transfer problem for a suitable equilibrium between matter and radiation (see chapter 6), subject to these conservation laws. Here also, we find that in many cases one is allowed to make assumptions that greatly reduce the complexity of the problem.

The density structure in the medium, $\rho(\mathbf{r}, t)$, is primarily determined by the conservation of mass and momentum. For relatively normal stars, such as those without a stellar wind, it is almost always justified to assume hydrostatic equilibrium. The temperature structure, $T(\mathbf{r}, t)$, is primarily determined by the interplay between the equations of transfer and energy conservation. Often the energy in a stellar atmosphere is transported by radiation, such that radiative equilibrium applies. In other cases the star considers it advantageous to transport energy by means of convection. We will not deal with this alternative means of energy transport in great detail, though we will discuss the principle of convection and the conditions in which it will occur.

9.1 Continuity equation

The material in an astrophysical medium may not be static or stationary, and for a general description we must take this into account. To do so, we use the basic equations of aero/fluid mechanics. In general, there are two methods commonly used to model gas/fluid flow. One method is to use a fixed set of coordinates in space and calculate the parameters of the gas as it flows through the coordinate frame. This is known as the Eulerian method. An alternative is to choose a set of coordinates fixed to a particle of the gas, moving with that particle, and to calculate the varying parameters in that coordinate frame (referred to as co-moving coordinates). This is known as the Lagrangian method.

Assume an arbitrary volume V contained by a closed surface S . V and S are fixed in space, so we are here adopting the Eulerian viewpoint. The mass flowing out of V per unit time through

the element of area $d\mathbf{S}$ of the surface is given by

$$\rho \mathbf{v} \cdot d\mathbf{S}, \quad (9.1)$$

where \mathbf{v} is the macroscopic (i.e. systemic) velocity in cm sec^{-1} and ρ the total mass density in gr cm^{-3} , and so the net rate at which mass flows out of V through S is given by

$$\oint_S \rho \mathbf{v} \cdot d\mathbf{S} = \int_V \nabla \cdot (\rho \mathbf{v}) dV, \quad (9.2)$$

where we have obtained the right-hand side by invoking Gauss's divergence theorem. The rate at which the mass in V decreases is given by

$$-\frac{\partial}{\partial t} \left(\int_V \rho dV \right) = \int_V \left(-\frac{\partial \rho}{\partial t} \right) dV, \quad (9.3)$$

where we can take $\partial/\partial t$ inside the integral because V is fixed in space. Obviously, the rate at which the mass in V decreases, i.e. eq. (9.3), must equal the rate at which mass flows out of V , across S , so

$$\int_V \left[\frac{\partial \rho}{\partial t} + \nabla \cdot (\rho \mathbf{v}) \right] dV = 0, \quad (9.4)$$

and since the volume V is arbitrary, it follows that

$$\frac{\partial \rho}{\partial t} + \nabla \cdot (\rho \mathbf{v}) = 0 \quad (9.5)$$

everywhere. This is known as the *continuity equation*. We can expand this equation and rewrite it as

$$\frac{\partial \rho}{\partial t} + \rho \nabla \cdot \mathbf{v} + \mathbf{v} \cdot \nabla \rho = \frac{\partial \rho}{\partial t} + \rho \frac{\partial v^i}{\partial x^i} + v^i \frac{\partial \rho}{\partial x^i} = 0 \quad (9.6)$$

where the double occurrence of index i in both terms in the second right-hand-side implies a summation over the components of the coordinate system.

We stress that $\partial \rho / \partial t$ is the Eulerian time derivative of the density, i.e. the rate of change of density at a fixed point in space. If we want the Lagrangian time derivative of the density, i.e. the rate of change of density moving with the fluid, we must include the contribution due to the displacement, $d\mathbf{r} = \mathbf{v} dt$, which occurs during the time interval dt . The net density change is

$$d\rho = \frac{\partial \rho}{\partial t} dt + d\mathbf{r} \cdot \nabla \rho, \quad (9.7)$$

and hence the Lagrangian time derivative of the density is

$$\frac{d\rho}{dt} = \frac{\partial \rho}{\partial t} + \mathbf{v} \cdot \nabla \rho = -\rho (\nabla \cdot \mathbf{v}), \quad (9.8)$$

where the final expression is obtained by substituting from equation (9.6). The Lagrangian time derivative is sometimes called the co-moving time derivative or fluid-frame derivative of the density.

Mass-loss rate

For a stationary one-dimensional radial spherical flow the mass continuity equation reduces to

$$\frac{1}{r^2} \frac{\partial(r^2 \rho v)}{\partial r} = 0 \quad (9.9)$$

from which we find

$$4\pi r^2 \rho(r) v(r) = \text{constant} \equiv \dot{M} \quad (9.10)$$

where \dot{M} is the *mass-loss rate* through a spherical surface of radius r , and v is the velocity in the radial direction. The cgs unit of mass loss is gr sec⁻¹, although it is custom to use the unit M_{\odot} per year: $1 M_{\odot}\text{yr}^{-1} = 6.303 \times 10^{25} \text{ gr sec}^{-1}$. It is straightforward to link the density of nuclei to the mass loss. If we introduce the *mean atomic weight*

$$\mu_a \equiv \frac{1}{m_{\text{amu}}} \sum_k m_k A_k \quad (9.11)$$

where m_k is the atomic mass of element k in atomic mass unit m_{amu} and A_k the abundance by number as defined by eq. (6.32), then

$$\rho(r) = m_{\text{amu}} \mu_a N_N(r) \quad (9.12)$$

such that

$$N_N(r) = \frac{\dot{M}}{4\pi m_{\text{amu}} \mu_a r^2 v(r)} \quad (9.13)$$

Statistical equilibrium

One may also write the equation of continuity separately for each species k in the medium. If these individual particles can occur in different states i we get

$$\frac{\partial n_{ik}}{\partial t} + \nabla \cdot (n_{ik} \mathbf{v}) = \sum_{j \neq i} (n_{jk} P_{ji} - n_{ik} P_{ij}) \quad (9.14)$$

Here n_{ik} is the volume density of particles k in energy level i and $P_{ij} = R_{ij} + C_{ij}$ the rate at which particles change from level i to j . The first term at the right-hand side of eq. (9.14) gives the number of particles per cm³ per second that enter level i . The second term at the right-hand side gives the number of particles per cm³ per second that leave level i .

In a static medium, or in a stationary medium in which equilibrium is reached in a time that is much shorter than the time it takes the characteristic flow velocity to change the local properties of the medium

$$\sum_{j \neq i} (n_{jk} P_{ji} - n_{ik} P_{ij}) = 0 \quad (9.15)$$

This is known as *statistical equilibrium* (SE). In general, the rate P_{ij} contains both radiative and collisional processes (see chapters 7 and 8).

Exercise 9.1

- a) Start with eq. (9.6) and show that in planar geometry the time-dependent continuity equation is given by

$$\frac{1}{\rho} \frac{\partial \rho}{\partial t} + \frac{\partial v_z}{\partial z} + \frac{v_z}{\rho} \frac{\partial \rho}{\partial z} = 0 \quad (9.16)$$

- b) Start with eq. (9.6) and show that in spherical geometry the time-dependent continuity equation for radial flow is given by

$$\frac{1}{\rho} \frac{\partial \rho}{\partial t} + v_r \left[\frac{1}{v} \frac{\partial v}{\partial r} + \frac{2}{r} + \frac{1}{\rho} \frac{\partial \rho}{\partial r} \right] = 0, \quad (9.17)$$

where v is the velocity in the radial direction.

- c) Start with eq. (9.10) and show that for a stationary radial flow the continuity equation is given by

$$\frac{1}{v} \frac{\partial v}{\partial r} + \frac{2}{r} + \frac{1}{\rho} \frac{\partial \rho}{\partial r} = 0 \quad (9.18)$$

Exercise 9.2

The total number of particles of species k is given by

$$N_k = \sum_i n_{ik} \quad (9.19)$$

If the mass of the individual particles of species k is m_k , then

$$\rho = \sum_k m_k N_k \quad (9.20)$$

- a) Give the continuity equation of species k
 b) Show that from a summation over all species one recovers the continuity equation (9.5) for the mass density.

9.2 Momentum equation

Consider again the volume of gas V . If the gas in this volume has pressure $p(\mathbf{r}, t)$, then the total force acting on the volume is the sum of the external pressure on the surface. This is given by the surface integral

$$-\oint_S p dS. \quad (9.21)$$

Transforming this into a volume integral using Gauss's divergence theorem, the net pressure force exerted on the arbitrary volume V is

$$-\oint_S p dS = - \int_V \nabla p \cdot dV, \quad (9.22)$$

and hence the net pressure force per unit volume is simply $-\nabla p$.

The equation of motion of this volume can be derived by equating the force per unit volume with the mass per unit volume multiplied by its acceleration. This is simply Newton's third law. The mass per unit volume is defined as the density ρ and the acceleration is the time derivative of the velocity, i.e. $d\mathbf{v}/dt$. So we have

$$-\nabla p = \rho \frac{d\mathbf{v}}{dt}, \quad (9.23)$$

and hence

$$\frac{d\mathbf{v}}{dt} = -\frac{\nabla p}{\rho}. \quad (9.24)$$

Here $d\mathbf{v}/dt$ is the co-moving acceleration of the gas, so equation 9.24 is the Lagrangian formulation of the equation of motion. The Eulerian formulation is obtained by substituting for $d\mathbf{v}/dt$ using

$$\frac{d\mathbf{v}}{dt} = \frac{\partial \mathbf{v}}{\partial t} + (\mathbf{v} \cdot \nabla) \mathbf{v}. \quad (9.25)$$

If the gas is also in a force field \mathbf{f} , for instance a gravitational field $\rho \mathbf{g}$, then an extra term must be included in eq. (9.24) to account for this. The force on unit volume due to an acceleration \mathbf{g} is simply $\rho \mathbf{g}$, and so eq. (9.24) becomes

$$\rho \left[\frac{\partial \mathbf{v}}{\partial t} + (\mathbf{v} \cdot \nabla) \mathbf{v} \right] = -\nabla p + \mathbf{f} \quad (9.26)$$

This is sometimes referred to as Euler's equation. The momentum equation primarily determines the density c.q. velocity structure of the medium.

Hydrostatic equilibrium

In a static medium (9.26) reduces to the equation of hydrostatic equilibrium

$$\nabla p = \mathbf{f} \quad (9.27)$$

Let us focus on planar atmospheres and derive the above equation again, but now in a heuristic way. In an atmosphere consisting of plane-parallel layers hydrostatic equilibrium implies an equilibrium between the force generated by the gradient of the gas pressure and the gravitational force at the stellar surface, which is assumed constant

$$g_* = \frac{GM_*}{R_*^2} \quad (9.28)$$

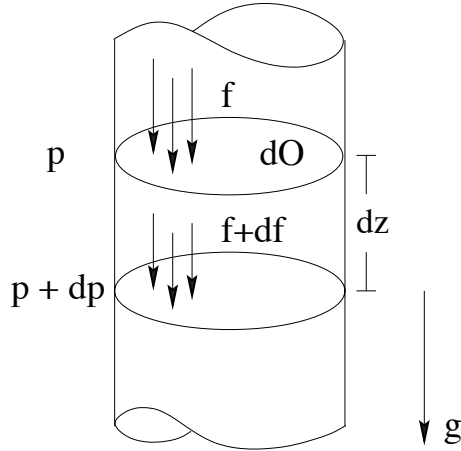


Figure 9.1: Schematic representation of hydrostatic equilibrium. The gas that is on top exerts a force f on surface dO , causing a pressure p . The weight of the volume $dOdz$ adds an amount df to the force, such that the pressure in the interval dz increases with an amount $dp = df/dO$.

where G is the gravitational constant. The gravitational force may be considered constant if *i*) the thickness of the atmosphere is much less than the stellar radius R_* – the inherent assumption of a planar atmosphere, and *ii*) the mass of the atmosphere is much smaller than the total mass of the star M_* , which holds for all stars.

Consider an elementary volume, with cross-section dO and length dz in the direction normal to the planar layers (see figure 9.1). The difference in pressure between the top and bottom of the volume is the force per unit surface of the mass of the volume. This force df is the product of density ρ , volume, and gravity g_* . For the pressure difference we find $dp = df/dO = -\rho g_* dz$, therefore

$$\frac{dp}{dz} = -\rho g_* \quad (9.29)$$

To illustrate the solution of this equation we assume that the total pressure in the atmosphere is dominated by the gas pressure, and that radiation pressure can be neglected. This allows us to use the ideal gas law eq. (6.30). If we introduce the *mean molecular weight* μ , which gives the mean mass per free particle in units of the atomic mass unit m_{amu} (an in this context perhaps somewhat confusing name) we find

$$p = \frac{\mathcal{R}\rho T}{\mu} \quad (9.30)$$

where $\mathcal{R} \equiv k/m_{\text{amu}}$ is the gas constant. This equation is also referred to as the *ideal gas law*. If we further assume that the atmosphere is isothermal, we find after substitution of eq. (9.30) in (9.29), for the solution of this first order differential equation

$$\rho(z) = \rho(z_0) \exp [-(z - z_0)/H], \quad (9.31)$$

where

$$H = \frac{\mathcal{R}T}{\mu g_*} \quad (9.32)$$

is the *density scale height* of the isothermal atmosphere. It measures the distance over which the density changes with a factor e^{-1} . For our sun this is about 150 km, a sizable fraction of the total geometrical thickness of the photosphere (~ 500 km). For the M1.5 Iab supergiant Antares (α Sco) with $T_{\text{eff}} = 3600$ K, $R_* = 650R_\odot$ and $\log g = 0$ one finds $H = 5\,000\,000$ km. This too is a sizeable fraction of the thickness of the photosphere of Antares. The result shows that for an increasing gravity the atmosphere will become more compact.

Radiation pressure

For extremely luminous stars (such as O-type stars, LBVs and Wolf-Rayet stars) the pressure that is exerted by the photons p_R (see eq. 3.30) is an important component of the total pressure $p = p_G + p_R$. Note that, so as to avoid confusion, we have introduced the subscript G to identify the gas pressure. We may rewrite the equation of hydrostatic equilibrium into

$$\frac{dp_G}{dm} = g_* - \frac{dp_R}{dm} \quad (9.33)$$

where m is the *column mass* (dimensions gr cm^{-2}), which serves as an independent measure of the depth in the atmosphere. The column mass is measured from the outside in, i.e.

$$dm \equiv -\rho dz \quad (9.34)$$

such that at depth z

$$m(z) = \int_z^\infty \rho(z) dz \quad (9.35)$$

gives the total mass of a column of cross-section unit cm^2 between the observer and z . The column mass is a very favourable variable as it allows for a very simple solution of the pressure structure in the atmosphere, $p(m) = g_* m + \text{constant}$.

Using eq. (3.28), (3.30), (4.33), and (4.38) we find for the outward directed acceleration due to the gradient of the radiation pressure

$$g_R(m) \equiv \frac{dp_R}{dm} = \frac{4\pi}{c} \int_0^\infty \chi'_{\nu} H_{\nu} d\nu \quad (9.36)$$

As the accelerations due to gravity g_* and radiation $g_R(m)$ have opposite signs one can have a situation where the net force in the atmosphere is zero (or even outward directed): the gas at this location is no longer bound to the star but “floats” on the photons (loosely speaking). This situation, for which $g_* = g_R$, is known as the *Eddington limit*. In hot O stars, where hydrogen is fully ionized throughout the atmosphere, the extinction is dominated by Thomson

scattering (see § 8.4). Using the fact that this process is wavelength independent, and using eq. (3.17), (3.18) and (3.19) we may derive an expression for the luminosity that is required to reach this situation of no net force in the atmosphere. We find for this *Eddington luminosity*

$$L_E = \frac{4\pi c G M_\star}{\sigma'_e} = 1.3 \times 10^4 \frac{1}{\sigma'_e} \frac{M_\star}{M_\odot} L_\odot \quad (9.37)$$

It is thought that the Eddington limit plays an important role in the life of very massive stars (with initial masses $M \gtrsim 40 M_\odot$) when they reach an evolutionary phase in which they are spectroscopically identified as LBV (see § 2.2).

Atmospheres that are not in hydrostatic equilibrium

In the above discussion we have assumed that the forces due to pressure gradients and gravity are in equilibrium. Yet there are stars that have, for a range of reasons, a stationary stellar wind. This wind causes the atmosphere to be extended. In many cases the stellar wind does not have a significant influence on the continuum emission of the star. For luminous O, LBV and Wolf-Rayet stars this, however, *is* the case (see § 2.2). Notably Wolf-Rayet stars may develop stellar winds that are so strong that the continuum radiation is formed in the wind. Acoustic waves in red giants and supergiants, and pulsations in asymptotic giant branch stars can also lead to very extended atmospheres. Stellar winds of hot stars will be discussed in more detail in chapter 16.

Exercise 9.3

- a) Assume that in a planar geometry the only force field present is f_z and that this field is acting in the z -direction only. Start with eq. (9.26) and show that in this geometry the time-dependent momentum equation is given by

$$\rho \left[\frac{\partial v_z}{\partial t} + v_z \frac{\partial v_z}{\partial z} \right] = - \frac{\partial p}{\partial z} + f_z \quad (9.38)$$

- b) Assume that in a spherical geometry the only force field present is f_r and that this field is acting along the radial direction only. Start with eq. (9.26) and show that in this geometry the time-dependent momentum equation for radial flow is given by

$$\rho \left[\frac{\partial v}{\partial t} + v_r \frac{\partial v}{\partial r} \right] = - \frac{\partial p}{\partial r} + f_r \quad (9.39)$$

Exercise 9.4

For general equations of state, the speed of sound is given by

$$v_s^2 = \frac{\partial p}{\partial \rho} \quad (9.40)$$

where the derivative is taken with respect to adiabatic change. It follows from eq. (9.30) that for an isothermal medium and a constant mean molecular weight μ , $v_s = \sqrt{\mathcal{R}T/\mu}$. Assume that the only force field present is gravity, such that $f_r = \rho g$ with $g = -GM/r^2$. Use the results eq. (9.18) and eq. (9.39) and show that for an isothermal medium in which the mean molecular weight is constant, the equation of motion for a stationary radial flow can be written as

$$\frac{1}{v} \frac{\partial v}{\partial r} = \left[\frac{2v_s^2}{r} - \frac{GM}{r^2} \right] / [v^2 - v_s^2]. \quad (9.41)$$

This equation has a singularity at the point where $v(r) = v_s$, where the denominator is zero and $\partial v/\partial r$ becomes infinite (which cannot be physical), unless the numerator is also zero there. As this equation traces the change of velocity in only one direction, i.e. r , the partial derivative $\partial/\partial r$ may be replaced by the total derivative d/dr . We return to this equation in Chapter 16.

Exercise 9.5

- a) Compute the density scale height of the Earth atmosphere at the surface. Assume our atmosphere to be isothermal.
- b) Compute the gas density at the Earth surface knowing that the surface pressure is 1.013×10^6 barye (cgs unit) or 1.013×10^5 Pa (SI unit).
- c) Compute the total column mass m (Eq. 9.35) and total gas mass of Earth's atmosphere.

Exercise 9.6

Show that for a static, spherical, isothermal atmosphere

$$\rho(r) = \rho(r_\odot) \exp \left[-\frac{(r - r_\odot)}{H} \frac{r_\odot}{r} \right] \quad (9.42)$$

Exercise 9.7

- a) Derive that the acceleration due to the gradient in the radiation pressure, g_R , is given by equation (9.36).
- b) Show that if $g_* = g_R$, the Eddington luminosity is given by equation (9.37), assuming the continuum extinction is dominated by Thomson scattering.

Exercise 9.8

Consider a homogeneous isothermal planar atmosphere, with temperature $T = 6\,000\text{ K}$; mean molecular weight $\mu = 0.6$, and a gravity $\log g = 4.4$ in c.g.s. units. The continuum mass extinction coefficient $\chi'_{\text{cont}} = 0.6\text{ cm}^2\text{ gr}^{-1}$. The atmosphere is in hydrostatic equilibrium. The gas may be considered to be ideal. The gas constant $\mathcal{R} = 8.31 \times 10^7$ (cgs).

- Compute the density scale height in this atmosphere?
- Derive an expression for the optical depth at position z_o in the atmosphere when it is given that $\rho(z_o) = \rho_o$.
- Compute the density in gr cm^{-3} at $\tau_{\text{cont}} = 1$.
- Explain why the (pressure broadened) hydrogen lines in supergiants are so narrow (flip ahead to Section 12.2 for more information).

9.3 Energy equation

Conservation of energy is expressed by the *energy equation*

$$\frac{\partial}{\partial t} \left(\frac{1}{2} \rho v^2 + \rho \epsilon \right) + \nabla \cdot \left[\left(\frac{1}{2} \rho v^2 + \rho \epsilon \right) \mathbf{v} \right] + \nabla \cdot (p \mathbf{v}) = \mathbf{f} \cdot \mathbf{v} - \nabla \cdot (\mathcal{F}_{\text{rad}} + \mathcal{F}_{\text{conv}} + \mathcal{F}_{\text{con}}) \quad (9.43)$$

where ϵ is the specific (i.e. per unit mass) internal energy and the term $\nabla \cdot (p \mathbf{v})$ the work done by the gas pressure p to accomplish a change in the specific volume (so the change of volume per mass unit, i.e. per $1/\rho$). Heating by radiation, convection and conduction are described by the divergences of \mathcal{F}_{rad} , $\mathcal{F}_{\text{conv}}$ and \mathcal{F}_{con} , i.e. the total radiative, convective and conductive flux, respectively. In principle other terms could be added to the energy equation, such as terms due to viscous processes. The energy equation primarily determines the temperature structure of the medium.

Radiative equilibrium

In a static medium in which all energy is transported in the form of radiation the energy equation reduces to

$$\nabla \cdot \mathcal{F}_{\text{rad}} = 0 \quad (9.44)$$

This is the equation of *radiative equilibrium*. For a planar atmosphere we find $d\mathcal{F}/dz = 0$, where we have dropped the subscript “rad” as hereafter we will only speak of radiative flux. So, the same amount of total flux passes through each planar layer. This is to be expected: as no energy is generated in the atmosphere of a normal star (for instance by thermonuclear

reactions) the only thing that needs to be done is to transport the energy outward. The constant total flux is given by eq. (3.18), which we here repeat

$$\mathcal{F} = \text{constant} = \sigma T_{\text{eff}}^4 \quad (9.45)$$

Note that the effective temperature T_{eff} does *not* represent a physical temperature, but is a measure of the total flux (see also § 6.6).

For a spherical atmosphere eq. (9.44) implies that $\partial(r^2 \mathcal{F})/\partial r = 0$, or

$$4\pi r^2 \mathcal{F}(r) = \text{constant} = L \quad (9.46)$$

where L is the luminosity of the star. So, for the case of spherical shells the total flux, and therefore the effective temperature, depends on distance. To conserve the concept of effective temperature (as best as possible) it is custom to identify T_{eff} with the total flux at the stellar surface R_\star (see eq. 3.19).

Equations 9.45 and 9.46 are *global* representations of the condition of radiative equilibrium. The total flux that enters the “inner boundary” of the atmosphere should also leave the at the “outer boundary”. We can however also formulate the requirement of radiative equilibrium in a *local* representation using the zero-order moment of the equation of transfer (eq. 4.37 or 4.40). For a planar geometry we find

$$4\pi \int_0^\infty \chi_\nu(z) [S_\nu(z) - J_\nu(z)] d\nu = 0 \quad (9.47)$$

An identical equation is found for the case of spherical shells, with z replaced by r . Each volume element of gas must fulfill the above requirement. This is why this is called the local representation of radiative equilibrium. The equation describes that the total amount of energy that is absorbed by an elementary volume of gas per second ($4\pi \int_0^\infty \chi_\nu J_\nu d\nu$) must be equal to the total amount of energy that is emitted from the volume in the same time interval ($4\pi \int_0^\infty \chi_\nu S_\nu d\nu = 4\pi \int_0^\infty \eta_\nu d\nu$).

The effect of scattering on radiative equilibrium

In eq. (9.47) we may replace the total extinction coefficient χ_ν by the “true” absorption coefficient κ_ν (see eq. 4.4) and the source function by the local Planck function. The reason for this is that scattering contributions drop out of the equation. Obviously, this is what one would intuitively expect should happen: the scattering of a photon does not lead to a change in the energy balance in the elementary volume and therefore can not contribute to eq. (9.47). To illustrate this we use a proto-type source function (see also eq. 4.31) that contains both a thermal and a scattering component, i.e.

$$S_\nu = \frac{\kappa_\nu B_\nu + \sigma_\nu J_\nu}{\kappa_\nu + \sigma_\nu} \quad (9.48)$$

Let us first briefly discuss this equation. Thermal emission, as expected, is described by the Kirchhoff-Planck relation (6.3), i.e. $\eta_\nu^{\text{th}} = \kappa_\nu B_\nu$. The contribution of scattering processes

to the emission is given by $\eta_\nu^{\text{sc}} = \sigma_\nu J_\nu$, where we have assumed that the scattering process is isotropic and coherent (for coherent scattering, see § 8.4). After all, for isotropic scattering the fraction of energy that is scattered out of a beam of light that is incident from direction \mathbf{n} , into a beam of solid angle $d\omega$ in for instance the direction of the observer, is $d\omega/4\pi$. For coherent scattering the contribution to the emission into this direction is $d\eta_\nu^{\text{sc}}(\mathbf{r}) = \sigma_\nu(\mathbf{r}) I_\nu(\mathbf{r}, \mathbf{n}) d\omega/4\pi$. Integrating over all incident directions yields $\eta_\nu^{\text{sc}} = \sigma_\nu J_\nu$.

Substitution of the proto-type source function in eq. (9.47) results in

$$4\pi \int_0^\infty \kappa_\nu(z) [B_\nu(z) - J_\nu(z)] d\nu = 0 \quad (9.49)$$

This equation shows that the total thermal emission $\int_0^\infty \kappa_\nu B_\nu d\nu$, which fixes the *local* temperature T , is determined by the mean intensity. The value of J_ν depends upon the *global* properties of the atmosphere because it follows from a solution of the transfer equation. Thus the temperature at a given point in the atmosphere is to some extent determined by the temperature at all other points and, at the same time, helps to establish the temperature structure elsewhere. This nonlocalness in the problem is a result of radiative transfer, by which photons moving from one point in the medium to another give rise to a fundamental coupling (i.e. interdependence) of the properties at those points.

Exercise 9.9

Show that the local constraint of radiative equilibrium, eq. (9.47), is already contained in eq. (4.28) and (4.29).

9.4 Convection

In a stellar atmosphere energy can also be transported by convection, i.e. by large scale motions of gas elements that obtain an excess energy content at some place and that deposit this excess energy at some other place. Convection becomes important in the somewhat deeper layers of the atmospheres of late type stars, starting at about middle F-stars. In the outermost part of the atmosphere, where $\tau < 1$ and photons can freely escape, the transport of energy by radiation is always more efficient than by convective motions. For stars of earlier spectral type than mid-F all of the atmosphere is in radiative equilibrium.

At the solar surface the convective motions are visible as a complex granulous pattern (see figure 9.2). The rising convective cells, called *granules*, are about 100 K warmer than the surrounding relatively dark cells. Because of this temperature difference the rising granules are about 25 percent brighter. The velocity of the cells is between 1 and 2 km sec⁻¹. The cells that go down have a velocity that typically is twice as large. There are at least two reasons why the falling gas moves faster than the rising gas. First, the darker areas cover less than half

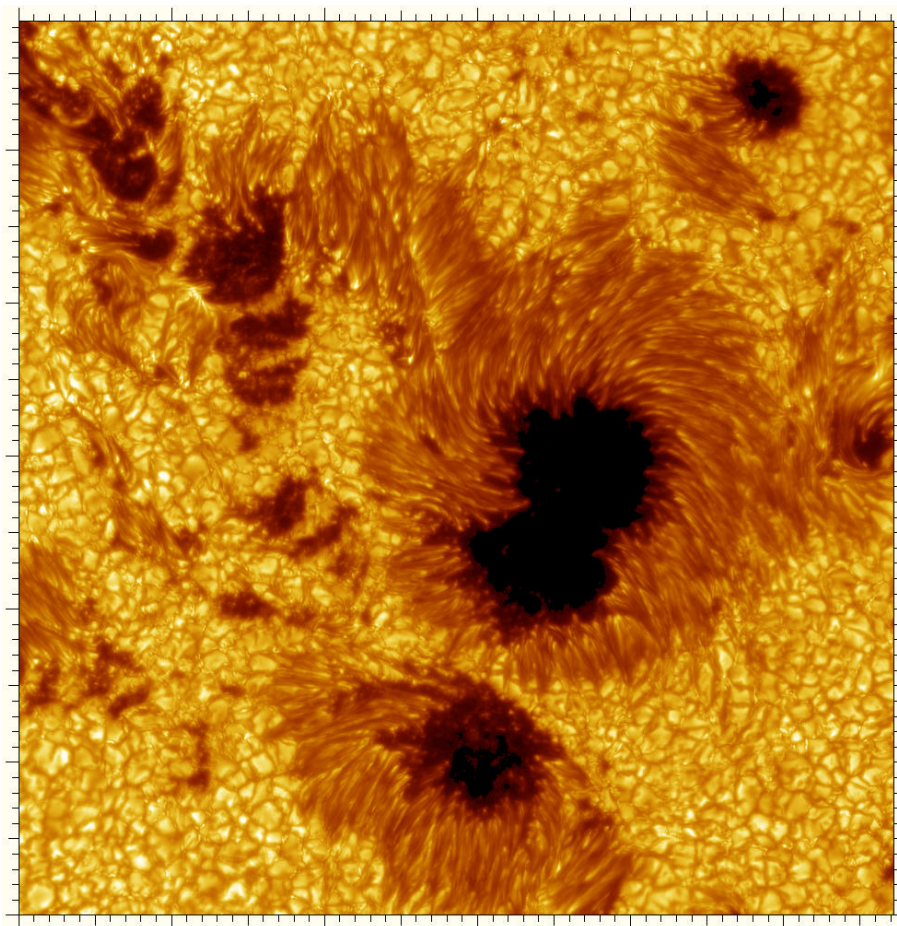


Figure 9.2: Detailed image of the surface of the sun. The tick marks are 1000 km apart. Though what we see here is part of a sunspot group near disk center, the irregular granular pattern can clearly be seen around the sunspot structures. The granular pattern is caused by temperature variations over the surface. The individual cells, or granules are the signature of convective motions and exist for about five minutes. The rising granules are about 100 K warmer compared to the relatively dark inter-granular regions that are falling; this higher T corresponds to a brightness difference of about 25 percent. The velocity of the rising granules is about 1 to 2 km sec^{-1} ; the velocities of the falling material is about twice as large. From: The institute for Solar Physics, Sweden.

of the solar surface. Conservation of mass flow thus requires the downward velocities to be larger than the upward velocities. More important, the continuum extinction is lower in the cooler areas, such that we see deeper layers, where the convective velocities are larger.

Convective motions are turbulent and consist of a complicated hierarchy of “eddies” or “bubbles” moving and interacting in an extremely involved way. Turbulence is a complex mathematical problem for which a definitive theory does not yet exist. Instead one adopts a phenomenological description that includes free scaling parameters. In this *mixing length theory*

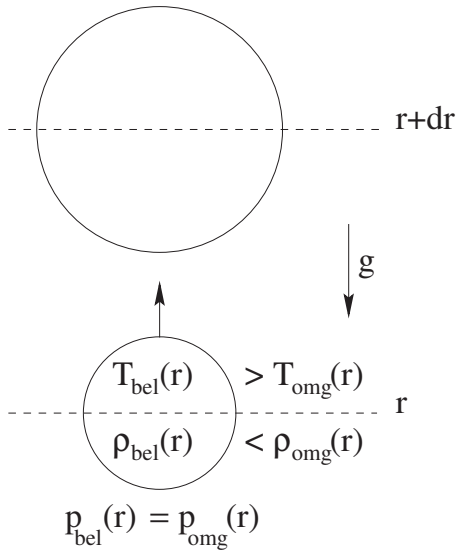


Figure 9.3: Schematic representation of convection. A gas bubble having a temperature slightly above that of its surrounding, and that does not exchange heat with these surroundings, will rise because the density in the bubble is lower than that of its surroundings.

it is assumed that the convective cells travel a certain distance (the mixing length) before they deposit their excess thermal energy into their surroundings. We will not give a detailed description of the physics of energy transfer by convection, rather we focus on deriving a criterion that will allow us to determine whether energy is transported by radiation or by convection.

Schwarzschild instability criterion

Let us forget about the complex of turbulent gas motions, and focus on the movement of a single identifiable “bubble” of gas. We assume this gaselement is hotter than its surroundings. In order for the bubble *not* to radiate this surplus of thermal energy the total optical depth measured over the dimensions of the bubble should be large, i.e. $\tau > 1$. We also assume that the motion of the bubble is subsonic, such that it will be in pressure equilibrium with its surroundings (an equilibrium that sets itself with the velocity of sound). Because of this the density in the bubble will be lower than that of its surroundings. According to Archimedes law the bubble will rise (see figure 9.3). We further assume that all during the rise of the bubble none of the surplus in energy will leak into the ambient medium – i.e. the convective bubble behaves adiabatically. The change in density in the cel, after it has ascended a distance dr , can then be described by $(d\rho)_{cel} = (d\rho/dr)_{ad} dr$. In a radiative surroundings the change in density over the same distance will be $(d\rho)_{sur} = (d\rho/dr)_{rad} dr$. As long as the density in the bubble is lower than that of its surroundings it will continue its rise upward in the atmosphere, and convection will persist. Convection thus occurs when $(d\rho/dr)_{cel} < (d\rho/dr)_{sur}$ (Recall

that both density gradients are negative), or, phrased differently

$$\left. \frac{d \log \rho}{d \log p} \right|_{ad} > \left. \frac{d \log \rho}{d \log p} \right|_{rad} \quad (9.50)$$

(the sign flips as also dp/dr is negative). For adiabatic circumstances *Poisson's law* is valid

$$p = \text{constant } \rho^\gamma \quad (9.51)$$

where the *adiabatic index* γ is the ratio between the specific heat at constant pressure and constant volume. One gets

$$\left. \frac{d \log \rho}{d \log p} \right|_{ad} = \frac{1}{\gamma} \quad (9.52)$$

Using the ideal gas law eq. (9.30) we find for this gradient in a radiative environment

$$\left. \frac{d \log \rho}{d \log p} \right|_{rad} = 1 - \left. \frac{d \log T}{d \log p} \right|_{rad} + \left. \frac{d \log \mu}{d \log p} \right|_{rad} \quad (9.53)$$

Substituting the results (9.52) and (9.53) into the convection criterion (9.50) yields

$$\left. \frac{d \log T}{d \log p} \right|_{rad} > \frac{\gamma - 1}{\gamma} + \left. \frac{d \log \mu}{d \log p} \right|_{rad} = \left. \frac{d \log T}{d \log p} \right|_{ad} \quad (9.54)$$

The last equality on the right-hand side can be verified by substitution of the ideal gas law into eq. (9.51) and subsequent differentiation. The above equation is known as the *Schwarzschild instability criterion*, after the person that thought of it. In terms of the temperature gradient dT/dr we may write the criterion for convection to occur as

$$\left| \frac{dT}{dr} \right|_{rad} > \left| \frac{dT}{dr} \right|_{ad} \quad (9.55)$$

This shows that an atmosphere will opt for the smallest temperature gradient: if $|dT/dr|_{rad}$ is larger than $|dT/dr|_{ad}$ it will switch to the transport of energy by convection.

Condition for convection to occur

Using the diffusion approximation 4.65, which for the radiative temperature gradient yields

$$\frac{dT}{dz} = -\frac{3}{16\sigma} \frac{\chi'_{R}\rho\mathcal{F}}{T^3} \quad (9.56)$$

where χ'_{R} is the Rosseland mean mass extinction coefficient (dimensions $\text{cm}^2 \text{ gr}^{-1}$), i.e. $\chi_R = \chi'_{R}\rho$, and equation (9.29) describing hydrostatic equilibrium, we may obtain an explicit formulation of the radiative gradient (9.54). We find

$$\left. \frac{d \log T}{d \log p} \right|_{rad} = -\frac{3}{16\sigma} \frac{\chi'_{R}\mathcal{F}p}{g_* T^4} = -\frac{3}{16} \frac{\chi'_{R}p}{g_*} \left(\frac{T_{\text{eff}}}{T} \right)^4 \quad (9.57)$$

The atmosphere will thus become unstable for convection if the extinction becomes too large. For increasing extinction it will be harder to transport energy by means of photons, since radiation gets effectively trapped. The star has two ways to solve for this problem. One way is to increase in size, as $(d \log T / d \log p)_{\text{rad}} \propto p/T^4 \propto \rho/T^3$, and therefore the value of the radiative gradient can go down if at the position of temperature T the density would be lower. In other words, the star needs to swell. The second possibility is for the star to switch to a transport of energy by convection the moment that criterion (9.54) is fulfilled.

It is more likely for convection to take over if the adiabatic gradient is small. This may happen when changes in the ionization or in the chemistry of the gas occur. We first discuss the effects of chemistry. Stars of relatively late spectral type (G or later) show a strong increase in molecular abundances. The formation of molecules changes the adiabatic index γ from 5/3 for a fully mono-atomic gas toward 7/5 for a fully di-atomic gas. The result is that the factor $(\gamma - 1)/\gamma$ in eq. (9.54) goes down from 0.4 to 0.29. The presence of molecules thus increases the chance for convection to occur. The adiabatic gradient is also lower in regions where hydrogen (or helium) gets ionized. Here the gradient $d \log \mu / d \log p$ is negative, lowering the threshold at which convection starts. Progressing from deep layers towards the surface, i.e. in the direction of decreasing temperature, the extinction of hydrogen will increase strongly in the zone in which this element recombines, notably due to bound-free processes. This requires a steeper temperature gradient for energy to be transported by radiation, and thus increases the likelihood that convection takes over. The effect of recombination in a convective cell (that does not exchange heat with its environment) is that extra energy is added to the gas (13.6 eV per recombination of electron and proton), causing the bubble to expand further, which sustains convection. Zones of molecule formation in extremely cool stars cause a similar effect. Such zones are therefore advantageous for two reasons, both for initiating and sustaining convection.

10

Grey atmosphere in radiative equilibrium

The definition of a *grey medium* is that the extinction coefficient is independent of frequency, i.e. $\chi_\nu = \chi$. In many cases this is a very unrealistic assumption. For instance, think about absorption lines and ionization edges. These show an extreme frequency dependent behavior. The only real example of a grey extinction is that of Thomson scattering on free electrons. Still, studying the grey atmosphere problem is extremely useful. First, because the grey problem very nicely illustrates how the temperature structure is the result of a combined solution of the transfer equation and the energy equation. Second, because the end result for $T(r)$ compares remarkably well to those obtained from advanced models, and third, because the latter implies that this simple model may serve as an excellent starting model for the iterative methods that are required to construct LTE and NLTE atmosphere models.

10.1 Description of the grey atmosphere

We assume that the atmosphere consists of planar layers. The equation of transfer for a grey medium follows from eq. (4.34) and is given by

$$\mu \frac{dI_\nu}{d\tau} = I_\nu - S_\nu \quad (10.1)$$

Note that the optical depth is no longer frequency dependent. Integration of this equation over frequency yields

$$\mu \frac{dI}{d\tau} = I - S \quad (10.2)$$

where I is the total specific intensity (eq. 3.3) and S is the total source function (eq. 4.32).

We require the atmosphere to be in radiative equilibrium. From eq. (9.47) it follows that

$$\int_0^\infty \chi S_\nu d\nu = \int_0^\infty \chi J_\nu d\nu \quad (10.3)$$

Because $\chi \neq \chi_\nu$, the equation reduces to $S = J$. If the source function can be written as eq. (9.48) it also holds that $J = B$ (see eq. 9.49), and therefore $S = B$. Using Stefan-Boltzmann's law (eq. 6.11) we finally obtain $J = (\sigma/\pi)T^4$. This implies that if we derive a solution for $J(\tau)$, we may immediately couple it to the temperature, automatically fulfilling the requirement of energy conservation.

Integration of the 0th order moment of the equation of transfer over frequency (eq. 4.37) yields

$$\frac{dH}{d\tau} = J - S = 0 \quad (10.4)$$

implying that the total Eddington flux $H = \text{constant} = \sigma T_{\text{eff}}^4 / 4\pi$.

Integration of the 1st order moment of the equation of transfer over frequency (eq. 4.38) results in

$$\frac{dK}{d\tau} = H \quad (10.5)$$

which has an elementary solution $K(\tau) = H \times (\tau + \text{constant})^1$. If we also integrate the Eddington factor f_ν over frequency, which gives $f = K/J$, we find

$$3f(\tau)J(\tau) = 3H(\tau + \text{constant}) \quad (10.6)$$

and for the temperature as a function of optical depth

$$3f(\tau)T^4(\tau) = \frac{3}{4}T_{\text{eff}}^4(\tau + \text{constant}) \quad (10.7)$$

To know the exact behavior $T(r)$ we thus need to determine the run of $f(\tau)$ throughout the atmosphere. As we have seen in § 3.6, deep in the atmosphere, where the radiation field is almost isotropic, $f \rightarrow 1/3$, such that

$$J(\tau) \rightarrow 3H\tau \quad \forall \tau \gg 1 \quad (10.8)$$

At depth, the mean intensity is a linear function of optical depth. Close to the surface we obviously expect that $f(\tau) \neq 1/3$, and thus $J(\tau)$ can not be described by this simple relation. To account for this, we could define a general relation for the exact expression of the mean intensity that looks like

$$J(\tau) = 3H(\tau + q(\tau)) \quad (10.9)$$

where the anisotropy of the radiation field has been absorbed in the function $q(\tau)$. This $q(\tau)$ is known as the *Hopf-function*. There is an elegant, though somewhat complex analytical solution of the Hopf-function that requires numerical integration. We will return to this solution below. Using the Hopf-function we find for the general solution of the grey temperature structure

$$T^4(\tau) = \frac{3}{4}T_{\text{eff}}^4(\tau + q(\tau)) \quad (10.10)$$

¹Do not get confused: the solution is $K(\tau) = H\tau + \text{constant}$. As H is a constant one may define $\text{constant}' = H \times \text{constant}$.

τ	$q(\tau)$	τ	$q(\tau)$	τ	$q(\tau)$	τ	$q(\tau)$
0.00	0.577351	0.20	0.649550	0.8	0.693534	3.0	0.709806
0.01	0.588236	0.30	0.663365	1.0	0.698540	3.5	0.710120
0.03	0.601242	0.40	0.673090	1.5	0.705130	4.0	0.710270
0.05	0.610758	0.50	0.680240	2.0	0.707916	5.0	0.710398
0.10	0.627919	0.60	0.685801	2.5	0.709191	∞	0.710446

Table 10.1: *The exact solution of the Hopf function $q(\tau)$ for a planar atmosphere. The limit value $q(0) = 1/\sqrt{3}$.*

Eddington approximation

To get a fully explicit solution of the grey temperature structure we pursue an idea of Eddington and assume that everywhere in the atmosphere $f = 1/3$. This assumption, you'll never guess, is called the *Eddington approximation*. For the total mean intensity we obtain from eq. (10.6)

$$J(\tau) = 3H(\tau + \text{constant}) \quad (10.11)$$

This is a linear function of optical depth, which therefore also holds for the source function, as in a grey medium $J = S$. It implies that also the Eddington-Barbier approximation is valid (see § 4.6). From an integration of eq. (4.51) over frequency we know that the emerging total flux is given by

$$H^+(0) = H = \frac{1}{4}S(\tau = 2/3) \quad (10.12)$$

Combining the above two equations one finds for the constant a value of $2/3$. For the temperature we find

$$T^4(\tau) = \frac{3}{4}T_{\text{eff}}^4(\tau + \frac{2}{3}) \quad (10.13)$$

In the Eddington approximation, therefore, $q(\tau) \equiv 2/3$. The real value of the Hopf function smoothly varies between $q(0) = 0.577$ and $q(\infty) = 0.710$, which is never that far off from the Eddington approximation. Table 10.1 gives for a number of optical depths the exact solution of the Hopf function.

Result 10.13 shows that in a grey atmosphere the temperature structure follows from the equation of transfer and the energy equation. The momentum equation, let us assume hydrostatic equilibrium, does not enter in the problem. In other words, the temperature in a grey atmosphere, as a function of optical depth, does not depend on the gravity g_* . However, the equation of hydrostatic equilibrium does control the relation between optical depth and geometrical depth. We will return to this below.

The grey temperature structure is a monotonous function of optical depth. Why is this so? Actually, it follows from the condition of radiative equilibrium, which requires that the total radiative flux is constant throughout the atmosphere. The relation between the radiative flux and the mean intensity measures the degree of anisotropy of the medium (see § 3.6). With increasing (optical) depth in the atmosphere the degree of anisotropy decreases. The only

means of keeping the flux constant is by increasing the energy density of radiation (which is proportional to J). As $J \propto T^4$, the temperature has to increase.

The Eddington approximation also predicts that $T = T_{\text{eff}}$ for $\tau = 2/3$. This result confirms that the “effective depth” of continuum formation is at $\tau \sim 2/3$ (see also eq. 4.51). Note that a photon that is emitted at position $\tau = 2/3$ in the outward direction has a chance of order $e^{-2/3} \sim 0.5$ to escape from the atmosphere by direct flight. This intuitively agrees with what one would expect about the place where the continuum is formed. Finally: equation (10.13) predicts that the temperature at the outer boundary $T(0)/T_{\text{eff}} = (1/2)^{1/4} = 0.8409$. The compares well with the exact value $T(0)/T_{\text{eff}} = 0.8114$.

Limb darkening

In the Eddington approximation we obtain the angle dependence of the emerging radiation by substituting $S(\tau) = 3H(\tau + 2/3)$ in eq. (4.47) and doing the integration. One finds

$$I(0, \mu) = 3H \left(\mu + \frac{2}{3} \right) \quad (10.14)$$

For the relative run of intensity over the stellar disk we then get

$$\frac{I(0, \mu)}{I(0, 1)} = \frac{3}{5} \left(\mu + \frac{2}{3} \right) \quad (10.15)$$

The intensity at the edge of the stellar disk ($\mu = 0$) is thus 40 percent of that at the center of the disk ($\mu = 1$). The effect is referred to as *limb darkening* and the result we have obtained is in first approximation in good agreement with the observed intensity change over the solar disk. It even agrees so well, that it spurred Karl Schwarzschild in 1914 to propose that the outer layers of the sun are in radiative equilibrium, and not in convective equilibrium as was expected on the basis of observations of the solar granulation (see § 9.4).

10.2 Constructing the grey atmosphere

Having obtained the temperature structure we still need to determine the pressure and density structure. In a grey atmosphere the equation of hydrostatic equilibrium (see eq. 9.33 and 9.36) reduces to

$$\frac{dp_G}{dm} = g_\star - \frac{4\pi}{c} \chi' H = g_\star - \frac{\sigma}{c} \chi' T_{\text{eff}}^4 \quad (10.16)$$

For the relation between optical depth and column mass one gets

$$d\tau = (\chi/\rho) dm = \chi' dm \quad (10.17)$$

where χ' is the mean extinction coefficient in $\text{cm}^2 \text{ gr}^{-1}$, which only depends on the abundances A_k , for all chemical elements k , and the state of the gas. For the latter we will assume LTE.

We define a reference point z_\circ at the outer edge of the atmosphere, where the optical depth $\tau(z_\circ) \equiv \tau_\circ$ is small. The temperature at this position follows from eq. (10.10) or (10.13) and will be almost identical to the limiting value $T(0)$. In order to determine the state of the gas we need to know, in addition to the temperature $T(\tau_\circ) \equiv T_\circ$, the density $\rho(\tau_\circ) \equiv \rho_\circ$. We now assume that beyond z_\circ , so even farther out, the state of the gas no longer changes. As in these outer layers, for all practical purposes, the temperature is constant, we obtain

$$\tau_\circ = \chi' \circ \int_{z_\circ}^{\infty} \rho(z) dz = \chi' \circ \rho_\circ H_\circ = \chi' \circ m_\circ \quad (10.18)$$

where we have used eq. (9.31) and (9.35), and where the density scaleheight $H_\circ = \mathcal{R}T_\circ / \mu_\circ g_{\text{eff}}$, and $g_{\text{eff}} = g_\star - g_R(m_\circ)$. The quantities $\chi' \circ$ and μ_\circ are not known, after all, to know these requires knowledge of the state of the gas, for which we need ρ_\circ , which is the very quantity we aim to determine. This means we need to iterate for a moment at the position z_\circ to get the correct ρ_\circ . Take as a starting solution an arbitrary mean extinction, say $\chi' \circ = 0.5 \text{ cm}^2 \text{ gr}^{-1}$. This yields by means of eq. (10.18) a value for the density ρ_\circ . Set the mean molecular weight μ_\circ equal to the mean atomic weight μ_a (see eq. 9.11). We can then compute the state of the gas from $N_\circ = \rho_\circ / (\mu_\circ m_{\text{amu}})$ and T_\circ following the method described in § 6.5. This results in new values for $\chi' \circ$ and μ_\circ , from which a new value of the density can be obtained, which, in turn, can be used to derive a new state of the gas, etcetera; until ρ_\circ is converged. From the ideal gas law eq. (9.30) we find the gas pressure $p_{G,\circ} = N_\circ k T_\circ$.

We may now determine the structure of the entire atmosphere by integrating eq. (10.16) in the inward direction using an integration scheme for normal differential equations, such as for instance a 4th order Runge-Kutta method. Use the value $\chi' \circ$ to take a small step dm c.q. $d\tau$; this yields $p_G(m_\circ + dm)$; determine using eq. (10.10) or (10.13) the value $T(m_\circ + dm)$; from the ideal gas law we then find $N(m_\circ + dm)$, which gives us all we need to determine the state of the gas at $m_\circ + dm$. Take the next step, etcetera. Stop the integration if the total optical depth $\tau \sim 100$. This concludes the computation of the grey atmosphere.

However, there is one problem we have so far not discussed, which is how to determine a mean (i.e. grey) extinction coefficient for a gas of which the excitation and ionization state is known. This will be discussed in the next section.

Exercise 10.1

Which fraction of the mass of the sun is in its atmosphere? Assume that the sun has an isothermal gray atmosphere for which $\chi'(z) = 0.8 \text{ cm}^2 \text{ gr}^{-1}$. We define the atmosphere to reach down to $\tau = 20$.

10.3 Mean extinction coefficients

In a realistic situation, the extinction coefficient will be strongly frequency dependent. Especially so, when spectral lines are present. A grey extinction coefficient is therefore a quantity that needs to be defined. It implies that a grey atmosphere can at most give a – to some degree successful or otherwise – approximation of reality. Still, it would be useful if we could preserve some of the results of the grey atmosphere problem, by making a careful choice of mean extinction coefficients. To start out, we recapitulate the transfer equations and its first two moments in both the monochromatic and frequency-integrated grey case:

$$\begin{array}{ll} \mu \frac{dI_\nu}{dz} = \chi_\nu (S_\nu - I_\nu) & \mu \frac{dI}{dz} = \chi (J - I) \\ \frac{dH_\nu}{dz} = \chi_\nu (S_\nu - J_\nu) & \frac{dH}{dz} = 0 \\ \frac{dK_\nu}{dz} = -\chi_\nu H_\nu & \frac{dK}{dz} = -\chi H \end{array}$$

The monochromatic equations are on the left; the frequency-integrated grey equations are on the right. We will now discuss two means of defining a mean extinction coefficient, the flux-weighted mean, and the Rosseland mean.

Flux-weighted mean extinction

Say, we are interested in a mean extinction such that the 1st order moment of the transfer equation reduces to the grey case. Integration of the monochromatic equation over frequency yields

$$-\frac{dK}{dz} = - \int_0^\infty \frac{dK_\nu}{dz} d\nu = \int_0^\infty \chi_\nu H_\nu d\nu = \chi_F H \quad (10.19)$$

where

$$\chi_F \equiv \frac{1}{H} \int_0^\infty \chi_\nu H_\nu d\nu \quad (10.20)$$

is the *flux-weighted mean extinction coefficient*. Note that the choice of χ_F does not reduce the nongrey transfer problem completely to the grey case, for the transfer equation and its 0th order moment do not transform to their respective grey equivalents with this choice of mean extinction. Furthermore, there is the practical problem that H_ν is not known *a priori*, and therefore χ_F cannot actually be calculated until after the transfer equation is solved. This latter difficulty can be overcome by an iteration between the construction of the grey model and the calculation of χ_F . Although the desired goal has not been fully attained, the fact that the flux-weighted mean preserves the K -integral is important, for it implies that the correct value is recovered for the radiation pressure p_R , as well as for the radiation force dp_R/dz . This

is of relevance for the determination of the density structure from the equation of hydrostatic equilibrium (see e.g. eq. 10.16).

Rosseland mean extinction

Say, we are interested in a mean extinction such that the correct value of the integrated flux H is conserved. That is, that we fulfill the constraint of radiative equilibrium. Using the 1st order moment of the transfer equation we obtain

$$-\int_0^\infty \frac{1}{\chi_\nu} \frac{dK_\nu}{dz} d\nu = \int_0^\infty H_\nu d\nu = H = -\frac{1}{\chi} \frac{dK}{dz} \quad (10.21)$$

where

$$\frac{1}{\chi} = \frac{\int_0^\infty (1/\chi_\nu) (dK_\nu/dz) d\nu}{\int_0^\infty (dK_\nu/dz) d\nu} \quad (10.22)$$

Again we face the practical difficulty that K_ν is not known *a priori*, and therefore χ defined according to the above definition can not be determined until the transfer equation is solved.

Still, it can be meaningful to use this definition of the mean extinction. However, we need to make an assumption. To do so, we use the fact that at great optical depth (i.e. $\tau_\nu \gg 1$), where the radiation field is almost isotropic and the properties of the material medium are (locally) very close to thermodynamic equilibrium, $K_\nu \rightarrow 1/3J_\nu$ (see § 3.6), and $J_\nu \rightarrow B_\nu$ (see § 6.2). In that case

$$\frac{dK_\nu}{dz} \simeq \frac{1}{3} \frac{dB_\nu}{dz} = \frac{1}{3} \frac{dB_\nu}{dT} \frac{dT}{dz} \quad (10.23)$$

which yields for the mean extinction

$$\frac{1}{\chi_R} \equiv \frac{\int_0^\infty (1/\chi_\nu) (dB_\nu/dT) d\nu}{\int_0^\infty (dB_\nu/dT) d\nu} \quad (10.24)$$

This is the *Rosseland mean extinction coefficient*, which was already introduced in § 4.6 in the derivation of the diffusion approximation (see eq. 4.63). It is an harmonic mean, i.e. the largest contributions are from frequency regions where χ_ν is smallest and the transported flux is largest. The use of the Rosseland mean optical depth scale τ_R will, at great optical depth, recover the correct shape of the asymptotic transfer equation (eq. 4.62), and, therefore, the correct total flux (eq. 4.65). In regions of large optical depth the temperature structure of a stellar atmosphere in radiative equilibrium is thus given by

$$T^4(\tau_R) = \frac{3}{4} T_{\text{eff}}^4 (\tau_R + q(\tau_R)) \quad (10.25)$$

For small optical depths the above approximation is no longer valid, as flux conservation near the stellar surface can no longer be guaranteed. Consequently, the temperature structure will deviate from eq. (10.25).

Exercise 10.2

Show that at large optical depth eq. (10.25) reduces to diffusion equation 4.65. Use table 10.1 to determine the behavior of $q(\tau_R)$ for $\tau_R \gg 1$.

Exercise 10.3

Ponder on the results in this chapter and write down an expression for the Rosseland optical depth from the surface to the center of a star. Estimate the total radial Rosseland optical depth for the Sun, using information from the internet if needed.

LTE atmosphere in hydrostatic and radiative equilibrium

In this chapter we discuss the construction of the LTE model atmosphere. The field of LTE atmospheres is fully dominated by the model grid and the computer code ATLAS of Bob Kurucz. We will therefore limit the discussion of LTE to this grid. Realize, however, that a number of other independent codes exist, mainly aimed at studying very cool stars.

11.1 Constructing the LTE atmosphere

We assume that the atmosphere consists of planar layers and that both hydrostatic and radiative equilibrium hold. The relevant transfer equation is eq. (4.39), which we repeat for clarity

$$\frac{d^2(f_\nu J_\nu)}{d\tau_\nu^2} = J_\nu - S_\nu = \frac{\kappa_\nu}{\kappa_\nu + \sigma_\nu}(J_\nu - B_\nu) \quad (11.1)$$

The second equality follows after substitution of the proto-type source function eq. (9.48). The extinction coefficient κ_ν is here the sum over all bound-bound, bound-free, and free-free absorption cross sections that may occur; σ_ν is the sum over all scattering processes. Recall that we derived the left part of this equation using the moments of the transfer equation. Note that we could also have obtained this result by integrating the 2nd order differential equation for the symmetric average (eq. 5.17) over all solid angles. (In view of the definition of the symmetric average this integration would have been over the angles $0 \leq \mu \leq 1$). This yields an identical result. With this in mind, it is straightforward to derive the boundary conditions of eq. (11.1), i.e., we only need to integrate the boundary conditions of the symmetric average eq. (5.20) and (5.21) in a similar way. After having multiplied by μ , we obtain for the condition at the outer edge $\tau_\nu = 0$

$$\left. \frac{d(f_\nu J_\nu)}{d\tau_\nu} \right|_0 = g_\nu(0)J_\nu(0) \quad (11.2)$$

where the Eddington factor $g_\nu(0) = H_\nu(0)/J_\nu(0)$, which we, inspired by eq. (10.9) for the grey problem, set to the initial value $1/\sqrt{3}$ (see table 10.1). For the outer edge $\tau_\nu = \tau_{\max}$ we find

$$\frac{d(f_\nu J_\nu)}{d\tau_\nu} \Big|_{\tau_{\max}} = \frac{1}{3} \left(\frac{1}{\chi_\nu} \left| \frac{dB_\nu}{dz} \right| \right)_{\tau_{\max}} \quad (11.3)$$

Discretization of these equations is done using the finite difference method as explained in § 5. In eq. (11.1) we obviously choose the outermost right-hand-side term (i.e. not middle one) for discretization, as this allows us to account explicitly for the scattering term in the source function.

The radiation quantities for which we solve directly are J_ν and f_ν , therefore we choose to write the equation of hydrostatic equilibrium as

$$\frac{dp_G}{dm} = g_\star - \frac{4\pi}{c} \int_0^\infty \frac{d(f_\nu J_\nu)}{dm} d\nu \quad (11.4)$$

where we have used eq. (3.28), (3.30), (3.31) and (9.33). Discretization of this 1st order differential equation yields

$$N_d k T_d - N_{d-1} k T_{d-1} + \frac{4\pi}{c} \sum_{n=0}^N w_n (f_{dn} J_{dn} - f_{d-1,n} J_{d-1,n}) = g_\star (m_d - m_{d-1}) \quad (11.5)$$

where $\{m_d\}, d = 0, \dots, D$ is the set of column masses, such that $d = 0$ describes the outer edge of the atmosphere, and $d = D$ the inner edge; w_n are the frequency integration weights of the set $\{\nu_n\}, n = 0, \dots, N$ frequency points.

If we use the grey result (eq. 10.10) as a starting value of the temperature structure, to which we refer as $T_0(m)$, we may determine an initial value for the total particle density $N_0(m)$ analogously to the way we have done this in the grey problem (see § 10.2). The only difference is that we now need to assume a starting value for the mean intensity, for which we take $J_\nu(m) = B_\nu(T_0(m))$, and for the Eddington factor, for which we assume $f_\nu(m) = 1/3$. At each grid point we determine the state of the gas, based on the local values N_d and T_d . This then allows us to compute the extinctions κ_{dn} and σ_{dn} . Once we have derived the structure in this way, the radiation field J_{dn} can be derived from a solution of the transfer equation using the current values f_{dn} . These Eddington factors can then be updated by doing a formal solution, using first the new J_{dn} to update the total source function. This implies that we need to solve eq. (5.17) for the symmetric mean u_{dmn} for each combination of frequency n and angle of incidence m . The new Eddington factors follow from

$$f_{dn} = \frac{K_{dn}}{J_{dn}} = \frac{\sum_{m=0}^M w_m \mu_m^2 u_{dmn}}{\sum_{m=0}^M w_m u_{dmn}}, \quad (11.6)$$

where w_m are the angle integration weights of the set $\{\mu_m\}, m = 0, \dots, M$. In a similar way we may determine new values for g_{0n} , required for the boundary condition (11.2).

The new mean intensities are used to test the equation of radiative equilibrium. In LTE this is eq. (9.49), which we here repeat

$$4\pi \int_0^\infty \kappa_\nu(z) [B_\nu(z) - J_\nu(z)] d\nu = 0 \quad (11.7)$$

and which in discrete form is given by

$$4\pi \sum_{n=0}^N w_n \kappa_{dn} (B_{dn} - J_{dn}) = 0 \quad (11.8)$$

where again w_n are the frequency integration weights of the set $\{\nu_n\}$, $n = 0, \dots, N$ frequency points. From this equation we determine a new value for the temperature T_d at each grid point. How to do this is discussed in the next section. With this new run of temperatures we redo the above described process, and we keep iterating until T_d is converged. This gives the LTE model atmosphere.

Finally, the emerging spectrum of the LTE model is given by

$$\mathcal{F}_\nu(0) = 4\pi H_\nu(0) = 4\pi g_\nu(0) J_\nu(0) \quad (11.9)$$

The general source function for a gas

At the start of this section we have rather carelessly adopted the proto-type formalism (9.48) for the total source function. But, what is the correct expression for the total source function of a gas anyway?

From definition (4.30) we know that the total source function is nothing else than the sum of all emission processes divided by the sum of all extinction processes. In the most general case we find for the total non-LTE extinction per centimeter

$$\begin{aligned} \chi_\nu &= \sum_k \sum_j \left\{ \sum_l \left\{ \sum_{u>l} \left[n_{ljk} - \frac{g_{ljk}}{g_{ujk}} n_{ujk} \right] \alpha_{lu,jk}(\nu) + \right. \right. \\ &\quad \left. \left. \left[n_{ljk} - n_{ljk}^* e^{-h\nu/kT} \right] \alpha_{l,j+1,k}(\nu) \right\} + \alpha_{jk}(\nu, T) n_e N_{jk} \left(1 - e^{-h\nu/kT} \right) \right\} + n_e \sigma_T \end{aligned} \quad (11.10)$$

where $\alpha_{lu,jk}$ and α_{ljk} are the extinction coefficients per particle, given by eq. (7.20) and (8.1), respectively; α_{jk} is defined as the leading part of eq. (8.17). The summation is over all elements k , ionization states j and excitation states l . Here u denotes a higher excitation state than l . The first term gives the line extinction, corrected for stimulated emission. The second term represents the bound-free extinction, again corrected for stimulated emission. Why for this last process the LTE population is used is immediately clear if one subtracts eq. (8.10) from (8.1). The third term gives the extinction by free-free transitions and the last term is that of electron scattering.

For the total non-LTE thermal emission coefficient (dimensions $\text{erg cm}^{-3} \text{ sec}^{-1} \text{ hz}^{-1} \text{ sr}^{-1}$) it follows that

$$\eta_\nu = \frac{2h\nu^3}{c^2} \sum_k \sum_j \left\{ \sum_l \left\{ \sum_{u>l} n_{ujk} \frac{g_{ljk}}{g_{ujk}} \alpha_{lu,jk}(\nu) + n_{ljk}^* \alpha_{l,j+1,k}(\nu) e^{-h\nu/kT} \right\} + n_e N_{jk} \alpha_{jk}(\nu, T) e^{-h\nu/kT} \right\} \quad (11.11)$$

The three terms again describe bound-bound (i.e. line), bound-free, and free-free transitions. The emission by scattering is treated separately in the proto-type source function (and is given by $\eta_\nu = n_e \sigma_T J_\nu$ for an isotropic source function) and is therefore not included in η_ν .

LTE source function for a gas

If LTE holds, then the extinction and thermal emission per centimeter is given by

$$\chi_\nu^* = \sum_k \sum_j \left\{ \sum_l \left\{ \sum_{u>l} n_{ujk}^* \alpha_{lu,jk}(\nu) + n_{ljk}^* \alpha_{l,j+1,k}(\nu) \right\} + n_e N_{jk} \alpha_{jk}(\nu, T) \right\} \times (1 - e^{-h\nu/kT}) + n_e \sigma_T \quad (11.12)$$

$$\eta_\nu^* = \frac{2h\nu^3}{c^2} e^{-h\nu/kT} \times \sum_k \sum_j \left\{ \sum_l \left\{ \sum_{u>l} n_{ujk}^* \alpha_{lu,jk}(\nu) + n_{ljk}^* \alpha_{l,j+1,k}(\nu) \right\} + n_e N_{jk} \alpha_{jk}(\nu, T) \right\} \quad (11.13)$$

That indeed this is equivalent to the proto-type source function eq. (9.48) and that the thermal part of the source function fulfills the Kirchhoff-Planck relation (6.3) will be investigated in exercise 11.1.

Exercise 11.1

- a) Show that, using $\kappa_\nu^* = \chi_\nu^* - n_e \sigma_T$ one recovers $\eta_\nu^* = \kappa_\nu^* B_\nu(T)$, as expected from the Kirchhoff-Planck relation (6.3).
- b) Show that in LTE the proto-type source function is given by eq. (9.48).

11.2 Obtaining the temperature structure

The determination of the temperature structure is, in fact, the very heart of the problem of constructing LTE models. As discussed, we adopt the grey solution as the initial estimate of

$T(m)$ in the LTE case. If we substitute this initial solution in eq. (11.7) we will normally find that the newly determined radiation field (the solution of eq. 11.1, 11.2, and 11.3) does not fulfil the constraint of radiative equilibrium. It is therefore necessary to adjust $T(m)$ iteratively in such a way that the radiation field ultimately satisfies the requirement of energy balance. There are basically two strategies we may use to make this happen: (A) temperature correction procedures, and (B) the linking together of the requirement of radiative equilibrium and solving radiation transfer. We will discuss the basic principle of each family of methods.

(a) Lambda iteration

The solution of the mean intensity for frequency ν from the current value of the temperature $T(m)$ can formally be written as

$$\mathbf{T}_{\tau_\nu} \mathbf{J}_\nu = \mathbf{B}_\nu \quad (11.14)$$

where \mathbf{T}_{τ_ν} is the $(D \times D)$ transfer matrix; \mathbf{J}_ν is the vector of mean intensities for all depth points d , and \mathbf{B}_ν is the vector of local Planck functions (given by the temperature $T(m)$). The transfer matrix can be constructed by discretization of eq. (11.1), and of its boundary conditions (11.2) and (11.3). If we adopt the central difference representation (such as described in section 5.2) we obtain a tri-diagonal matrix *à la* eq. (5.32). Inversion of this equation yields

$$\mathbf{J}_\nu = \mathbf{T}_{\tau_\nu}^{-1} \mathbf{B}_\nu = \Lambda_{\tau_\nu} \mathbf{B}_\nu \quad (11.15)$$

where Λ_{τ_ν} is the *lambda matrix* or *lambda operator*. The iteration scheme described in section 11.1 is therefore often referred to as *lambda iteration* because, formally, the mean intensity is obtained by applying the Λ_{τ_ν} operator to the current $T(m)$, yielding J_ν , which in turn is used to improve $T(m)$.

The most obvious method of lambda iteration is to improve the temperature after each iteration step in the following way. We assume that the requirement of radiative equilibrium is fulfilled if we correct the current temperature $T(m)$ by $\Delta T(m)$, such that

$$4\pi \int_0^\infty \kappa_\nu(T) [B_\nu(T(m) + \Delta T(m)) - J_\nu] d\nu = 0 \quad (11.16)$$

If we expand the Planck function to within first order, i.e.

$$B_\nu(T + \Delta T) \simeq B_\nu(T) + \Delta T \left. \frac{\partial B_\nu}{\partial T} \right|_T \quad (11.17)$$

we find

$$\Delta T = \frac{\int_0^\infty \kappa_\nu(T) [J_\nu - B_\nu(T)] d\nu}{\int_0^\infty \kappa_\nu(T) (\partial B_\nu / \partial T)_T d\nu} \quad (11.18)$$

It must be emphasized that the value of J_ν in these equations denotes the value computed from the old $T(m)$ values. If one carries through this process and recomputes a new model with the new temperature distribution, one usually obtains some improvement in satisfying the requirement of radiative energy conservation. However, one often has to pass through

hell to achieve convergence. The main reasons for this are: (1) It is only with difficulty that information on the non-local nature of the radiation field can penetrate regions of high optical depth, after all it is damped by the term $\exp(-\tau_\nu)$. If the initial values for $T(m)$ are far from the actual solution, it will typically take on the order of $\tau_\nu(D)$ iterations to propagate this information (and, to be more specific: this is information about the boundary conditions of the problem) through the medium. It takes so long for this information to seep through because the mean optical photon path by which the radiation field can make itself be known (per solution of the transfer equation, so per iteration) is only $\langle \tau_\nu \rangle = 1$ (see eq. 4.25). Therefore, if the solution of $J_\nu(m)$ is vastly different from the local value of the Planck function, it will take on the order of $\tau_\nu(D)$ iterations to correct for this. (2) The temperature correction $\Delta T(m)$ computed in the lambda iteration procedure may be complete nonsense because the effect of the correction does not (directly) affect the values $J_\nu(m')$, i.e. the radiation field elsewhere in the medium. After all, the mean intensity is assumed constant when computing the temperature corrections.

The need for other methods to solve the LTE atmosphere problem (and other transfer problems) appears obvious. One very successful alternative method was first introduced in astrophysics by Cannon in 1973. This is the *method op postponed corrections*, better known as *operator splitting* or *approximate lambda iteration*.

(b) Approximate lambda iteration

At the basis of the approximate lambda iteration is the realization that some parts of the physical coupling between medium and radiation field are more important than others. The method aims to split the problem at hand in such a way that the problematic regions (those where the optical depth is large) are separated from those where no problems occur (the optically thin regimes). The trick is to weave together the requirement of radiative equilibrium and the solution of the transfer equation in those regions where problems occur. In other parts of the medium we do not do anything special, we simply use the lambda iteration technique to come to a solution. Because the optical depth in the problematic regimes is large (per definition) it implies that the trick solution should act more or less *locally*. The splitting therefore focuses on defining the *local* and *non-local* medium, and the separation of the two. So, lets do that.

The formal solution of the mean intensity can be considered as a linear operation on the source function, i.e.

$$J_\nu = \Lambda_\nu S_\nu \quad (11.19)$$

Note that for this more general discussion we have chosen to have the lambda operator act on S_ν (see the first equality in eq. 11.1) and not B_ν (see the second equality in the same equation). This will be repaired once we return to the LTE atmosphere problem. We now formulate the idea of the splitting as follows

$$\Lambda_\nu = \Lambda_\nu^* + (\Lambda_\nu - \Lambda_\nu^*) \quad (11.20)$$

where Λ_ν^* is an appropriately chosen *approximate lambda operator* which acts on the state of the medium and/or radiation field that still has to be determined. The operator $(\Lambda_\nu - \Lambda_\nu^*)$

acts on the known, i.e. current state (in our LTE atmosphere problem this is the temperature $T(m)$). In short

$$J_\nu^{\text{new}} = \Lambda_\nu^* S_\nu^{\text{new}} + (\Lambda_\nu - \Lambda_\nu^*) S_\nu^{\text{old}} \quad (11.21)$$

where “new” denotes that the source function is dependent on the state of the medium that still has to be determined, and “old” refers to the state of the medium as determined in the previous iteration. Note that *any* choice of Λ_ν^* that leads to convergence will provide the correct physical solution. After all, if $S_\nu^{\text{new}} \rightarrow S_\nu^{\text{old}}$ then $J_\nu \rightarrow \Lambda_\nu S_\nu$. To actually achieve convergence, as discussed above, Λ_ν^* in regions of large optical depth should (locally) be a good approximation of the exact operator Λ_ν . Beware: not necessarily the best approximation, good is in principle good enough.

Based on the above discussion it may be clear that for this problem the ideal choice of a strictly local operator is

$$\Lambda_\nu^* \equiv \text{diag} [\mathbf{T}_{\tau_\nu}^{-1}] \quad (11.22)$$

For a diagonal matrix acts on the local source function. This definition has been proposed in 1986 by Olson, Auer, & Buckler and is often called the *OAB operator*. The problem with this definition seems, at first sight, that the explicit determination of this approximate lambda operator is cumbersome and computationally expensive, as it needs inversion of the transfer matrix \mathbf{T}_{τ_ν} , which requires order D^3 computations. However, Rybicki & Hummer (1991) have shown that for a tri-diagonal matrix system this type of problem can be solved in order D computations if one combines the forward recursive sweep and back substitution (see section 5.2) with a backward recursive sweep and back substitution.

We now return to the problem of LTE atmospheres (and switch back to using the second equality in eq. 11.1). With the new radiation field given by

$$J_\nu^{\text{new}} = \Lambda_\nu^* B_\nu^{\text{new}} + (\Lambda_\nu - \Lambda_\nu^*) B_\nu^{\text{old}} = \Lambda_\nu^* B_\nu^{\text{new}} + \Delta J_\nu^{\text{old}} \quad (11.23)$$

where $B_\nu^{\text{new}} = B_\nu(T(m) + \Delta T(m))$ and $B_\nu^{\text{old}} = B_\nu(T(m))$, one finds after substitution in eq. (11.7)

$$4\pi \int_0^\infty \kappa_\nu \left[(1 - \Lambda_\nu^*) B_\nu(T(m) + \Delta T(m)) - \Delta J_\nu^{\text{old}} \right] d\nu = 0 \quad (11.24)$$

The term $\Delta J_\nu^{\text{old}}$ describes the non-local contribution to the mean intensity; the local contribution to J_ν is, by means of this operator splitting, computed explicitly on the basis of the “correct” temperature $T(m) + \Delta T$. The constraint of radiative equilibrium is in this way (partly) woven together with the solution of the equation of transfer. The temperature corrections $\Delta T(m)$ again follow using a first order expansion of the Planck function (see eq. 11.17 and 11.18).

The convergence properties of this approximate lambda iteration method are excellent. The non-local radiation field, which in optically thick parts of the medium is only a small fraction of the total radiation field, is isolated and “drives” as it were the solution towards convergence. This is essential as it is this non-local radiation field that needs to make sure that all points in the medium know what the boundary conditions are. Locally the radiation field is determined

in compliance with the radiative energy conservation. In this way of dealing with the problem the corrections $\Delta T(m)$ are reliable (recall that this need not be the case in standard lambda iteration).

Other definitions of Λ_ν^* have been proposed in order to solve transfer problems. Examples are the *core saturation operator* and the *Scharmer operator*, both introduced by Scharmer in 1981.

To actually compute detailed LTE model atmospheres we obviously need to know how to describe the spectral lines in detail. This we will discuss in the next chapter. In anticipation of this discussion we already discuss aspects of the end result in the next section using the LTE models computed by Bob Kurucz.

11.3 Kurucz models

In the Kurucz models it is assumed that LTE and hydrostatic equilibrium are valid, and that the energy is transported by either radiation or convection. In the final set of models the potential contribution of over 58,000,000 million spectral lines has been taken into account. Information on the Kurucz models can for instance be found at <http://cfaku5.cfa.harvard.edu> or <http://kurucz.harvard.edu>.

A very large standard grid is available, in which for 19 different sets of abundances, 76 effective temperatures and 11 gravities, the atmospheric structure and emerging spectrum have been computed (so a total of 15 884 models). The specification of the abundance pattern is always such that the total mass fraction of all elements more heavy than helium, the so-called *metal abundance* Z , are scaled to the solar abundances $Z_\odot = 0.018$. In this way the $\log Z/Z_\odot$ value is varied between +1.0 and -5.0. The values for the effective temperature range between $3\,500 \leq T_{\text{eff}} \leq 50\,000$ K, and that of the logarithm of the gravity between $0.0 \leq \log g \leq 5.0$.

An extensive library of synthetic spectra based on Kurucz's code that covers the 2500-10500 Å wavelength range at resolving powers (see Eq. 12.3) 20,000, 11,500, 8,500 and 2,000 has been presented by Munari et al. (2005, A&A 442, 1127). Their spectra are electronically available as absolute fluxes as well as continuum normalized fluxes at
<http://archives.pd.astro.it/2500-10500/>

The purpose of these models is to derive the important quantities T_{eff} , $\log g$, and the chemical abundance pattern by comparing them to observed energy distributions. Also, these models provide colors, ionizing fluxes – relevant for nebular studies – and limb darkening profiles – relevant for studies of the light curves of eclipsing binaries and exo-planet transits. After correcting for interstellar extinction (see § 18.2), scaling of an appropriate model with an absolute measurement of the flux (for instance the V magnitude or a part of the spectrum for which an absolute calibration is available) then yields a value for the angular diameter (see

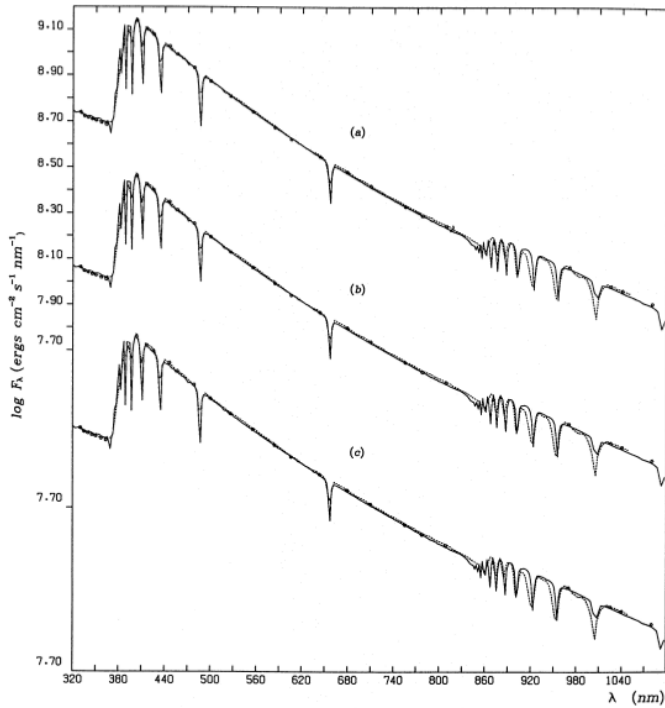


Figure 11.1: Comparison of the observed and predicted absolute flux $\log \mathcal{F}_\lambda$ of the A0 V star Wega (α Lyrae). The computed fluxes (solid line) are for $\log g_\star = 3.95$, $[M/H] = -0.5$, $\xi_{\text{micro}} = 2 \text{ km sec}^{-1}$, $N_{\text{He}}/N = 0.089$ (i.e. solar) and (a) $T_{\text{eff}} = 9550 \text{ K}$ and $E(B-V) = 0$; (b) $T_{\text{eff}} = 9600 \text{ K}$ and $E(B-V) = 0.005$; (c) $T_{\text{eff}} = 9650 \text{ K}$ and $E(B-V) = 0.01$ (Castelli & Kurucz 1994, A&A 281, 817).

eq. 3.25). If we know the distance to the object, for instance from a parallax measurement, we then have a value for the stellar radius. Using eq. (3.19) this yields a value for the luminosity, and, with eq. (9.28), the mass. A comparison with evolutionary tracks plotted in the Hertzsprung-Russell diagram of L_\star versus T_{eff} , then reveals the age and evolutionary stage of the star.

We briefly discuss some aspects of the Kurucz models.

Atmospheric structure

Table A.5 gives for a number of effective temperatures T_{eff} and gravities $\log g$ a sampling of the most important structural parameters as a function of the continuum optical depth at $\lambda 5000 \text{ \AA}$. A gravity $\log g = 4$ is typical for main sequence stars (luminosity class V); $\log g = 1$ is characteristic for the rarefied atmospheres of giants (luminosity class III). Note that e.g. the density ρ at $\tau \sim 1$ in the giant star is two orders of magnitude less than in the dwarf star. Deep down ($\tau \sim 10$) in the atmospheres of cool stars convection is the most important mode of energy transport; in higher layers – where the mean free path of the photons start

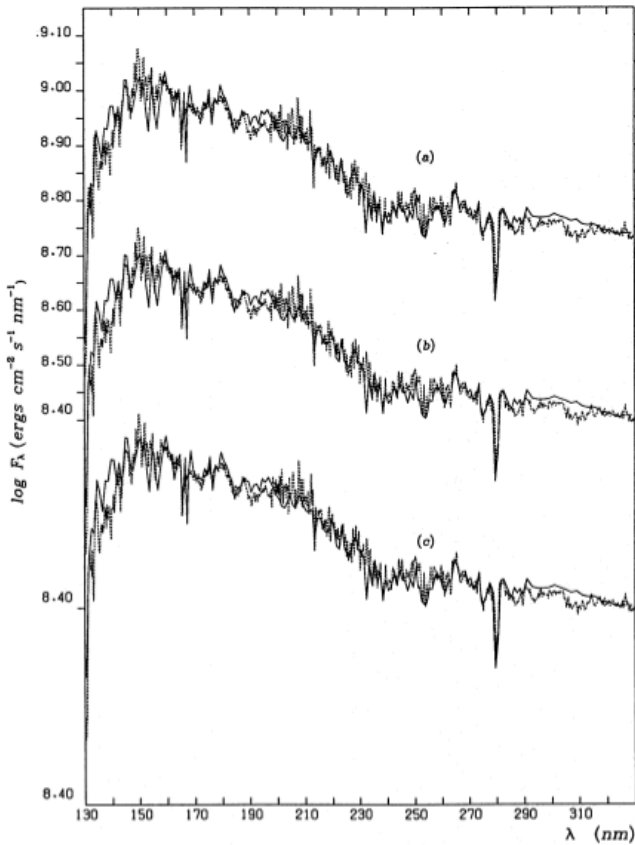


Figure 11.2: Comparison of the observed and predicted flux $\log \mathcal{F}_\lambda$ of the A0 V star Wega (α Lyrae). The computed fluxes (solid line) are for $\log g_* = 3.95$, $[M/H] = -0.5$, $\xi_{\text{micro}} = 2 \text{ km sec}^{-1}$, $N_{\text{He}}/N = 0.089$ (i.e. solar) in (a) $T_{\text{eff}} = 9550 \text{ K}$ and $E(B-V) = 0$; (b) $T_{\text{eff}} = 9600 \text{ K}$ and $E(B-V) = 0.005$; (c) $T_{\text{eff}} = 9650 \text{ K}$ and $E(B-V) = 0.01$ (Castelli & Kurucz 1994, A&A 281, 817).

to become large – energy is transported by radiation. In stars with $T_{\text{eff}} \geq 10\,000$ convection does not occur anywhere in the atmosphere. In hotter stars hydrogen gets ionized, such that $n_e \sim N_N$, where N_N is the H dominated number density of nuclei. In hot stars radiation pressure becomes so important that even $p_R > p_G$.

Standard star Wega

The Kurucz models are calibrated using a number of standard stars. Obviously the sun is the most important of these calibrators, but also the A0 V star Wega (α Lyrae) is often used for this purpose. The computed T_{eff} and $\log g$ of Wega depend on the amount of interstellar extinction $E(B-V)$ and the helium abundance. The numbers that follow are meant to give an impression of the accuracy by which the parameters of the best studied stars are known. Figure 11.1 and 11.2 show how the ultraviolet, optical, and near-infrared part of the spectrum

can be predicted. The spectral resolution of the models plotted in these figures is modest, so ignore the fits to individual lines and focus on the global fit to the energy distribution. The models range in T_{eff} from 9 550 to 9 650 K, depending on whether $E(B-V)$ is 0.0 or 0.01 magn. An accurate measurement of the reddening is therefore required to get a very precise fix of the effective temperature. The derived gravity is linked to that of the helium abundance. A lower limit of $\log g = 3.95$ follows for $T_{\text{eff}} = 9 550$ K and a solar helium abundance $N_{\text{He}}/N_{\text{H}} = 0.0977$ (i.e. $N_{\text{He}}/N = 0.089$). However, a model with $N_{\text{He}}/N_{\text{H}} = 0.0677$ (i.e. $N_{\text{He}}/N = 0.063$) instead of a solar value yields – at fixed temperature – a gravity $\log g = 3.98$. These computations show that the error in the determination of the temperature is about 50 K, while the fit to the gravity sensitive $H\gamma$ line shows an error in the logarithm of the gravity of about 0.05 dex (see figure 11.4). All computations assume a solar scaled metal abundance $[\text{M}/\text{H}] = -0.5$, and a atmospheric depth independent microturbulent velocity $\xi_{\text{micro}} = 2 \text{ km sec}^{-1}$. This microturbulent velocity is a free parameter in the Kurucz models that has not yet been discussed and is of relevance when making detailed fits to the spectral lines (see section 12.2).

Energy distribution

Figure 11.3 shows examples of energy distributions computed by Kurucz. Look whether you can understand the global trends using the physics discussed in these lecture notes.

$U-B$ vs. $B-V$ diagram

The Kurucz color-color diagram of $U-B$ vs. $B-V$ is given in figure 11.5. The top panel gives this diagram on the same scale as that of figure 2.11 and 6.6; the bottom panel shows an enlargement of the regime where these indices are the most sensitive for gravity. Labels indicate the effective temperature and logarithm of the gravity of the grid of models. Notice that a star that has $T_{\text{eff}} = 6 500$ K is 'redder' in its $B-V$ color if the gravity is larger, but is 'bluer' in its $U-B$ color. This is a reflection of the behavior of the optical spectrum as a function of g . For the two extreme values of the gravity these spectra are plotted in the right panel of Fig. 11.6. Remember that the U -filter is positioned mainly in the Balmer continuum (i.e. at the short-wavelength side of 3646 Å; see Fig. 6.4) and the B - and the V -filter are not. The star with the high gravity has a relatively high flux in U and low flux in B ; therefore a relatively 'blue' $U-B$ color. Comparison of the flux in the B - and V -filter shows that the high gravity model has (relatively speaking) less flux in the B -filter than in the V -filter; therefore a relatively 'red' $B-V$ color.

Kurucz colors and bolometric correction BC_V

An extensive set of synthetic colors can be found at one of the http addresses listed in the beginning of this subsection, in the folder *Grids of model atmospheres*. In 2008 opacities and abundances have been updated. Color information regarding $U-B$, $B-V$, $V-R$,

Table 11.1: Polynomial relations expressing the $B-V$ color and BC_V as a function of effective temperature (Flower 1996, ApJ 469, 355). The $B-V$ relation for supergiants is slightly different from that of other luminosity classes.

Coefficient	$B-V$ color		Bolometric Corrections		
	$B-V = a + b \log T_{\text{eff}} + c(\log T_{\text{eff}})^2 + ..$	$BC_V = a + b \log T_{\text{eff}} + c(\log T_{\text{eff}})^2 + ..$	$\log T_{\text{eff}} > 3.90$	$3.90 < \log T_{\text{eff}} < 3.70$	$\log T_{\text{eff}} < 3.70$
a	3.979145	4.0125597	-0.188115	-0.370510	-0.190537
b	-0.654499	-1.055043	-0.137146	0.385673	0.155145
c	1.740690	2.133395	-0.636234	-0.150651	-0.421279
d	-4.608815	-2.459770	0.147413	0.261725	0.381476
e	6.792600	1.349424	-0.179587	-0.170624	-
f	-5.396910	-0.283943	0.788732	-	-
g	2.192970	-	-	-	-
h	-0.359496	-	-	-	-

$V-I$, $V-J$, $V-K$, $V-L$ is supplied for various chemical compositions and a few micro-turbulent velocities. For instance, for a solar composition and $\xi_{\text{micro}} = 2 \text{ km sec}^{-1}$ the grid P00ODFNEW and tables ubvp00k02odfnew.dat and rijklp00k2odfnew.dat supply the relevant information. The former table also provides bolometric corrections BC_V in the V -band.

The Kurucz colors make use of measured filter transmissions in the Johnson system. For the rest, they are fully synthetic in nature, i.e. they rely on the Kurucz models. Obviously, any model is susceptible to uncertainties. For the Kurucz models these include an incomplete line list, assumptions in the treatment of convection, turbulence and line broadening and the assumption of LTE. For this reason, others have determined colors using 'more' empirical approaches. For instance, Worley & Lee (2011, ApJS 193, 1) use a catalog of *observed* photometric data of nearby stars that have been analyzed using (mainly) Kurucz models to yield T_{eff} , $\log g$, and [Fe/H]. These tables are available at <http://astro.wsu.edu/models> together with a small fortran program that provides Johnson $U-B$, $B-V$, $V-R$, $V-I$, $J-K$, $H-K$, $V-K$ and the bolometric correction.

Useful relations between $B-V$ color and effective temperature and/or bolometric correction have been derived by several authors. For instance, Flower (1996, ApJ 469, 355) provides polynomial fits (see table 11.1) as well as an extensive table.

Limb darkening

The amount of information in the Kurucz-models on limb darkening (see § ??), i.e. the run of specific intensity from the center of the stellar disk to the edge, is immense. This information is available for each viewing angle μ , for each frequency point. In practice this information is usually described with a limb-darkening law (that describes the angle dependence) for a number of photometric bands. The first to propose a limb-darkening law was Milne (1921,

MNRAS 81, 361)

$$\frac{I_m(\mu)}{I_m(1)} = 1 - u_m(1 - \mu) \quad (11.25)$$

where $I_m(\mu)$ is the specific intensity in the photometric filter m (see § 2.6)

$$I_m(\mu) = \frac{\int_0^\infty I_\nu(\mu) \mathcal{S}_m(\nu) d\nu}{\int_0^\infty \mathcal{S}_m(\nu) d\nu}. \quad (11.26)$$

$I_m(1)$ is the specific intensity at the center of the stellar disk. Milne thus proposed limb-darkening to be linear phenomenon. For a number of Kurucz-models the limb-darkening coefficients u_m are give in table A.4. This linear description turned out to be a fairly good approximation for solar-type stars. More accurate laws are the quadratic law: $I_m(\mu)/I_m(1) = 1 - a_m(1 - \mu) - b_m(1 - \mu)^2$; de square root law: $1 - c_m(1 - \mu) - d_m(1 - \sqrt{\mu})$; and the logarithmic law: $1 - e_m(1 - \mu) - f_m \mu \ln \mu$. A very accurate description is given by Claret (2000, A&A 363, 1081)¹

$$\begin{aligned} \frac{I_m(\mu)}{I_m(1)} &= 1 - a_{1,m}(1 - \mu^{1/2}) - a_{2,m}(1 - \mu) - a_{3,m}(1 - \mu^{3/2}) - a_{4,m}(1 - \mu^2) \\ &= 1 - \sum_{k=1}^4 a_{k,m}(1 - \mu^{k/2}) \end{aligned} \quad (11.27)$$

Limb darkening is extremely important in the study of the light curves of eclipsing binaries and transiting extra-solar planets, the determination of stellar diameters, and the analysis of line profiles from rotating stars.

Exercise 11.2

In this computer exercise we make a model for the effect on the lightcurve of a star due to the transit of an exo-planet. We model the transit as an eclipse of a spherical star by an opaque, dark sphere. In what follows, a is the center-to-center distance between the star and the planet, R_p is the radius of the planet; R_\star is the stellar radius; $z = a/R_\star$ is the normalized separation of the centers, and $p = R_p/R_\star$ is the size ratio of the two objects. The flux relative to the unobscured flux \mathcal{F}_ν^* is (Mandel & Agol 2000, ApJ 580, L171)

$$\frac{\mathcal{F}_\nu(p.z)}{\mathcal{F}_\nu^*} = 1 - \Psi(p, z), \quad (11.28)$$

where

$$\Psi(p, z) = \begin{cases} 0, & 1 + p \leq z, \\ \frac{1}{\pi} \left[p^2 e_0 + e_1 - \frac{1}{2} \sqrt{4z^2 - (1 + z^2 - p^2)^2} \right], & |1 - p| < z \leq 1 + p, \\ p^2, & z \leq 1 - p, \\ 1, & z \leq p - 1, \end{cases} \quad (11.29)$$

and $e_0 = \cos^{-1}[(p^2 + z^2 - 1)/2pz]$ en $e_1 = \cos^{-1}[(1 - p^2 + z^2)/2z]$.

¹For the entire Kurucz grid all coefficients can be found at
<http://vizier.cfa.harvard.edu/viz-bin/VizieR?-source=J/A+A/363/1081>.

- a) Welke vier situaties worden in eq. (11.29) beschreven?
- b) Geef een relatie die de inclinatie beschrijft. Laat aan de hand van je computerprogramma grafisch het effect van inclinatie en p zien.

Voeg nu het effect van randverzwakking toe aan je model. Neem aan dat de specifieke intensiteit van de ster onder het door de planeetschijf afgedekte deel van het steropervlak constant is en gegeven is door de specifieke intensiteit op het punt waar het middelpunt van de planeetschijf zich bevindt. Deze benadering is typisch beter dan 2% van $1 - \Psi(p, 0)$ als $p < 0.1$. Neem tijdens ingress en egress voor de constante specifieke intensiteit de waarde die halverwege de rand van de ster en het verste punt van de planeet op de sterschijf ligt.

- c) Neem aan dat de ster $T_{\text{eff}} = 5\,500$ en $\log g = 4.5$ heeft en dat de randverzwakking kan worden beschreven met een lineaire wet (zie tabel A.4 voor de relevante randverzwakkingscoëfficiënt). Laat opnieuw grafisch het effect van inclinatie en p zien.

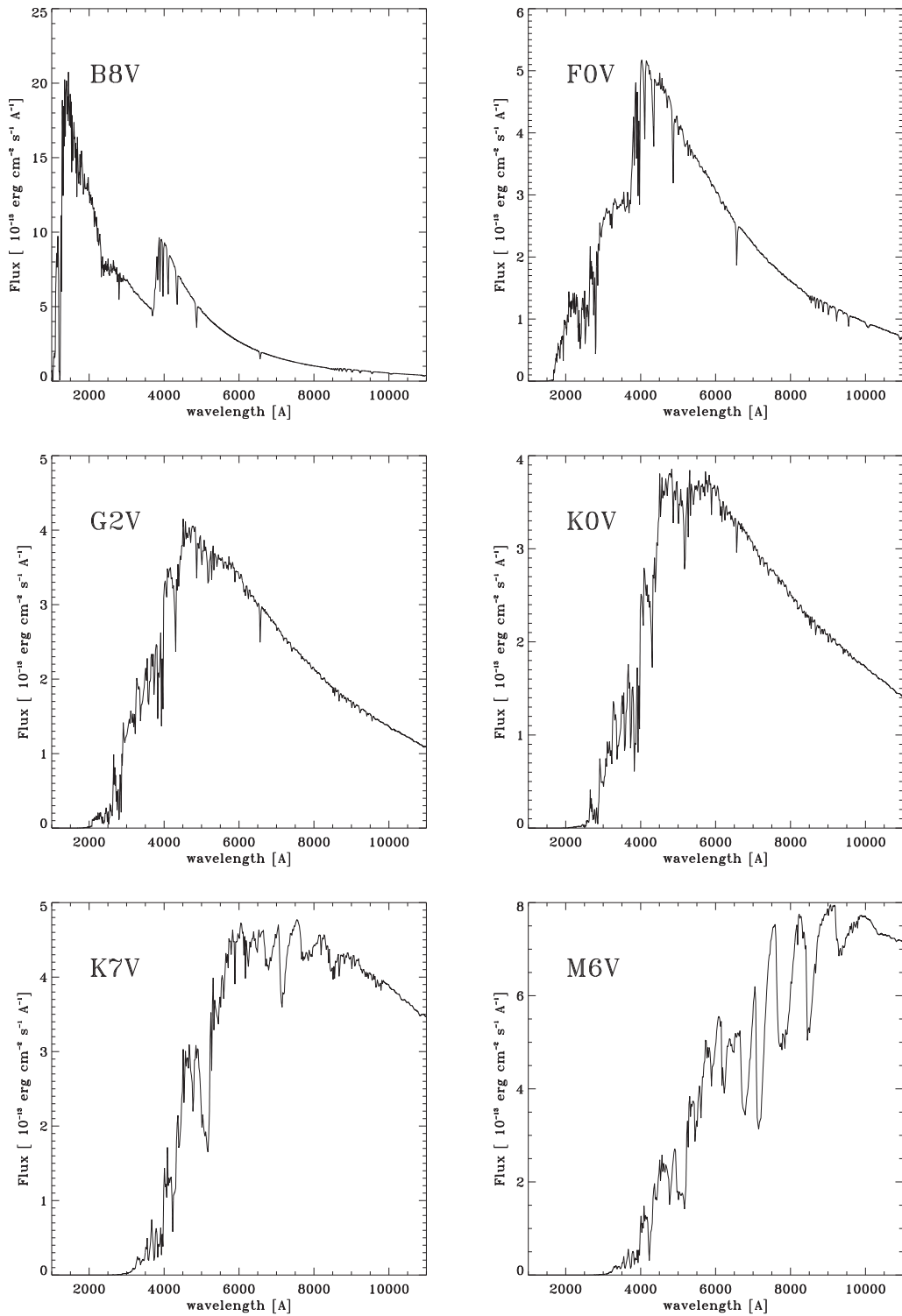


Figure 11.3: Examples of the energy distributions of Kurucz models for mains sequence star with solar abundances.

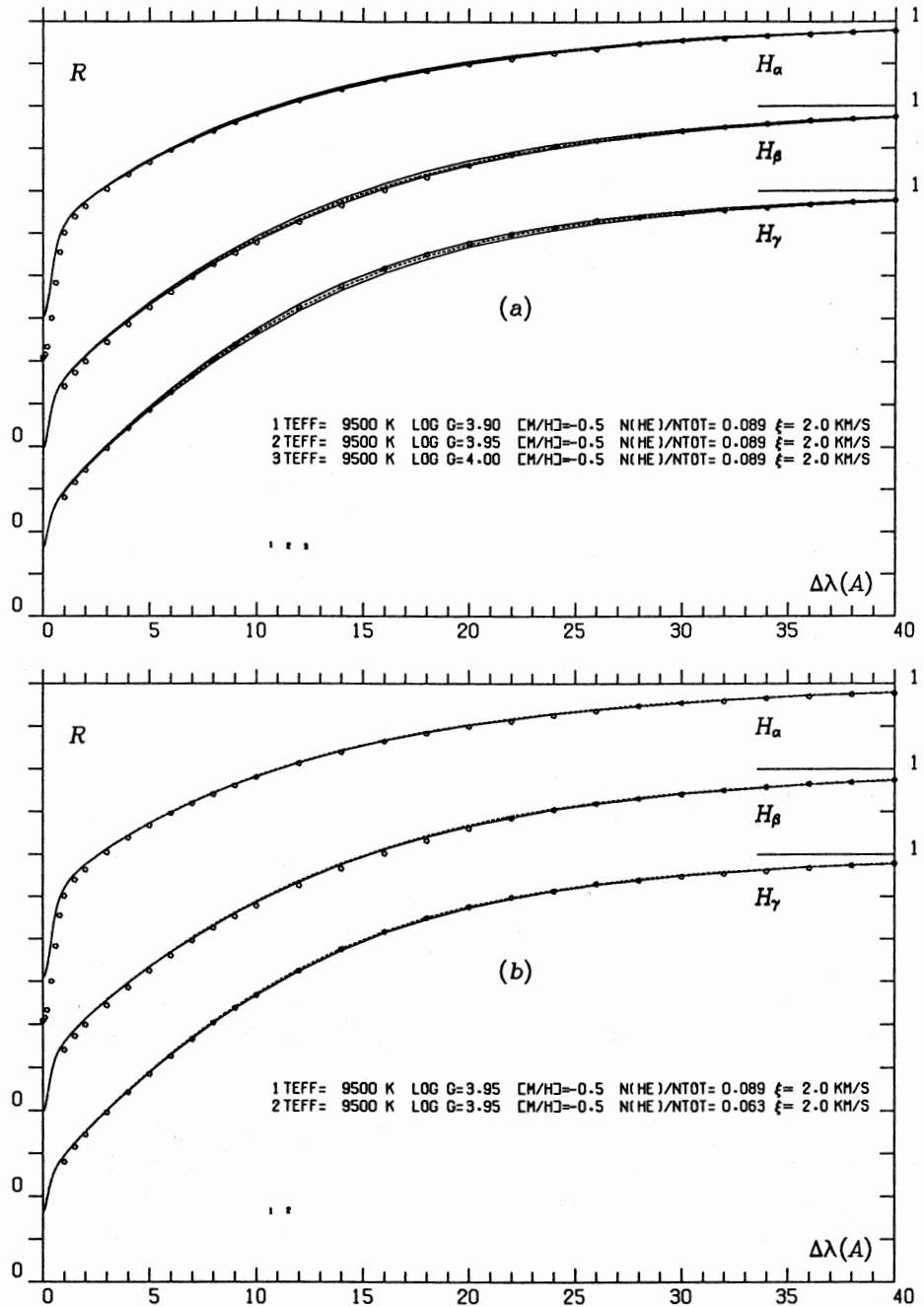


Figure 11.4: Comparison of observed and computed $H\alpha$, $H\beta$ and $H\gamma$ profiles for the A0 V star Wega (α Lyrae). For both models shown $T_{\text{eff}} = 9500$ K, $[M/H] = -0.5$ en $\xi_{\text{micro}} = 2 \text{ km sec}^{-1}$. In (a) $N_{\text{He}}/N = 0.089$ (i.e. solar) and $\log g = 3.90$ (upper solid line), 3.95 (dashed line), and 4.00 (lower solid line). In (b) $\log g = 3.95$ and the helium abundance $N_{\text{He}}/N = 0.089$ (solid line) and 0.063 (dashed line).

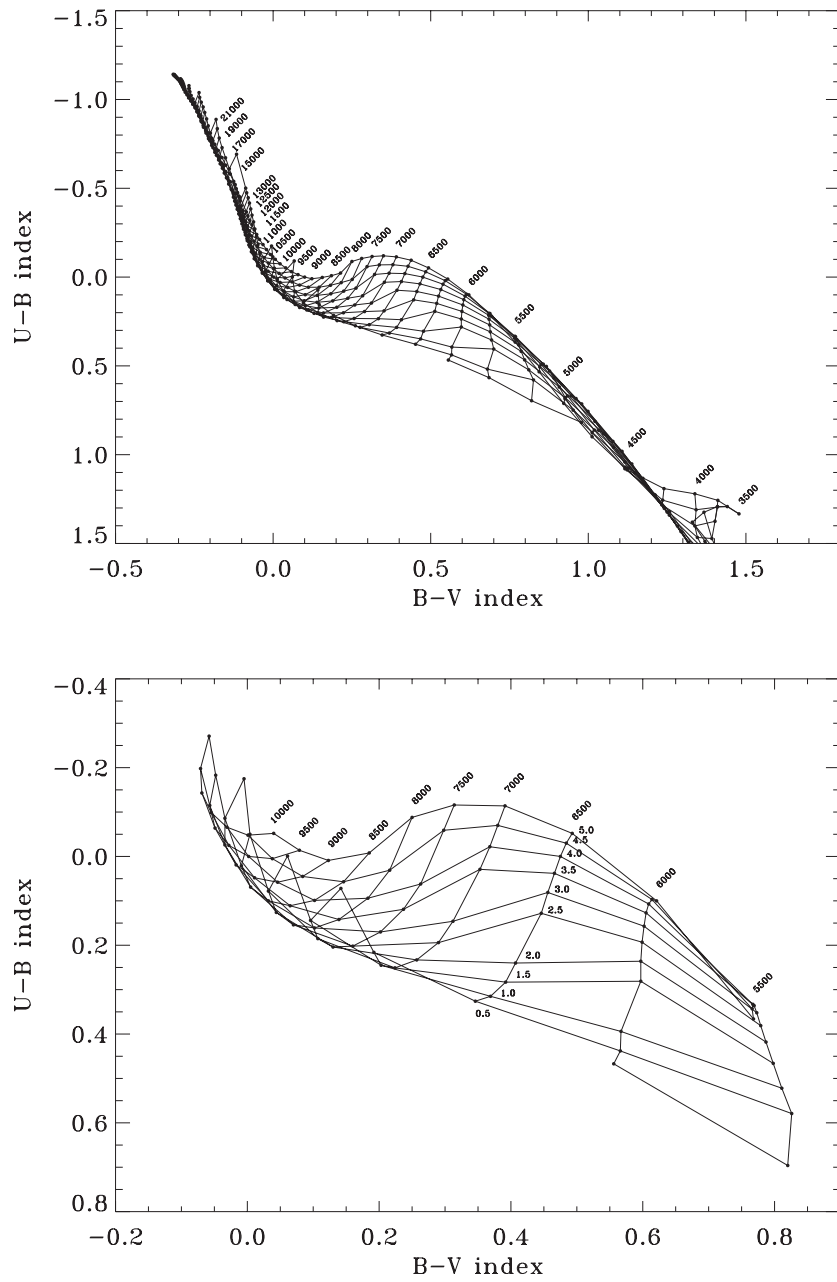


Figure 11.5: Relation between the color indices $U-B$ and $B-V$ for Kurucz models with solar abundances and 2 km sec^{-1} micro turbulent velocity. Top: global view. Bottom: detail. Labels provide T_{eff} and $\log g$.

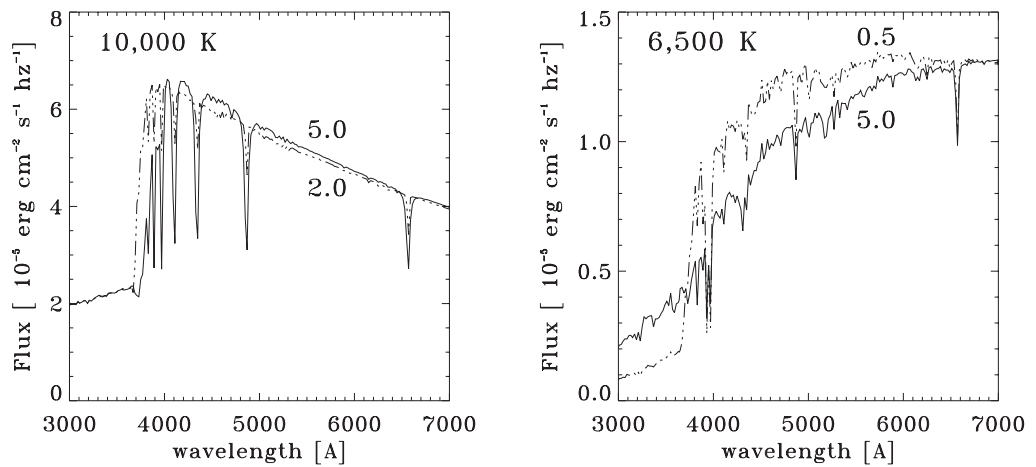


Figure 11.6: Kurucz models with a solar abundance pattern and a micro-turbulent velocity of 2 km sec^{-1} for $10\,000 \text{ K}$ (left panel) and $6\,500 \text{ K}$ (right panel) and different values of the gravity. $\log g = 5.0$ (that could be a dwarf star); 2.0 (a bright giant or supergiant), en 0.5 (a supergiant).

12

Spectral lines

The intensity distribution in the spectral line primarily reflects the run of the source function throughout the stellar atmosphere: in the line core one “sees” layers that are relatively high up in the atmosphere; in the line wings one sees much deeper (see § 4.6). This coupling exists due to the profile function ϕ_ν , which causes the opacity in the line core to be much higher than in the line wing. In this chapter we will study the line profile in more detail. We first define a means to describe the strength of a spectral line. Next, the processes that shape the spectral line are reviewed. We end with a discussion of the curve-of-growth method.

12.1 Describing the line profile

The most complete description of the spectral line is given by its *profile*. The *relative depression* or *absorption depth* of the profile is strictly speaking defined as

$$d_\lambda \equiv 1 - \frac{I_\lambda}{I_\lambda^c} \quad (12.1)$$

where I_λ^c is the continuum intensity at the wavelength λ . In the presence of a spectral line it is by definition impossible to measure the continuum intensity, therefore its value is determined by interpolation of the continuum intensity at both sides of the line profile. In case the absorption depth is positive, the line is an absorption line; in case d_λ is negative, we are dealing with an emission line.

As for almost all stars one can only measure the flux – and not the specific intensity as a function of position on the stellar disk – the absorption depth is often described by

$$D_\lambda \equiv 1 - \frac{\mathcal{F}_\lambda}{\mathcal{F}_\lambda^c} \quad (12.2)$$

where \mathcal{F}_λ^c is the continuum flux at wavelength λ . Also the continuum flux at a wavelength in the line profile can not be measured directly, and therefore it also follows from interpolation of the continuum flux at both sides of the line.

Before the absorption profile can be used as a diagnostic of the stellar atmosphere it needs to be corrected for instrumental distortions. This distortion, which always leads to degradation of the line profile, is described by the *instrumental profile*. Say a light source emits an emission line of infinitesimal width. The profile of this line can be described by a δ -function. Measurement of this line by an instrument shows a smeared profile (typically a Gaussian profile), of which the sharpness is determined by the quality and/or settings of the spectrograph. A measure of this sharpness is the *spectral resolution* or *resolving power*

$$R \equiv \lambda / \Delta\lambda \quad (12.3)$$

Here $\Delta\lambda$ is the bin-width of the flux measurement. For excellent instruments R can be larger than 100 000.

Equivalent width

The concept of *equivalent width* of a spectral line was developed by Marcel Minnaert (1893–1970)¹. The equivalent width is the line profile integrated absorption depth, i.e.

$$W_\lambda(\text{line}) \equiv \int_{\text{line}} D_\lambda d\lambda = \int_{\text{line}} \left(1 - \frac{\mathcal{F}_\lambda}{\mathcal{F}_\lambda^c}\right) d\lambda \quad (12.4)$$

and is – in case of an absorption line – equivalent to the width of a fully blackened rectangular profile of identical surface area (see figure 12.1). It is custom to measure W_λ in (milli-) Angström or in the velocity unit km sec⁻¹. In case of an absorption line $\mathcal{F}_\lambda^c \times W_\lambda$ is equal to the total continuum energy that is removed by the line. In case of an emission line W_λ will be negative, and $-\mathcal{F}_\lambda^c \times W_\lambda$ describes the total energy that is added by the line to the continuum. The equivalent width is a suited measure for the strength of the spectral line, as it is, for instance, much less sensitive to smearing of the profile as a result of the finite resolution of the spectrograph, than is, for instance, the central absorption depth. For an accurate measurement of W_λ it usually suffices to have a spectral resolution of $R \sim 20\,000$. The equivalent width offers a quantitative measure of the line profile in cases where the flux levels are too low to observe a detailed line profile. Finally, the equivalent width is independent of interstellar extinction (see § 18).

If the source is spatially resolved, one can determine the equivalent width from

$$w_\lambda(\text{line}) \equiv \int_{\text{line}} d_\lambda d\lambda \quad (12.5)$$

Total line flux

The line profile integrated flux or *total line flux* is

$$\mathcal{F}(\text{line}) \equiv \int_{\text{line}} (\mathcal{F}_\nu - \mathcal{F}_\nu^c) d\nu = \int_{\text{line}} (\mathcal{F}_\lambda - \mathcal{F}_\lambda^c) d\lambda \quad (12.6)$$

¹Born in Ghent, Belgium, Minnaert worked at the Utrecht astronomical observatory Sonnenborgh from shortly after World War I. From 1937 until 1962 he was the director of the observatory.

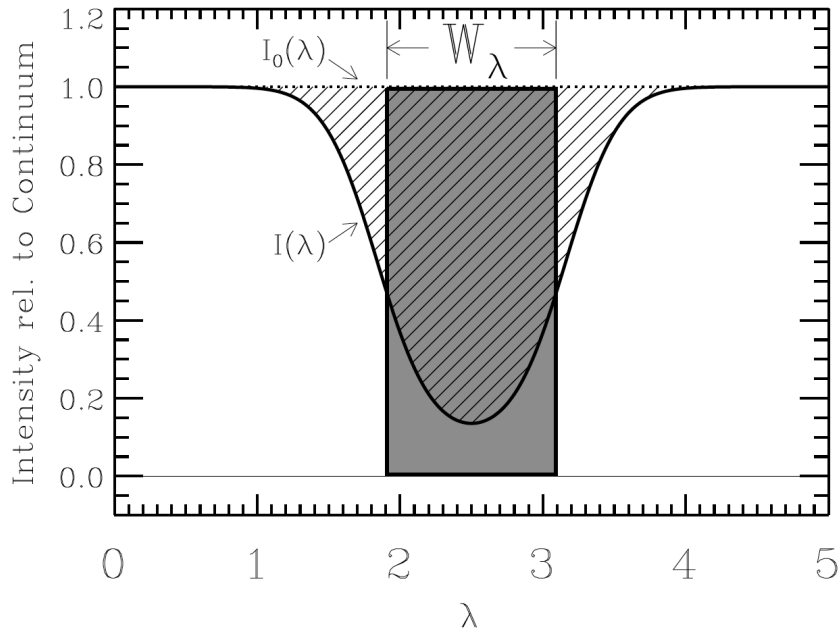


Figure 12.1: Schematic representation of the flux behaviour of a spectral line (i.e. the profile). The equivalent width W_λ is equal to the surface area of the spectral line divided by the continuum flux. *Figure: Edward Jenkins*

The total line flux (measured at distance d) is especially important in studies of emission lines, and therefore is defined such that a positive value results if $\mathcal{F}_\nu > \mathcal{F}_\nu^c$. One obtains $\mathcal{F}(\text{line}) = -\mathcal{F}_\lambda^c \times W_\lambda = -\mathcal{F}_\nu^c \times W_\nu$. In, for instance, planetary nebulae the continuum flux can be so low that it can not be measured (accurately), i.e. $\mathcal{F}_\nu \gg \mathcal{F}_\nu^c$. The continuum contribution can then simply be omitted when computing the total line flux. Note that the total line flux – in contrast with the equivalent width – is dependent on the amount of interstellar extinction.

Related to the total line flux is the *luminosity in the line*, i.e.

$$L(\text{line}) = 4\pi d^2 \mathcal{F}(\text{line}) \quad (12.7)$$

Exercise 12.1

Show that the equivalent width in frequency units is

$$W_\nu(\text{line}) \equiv \int_{\text{line}} \left(1 - \frac{\mathcal{F}_\nu}{\mathcal{F}_\nu^c} \right) d\nu \quad (12.8)$$

and that it is related to the equivalent width in wavelength units as $W_\nu = c/\lambda^2 W_\lambda$.

Exercise 12.2

Is the equivalent width dependent on interstellar extinction. Why (not)?

12.2 Line broadening

There are several processes that can influence the shape of the line profile. We first briefly enumerate these processes, then we discuss each of them separately:

- natural broadening or radiation damping, due to the finite lifetime of excited states
- collisional or pressure broadening, due to the physical interaction of atoms and ions
- Doppler broadening due to the thermal motions of particles
- Doppler broadening due to turbulent (i.e. non-thermal) motions.
- broadening due to the rotation of the star
- broadening due to the presence of a stellar wind

Natural broadening

Spontaneous de-excitations cause the lifetime of an excited state to be statistically distributed around a finite value. The Heisenberg uncertainty principle implies that the uncertainty in lifetime must be coupled to an uncertainty in the energy of the transition. In different words, one expects a broadening of the line, which is referred to as *natural broadening* or *radiation damping*. The term “natural” implies that this broadening occurs even if no other particles are present; the term “damping” results from the classical description of the atom as a driven-damped classical oscillator. It is custom to correct the classical result for quantum mechanical effects using the oscillator strength (see § 7.3). Without its formal derivation we give that the profile that belongs to natural broadening is a *Lorentz profile*, i.e.

$$\phi(\nu - \nu_{lu}) = \frac{\gamma^{\text{cl}}/4\pi^2}{(\nu - \nu_{lu})^2 + (\gamma^{\text{cl}}/4\pi)^2} \quad (12.9)$$

where γ^{cl} is the *classical damping constant* (dimensions s^{-1}), which in the classical description has the value

$$\gamma^{\text{cl}} = \frac{8\pi^2 e^2 \nu_{lu}^2}{3m_e c^3} = \frac{8\pi^2 e^2}{3m_e c \lambda_{lu}^2} \quad (12.10)$$

In the line wings the Lorentz profile drops off as $\Delta\nu^{-2}$. If we use as a characteristic width of the profile the *Lorentz width*, defined as the half width at half maximum, i.e.

$$\Delta\nu_L = \nu - \nu_{lu} \equiv \frac{\gamma^{\text{cl}}}{4\pi} \quad \text{hz}^{-1} \quad (12.11)$$

then, using $\phi(\nu) d\nu = \phi(x) dx$, we may write the Lorentz profile in its dimensionless form as

$$\phi(x) = \frac{1}{\pi} \frac{1}{x^2 + 1} \quad (12.12)$$

where $x = \Delta\nu/\Delta\nu_L$. The Lorentz profile fulfils the normalization requirement eq. (7.2). Note that the characteristic natural line width in wavelength units, i.e. $\Delta\lambda_L = \lambda_{lu}^2 \gamma^{\text{cl}} / 4\pi c \text{ cm}^{-1}$, is constant and given by $6 \cdot 10^{-5} \text{ \AA}$. This is a very small value. Usually, other line broadening mechanisms are more important.

The quantum mechanical equivalent of the damping constant is given by

$$\Gamma = \Gamma_u + \Gamma_l = \sum_{i < u} A_{ui} + \sum_{i < l} A_{li} \quad (12.13)$$

It is the sum of all possible spontaneous de-excitations from the upper level plus that of all from the lower level (per second). Also the lower level plays a role because the width of the spectral line is determined by the uncertainty in energy of both levels. One may simply add the contributions of the upper and lower level as a convolution of two Lorentz profiles with half width Γ_u and Γ_l yields again a Lorentz profile of which the half width is $\Gamma_u + \Gamma_l$. To get an impression of how the classical values of the half width compare to the quantum mechanical values: for the strong H α -line of hydrogen we find $\Delta\lambda_L = 6.5 \cdot 10^{-4} \text{ \AA}$ or 0.03 km sec^{-1} . This compares roughly with the classical value. Weak lines, with smaller values of the Einstein coefficients A_{ul} will have smaller natural line widths. For an idealized two level atom it holds that $\Gamma = A_{ul}$.

Collisional broadening

Radiating or absorbing atoms and ions in a gas can not be treated as strictly independent particles. The densities are usually so high that the atoms and ions will “feel” other particles, even if this does not result in an extinction or emission of a photon (such as e.g. in a free-free interaction). These other particles can be electrons, ions or atoms of the same kind, or also, in case of cool stars, molecules. In the simplest representation, the energy levels of the atom or ion that absorbs a photon will be somewhat disturbed by Coulomb interaction with other nearby particles, such that (temporarily) their energy will be modified. The extend by which these energy levels will be affected is a function of distance to, and the amount and nature of the perturbing particles. The perturbation of the energy levels leads to a line broadening. This process is referred to as *collisional or pressure broadening*.

In many cases the perturbation of the level energies as a function of distance to the particles that are responsible for it can be approximated by a powerlaw, i.e. $\Delta E \propto r^{-p}$ where p is

Table 12.1: Overview of collisional broadening mechanisms, and an indication of the type of stars for which these are relevant (adapted from Rob Rutten).

p	Mechanism	Profile	Atom/Ion	Perturbers	Spectral Types
2	linear Stark	Holtzmark	H, hydrogenic	ions	early-type
		Lorentz?	H, hydrogenic	electrons	early-type
3	resonance	Lorentz	atom A (read: H)	atom A (read: H)	solar
4	quadratic Stark	Lorentz	non-hydrogenic	electrons, ions	early-type
6	van der Waals	Lorentz	atom B	atom A (read: H)	late-type

an integer number which depends on the type of interaction. One may expect that the upper level of the transitions is more severely affected by the interaction than is the lower level. The perturbation of the spectral line is simply the difference between of the two independent levels, i.e.

$$\Delta E_u - \Delta E_l = h\Delta\nu = \frac{C_p(l, u)}{r(t)^p} \quad (12.14)$$

The interaction constant C_p needs to be measured or computed for each transition and type of interaction (see table 12.1).

The lowest order broadening, $p = 2$, is the *linear Stark effect*. It is particularly important for neutral hydrogen and causes the broad line wings of the Balmer lines, such as H α , H β , H γ and H δ , in main sequence stars (see § 2.1). Also hydrogen like lines, such as the He II and Rydberg lines – i.e. lines between levels with high main quantum numbers – are sensitive for the linear Stark effect. The nature of the interaction is based on the fact that neutral hydrogen has a permanent dipole character as the electron is not capable of fully shielding the proton. The perturbing particles are protons and electrons. The decline of the interaction force is the same as that of the Coulomb field of a point source, which implies that the perturbation of the level energies is dependent on the field strength in the ambient medium.

Resonance broadening describes the mutual interaction between neutral hydrogen atoms, and is based on the permanent dipole nature of these atoms. For this broadening mechanism the decay is described by $p = 3$. The effect plays a role in those stars in which neutral hydrogen itself is the main perturbing particle. This is the case for solar type stars, where it is relevant for the broadening of the H α line.

Lines of atoms and ions that are not hydrogen-like, and that therefore do not have a dipole moment, feel a *quadratic Stark effect* because of interactions with protons and electrons. For this effect $p = 4$. In early-type stars interactions of non-hydrogenic atoms and ions with electrons are the dominant cause of collisional broadening.

Interactions of non-hydrogen like atoms with neutral hydrogen are the dominant cause of collisional broadening in solar-type or even cooler stars. This type of collisional broadening is called *Van der Waals broadening* and has $p = 6$.

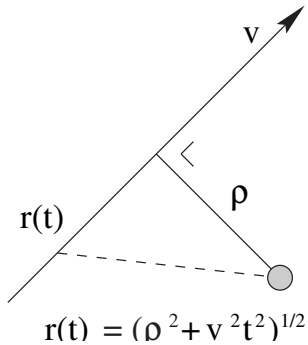


Figure 12.2: Schematic representation of the collision parameter ρ

It is beyond the scope of these lecture notes to give a detailed description of the theory of collisional broadening. We mention that there are two extreme formalisms to describe the problem. In the *impact approximation* the duration of the perturbation is short compared to the time between collisions. It is a meaningful way of describing perturbations that are effective over a short distance (i.e. the type of interactions that have high values of p). The result of the perturbation is described as a phase jump in the wave train emitted by the exciting or de-exciting atom. This Lindholm approximation causes a broadening that is described by a Lorentz profile – similar to natural broadening – with a damping constant Γ_p that may be added to eq. (12.13). The effective duration of the perturbation

is typically of the order $\Delta t_s \sim \rho_{\text{eff}}/v$, where ρ_{eff} is the effective collision parameter (see figure 12.2) and v is the velocity of the perturbing particle. The time interval between two collisions is given by $\Delta t_b = (N\pi\rho_{\text{eff}}^2 v)^{-1}$ where N is the density of the perturbers; v the velocity of these particles, and $\pi\rho_{\text{eff}}^2$ the effective collision cross section of the particle that suffers the collision. The cross section depends on the type of interaction potential (see eq. 12.14). The validity of the impact approximation therefore also depends on the density of the impacting particles. Only when this is sufficiently low, the approximation may be applied, as expected.

For increasing density the interaction time Δt_s will become shorter and shorter. At some point the particles that are being perturbed will feel a continuous interaction due to (partly) overlapping collisions. This allows for a *statistical approximation*, which is the other extreme of describing the collisional broadening problem. The linear Stark effect is described in this way because, due to the relatively slow decay of the interaction potential ($\Delta E \propto r^{-2}$), the effective cross sections is very large. In this approximation the profile function will deviate from the Lorentz profile and has a so-called Holtzman shape. In the line wings this profile decays as $\Delta\nu^{-5/2}$, whereas the Lorentz profile shows a $\Delta\nu^{-2}$ dependence.

Doppler broadening

The motion of a radiating particle along the line of sight will cause a Doppler shift given by

$$\frac{\Delta\nu}{\nu} = -\frac{\Delta\lambda}{\lambda} = \frac{\xi}{c} \quad (12.15)$$

Here ξ is the velocity component in the line of sight. A positive Doppler shift, i.e. due to a particle that is moving in the direction of the observer, implies a blue shift. Is the atom or ion moving towards the observer with this velocity ξ , then it will absorb a photon that has a frequency ν in the reference frame of the observer in its own reference frame (which we would

consider to be moving, and therefore is called the co-moving frame) at a redshifted frequency

$$\nu' = \nu \left(1 - \frac{\xi}{c}\right) \simeq \nu - \nu_{lu} \frac{\xi}{c} \quad (12.16)$$

The distribution of thermal velocities in the line of sight is given by the one dimensional Maxwellian velocity distribution (see eq. 6.17)

$$\frac{n(\xi)}{N} d\xi = \frac{1}{\xi_D \sqrt{\pi}} \exp \left[-(\xi/\xi_D)^2 \right] d\xi \quad (12.17)$$

where

$$\xi_D = \left(\frac{2kT}{m} \right)^{1/2} = 12.895 \left(\frac{T}{10^4 A} \right)^{1/2} \text{ km s}^{-1} \quad (12.18)$$

is the *Doppler velocity*, with m the mass and A the atomic weight (in amu) of the particle.

If thermal Doppler broadening is the only source of line broadening, such that in the co-moving frame the profile function may be replaced by a delta function $\delta(\nu' - \nu_{lu})$ – as in this case the energy levels of the transition are infinitely sharp and the extinction will occur only at a single (shifted) frequency – then one finds for the profile function in the reference frame of the observer

$$\begin{aligned} \phi(\nu - \nu_{lu}) &= \int_{-\infty}^{+\infty} \delta(\nu' - \nu_{lu}) \frac{n(\xi)}{N} d\xi = \int_{-\infty}^{+\infty} \delta \left(\nu - \nu_{lu} \frac{\xi}{c} - \nu_{lu} \right) \frac{n(\xi)}{N} \frac{d\xi}{d\nu} d\nu \\ &= \frac{n((\nu - \nu_{lu})c/\nu_{lu})}{N} \frac{c}{\nu_{lu}} \end{aligned} \quad (12.19)$$

where in the second right hand side we have switched to the usual unit of the profile function (i.e. hz^{-1}) and in the third right hand side we have taken $\xi = (\nu - \nu_{lu})c/\nu_{lu}$, such that $d\xi/d\nu = c/\nu_{lu}$. One finds

$$\phi(\nu - \nu_{lu}) = \frac{1}{\sqrt{\pi} \Delta \nu_D} \exp \left[-(\Delta \nu / \Delta \nu_D)^2 \right] \quad (12.20)$$

where $\Delta \nu_D$ is the *Doppler width*, which is defined as

$$\Delta \nu_D \equiv \frac{\xi_D}{c} \nu_{lu} = \frac{\nu_{lu}}{c} \left(\frac{2kT}{m} \right)^{1/2} \quad (12.21)$$

Equation (12.20) is referred to as the *Doppler profile*. In a stellar spectrum one observes the combined effect of a large number of atoms, that each have their own thermal velocity projected along the line of sight. As ξ_D is proportional to $A^{-1/2}$ large differences in the characteristic width of thermal profile functions may exist. For a star like the sun ($T \sim 6000$ K) the Doppler width for hydrogen is typically 10 km sec^{-1} , while for iron it is only 1.3 km sec^{-1} – more than seven times as small.

The dimensionless Doppler profile function follows after introducing $x = \Delta \nu / \Delta \nu_D$

$$\phi(x) = \frac{1}{\sqrt{\pi}} \exp(-x^2) \quad (12.22)$$

This function is properly normalized to unity.

Turbulent broadening

The profiles of spectral lines are often broader than one would expect on the basis of the known broadening mechanisms. Examples of physical processes that might cause this broadening are (several types of) waves and turbulent convection. One collectively refers to the motion fields caused by these effects as *turbulence*. We implicitly ignore these turbulent motions when we assume that the stellar atmosphere is time-independent and consists of homogeneous layers. To “compensate” for this simplification we use two *ad-hoc* fit parameters, first introduced by Otto Struve (1897–1963). These are the *microturbulent velocity* and the *macroturbulent velocity*.

It is assumed that the microturbulent motions are random in nature and that they show a Gaussian velocity distribution and correspond to characteristic length scales that are significantly smaller than the geometrical thickness of the line-forming layer in the atmosphere. The effect of microturbulence is a broadening of the profile function. Convolution with the thermal velocity distribution (which truly is Gaussian in nature) yields a new Gauss distribution with a Doppler width

$$\Delta\nu_D \equiv \frac{\nu_{lu}}{c} \sqrt{\xi_D^2 + \xi_{\text{micro}}^2} \quad (12.23)$$

where ξ_{micro} is the microturbulent velocity. Micro turbulence may cause an increase in the equivalent line width. If “saturation” occurs at line centre – i.e. all photons that can be absorbed at line centre are indeed absorbed – the presence of microturbulent velocity fields will have the effect that the available wavelength regime over which photons can be absorbed is increased. In other words, more particles will be able to absorb line (wing) photons, such that W_λ can increase further (see section 12.4).

Also the macroturbulent velocity distribution is often assumed Gaussian. Here, however, one assumes that the characteristic length scales of the gas elements that experience macroturbulence is larger than the geometrical thickness of the line-forming layer. If one could observe the stellar disk with sufficient spatial resolution, the macroturbulence would manifest itself as small “wiggles” on the spectral lines. During excellent atmospheric conditions this has indeed been observed for the sun (one finds velocity amplitudes of ~ 0.3 to ~ 3 km sec $^{-1}$). The surface integrated effect of macroturbulence is that the line profiles become broader and less deep; the equivalent line width of the spectral line is not affected. The assumption of a Gaussian distribution of the moving elements responsible for the macroturbulent motion field is only justified when the velocity fluctuations are not coupled to temperature fluctuations, such as could occur if rising gas elements have a higher temperature relative to those that sink (think about granulation on the solar surface). If this is the case, then one should apply a “multiple-stream model” for which asymmetric line profiles may occur.

Macroturbulence is (most simplistically) accounted for by convolving the computed absorption depth with a Gaussian velocity distribution

$$D_\lambda = D_\lambda^{\text{comp}} * \frac{1}{\xi_{\text{macro}} \sqrt{\pi}} \exp(-\xi^2 / \xi_{\text{macro}}^2) \quad (12.24)$$

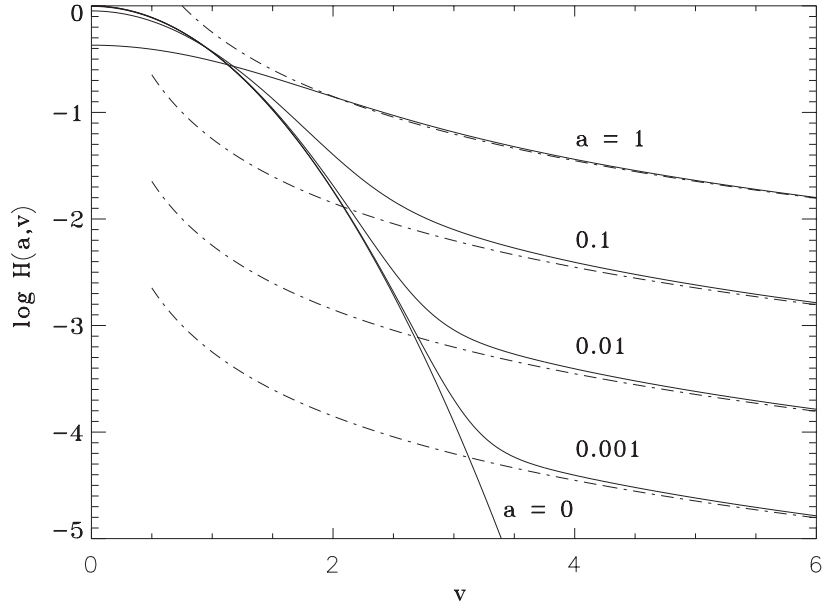


Figure 12.3: The Voigt function $H(a, v)$ as function of v for different values of the damping parameter a . The dashed line gives the approximation $H(a, v) \approx a / \sqrt{\pi v^2}$ for the damping wings of a Lorentz profile.

Voigt profile function

If the collisional broadening may be described by a Lorentz profile (such as in the impact approximation) the total damping profile will again be a Lorentz profile, with damping constant $\gamma = \Gamma + \Gamma_p$. Assuming the collisional broadening and the thermal broadening are independent processes, the final profile function will be a convolution of a Lorentz and a Doppler profile. As the damping profile is properly normalized we may replace the δ -function in eq. (12.19) by a Lorentz profile. This yields

$$\begin{aligned} \phi(\nu - \nu_{lu}) &= \left[\frac{1}{\sqrt{\pi} \Delta \nu_D} \exp \left[-(\Delta \nu / \Delta \nu_D)^2 \right] \right] * \left[\frac{\gamma / 4\pi^2}{(\nu - \nu_{lu}(\xi/c) - \nu_{lu})^2 + (\gamma / 4\pi)^2} \right] \\ &= \frac{1}{\sqrt{\pi} \Delta \nu_D} \int_{-\infty}^{+\infty} \frac{(\gamma / 4\pi^2) \exp \left[-(\Delta \nu / \Delta \nu_D)^2 \right]}{(\nu - \nu_{lu}(\xi/c) - \nu_{lu})^2 + (\gamma / 4\pi)^2} d\nu \\ &= \frac{1}{\sqrt{\pi} \Delta \nu_D} H(a, v) \end{aligned} \quad (12.25)$$

where

$$H(a, v) \equiv \frac{a}{\pi} \int_{-\infty}^{+\infty} \frac{\exp(-y^2)}{(v - y)^2 + a^2} dy \quad (12.26)$$

$$y \equiv \frac{\xi}{\xi_D} = \frac{\xi}{c \Delta\nu_D} \frac{\nu_{lu}}{\Delta\nu_D} = \frac{\xi}{c \Delta\lambda_D} \frac{\lambda_{lu}}{\Delta\lambda_D} \quad (12.27)$$

$$v \equiv \frac{\nu - \nu_{lu}}{\Delta\nu_D} = \frac{\lambda - \lambda_{lu}}{\Delta\lambda_D} \quad (12.28)$$

$$a \equiv \frac{\gamma}{4\pi\Delta\nu_D} = \frac{\lambda^2}{4\pi c \Delta\lambda_D} \frac{\gamma}{\lambda^2} \quad (12.29)$$

The function $H(a, v)$ is the *Voigt function*. Examples of Voigt profiles are given in figure 12.3. The Voigt profile is not normalized, but has a surface $\sqrt{\pi}$ in units of v . The maximum value at profile centre is about $H(a, v = 0) \sim 1 - a$ for $a < 1$. In most astrophysical circumstances the value of a is between 10^{-3} and 10^{-1} . For $a \ll 1$ the Voigt function can be approximated quite accurately by the sum of a Gaussian core and the damping wings of the Lorentz profile, i.e.

$$H(a, v) \simeq \exp(-v^2) + \frac{a}{\sqrt{\pi}v^2} \quad (12.30)$$

For $a \sim 10^{-2}$ the transition between the Doppler core and the Lorentz wings is near $v = 2.7$, where $H(a, v) \sim 10^{-3}$. It shows that the Doppler core extends quite far. Only for really strong lines the wings will be sufficiently strong to be insensitive to the Doppler velocity:

$$\phi(\nu - \nu_{lu}) \sim \frac{1}{\sqrt{\pi}\Delta\nu_D} \frac{a}{\sqrt{\pi}v^2} = \frac{1}{\sqrt{\pi}\Delta\nu_D} \frac{\gamma}{4\pi\Delta\nu_D} \frac{\Delta\nu_D^2}{\sqrt{\pi}\Delta\nu^2} = \frac{\gamma}{4\pi^2\Delta\nu^2} \quad (12.31)$$

This shows that the fact that in most cases collisional broadening is poorly known is irrelevant, after all the profiles are Doppler shaped until far in the line wings.

Exercise 12.3

In this exercise we will derive the Lorentz profile eq. (12.9) following the classical description of Hendrik Antoon Lorentz (1853 – 1928), professor in theoretical physicist at Leiden University and winner of the Nobel prize in 1902. We assume the bound electron in the atom may be described by a (one dimensional) damped harmonic oscillator suffering from periodic excitation with angular frequency ω in an electromagnetic field $E_0 e^{i\omega t}$. The eigen angular frequency of the damped oscillations is ω_0 ; the damping constant is γ . The equation of motion for this system is therefore given by

$$m_e \ddot{x} + \gamma m_e \dot{x} + m_e \omega_0^2 x = e E_0 e^{i\omega t}, \quad (12.32)$$

where we have introduced $\partial x / \partial t = \dot{x}$ and $\partial^2 x / \partial t^2 = \ddot{x}$ to simplify the notation and e is the charge of the electron. The first term on the left hand side is the force due to inertia; the second term is the damping force, the third term is the restoring force.

- a) Using the ansatz $x(t) = x_0 e^{i\omega t}$, first write down an expression for (the complex solution) $x(t)$ in terms of the unknowns of the problem.

As the solution is complex in nature, Larmor's law (see eq. 8.16) implies that the radiated power is given by

$$p(t) = \frac{2}{3} \frac{e^2}{c^3} [\Re(\ddot{x}(t))]^2. \quad (12.33)$$

To obtain the mean radiated power \bar{p} requires us to average the radiated power over one period, i.e. to determine $[\Re(\ddot{x}(t))]^2$.

- b) Derive the expression for \bar{p} . Recall that

$$\sin \omega t = \frac{e^{i\omega t} - e^{-i\omega t}}{2i} \quad \text{and} \quad \cos \omega t = \frac{e^{i\omega t} + e^{-i\omega t}}{2} \quad (12.34)$$

You will find that the average power yields an expression of the form

$$\bar{p} = \frac{2}{3} \frac{e^4 E_0^2}{m_e^2 c^3} f(\nu), \quad (12.35)$$

where $f(\nu)$ is the function describing the frequency dependence of the radiation. To obtain the normalized profile function or Lorentz profile $\phi(\nu)$, fulfilling requirement eq. (7.2), one should determine a normalizing constant C , such that, for instance, $f(\nu) = \phi(\nu)/C$.

- c) Determine the constant C and derive the Lorentz profile $\phi(\nu)$, realizing that $\Delta\nu = \nu - \nu_0 \ll \nu \simeq \nu_0$. Recall that

$$\int_{-\infty}^{+\infty} \frac{dx}{1+x^2} = \pi. \quad (12.36)$$

In the ‘classical’ picture of a driven-damped oscillator, the damping of the system must be exactly compensated by the periodic excitation. This implies that the power associated with the damping force $F_{\text{damp}} = \gamma m_e \dot{x}(t)$, i.e. $p_{\text{damp}}(t) = \gamma m_e \dot{x}^2(t)$, and the mean radiated power $p(t) = (2e^2/3c^3) \ddot{x}^2(t)$ should cancel out.

- d) Use the ansatz $x(t) = x_0 e^{i\omega t}$ (again) to show that the classical damping constant is given by eq. (12.10).

Exercise 12.4

Before model atmospheres became available it was customary to estimate an electron density from the Inglis-Teller formula which relates the principal quantum number n_{Balmer}^{\max} of the “last resolvable line” (i.e. the one with the highest frequency) of the hydrogen Balmer series to the electron density n_e according to the law

$$\log n_e = 23.26 - 7.5 \log n_{\text{Balmer}}^{\max} \quad (12.37)$$

For the A2 I star α Cyg it is found that $n_{\text{Balmer}}^{\max} = 29$; for the A3 V star Sirius one finds $n_{\text{Balmer}}^{\max} = 18$.

- a) Explain why there is a relation between n_e and n_{Balmer}^{\max} .
- b) Obviously, the electron density is a function of depth in the stellar atmospheres. Which electron density is probed when applying the Inglis-Teller formula: n_e at ...
1. the depth at which the continuum optical depth in the optical is about unity.
 2. the depth at which the continuum optical depth in the infrared is about unity.
 3. the depth at which the optical depth of optical Balmer lines is about unity.
 4. the depth at which the optical depth of infrared Balmer lines is about unity.

Explain your answer.

- c) Discuss why α Cyg has a higher n_{Balmer}^{\max} than Sirius.

12.3 Rotational broadening

Line broadening through motion of the stellar surface

We first discuss the general theory of line broadening through motion of the stellar surface (following Underhill, 1968, BAIN 19, 526). The coordinate system adopted is shown in Fig. 12.4. Here the (x, y) -plane is the plane of the sky and the z -axis points towards the observer. The origin, O , of the coordinate system is at the centre of the star. The position of any point P on the surface of a star is determined by the distance R which is the distance OP , the angle φ which gives the rotation of the plane through the z -axis and the line OP about the z -axis, and the angle θ which is measured in the plane zOP from the z -axis towards the xy -plane. The angle φ varies from 0 to 2π ; the angle θ varies from 0 to $\pi/2$.

Let ds be an element of surface around the point P perpendicular to the line OP and let ds_z be the projected element of area perpendicular to the z -axis. Let $I_z(\lambda\nu)$ be the specific intensity at wavelength $\lambda\nu$ (as seen by someone at P who is co-moving with the rotating star) emergent at the point P in a direction parallel to the z -axis. The flux emitted by the star (in its own reference frame) in the direction of the observer is (see also the description of the ray-by-ray solution in section 3.4)

$$\mathcal{F}_{\lambda\nu} = \int_S I_z(\lambda\nu) ds_z \quad (12.38)$$

where the integration is carried out over the total surface S which faces in the direction of the observer. In general ds_z can be expressed as an analytical function of the angles φ and θ and of a unit distance R_\circ . The exact form of the relation depends upon the shape of the star. For a spherical star $R(\theta, \varphi) = R_\circ$, where the latter is the stellar radius. The integration over the surface is performed by letting φ and θ vary over their whole range. If the element of surface at point P has a component of velocity $v_z(P)$ in the z -direction, such that v_z is positive for a surface element moving away from the distant observer, radiation of wavelength

$$\lambda\nu = \lambda \left(1 - \frac{v_z}{c}\right) \quad (12.39)$$

as seen by a co-moving observer at P , will appear to a distant observer to have the wavelength λ . To this external distant stationary observer the wavelength $\lambda\nu$ is a function of the position of point P on the stellar surface. Thus the flux at wavelength λ , as seen by the distant observer, may be found from

$$\mathcal{F}_\lambda = \int_S I_z(\lambda\nu) ds_z \quad (12.40)$$

The above equation is entirely general. Particular cases such as the change in shape of spectral lines due to rotation of the star, to pulsation or to macro-turbulence can be investigated by substituting in eq. (12.40) particular expressions for $I_z(\lambda\nu)$ and for s_z . In the following the case of the line profile resulting from a rotating star will be investigated.

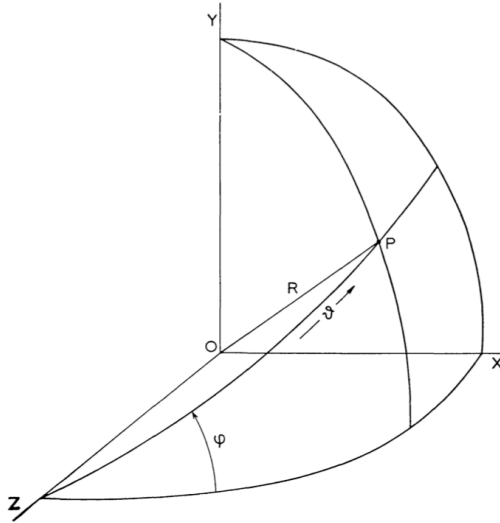


Figure 12.4: The coordinate system used in describing rotational broadening. From: Underhill, 1968, *BAIN* 19, 526.

The particular case of a rigidly rotating star

Consider the case of a spherical star of radius R rotating about the y -axis as a rigid body with an equatorial velocity v_R . It follows that at point $P(\theta, \varphi)$

$$ds_z = R \sin \theta \cos \theta d\theta d\varphi \quad (12.41)$$

and

$$v_R(P) = v_R \sin \theta \cos \varphi. \quad (12.42)$$

Futhermore one can write with adequate accuracy

$$\lambda' = \lambda - \frac{v_R}{c} \lambda_{lu} \sin \theta \cos \varphi \quad (12.43)$$

where λ_{lu} is the wavelength at the centre of the line and λ is any neighbouring wavelength such that $\Delta\lambda = \lambda - \lambda_{lu}$ is small with regard to λ_{lu} . The emergent intensity in the direction of the z -axis, I_z at the point P is a function of the angles θ and φ as a result of, for instance, limb darkening or effects of rotation. It also depends on the angles θ and φ through the wavelength λ' , see eq. (12.43). In general, even for the case of a spherical star a numerical approach is taken. However, if we assume the intrinsic profile of the line to be infinitely narrow and independent of position on the stellar disk and when the limb darkening in the continuum spectrum may be represented by a linear function of μ (such as the limb darkening law proposed by Milne, see vgl. 11.25) the line broadening may be treated analytically. This has first been shown by Shajn & Struve (1929, MNRAS 89, 222). Following Unsöld (in

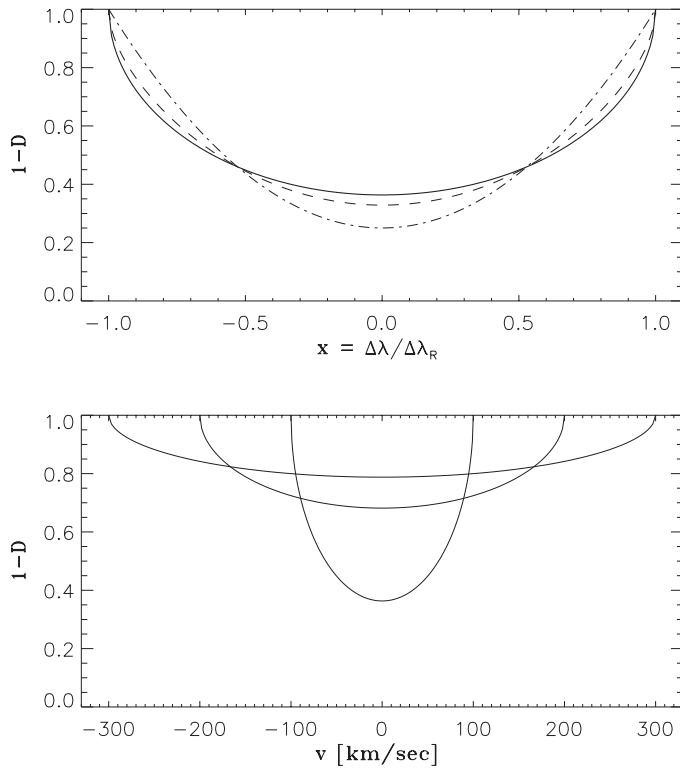


Figure 12.5: Rotational broadening profiles for a rigidly rotating spherical star assuming the intrinsic profile of the line to be infinitely narrow and independent of position on the stellar disk. The adopted limb darkening law is a linear function of μ , given by eq. (12.46). Plotted is the line flux relative to the continuum, i.e. $1 - D(x)$. Top panel: the horizontal axis shows the wavelength shift $\Delta\lambda$ in units of $\Delta\lambda_R$ (so in units of x). Profiles for $\beta = 0$ (solid line), $3/2$ (dashed line) and ∞ (dashed-dotted line) are shown. Bottom panel: the horizontal axis shows the wavelength in velocity units relative to line center. For three values of $v_R \sin i$ (and β fixed to zero) de profile of a line that has an equivalent width in velocity space W_v of 100 km sec^{-1} is shown.

Physic der Sternatmosphären, 1955), we introduce the rotational displacement of the line

$$\Delta\lambda = \frac{\lambda_{lu}}{c} \omega x \sin i \quad (12.44)$$

where the angular velocity ω is a vector in the (y, z) -plane that is inclined at an angle i from the z -axis towards the observer in the direction of the y -axis. If $i = 0^\circ$, we see the star pole-on; if it is 90° , we see the star face-on. The angular speed is $\omega = |\omega|$. If we see the star face-on, the rotational velocity at the equator is $v_R = \omega R$. If we see the star at an inclination, this maximum rotational velocity is only $v_R \sin i$. The maximum velocity displacement is therefore $\Delta\lambda_R = (\lambda_{lu}/c) \omega R \sin i = (\lambda_{lu}/c) v_R \sin i$.

Let us introduce the normalized x and y distance $x' = x/R$ and $y' = y/R$, such that

$$\frac{\Delta\lambda}{\Delta\lambda_R} = x'. \quad (12.45)$$

Following Unsöld, we adopt for the emergent intensity

$$I(\mu) = \alpha (1 + \beta \cos \theta) = \alpha (1 + \beta \mu) \quad (12.46)$$

where, as usual, θ is the angle between the radial direction and that of the beam towards the observer. The angle μ will be the same for each circle around O , i.e.

$$\sin \theta = \sqrt{x'^2 + y'^2} \quad (12.47)$$

such that

$$I(\mu) = \alpha \left(1 + \beta \sqrt{1 - (x'^2 + y'^2)} \right). \quad (12.48)$$

If we normalize the flux in the line to unity in x' space, we find for the absorption depth

$$D_{x'} = \frac{\int_0^{\sqrt{1-x'^2}} I(x', y') dy'}{\int_{-1}^{+1} \int_0^{\sqrt{1-x'^2}} I(x', y') dy' dx'} = \frac{\frac{2}{\pi} \sqrt{1-x'^2} + \frac{\beta}{2}(1-x'^2)}{1 + \frac{2}{3}\beta} \quad (12.49)$$

For $\beta = 0$, i.e. no limb darkening, the line profile shape is that of an ellips. For the limb darkening law derived for the gray atmosphere (eq. 10.15) the coefficients $\alpha = 2/5$ and $\beta = 3/2$. In figure 12.5 examples of rotationally broadened profiles are shown. The top panel shows the effect of the limb-darkening coefficient β . In the lower panel $\beta = 0$ is adopted, but profiles are plotted as a function of velocity shift relative to line center. This shows the effect of different values of $v_R \sin i$. Rotation of the stellar surface will not affect the equivalent width of the spectral line as only the observed velocity (frequency) of line flux is changed. The equivalent width in velocity space $W_v = 100 \text{ km sec}^{-1}$. Notice that analyzing rapidly rotating stars seen fairly edge on tends to become more challenging as the lines will become shallow and broad, making them more difficult to distinguish from the continuum, especially so if the density of spectral lines in a given frequency interval is large and/or the spectrum has a fairly low signal-to-noise ratio.

Exercise 12.5

Derive the rotational broadening profile eq. (12.49). Remember that

$$\int \sqrt{a^2 - x^2} dx = \frac{1}{2} \left(x \sqrt{a^2 - x^2} + a^2 \arcsin \frac{x}{a} \right) \quad (12.50)$$

12.4 Curve of growth

In the not so distant past, the *curve of growth* analysis, developed by Marcel Minnaert, was a commonly used method to analyse stellar atmospheres as it provides a simple and quick way to estimate a number of important parameters – such as column depths, excitation- and ionization temperatures, and abundances – by only using equivalent line widths. These can be determined accurately for faint stars, where it is difficult to measure detailed line profiles. Nowadays the method is not often employed anymore, as thanks to the rapid development in computer technology it has become fairly easy and efficient to use LTE/NLTE model atmospheres. Nonetheless, we will discuss the curve of growth in detail as the method provides great insight in the physics of the formation of line profiles.

We consider a simple model for a stellar atmosphere consisting of two components: a geometrically deep layer responsible for the continuum, which emits at a brightness temperature T_b , and a homogeneous layer that is located further out, where the spectral line is formed, and that emits according to a Planck function at temperature T_L . We will assume that $T_L < T_b$, such that an absorption line is formed. Note that if the temperature in the line forming layer would be higher than T_b the following discussion will remain valid.

The emerging intensity follows from eq. (4.43) and is equal to

$$I_\lambda = B_\lambda(T_b)e^{-\tau_\lambda} + B_\lambda(T_L)[1 - e^{-\tau_\lambda}] \quad (12.51)$$

where τ_λ is the optical depth in the spectral line. If we neglect the contribution of stimulated emission in the line extinction coefficient, such that eq. (7.29) reduces to

$$\chi_\lambda = \alpha_{lu}(\lambda)n_l = \frac{\pi e^2}{m_e c} \frac{\lambda_{lu}^2}{c} f_{lu} \frac{1}{\sqrt{\pi \Delta \lambda_D}} n_l H(a, v) \quad (12.52)$$

where we have specified the profile function by the Voigt profile eq. (12.25), and if we defined the integrated *column depth* in cm^{-2} of particles in level l that are in the line of sight throughout the line forming region

$$N_l \equiv \int n_l(s) ds \quad (12.53)$$

we obtain for the line optical depth

$$\tau_\lambda = \alpha_{lu} N_l = \frac{\pi e^2}{m_e c} \frac{\lambda_{lu}^2}{c} f_{lu} \frac{1}{\sqrt{\pi \Delta \lambda_D}} N_l H(a, v) = \frac{\tau_o}{H(a, 0)} H(a, v) \simeq \tau_o H(a, v) \quad (12.54)$$

where $\Delta \lambda_D$ is the Doppler width, a and v the Voigt parameters as defined in eq. (12.29), and τ_o the optical depth at line centre. Often $a \ll 1$, such that $H(a, 0) \simeq 1 - a$, which justifies the last equality. For the relative depression d_λ we get

$$d_\lambda = 1 - \frac{I_\lambda}{I_\lambda^c} = \frac{B_\lambda(T_b) - B_\lambda(T_L)}{B_\lambda(T_b)} (1 - e^{-\tau_\lambda}) \equiv d_\lambda^{\max} (1 - e^{-\tau_\lambda}) \quad (12.55)$$

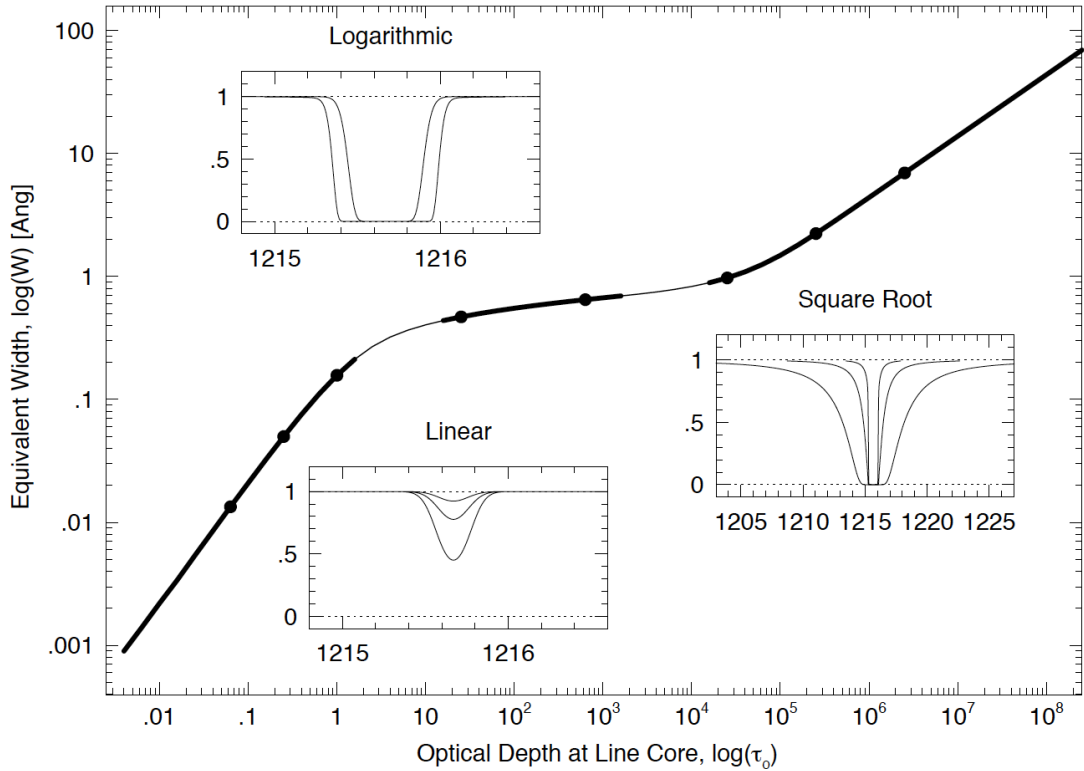


Figure 12.6: The curve of growth for a Ly α of H1 with a Doppler velocity $\xi_D = 30 \text{ km sec}^{-1}$. The three regimes discussed in the text, the linear (weak lines), flat (saturated lines), and damping part (strong lines) are shown by thicker curves. The approximations describing these regimes are Eq. 12.57, 12.58, and 12.60, respectively. Corresponding line absorption profiles are shown for each regime and their locations on the COG are marked with filled dots. Figure: Chris Churchill.

with d_λ^{\max} the maximum depression. This yields for the equivalent line width

$$w_\lambda = d_\lambda^{\max} \int_{\text{line}} (1 - e^{-\tau_\lambda}) d\lambda \quad (12.56)$$

Figure 12.6 shows how the line profile and equivalent line width depend on optical depth τ_0 for a line that has $d_\lambda^{\max} = 1$, i.e. in case the source function in the line forming layer is negligibly small compared to the continuum source function. The behaviour of the equivalent width may be characterized by three regimes.

Weak lines

First, the regime of weak lines, for which $\tau_\lambda \ll 1$. In this limit the relative depression reduces to $d_\lambda \simeq d_\lambda^{\max} \tau_\lambda$. Say, we can measure the absorption depth of the profile with an accuracy of one promille of the continuum intensity. Figure 12.3 tells us that for a spectral line that has

$a = 0.01$ the Doppler core will extend up to $H(a, v) \sim 0.01$. A weak line with a relative depression of 0.1 at line centre would then reach the measurement noise level at the point where the Lorentz wing is about to become dominant. For weak lines we may thus replace the Voight function $H(a, v)$ by $\exp[-(\Delta\lambda/\Delta\lambda_D)^2]$, which has surface $\sqrt{\pi}\Delta\lambda_D$. This yields

$$w_\lambda \simeq d_\lambda^{\max} \tau_o \sqrt{\pi} \Delta\lambda_D = \frac{\pi e^2}{m_e c} \frac{\lambda_{lu}^2}{c} f_{lu} d_\lambda^{\max} N_l \quad (12.57)$$

The equivalent width increases linearly with column depth N_l . The curve of growth therefore first shows a linear increase of w_λ with line strength. Note that the equivalent width is independent of the profile function.

Saturated lines

If $\tau_o > 1$, the core of the line becomes saturated. The intensity at line centre reaches the value $B_\lambda(T_L)$ reflecting the maximum depression d_λ^{\max} . The width of the line wings still increases, however, the corresponding increase in the equivalent width is no longer linear with τ_o , but proceeds at a slower pace. It approximately holds that

$$w_\lambda \approx d_\lambda^{\max} Q(\tau_o) \Delta\lambda_D \quad (12.58)$$

where one can estimate the value for $Q(\tau_o)$ using figure 12.6. For increasing optical depth, $Q(\tau_o)$ increases from about 2 to 6 in this ‘shoulder part’ of the curve of growth. An approximate analytical expression for this function is $Q(\tau_o) = 2\sqrt{\ln \tau_o}$, valid from $\tau_o \gtrsim 3$. This regime of the curve of growth is therefore (also) often referred to as the ‘logarithmic part’.

Strong lines

For very strong lines, i.e. lines for which $\tau_o \gg 1$, the line core does no longer change much. However, the far line wings will still have $\tau_\lambda < 1$. For a sufficiently large τ_o both wings will contribute significantly because they are formed in the damping part of the Voigt profile, i.e. where $H(a, v) \simeq a/(\sqrt{\pi}v^2) = (a/\sqrt{\pi})(\Delta\lambda_D/\Delta\lambda)^2 \sim 1/\Delta\lambda^2$. This decrease with wavelength is much less dramatic than the exponential decay of the Doppler core. In the damping part of $H(a, v)$ we may write

$$\tau_\lambda = \tau_o \frac{a}{\sqrt{\pi}v^2} = \tau_o \frac{a}{\sqrt{\pi}} \frac{\Delta\lambda_D^2}{\Delta\lambda^2} \quad (12.59)$$

Using the transformation $u^2 = 1/\tau_\lambda$, we obtain after substitution in eq. (12.56) for the equivalent width

$$\begin{aligned} w_\lambda &\simeq d_\lambda^{\max} \Delta\lambda_D \sqrt{\tau_o \frac{a}{\sqrt{\pi}}} \int_{\text{lijn}} (1 - e^{-1/u^2}) du \\ &= d_\lambda^{\max} \Delta\lambda_D \sqrt{\tau_o a} 2\pi^{1/4} \end{aligned} \quad (12.60)$$

For the last equality we used the standard integral

$$\int_{-\infty}^{+\infty} \left(1 - e^{-1/x^2}\right) dx = 2\sqrt{\pi} \quad (12.61)$$

The assumption that we have used here to derive the curve of growth, i.e. an atmosphere consisting of a homogeneous layer that is in LTE, such that $S^\ell = B_\lambda(T_L)$, placed in front of a layer from which a continuum is emitted that is also a Planck field, is called the *Schuster-Schwartzschild* model. It will not come as a surprise that this model does not provide a very realistic representation of the stellar atmosphere. An improvement that can still be done analytically is the *Milne-Eddington approximation*. Here it is assumed that the source function is a linear function of the continuum optical depth, that LTE holds, and that the profile function $\phi(\lambda - \lambda_{lu})$ and the ratio between the line and continuum extinction $\wp_\lambda = \chi_\lambda/\chi_c$ are independent of depth in the atmosphere. The result $w_\lambda(\tau_o)$ turns out to be identical to the Schuster-Schwartzschild result if τ_o is replaced by \wp_λ . We therefore do not discuss details of this approximation.

Empirical curve of growth

In real life the curve of growth method is applied somewhat different than described above. On the vertical axis one plots $\log W_\lambda/\lambda$. One therefore does not divide by $\Delta\lambda_D = \lambda\xi_D/c$, after all the Doppler and microturbulent velocities ξ_D are not known, but by the wavelength, such that we obtain a quantity that is independent of wavelength of the applied set of lines. The horizontal axis, in principle, contains the column depth of the particles responsible for the spectral line, i.e. $N_l = \int n_{ljk} ds$. Splitted out in terms of excitation, ionization, and elemental abundance, one obtains for the particle density

$$\begin{aligned} n_{ljk} &= \frac{n_{jlk}}{N_{jk}} \frac{N_{jk}}{N_k} \frac{N_k}{N_N} N_N \\ &= \frac{g_{ljk}}{U_{jk}(T_{\text{ext}})} e^{-E_{ljk}/k T_{\text{ext}}} q_{jk}(T_{\text{ion}}) A_k N_N \end{aligned} \quad (12.62)$$

where we have adopted the LTE formalism. The excitation fraction is described by eq. (6.24) and the ionization fraction q_{jk} by eq. (6.35). T_{ext} is the excitation temperature and T_{ion} the ionization temperature. In LTE these are locally equivalent. However, the curve of growth measures column densities, implying that T_{ext} and T_{ion} represent temperatures that correspond to excitation and ionisation fractions that are averaged over this entire column. These mean temperatures need not be equal, therefore they both are introduced.

In many applications of the curve of growth the excitation energy is expressed in electron volt. Using that the temperature associated with 1 eV is equal to $E/k = 11604.8$ K, one finds

$$e^{-E_{ljk}(\text{erg})/kT} = e^{-11604.8 E_{ljk}(\text{eV})/T} = 10^{-5039.9 E_{ljk}(\text{eV})/T} \quad (12.63)$$

Taking the energy in eV, the horizontal axis of the curve of growth becomes

$$\log X = \log C + \log(g_{ljk} f_{lu} \lambda_{lu}) - 5039.9 E_{ljk}/T_{\text{ext}} \quad (12.64)$$

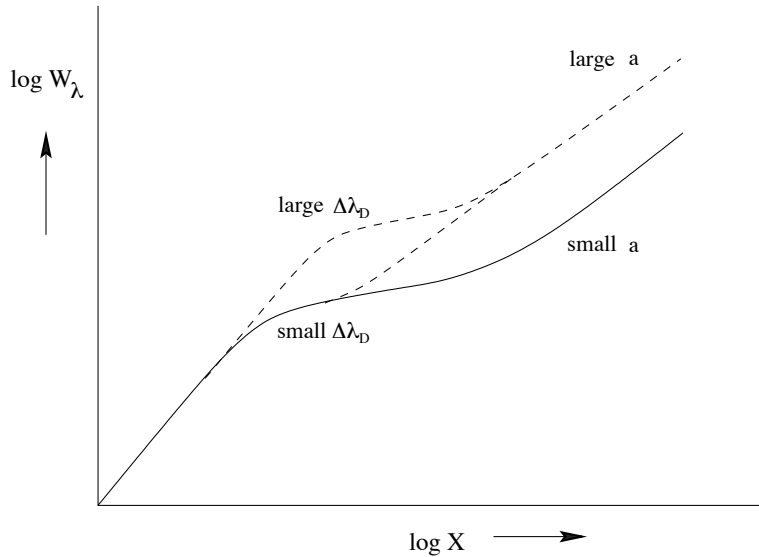


Figure 12.7: Schematic explanation of the way the curve of growth works. For a large turbulent velocity ξ_D , proportional to $\Delta\lambda_D$, the line will saturate later. Therefore the shoulder part of the curve of growth is further to the right. For a large value of the damping constant, proportional to a , this shoulder part will switch sooner to the \sqrt{X} dependence for strong lines.

where

$$C = \frac{\pi e^2}{m_e c} \frac{D_\lambda^{\max}}{\sqrt{\pi \xi_D}} q_{jk}(T_{\text{ion}}) A_k N_N \quad (12.65)$$

and N_N is the column density of nuclei; D_λ^{\max} the saturation absorption depth as measured in the flux; ξ_D is the thermal plus turbulent velocity averaged over the line forming region (see eq. 12.23), and q_{jk} is the mean ionization, averaged over the same region, and described by the temperature T_{ion} .

A systematic (practical) method is to build up the curve of growth in several steps. First, one could plot only those lines that originate from the groundlevel of one particular ion. These lines differ in gf -value (see § 7.3) but not in any other parameter. The next step is to plot lines from a different lower level. Because of the excitation term $5039.9 E_{ljk} / T_{\text{ext}}$ this new curve of growth will be shifted relative to the first one. By shifting both curves on top of each other as best as possible the excitation temperature may be derived. The ionization temperature is derived by comparison of the curves for different ions with model predictions. Note that the ionization equilibrium will be a function of temperature and electron density (see eq. 6.26). The latter implies that the shifting due to ionization is, at least in principle, also a measure of the total particle density, and therefore of the surface gravity. Abundances may then be determined by shifting curves of growth for different elements, and comparing these shifts with predictions.

In determining T_{ext} , T_{ion} , and A_k , using the method described above, relatively weak lines

positioned on the linear part of the curve of growth may be used. In this regime the lines are independent of Doppler and microturbulent velocity as each photon that can be absorbed by the line will be extinguished, regardless of whether it is a line centre or a line wing photon. For saturated lines that are located on the shoulder part of the curve of growth this is not so. Saturation implies that (at first) at line centre more potentially extinguishing particles are present than there are continuum photons offered to the line forming layer. The value of X for which the equivalent width is no longer linear will depend on the value of the microturbulent velocity. If ξ_{micro} is relatively large, the flattening of the curve of growth will occur later. This is so because for large turbulent velocities the intrinsic profile will be broader, therefore less particles can extinct at line centre, such that saturation will occur later, at larger X . This dependence of the curve of growth on ξ_{micro} is pictured in figure 12.7. It may be clear that from a comparison of these regions of the curve of growth with model predictions one may determine the microturbulent velocity.

In principle, one may use the parts of the curve of growth that are caused by the damping wings of strong line to determine the gravity. In a star with a relatively large value of $\log g$ the particle density in the line forming region will be larger. Therefore, the curve of growth of a given line, such as the sodium D₂ in the solar spectrum, will switch sooner from the shoulder part to the \sqrt{X} dependence of strong lines. To use this part of the curve of growth as a diagnostic it is essential that the damping constant γ is well known. After all, γ has a similar effect on the curve of growth as has $\log g$, such that a poorly known damping constant will introduce a large uncertainty in the gravity. This is also pictured in figure 12.7.

13

Scattering

Arguably the most fundamental *physical* complication inherent in solving radiation transfer problems is that of scattering. Scattering has the effect that the radiation field gets decoupled from local source and sink terms. Because of scatterings, photons may travel large distances through the medium without interacting with this medium. Therefore, due to a strongly deviant radiation field generated at some distant place, the local radiation field may be completely different from the radiation that is produced locally (by the local thermal source function). It is therefore scattering that makes that radiation transfer is a *global* problem and that communicates to regions of large optical depth that the medium has an open edge, through which photons escape. The above states that even at large optical depth, scattering may cause the mean intensity $J_\nu(\mathbf{r}, t)$ to be strongly deviant from the locally produced thermal radiation $B_\nu(T(\mathbf{r}, t))$.

We will investigate the effect of scattering using (1) continuum formation, and (2) line formation in a homogeneous semi-infinite medium. It may be clear that we – in order to determine the effect of scattering – can no longer assume the relevant (continuum or line) source function to be given by the local Planck function. For the line formation example this implies that we may no longer assume LTE. The source function now needs to include a scattering component, therefore it will have the more general form of eq. (9.48). Working out this proto-type source function in some more detail, to get a sense of what to expect, we get

$$S_\nu = \frac{\kappa_\nu B_\nu + \sigma_\nu J_\nu}{\kappa_\nu + \sigma_\nu} = \epsilon_\nu B_\nu + (1 - \epsilon_\nu) J_\nu \quad (13.1)$$

where

$$\epsilon_\nu = \frac{\kappa_\nu}{\kappa_\nu + \sigma_\nu} \quad (13.2)$$

Here ϵ_ν is the *thermal coupling parameter* or *destruction probability*. In case only thermal emission processes play a role, one has $\epsilon_\nu = 1$, therefore $S_\nu = B_\nu$. If only scatterings occur, such that $\epsilon_\nu = 0$, one finds $S_\nu = J_\nu$.

13.1 Continuum scattering

For several types of stellar atmospheres the thermal coupling parameter ϵ_ν for continuum radiation may be very small in a large fraction of the atmosphere. For instance, scattering of light by free electrons is the dominant source of extinction in the outer layers of hot stars. For hot stars even relatively deep layers may show ϵ_ν values of the order of only 10^{-4} , until, finally, for ever increasing density, free-free processes (recall $\chi_\nu^{\text{ff}} \propto \rho^2$) win from Thomson scattering (recall: $\chi_e \propto \rho$). In cool stars that have a low metal abundance, hydrogen will be neutral in the upper part of the atmosphere and free electrons will be scarce. Here Rayleigh scattering on H and H₂ will dominate the H⁻ extinction and ϵ_ν will be almost zero up to large depth (when finally hydrogen will rather abruptly excite and ionize, and ϵ_ν will quickly approach unity).

We will now show that if $\epsilon_\nu \rightarrow 0$ the continuum radiation field may (will!) differ from the local Planck function up to large optical depth. To do so we adopt a geometry of planer layers and assume that the Planck function is a linear function of optical depth, i.e.

$$B_\nu(\tau_\nu) = a_\nu + b_\nu \tau_\nu \quad (13.3)$$

Below, we will even assume the medium to be homogeneous, i.e. $b_\nu = 0$. Until then we keep things somewhat more general. We do already assume that ϵ_ν is constant. The 0th order moment of the transfer equation (eq. 4.37) can be written as

$$\frac{dH_\nu}{d\tau_\nu} = J_\nu - S_\nu = \epsilon_\nu(J_\nu - B_\nu) \quad (13.4)$$

If we use the Eddington approximation (we embark on a journey towards large optical depth, where $f_\nu \rightarrow 1/3$) to re-work the 1st order moment (eq. 4.38) to

$$\frac{dK_\nu}{d\tau_\nu} = \frac{1}{3} \frac{dJ_\nu}{d\tau_\nu} = H_\nu \quad (13.5)$$

we find after substitution

$$\frac{1}{3} \frac{d^2J_\nu}{d\tau_\nu^2} = \frac{1}{3} \frac{d^2(J_\nu - B_\nu)}{d\tau_\nu^2} = \epsilon_\nu(J_\nu - B_\nu) \quad (13.6)$$

where the second equality is allowed because of the particular form of eq. (13.3). The general solution of this differential equation is

$$J_\nu - B_\nu = \alpha_\nu e^{-\sqrt{3\epsilon_\nu}\tau_\nu} + \beta_\nu e^{+\sqrt{3\epsilon_\nu}\tau_\nu} \quad (13.7)$$

As we require that $J_\nu \rightarrow B_\nu$ for $\tau_\nu \rightarrow \infty$ it must hold that $\beta_\nu = 0$. To determine α_ν we use the boundary condition $H_\nu(0) = g_\nu(0)J_\nu(0)$. The value of the Eddington factor depends on the geometry of the problem. In the case of a sharply peaked radiation field $g_\nu(0) = 1$ (see § 3.6). However, here it is much more appropriate to adopt the solution of the grey atmosphere:

$g_\nu(0) = 1/\sqrt{3}$ (see eq. 10.9 and table ??). The boundary condition equation then becomes (see eq. 13.5)

$$J_\nu(0) = \sqrt{3}H_\nu(0) = \frac{1}{\sqrt{3}} \left. \frac{dJ_\nu}{d\tau_\nu} \right|_0 \quad (13.8)$$

such that we find for the mean intensity

$$J_\nu(\tau_\nu) = a_\nu + b_\nu\tau_\nu + \frac{b_\nu/\sqrt{3} - a_\nu}{1 + \sqrt{\epsilon_\nu}} e^{-\sqrt{3\epsilon_\nu}\tau_\nu} \quad (13.9)$$

and for the source function

$$S_\nu(\tau_\nu) = a_\nu + b_\nu\tau_\nu + (1 - \epsilon_\nu) \frac{b_\nu/\sqrt{3} - a_\nu}{1 + \sqrt{\epsilon_\nu}} e^{-\sqrt{3\epsilon_\nu}\tau_\nu} \quad (13.10)$$

As already implied by eq. (13.1) for small ϵ_ν the source function will be almost equal to the mean intensity. Note that for $\tau_\nu \rightarrow \infty$ one recovers $J_\nu \rightarrow B_\nu$ and $S_\nu \rightarrow B_\nu$, as one should. The above solutions clearly show the physics of the scattering problem. First, at the surface J_ν is remarkably different from B_ν . If we assume for simplicity that the medium is homogeneous, i.e. $b_\nu = 0$, we find that at $\tau_\nu = 0$

$$J_\nu(0) = \frac{\sqrt{\epsilon_\nu}}{1 + \sqrt{\epsilon_\nu}} B_\nu \quad (13.11)$$

For very small thermal coupling parameters ϵ_ν one obtains $J_\nu(0) \rightarrow \sqrt{\epsilon_\nu}B_\nu$, i.e. the mean intensity becomes much smaller than the Planck function. The run of the source function in a homogeneous medium is given in figure 13.1. It holds that $S_\nu(0) = \sqrt{\epsilon_\nu}B_\nu$ (a result that is much more general than one would expect given the rather rigorous approximations we have made here). For $\epsilon_\nu \ll 1$ we obtain $J_\nu(0) \rightarrow S_\nu(0)$. This illustrates that the mean intensity follows the source function, and not the Planck function. We also see that the discrepancy between J_ν and B_ν reached up to large depth in the medium. The exponential term shows that only $J_\nu \rightarrow B_\nu$ if $\tau_\nu \gtrsim 1/\sqrt{\epsilon_\nu}$. For media that are dominated by scatterings this can be a very large optical depth. When eventually the mean intensity approaches the Planck function we say that the radiation field is *thermalized*. $\tau_\nu = 1/\sqrt{\epsilon_\nu}$ is called the *thermalization depth*.

The following physical insight may help in gaining a better understanding of the concept of thermalization optical depth: the thermal coupling parameter $\epsilon_\nu = \kappa_\nu/(\kappa_\nu + \sigma_\nu)$ is simply the probability that a photon that is interacting with a particle is destroyed (i.e. converted into thermal energy). To be absolutely assure that the photon is destroyed it has to experience on the order of $n = 1/\epsilon_\nu$ interactions. If the trajectory of the photon through the medium is described by a *random walk*, with a mean optical photon path $\Delta\tau_\nu \sim 1$ (see § 4.3), the total optical depth it can travel before being destroyed will be given by

$$\tau_\nu = \sqrt{n} \Delta\tau_\nu = 1/\sqrt{\epsilon_\nu} \Delta\tau_\nu \sim 1/\sqrt{\epsilon_\nu} \quad (13.12)$$

Photons that are emitted at a larger optical depth most probably will not be able to escape without being thermalized first (which is why $J_\nu \rightarrow B_\nu$), while photons that are generated

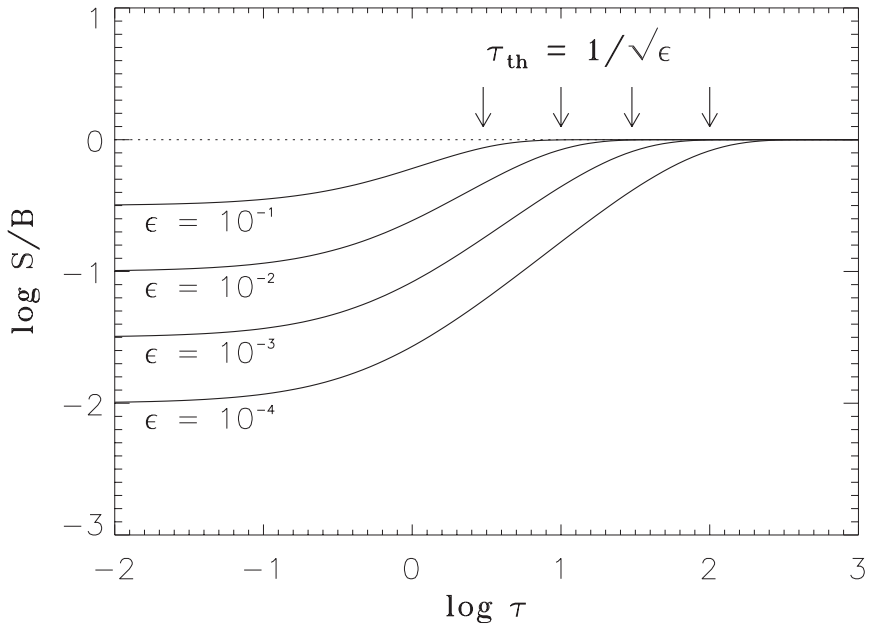


Figure 13.1: The continuum source function in a homogeneous semi-infinite medium as a function of the optical depth τ_ν . S_ν is normalized to the Planck function B_ν . The curves give solutions for different values of the destruction probability ϵ_ν .

at a smaller optical depth most likely are able to escape (causing J_ν to become less than the thermal value B_ν). Note that if $\epsilon_\nu = 1$, i.e. in each interaction the photon is destroyed, the thermalization optical depth $\tau_\nu \sim 1$, as expected, because in this case the optical depth scale is the same as the thermal optical depth scale ($d\tau_\nu = d\tau_\nu^{\text{therm}} \equiv \kappa_\nu dz$).

Exercise 13.1

Let us consider a geometry of planar layers. The source function is given by eq. (13.1) and the behaviour of the Planck function by eq. (13.3).

- a) Show that the Eddington flux is given by

$$H_\nu = \frac{1}{3} b_\nu - \sqrt{\frac{\epsilon_\nu}{3}} \frac{b_\nu/\sqrt{3} - a_\nu}{1 + \sqrt{\epsilon_\nu}} e^{-\sqrt{3\epsilon_\nu}\tau_\nu} \quad (13.13)$$

- b) Show that the flux is given by the diffusion approximation (vgl. 4.62) if $\tau_\nu \rightarrow \infty$

Exercise 13.2

Let us consider a geometry of planar layers. The source function is given by eq. (13.1) and the behaviour of the Planck function by eq. (13.3). We assume that the medium is homogeneous and that $\epsilon_\nu = 1$.

- a) Show that the mean intensity is given by

$$J_\nu(\tau_\nu) = B_\nu \left[1 - \frac{1}{2} e^{-\sqrt{3}\tau_\nu} \right] \quad (13.14)$$

- b) Explain why $J_\nu(0) = 1/2 B_\nu$.

13.2 Line scattering in a two-level atom

One of the best examples showing that the source function is composed of a thermal and a scattering contribution is that of the two-level atom. The two-level atom is an idealized problem. Real atoms have many energy levels, therefore, at first sight, this approximation may seem to be grossly inadequate. However it actually provides a surprisingly good description of line formation in a number of cases of interest. This is why we will discuss it here in certain detail.

The general formulation of the line source function in a two-level atom is given by eq. (7.25). If we assume complete redistribution this reduces to

$$S_\nu^\ell = \frac{n_u A_{ul}}{n_l B_{lu} - n_u B_{ul}} = \frac{2h\nu_{lu}^3}{c^2} \frac{1}{(g_u n_l)/(g_l n_u) - 1} \quad (13.15)$$

The last equality is identical to eq. (7.26). Note that the source function is dependent on the population ratio n_l/n_u . In LTE we assume that the line source function is equal to the local Planck function, i.e. $S_\nu^\ell = B_\nu$, implying that the ratios between level populations are given by the Boltzmann excitation equation. Consequently, it also implies that in LTE scattering processes do not play a role in determining the behaviour of the line source function. By that, the state of the gas can not depend on a radiation field that is generated elsewhere – where conditions may be completely different.

To study the effects of scatterings we must therefore not assume LTE. Rather, we must derive the ratio of the population of lower level 1 and upper level 2 from the statistical equilibrium equation (9.15). This equation states that the number of transitions into state 1 (or 2) should be equal to the number of transitions out of state 1 (or 2); phrased differently

$$n_1 (R_{12} + C_{12}) = n_2 (R_{21} + C_{21}) \quad (13.16)$$

Here R is the radiative- and C the collisional rate per particle per second. The radiative excitation rate is give by eq. (7.3); that of radiative de-excitation is the sum of eq. (7.1) and

(7.4). The collisional excitation rate is given by eq. (7.5). The relation between C_{12} and C_{21} follows from eq. (7.7), and for our two-level atom is given by

$$\frac{C_{21}}{C_{12}} = \left(\frac{n_1}{n_2} \right)^* = \frac{g_1}{g_2} \exp(h\nu_{12}/kT) \quad (13.17)$$

Source function of the two-level atom

Armed with the above knowledge, it follows, after substitution of the SE ratio for n_1/n_2 in the outermost right hand side term of equation (13.15), and using the Einstein relations eq. (7.14) and eq. (13.17), that

$$S^\ell = (1 - \epsilon) \bar{J}_{12} + \epsilon B_{\nu_{12}} \quad (13.18)$$

where

$$\epsilon = \frac{\epsilon'}{1 + \epsilon'} \quad \text{in which} \quad \epsilon' = \frac{C_{21} [1 - \exp(-h\nu_{12}/kT)]}{A_{21}} \quad (13.19)$$

The two-level approximation provides a good approximation for resonance lines. These usually occur in the ultraviolet part of the spectrum where the frequency is relatively high, therefore $h\nu/kT \gg 1$. This implies that ϵ may be approximated by

$$\epsilon \approx \frac{C_{21}}{C_{21} + A_{21}} \quad (13.20)$$

which shows that it simply represents the thermal coupling parameter or destruction probability, i.e. the probability that an absorbed photon is destroyed by a collisional de-excitation process (C_{21}) rather than being conserved by re-emission in a spontaneous de-excitation (A_{21}). Equation (13.18) is the most fundamental equation of the problem. The first term at the right hand side reflects the creation of photons by scattering, i.e. by emission following the absorption of photons. The second term reflects the thermal creation of photons, i.e. by emission following collisional excitations.

We will assume that the profile function is given by a pure Doppler profile, i.e. we neglect natural line broadening and accept that the only broadening is due to the thermal motions of atoms. For a description of this profile we use its dimensionless form eq. (12.22). The absorption in the line can then be described as

$$\chi_x = \chi\phi(x) \quad (13.21)$$

By analogy we obtain for the emission $\eta_x = \eta\phi(x)$. Note that the extinction χ_x is not equal to the extinction at line centre, χ_0 . In case of a Doppler profile it holds that $\chi_0 = \chi/\sqrt{\pi}$. The optical depth τ corresponding to the frequency-independent opacity χ is called the *frequency-averaged opacity* in the line, and is the logical optical depth scale in terms of which we will discuss the two-level atom. The optical depth τ and the monochromatic optical depth are related by

$$\tau_x = \tau\phi(x) \quad (13.22)$$

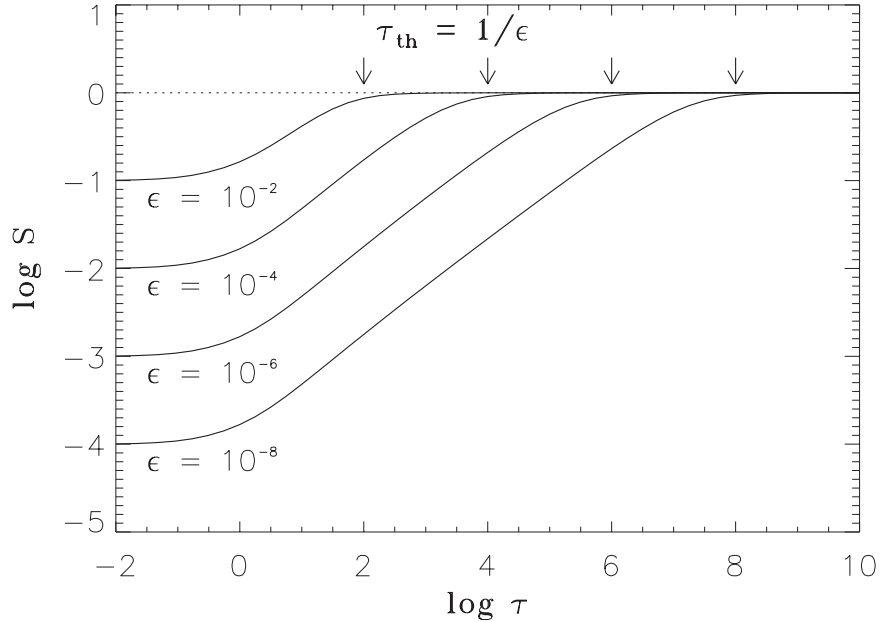


Figure 13.2: The source function of the two-level atom in a homogeneous semi-infinite medium as a function of the frequency averaged optical depth τ . S is normalized to the Planck function $B_{\nu_{12}}$. The curves give solutions for different values of the destruction probability ϵ , labeled in the figure.

Interpretation of the two-level atom

From a mathematical point of view the source function (eq. 13.18) is still a linear function of the mean intensity. This implies, that although there is a global coupling between the radiation field and the material medium, the problem is still relatively simple and can, for instance, be solved with the Feautrier method. This solution method will be presented in some detail at the end of this section. We first take a closer look at the meaning of the solution of the two-level atom, presented in figure 13.2. To obtain this solution we have used the fact that the medium is homogeneous, ϵ , B_ν , and χ are independent of τ .

What do we learn from this result? In the limit $\tau \rightarrow 0$ the source function $S^\ell \rightarrow \sqrt{\epsilon} B_{\nu_{12}}$. This result is valid regardless of the exact shape of the profile function. Several rigorous mathematical proofs of this result exist, but these will not be discussed here. For us it is important that $S^\ell(0) < B_{\nu_{12}}$. Why is this so? In a homogeneous medium departures from LTE (i.e. $S_\nu^\ell \neq B_\nu$) arise only because of the presence of a boundary through which photons escape. In regions of high opacity, where the line photons do not yet “feel” the presence of the boundary, all microscopic processes depicted in figure 7.1 are in detailed balance. Phrased differently: LTE holds. However, as soon as photons do start to feel the edge, radiative excitations will

no longer be balanced by radiative de-excitations. Since the absorption rate depends on the number of photons present, while the spontaneous emission rate does not (we neglect for simplicity the stimulated emission), the number of radiative excitations drops below the number of de-excitations as soon as photons start to escape. The lower level will consequently start to be depopulated with respect to LTE, while the upper level will be underpopulated. Since the source function measures the number of photons created per unit optical depth, and since the number of created photons is proportional to the population of the upper level (because this is the level from which the atomic transitions accompanied by the photon emission occur), the source function has to drop below the Planck function, i.e. S^ℓ will be less than $B_{\nu_{12}}$.

At some optical depth the source function will start to deviate from the Planck function. This optical depth is called the *thermalization depth* τ_{th} . Figure 13.2 shows that for a Doppler profile $\tau_{\text{th}} \sim 1/\epsilon$. Note that for a typical value $\epsilon = 10^{-6}$ the optical depth at which this occurs is very large: $\tau \sim 10^6$. Why is this so? After all, one would expect that the boundary is first felt by an “average” photon when $\tau \sim 1$.

The reason is that in a spectral line it is not the “average” photon that is responsible for the transfer and escape of photons. To better understand this, let us follow the trajectory of a photon from the point where it is created by a thermal emission. We assume that this happens at large optical depth. It is very likely that the newly created photon has a frequency that is close to that of line center. After all, this is where the profile function $\phi(x)$ has its maximum. For this frequency the monochromatic optical depth $\tau_x = \tau\phi(x)$ is large and therefore the geometrical distance the photon will travel – i.e. the distance corresponding to $\Delta\tau_x \sim 1$ – will be small (see § 4.3). Probably a similar scenario will unfold in the next scattering events. This yields the following picture of the path a photon will follow in case of complete redistribution: the particle of light will experience many successive scatterings, all at a frequency close to line center; the geometrical distance the photon will cover in all these interactions is, however, small. But, in the rare occasion that the photon is emitted in the wing of the profile function, where the optical depth is orders of magnitude less, it suddenly can travel a large distance. This situation is schematically shown in figure 13.3. Phrased differently: the transfer of photons in the core of the line is very inefficient; the crossing of geometrical space occurs during the rare excursions of the photons into the line wings. It is now clear why the thermalization optical depth is so large: it is determined by photons in the line wings that have an average mean free path that is much larger than that of photons in the line core. However, realize that it is the line core photons that define the frequency mean optical depth τ .

Why is the thermalization depth a function of destruction probability? The total number of successive scatterings is of the order $1/\epsilon$; if the photon has not escaped before it has experienced $1/\epsilon$ scatterings it will be destroyed by means of a collisional deexcitation. It will not have been aware of a boundary to the medium. This illustrates that ϵ must play a role in determining the thermalization depth. But why is $\tau_{\text{th}} \propto 1/\epsilon$, and not, for instance, proportional to $1/\sqrt{\epsilon}$ as is to be expected in case the photon distances itself from its point of creation by means of a random walk (see § 13.1)? Essentially, the answer is already given above: if the

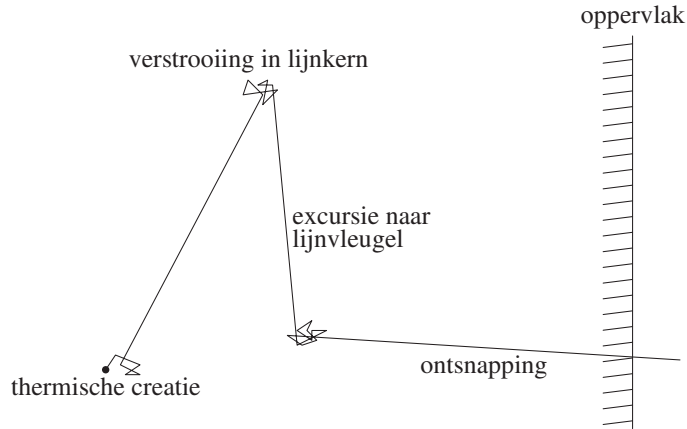


Figure 13.3: Schematic representation of a trajectory of a photon in a gas of two-level atoms (from Hubeny, in *Stellar Atmospheres: Theory and Observation*).

photon escapes, it does so in the line wing by means of one long flight in the right direction, i.e. in the direction of the surface. (As long as the photon has a frequency close to that of line center it follows a more or less “random walk”, however, as discussed, it does not travel a significant geometrical distance.)

We may quantify the above consideration using the *escape probability* formalism.

Escape probability

The probability that a photon with frequency ν and propagating in the direction specified by angle μ escapes in a single flight is given by

$$p_{\nu\mu} = e^{-\tau_{\nu\mu}} \quad (13.23)$$

This follows from the physical meaning of optical depth (see section 4.3). In a plane-parallel medium it holds that $\tau_{\nu\mu} = \tau_\nu/\mu$. The angle-averaged escape probability is thus given by

$$p_\nu = \frac{1}{2} \int_0^1 e^{-\tau_\nu/\mu} d\mu \quad (13.24)$$

where the integration only extends for angles $\mu \geq 0$, since photons moving in the inward direction ($\mu \leq 0$) cannot escape. The angle- and frequency-averaged escape probability for photons in a single spectral line is given by

$$p_{\text{esc}} = \int_{-\infty}^{+\infty} \phi_x p_x(\tau_x) dx \quad (13.25)$$

where we have switched to the frequency variable x and the frequency averaged optical depth τ . Notice that at the surface $p_{\text{esc}}(0) = 1/2$, because a photon is either emitted in the outward

direction, in which case it certainly escapes, or in the inward direction, in which case it does not escape.

We now need compare the escape probability p_{esc} to the photon destruction probability $p_{\text{des}} = \epsilon$. If $p_{\text{esc}} \ll p_{\text{des}}$, photons are likely thermalized before escaping from the medium. In other words: the line photons do not feel the presence of the boundary, and therefore $S^\ell \sim B_{\nu_{12}}$. If $p_{\text{esc}} \gg p_{\text{des}}$, photons likely escape before being thermalized. It is therefore natural to define the thermalization optical depth τ_{th} , as

$$p_{\text{esc}}(\tau_{\text{th}}) \equiv p_{\text{des}} = \epsilon \quad (13.26)$$

i.e. as the optical depth for which photon escape (by direct flight) is equally probable as the destruction of photons by a collisional process.

Substitution of (13.25) in (13.26) yields the sought-after relation between τ_{th} and ϵ . This relation for the escape probability may be a bit too abstract to give a clear physical picture. To obtain a deeper understanding we will approximate the integral in equation 13.25 using a dichotomous model. To do so we divide the frequencies x in two categories: the “optically thick” frequencies, for which $\tau_x > 1$, and the “optically thin” frequencies, for which $\tau_x < 1$. The *critical frequency* that divides the two regimes is given by

$$\tau\phi(x_c) = 1 \quad (13.27)$$

For the Doppler profile (12.22) it follows that

$$x_c = \sqrt{\ln(\tau/\sqrt{\pi})} \quad (13.28)$$

i.e. the critical frequency is a function of the frequency averaged optical depth τ . In our dichotomous model we now assume that all photons having an “optically thick” frequency will be absorbed, while all frequencies have an “optically thin” frequency will escape by a direct flight in the outward direction. The photon has a probability $\frac{1}{2}\phi(x)dx$ to be emitted in the outward direction with a frequency in the interval $(x, x + dx)$. In this picture the total escape probability of the photon is given by

$$p(\tau) = \frac{1}{\sqrt{\pi}} \int_{x_c}^{\infty} \exp(-x^2) dx = \frac{1}{2} \operatorname{erfc}(x_c) \approx \frac{\exp(-x_c^2)}{2\sqrt{\pi}x_c} \quad (13.29)$$

where $\operatorname{erfc}(x)$ is the complimentary error-function. The asymptotic behavior of this function is given by the expression at the far right hand side. Finally, substitution of (13.28) in (13.29) yields

$$p(\tau) \approx \frac{1}{2\tau\sqrt{\ln(\tau/\sqrt{\pi})}} \quad (13.30)$$

which within a factor of two (it is twice as large) is equal to the exact asymptotic expression, i.e. if we would not have adopted the dichotomous model. Equating the obtained result to the escape probability ϵ we get

$$\tau_{\text{th}} = \frac{1}{2\epsilon\sqrt{\ln(\tau_{\text{th}}/\sqrt{\pi})}} \approx \frac{\text{constant}}{\epsilon} \quad (13.31)$$

where the constant is of the order unity. This, finally, yields the anticipated result: the thermalization optical depth scales as $\tau_{\text{th}} \propto 1/\epsilon$.

Numerical solution using Feautrier

We will now describe a way to numerically solve the two-level atom. In doing so we will assume the line to be formed in a homogeneous semi-infinite medium, i.e. ϵ, B_ν en $\phi(x)$ do not depend on τ . However, each of these parameters may be chosen to be depth-dependent without causing additional complications. The source function (13.18) can be written as

$$S^\ell(\tau) = (1 - \epsilon) \int_{-\infty}^{\infty} \phi(x) J(\tau, x) dx + \epsilon B \quad (13.32)$$

$$= (1 - \epsilon) \int_{-\infty}^{\infty} \phi(x) dx \int_0^1 u(\tau, \mu, x) d\mu + \epsilon B \quad (13.33)$$

with u the symmetric average of the specific intensity (see equation 5.13). Notice that we have dropped the frequency subscript of the Planck function; B_x will not change significantly over the width of the line profile and may be computed once at, say, $x = 0$.

In order to switch to the difference representation, we introduce a set of optical depth points $\{\tau_d\}, d = 0, \dots, D$ for which $\tau_0 < \tau_1 < \dots < \tau_D$; a set of angle points $\{\mu_m\}, m = 0, \dots, M$; and a set of frequency points $\{\nu_n\}, n = 0, \dots, N$. Using this grid notation we obtain for the difference form of the source function

$$S_d = (1 - \epsilon) \sum_{n=0}^N a_n \sum_{m=0}^M b_m u_{dmn} + \epsilon B \quad (13.34)$$

where a_n and b_m are the quadrature weights of frequency and angle, respectively. In other words

$$\int_{-\infty}^{+\infty} \phi(x) f(x) dx \rightarrow \sum_{n=0}^N a_n f(x_n) \quad (13.35)$$

$$\int_0^{+1} f(\mu) d\mu \rightarrow \sum_{m=0}^M b_m f(\mu_m) \quad (13.36)$$

The transfer equation can again be reduced to the standard 2nd order differential form

$$\mu_m^2 \frac{d^2 u_{mn}}{d\tau^2} = \phi_n^2 (u_{mn} - S) \quad (13.37)$$

The source function connects *all* frequencies and angles. Important to realize is that the source function is a linear function of the specific intensity. The set of equations (13.37) therefore represents a system of linear differential equations.

For ease of notation we can group all angles and frequencies in a single set of grid points i for which $(\mu_i, \nu_i) = (\mu_m, \nu_n)$ for $i = m + n \times M$. We choose to introduce a column vector \mathbf{u}_d ,

with dimension $I = M \times N$, consisting of the angle-frequency components at depth d , i.e. $(\mathbf{u}_d)_i = u_{di}$. Transfer equation (13.37) can then be written as a matrix equation

$$-\mathbf{A}_d \mathbf{u}_{d-1} + \mathbf{B}_d \mathbf{u}_d - \mathbf{C}_d \mathbf{u}_{d+1} = \mathbf{L}_d \quad (13.38)$$

This equation is identical to (5.31), however the meaning of \mathbf{u}_d and the coefficients \mathbf{A}_d , \mathbf{B}_d and \mathbf{C}_d is different. In the Feautrier scheme eq. (5.32) \mathbf{A}_d are \mathbf{C}_d are now $(I \times I)$ matrices of which the diagonals contain terms given by the difference form of the transfer equation. \mathbf{B}_d is a full $(I \times I)$ matrix of which the diagonal again contains terms given by difference form of the transfer equation, but which also has off-diagonal terms that represent the integral over the angle-frequency points of the source function (13.34). \mathbf{L}_d is a vector that contains the thermal sources. The total system has a *blok tri-diagonal structure* for which the solution proceeds with a forward-backward recursive sweep, as discussed in § 5.2.

However, to obtain the matrix coefficients \mathbf{D}_d and \mathbf{E}_d (the matrix analogs of (5.34) en (5.35) respectively) requires the actual inversion of the full matrices $\mathbf{F}_d \equiv \mathbf{B}_d - \mathbf{A}_d \mathbf{D}_{d-1}$. In real problems the number of frequency- and angle points I tends to become quite large quite easily making matrix inversions very CPU intensive. Therefore, this method – though very elegant – is often not very practical, not even for linear problems.

The alternative is to solve the problem by means of iteration. In an iterative procedure the approach is to simply solve transfer equation (13.37) by means of the standard Feautrier algorithm, i.e. with A_d , B_d and C_d being scalars for every angle-frequency point separately, using a *given* source function. In other words: we do a formal solution. The given source function is based on the specific intensity values obtained in the previous iteration. This method is known as *lambda iteration*. The drawback of the lambda iteration method is that in problems in which scattering processes play an important role – as is the case for the two-level atom – the convergence properties of the iteration procedure are very poor. However, there is a method, referred to as *approximate lambda iteration* – which we do not discuss here – that overcomes this problem in normal lambda iteration.

Exercise 13.3

- a) Derive the line source function of the two-level atom, i.e. equation (13.18)

14

NLTE mechanisms and models

14.1 LTE versus NLTE

As discussed in § 6.7 one assumes that in LTE the state of the material medium in an elementary volume $dV(\mathbf{r})$ is controlled by the local values of the temperature and density¹: $n_{ijk} = n_{ijk}(N(\mathbf{r}), T(\mathbf{r}))$ or $n_{ijk}(\rho(\mathbf{r}), T(\mathbf{r}))$ or $n_{ijk}(n_e(\mathbf{r}), T(\mathbf{r}))$. The remarkable thing here is that in LTE the radiation field $J(\mathbf{r})$ does not seem to play a role in setting the state n_{ijk} of the gas. In section 6.7 we pointed out that this is because in LTE it is assumed that collisional processes dominate the transitions of electrons between energy levels causing the line source function to equal the local Planck function, i.e. $S_\nu^\ell = B_\nu(T(\mathbf{r}))$. In that case, the general equation for determining n_{ijk} , the statistical equilibrium equation, reduces to the Boltzmann equation for the description of the excitation state (eq. 6.23) and the Saha equation for the description of the ionization state (eq. 6.26). We therefore already arrived at the conclusion that deviations from LTE will arise if

- i) collisional processes no longer dominate over radiative processes, *and*
- ii) the radiation field deviates from the local Planck function, i.e. $J_\nu(\mathbf{r}) \neq B_\nu(T(\mathbf{r}))$.

The first situation occurs if the density in the medium is low, as the rate of collisions scales with the electron density: $C \propto n_e$ (see eq. 7.5). The interstellar medium ($n_e \sim 10^{-2} - 10^{-1} \text{ cm}^{-3}$) in general and nebulae ($n_e \sim 10^3 - 10^6 \text{ cm}^{-3}$; see also section 2.4) in particular are environments in which the (electron) density is extremely low. Also in chromospheres and coronae and in stellar flares ($n_e \sim 10^8 - 10^{10} \text{ cm}^{-1}$) around cool stars and in stellar winds the density of the outflowing gas is low enough to cause departures from LTE. The typical nature of these departures are that the absence of an effective (collisional) coupling of the

¹Note that in LTE there can be (and will be) a non-local *indirect* coupling between the radiation field and the material medium through the equation of radiative equilibrium (see eq. 9.47) and to a lesser extent the equation of hydrostatic equilibrium, which contains a contribution from forces related to the gradient in the radiation pressure (see eq. 11.4).

levels leads to a depopulation of excited levels through spontaneous radiative de-excitations² and an overpopulation of the ground level. This raining down of electrons is referred to as *electron cascade*.

Can departures from LTE occur *in* the photosphere of stars? To evaluate this question we use the handy (but rough) relation describing the density at $\tau \sim 1$ in the photosphere that we derived in section 10.2 (see eq. 10.18), i.e.

$$\rho(\tau = 1) \sim \frac{1}{\chi' H} \propto \frac{g}{T} \quad (14.1)$$

This shows that densities are relatively high for cool main-sequence stars, such as the sun ($n_e \sim 10^{12} - 10^{15} \text{ cm}^{-3}$, see table A.5). This is one of the reasons why for these stars LTE is in general a fine approximation (for a second reason, see below). Also in white dwarfs, which have extreme values for the surface gravity g , the density is such that LTE is a good approximation. Yet even in these cases LTE may break down in the very outer layers of the atmosphere. This situation may not affect the continua and weak lines, which are formed deep in the atmosphere, but may produce deviations in the strengths of strong lines (e.g. hydrogen Balmer and Lyman transitions, the He I triplets, and the Ca H and K lines), mainly in the line cores.

The atmospheres of giants and supergiants (with their low g ; yielding $n_e \sim 10^{10} - 10^{13} \text{ cm}^{-3}$, see again table A.5) require, in general, NLTE treatment of both continuum and line formation. The dividing line is not well defined, but a rule of thumb is that the resonance lines of the dominant ions are likely formed under NLTE for $\log g \lesssim 3.5$ or so for most T_{eff} . For the O and early-B dwarfs (with their high T) it is also necessary to adopt NLTE.

Let us now reflect on the second situation. The mean intensity $J_\nu(\mathbf{r})$ will differ from $B_\nu(\mathbf{r})$ if the radiation field at \mathbf{r} is significantly affected by photons that are produced elsewhere, at a place where the conditions are substantially different from those at \mathbf{r} . We first consider the situation *in* a photosphere. Here, there is a fundamental difference between the sun and the hot O stars. In the sun the contribution of scatterings to the total extinction is small. Phrased differently, the thermal coupling parameter $\epsilon_\nu = \kappa_\nu / (\kappa_\nu + \epsilon_\nu)$ (eq. 13.1) is almost unity. This is the second reason why LTE works so well in the sun³. In O stars scatterings do contribute considerably to the total extinction (through Thomson scattering) such that ϵ_ν becomes small. Consequently, by means scatterings a radiation field that is produced elsewhere may reach \mathbf{r} and dominate $J_\nu(\mathbf{r})$.

Let us characterize the non-local radiation field by the radiation temperature T_R . To illustrate the situation we will describe the radiation field in this chapter by assuming that

$$J_\nu(r) = W(r)B_\nu(T_R), \quad (14.2)$$

²However, levels very close to the continuum remain in LTE. See paragraph COLLISIONAL COUPLING OF HIGH LEVELS WITH THE CONTINUUM in section 8.1.

³The two reasons mentioned are so important that the effect of a lower degree of ionization in the solar photosphere ($n_e/N_N \sim 10^{-4}$) relative to that in the photosphere of O stars ($n_e/N_N \sim 1$) is compensated.

where we have made use of equations (3.9) and (3.10) and of eq. (6.47). $W(r)$ is de geometrical dilution. In the atmospheres of giants and supergiants, and in those of O and early-B dwarfs, it is the condition $J_\nu \neq B_\nu(T)$ that causes departures from LTE. It can be either because $J_\nu > B_\nu(T)$ or $J_\nu < B_\nu(T)$.

Far away from the stellar surface, in the direction of the interstellar medium, $W(r) \ll 1$. The temperature in the interstellar medium is only 10 – 20 K in molecular clouds and may reach $\sim 10\,000$ K in gas that is ionized by a nearby O star. This implies that the radiation field $J_\nu(r)$ in the ISM will deviate very strongly from $B_\nu(T)$ and one may expect the state of the gas in the ISM to differ from LTE in important ways.

In the following sections we provide an overview of the mechanisms of a number of NLTE processes. Though we will deal with the principles of NLTE only, the title of a number of these sections could have been ‘NLTE mechanisms as diagnostics of low density media’ because a number of these processes *an sich* are interesting as they provide very usable diagnostics for the study of (rarified) gaseous media. In the discussion we especially aim at mechanisms for which only a limited number of transitions need to be considered, such as to provide a clear insight in the NLTE process. We first address NLTE radiation mechanisms in ionized gas clouds in interstellar space; only then do we consider the situation in stellar atmospheres.

14.2 Photo- and collisional ionization in a low density medium

So one may expect NLTE conditions in a low density medium, such as a gas cloud. Gas clouds, often called gaseous nebulae, around hot stars show emission lines of hydrogen, for instance H α . The emission arises because the hot star, at large distance, ionizes the nebular gas after which the free electrons again recombine to arbitrary levels. It is almost certain that a hydrogen atom in an excited state will de-excite to a lower energy level by means of a spontaneous de-excitation, before it can absorb a photon that may bring it into a higher excited state, or (again) ionizes the atom. As a result, the electrons rain down into the ground level. For instance, an electron that enters the atom at excitation level $i = 6$ may first cascade to level $i = 3$ emitting a Paschen γ photon at a wavelength of 10938 Å (see figure 6.4 en tabel 7.1). Next, it may rain down into level $i = 2$ emitting an H α $\lambda 6562$ photon and subsequently end up in the ground level after emitting a Ly α photon.

It may be surprising that a distant star is capable of ionizing nebulae for the dilution of the radiation fields is considerable. If we formulate the dilution factor as (eq. 3.10)

$$W(r) \simeq \frac{1}{4} \left(\frac{R_\star}{r} \right)^2 = 1.272 \times 10^{-16} \left(\frac{R_\star/R_\odot}{d/\text{pc}} \right)^2, \quad (14.3)$$

and the star has a radius of $10 R_\odot$ and is positioned at a distance of 0.1 pc from a nebula, we find that the geometrical dilution of the radiation field is a factor $W = 1.3 \cdot 10^{-12}$. So, even though the color temperature of the radiation field may be 30 000 K or higher, the energy

density (see eq. 3.12) is weakened by a factor $\sim 10^{12}$. Atomic processes that depend on radiation, such as photoexcitation and photoionization, therefore proceed at a rate that is a factor W lower compared to thermal equilibrium. However, though the rate of recombinations is independent of W it is proportional to the electron density n_e . Phrased differently ‘the gas recombines only laboriously’. This is why in the surroundings of a hot star conditions may arise in which hydrogen is highly ionized. These regions of ionized hydrogen are referred to as H II regions. Is the temperature of the star however lower than $\sim 30\,000$ K the stellar radiation field will simply fail to supply sufficient ultraviolet photons with $\lambda < 912$ Å to ionize the hydrogen gas at all.

Photoionization equilibrium

The above implies that the ionization equilibrium of hydrogen is given by

$$n_0 4\pi \int_{\nu_\circ}^{\infty} \alpha_\nu^{\text{bf}} \frac{J_\nu}{h\nu} d\nu = N^+ n_e \alpha_A(T), \quad (14.4)$$

where

$$\alpha_A(T) = \sum_{i=1}^{\infty} \alpha_{i,\text{H}}^{\text{RR}}(T) \quad (14.5)$$

is the total recombination coefficient and $\alpha_{i,\text{H}}^{\text{RR}}$ the recombination coefficient in cm^3 per sec into level i of neutral hydrogen (see eq. 8.8). Values for $\alpha_A(T)$ are given by, for instance, Osterbrock & Ferland (2006); see Table 17.1. The subscript A indicates Case A recombination; we will return to this in chapter 17.

The ionization fraction $q = n_0/N^+$ (see eq. 6.35). Equation 14.4 describes the photo-ionization equilibrium, and not the Saha ionization equation 6.26 that specifies this equilibrium in LTE conditions. Note that only photo-ionizations, spontaneous recombinations and spontaneous de-excitations feature in the photo-ionization equilibrium. The excitation conditions will also strongly deviate from the Boltzmann equation (6.23) as the NLTE departure coefficients $b_0 \gg 1$ and $b_i < 1 \forall i > 1$ (see vgl. 6.29).

Collisional ionization equilibrium

Do collisional ionizations not play a role in nebulae? Equation (8.13) shows that the rate of collisional ionizations per $\text{cm}^3 \text{ sec}^{-1}$ is proportional to

$$C_{i\kappa} \propto n_e x^{-2} T^{-3/2} e^{-x}. \quad (14.6)$$

Using eq. (12.63) it follows that

$$x = \frac{\Delta E}{kT} = \frac{E_{i\kappa}}{kT} = \frac{11604.8 E_{i\kappa}(\text{eV})}{T} \quad (14.7)$$

Notice that, as discussed at the end of section 8.1, this rate is a sensitive function of x . For $x \ll 1$ we find that $C_{ik} \propto T^{1/2}$. For $x \gg 1$ the probability of occurrence of collisional ionizations is strongly reduced because of the e^{-x} dependence. This behavior reflects that in this case only a small part of the velocity distribution of the free electrons (given by Maxwell) can be used for collisional ionization processes. For the hydrogen Lyman continuum the ionization energy is 13.6 eV and one finds $x = 157825/T$ (see figure 6.4). Applying the effective temperature for T we find that even for the hottest stars x is considerably above unity. In combination with the low electron density ($C_{ik} \propto n_e$) it follows that collisional ionizations are not important.

The situation is different in the (proto-typical case of the) solar corona, where the electron density $n_e \sim 10^9$ and the temperature $T > 10^6$ K (see section 15.2). Consequently, $x \ll 1$. The rate C_{ik} is therefore orders of magnitude larger than in nebulae. As will be discussed in chapter 15, the corona already starts some thousands of kilometers about the solar surface. At first sight, one might think that therefore the radiation field of the sun might also play a role in (photo)ionizing the corona. But the effective temperature of the sun is only 5570 K. The regime $\lambda < 912$ Å is thus located far in the Wien part of the spectrum, where the flux has dropped exponentially (see Fig. 6.2). Therefore, photoionization by the relatively 'cold' solar radiation field has no appreciable effect on the ionization balance of the highly charged coronal gas. The solar corona is hence characterized by a *collisional ionization equilibrium*, for hydrogen given by

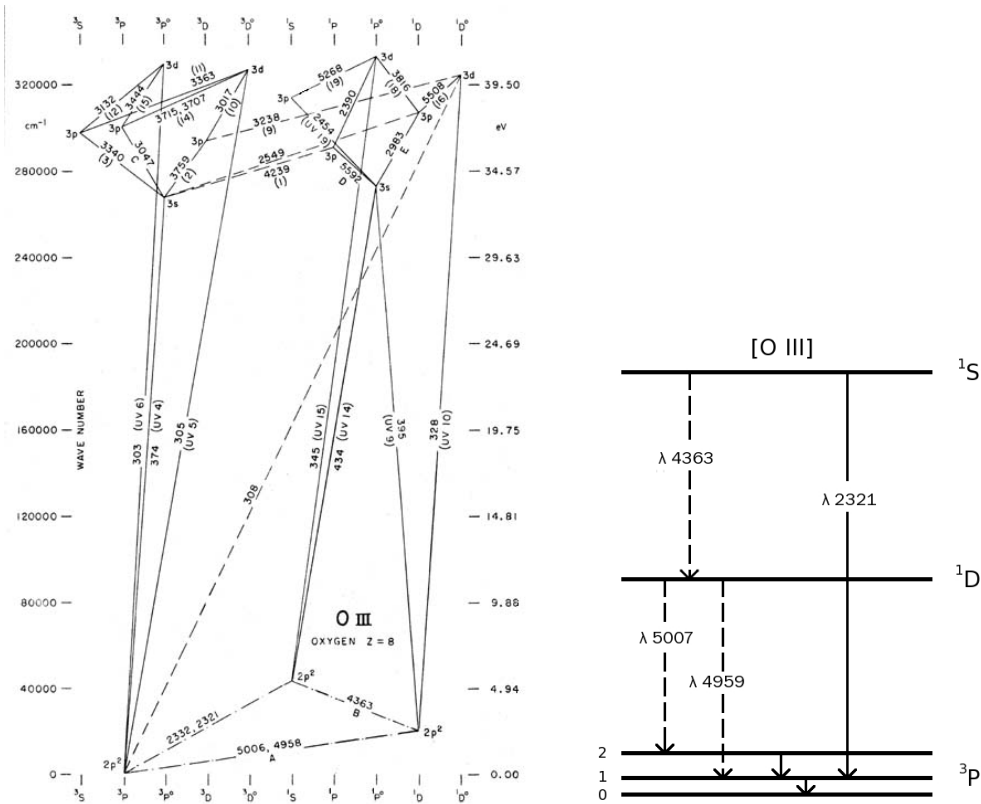
$$n_0 C_{0,H}(T) = n_0 n_e q_{0,H}(T) = N^+ n_e \alpha_A(T). \quad (14.8)$$

14.3 Excitations in a low density medium

In the previous section it was discussed that the interstellar radiation field, provided the radiation temperature T_R is sufficiently high, is capable of ionizing the nebular gas. Is this nebular material also excited, and if so, by what mechanism? We discuss the excitation of gas in a medium of low density using the oxygen O III ion as an example.

Forbidden transitions

Figure 14.1 shows the Grotrian diagram or energy level diagram of this ion. Note that O III has two energy levels that are fairly close to the $2p^2 3P$ ground level, i.e. the $2p^2 1S$ level with an excitation potential of 5.25 eV and the $2p^2 1D$ level with excitation potential 2.51 eV. Transitions between the same configuration (here $2p^2$) are called 'forbidden' as they violate *Laporte's parity rule* and are denoted with square brackets, e.g. $[O\text{ III}] \lambda 5007$. Forbidden transitions mostly have small Einstein coefficients A_{ul} . For instance, for $[O\text{ III}] \lambda 4959$ and $\lambda 5007$ these are 0.007 and 0.014 sec $^{-1}$. This implies that the mean lifetime of the 1D_2 level of O III is $\langle t \rangle = 1/0.021 = 36$ sec (see eq. 7.11). This is extremely long, and these levels



10 to 50 eV).

What about radiative excitations in the $2p^2\ ^3P - 2p^2\ ^1S$ and $2p^2\ ^3P - 2p^2\ ^1D$ transitions of O III? There are two reasons why these are unimportant relative to collisional excitations. First, because the interstellar radiation field at these wavelengths is extremely weak. Analogues to eq. (14.2) we may write (see also eq. 7.3)

$$J_\nu(r) = W(r) \int_0^\infty B_\nu(T_R) \phi(\nu) d\nu \quad (14.10)$$

where $\phi(\nu)$ is the profile function. Because the profile function is extremely narrow (i.e. it has the width of a spectral line) much less photons will be available for excitation compared to, for instance, that in the Lyman continuum discussed in the previous section. Second, we are here concerned with forbidden transitions. This implies that the chance that a photon from the already very weak radiation field is actually absorbed is very small.

For other lines, however, situations may occur in which the radiation field in a medium of low density can actually be very important and even dominate the excitation from the ground level. Interestingly, it is also O III that suffers from this. This principle has first been found by Ira Sprague Bowen (1898 –1973) in 1947 and is called *Bowen resonance fluorescence* (see section 14.4).

Critical electron density

The only process we still need to discuss is that of collisional excitations. These turn out to be negligible as long as the electron density is below a critical value. For the 1D_2 level the *critical electron density* $n_e^{\text{crit}} = 6.8 \times 10^5 \text{ cm}^{-3}$. For a higher electron density the level population will attain the LTE value relative to the ground level, given by Boltzmann equation (6.23). For lower densities the occupation will be lower than in LTE, however, because of the long lifetime the population of the meta-stable levels will be relatively high. So high even, that it will be only a few orders of magnitude below the LTE value.

The formal definition of the critical electron density for the population of level u is the one for which spontaneous de-excitations are equally important as collisional de-excitations. Therefore:

$$n_e^{\text{crit}} = \sum_{l < u} A_{ul} \left/ \sum_{l < u} q_{ul} \right. , \quad (14.11)$$

where we have summed over all levels lower than u .

The forbidden lines (one could also refer to them as collisionally excited lines) are discussed in more detail in chapter 17. It turns out that they are excellent diagnostics of the electron temperature T and electron density n_e in nebular gas.

14.4 Fluorescence

Insofar the discussion of NLTE processes in low density media dealt with excitations, these were collisional excitations. In case the nebular gas is ionized by the ultraviolet radiation field of a nearby star, relatively many photons of the resonance lines of hydrogen and helium will be present. As discussed in section 14.2, such photons will be created in recombination processes of H and He. If the density is not extremely low the nebular medium will be optically thick for H and He Lyman series photons. Phrased in a different way, these photons are ‘trapped’ and can only escape if they happen to reach the edge of the nebula. The radiation field in these optically thick lines will be much stronger than that suggested by equation 14.10, where it is assumed that the medium is optically thin at the line frequencies.

For a nebula that is irradiated by an early O star there will be a zone in the medium in which helium is predominantly present as He III. Obviously, there will be some He II in this zone, after all, there is a photo-ionization balance (*à la* that of hydrogen, see eq. 14.4). In case this balance implies that the amount of He II is such that the He II Ly α photons that are created by the recombination process are scattered many times before they can escape (i.e. the He II Ly α line is optically thick), there will be a strong radiation field at 303.78 Å, the wavelength of the He II Ly α line.

Now again consult the Grotrian diagram for O III in figure 14.1. Notice that, by coincidence, the wavelength of the $2p^2\ ^3P - 2p3d\ ^3P^\circ$ transition is almost identical to that of He II Ly α . To be precise, the most probable transition (having a relative probability of occurrence of 0.74) is the $2p^2\ ^3P_2 - 3d\ ^3P_2^\circ$ line at 303.80 Å; the next most likely transition (with a relative probability of 0.24) is the $2p^2\ ^3P_1 - 3d\ ^3P_2^\circ$ line at 303.62 Å. The many photons at these wavelengths created through the process of recombination and cascading of He III are used to populate the $2p3d\ ^3P^\circ$ level from the ground level. Using an alternative phrasing, these transitions are ‘resonating’ with the He II Ly α line. Many of the de-excitations in O III will proceed through the same transitions back to the ground level (again ‘the resonance’), but some will cascade via other (intermediate) levels. This is depicted in figure 14.2. These optical transitions are observed in many planetary nebulae.

With a very small relative probability of 0.02 the $2p3d\ ^3P_2$ level (labeled 4 in figure 14.2) will rain down in one of six levels $2p3p\ (^3S_1, ^3P_{1,2}^\circ, ^3D_{1,2,3}^\circ)$ (label 3) producing photons with wavelengths between 2809 Å en 3444 Å. From these levels 14 possibilities arise for further cascading. A number of these occur by way of the $2p3s$ level (label 2), with associated line transitions between 3024 Å en 3811 Å, into the $2p^2\ ^3P$ ground level (label 1). This mechanism, producing near-ultraviolet and violet lines between 2809 Å en 3811 Å, is called the *Bowen resonance fluorescence mechanism*, first described by Ira S. Bowen in 1947.

A second near-coincidence of a ground level transition of oxygen with a resonance line of hydrogen or helium is that of H I Ly β λ1025.72 Å with the O I transition $2p^4\ ^3P_2 - 2p^33d\ ^3D_3^\circ$, that has a wavelength of 1025.75 Å. This requires the presence of neutral oxygen in the H II

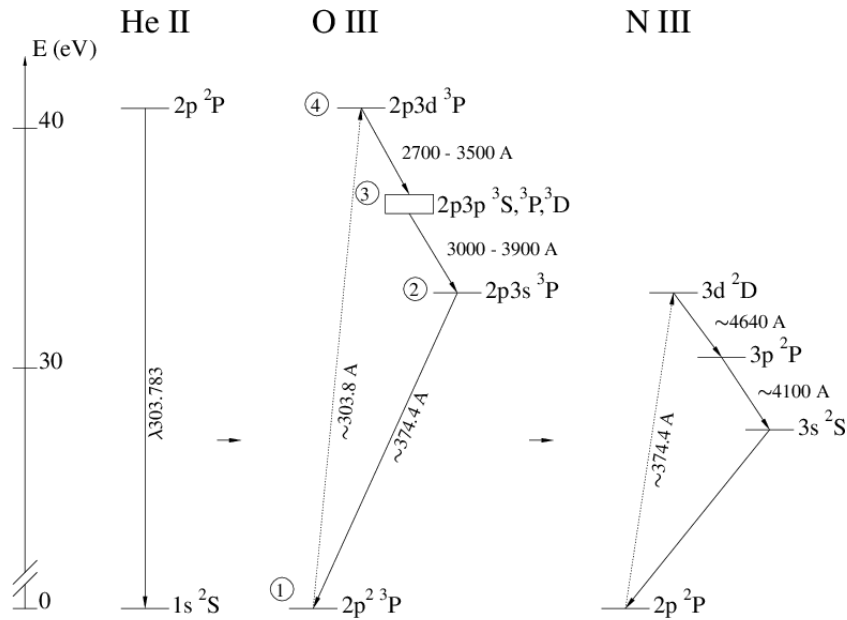


Figure 14.2: The Bowen fluorescence mechanism: ‘resonant’ excitation of O III lines by He II.

nebula, which is the case due to rapid charge transfer between oxygen and hydrogen.

The line-fluorescence mechanism shows that NLTE effects can be subtle. This type of fluorescence does occur in stellar atmospheres, but here we discussed it in the context of gaseous nebulae where it is prominently visible.

Continuum fluorescence

When considering fluorescence one usually means *line* fluorescence. However, it is possible to have a fluorescence effect in rarefied media by continuum radiation from a nearby star. Unlike the case of line fluorescence, in which one specific level is excited, continuum fluorescence is likely to excite a range of levels of an ion (or of multiple ions). The pumping of the levels usually occurs from the ground level through strong (di-pole) allowed transitions. For it to be considered a fluorescence process the radiation field in the line (or lines), $B_{lu}\bar{J}_{lu}$, must dominate over collisional excitations, $n_e q_{lu}$.

An example of continuum fluorescence is the excitation of [Ni II] $\lambda 7379$ in the circumstellar ejecta surrounding the Be star P Cygni (the first star in which P Cygni line profiles have been observed, see section 16.2). The ionization potentials of Fe and Ni are very similar, 7.9 and 16.2 eV for the ground level of Fe I and Fe II, and 7.6 and 18.2 eV for Ni I and Ni II. One may thus expect these ions to co-exist in the same region. It is therefore quite remarkable that the emission in the [Ni II] $\lambda 7379$ line in the shell surrounding P Cygni is much stronger than that of apparently comparable lines of [Fe II] in the same spectral regime; sometimes even by up

to a factor of 1000 stronger over what is expected on the basis of the abundance ratio between nickel and iron ($A_{\text{Fe}}/A_{\text{Ni}} \sim 20$; see table 15.2).

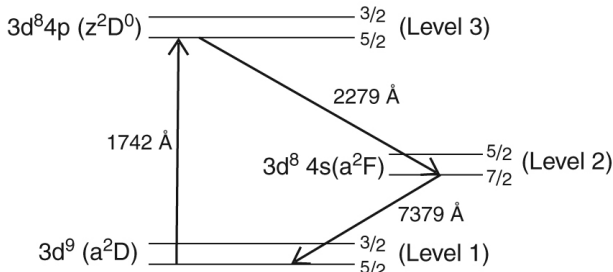


Figure 14.3: Energy-level diagram illustrating the [Ni II] continuum fluorescence. From: Pradhan & Nahar, Atomic Astrophysics and Spectroscopy.

A spontaneous de-excitation from this level to the excited $a^2F_{7/2}$ level (level 2) through the emission of a UV photon of wavelength 2279 Å causes the population in level 2 to increase. The last step in the fluorescence mechanism is the emission of a photon of wavelength 7379 Å in the forbidden transition $a^2D_{5/2} - a^2F_{7/2}$ when the electron cascades down from level 2 → 1. Two other forbidden lines in the system drawn in figure 14.3 are pumped in the same way: $a^2D_{3/2} - a^2F_{5/2}$ at 7413 Å and $a^2D_{5/2} - a^2F_{5/2}$ at 6668 Å. The transition $a^2D_{5/2} - a^2F_{7/2}$ is much weaker.

The critical electron density for this process is $n_e^{\text{crit}} \sim 10^7 \text{ cm}^{-3}$. Only at lower densities continuum fluorescence will occur. At higher densities collisional excitations dominate from the ground level.

For Fe II the fluorescence process is much less important because the levels corresponding to level 2 in the case of nickel can not be reached by means of allowed transitions (in the case of Ni, transitions 1 → 3 en 3 → 2). Allowed transitions that could correspond to the 1 → 3 transition turn out to have substantially lower critical electron densities compared to the value mentioned for Ni II, which is also unfavorable for the occurrence of fluorescence.

14.5 The NLTE behavior of hydrogen in O stars

We now study the NLTE behavior of hydrogen *in* the atmosphere of a hot O star. As discussed in the introduction to this chapter we may expect NLTE effects to play a role, especially because of the relatively low gravity. As an example we will focus on a pure-hydrogen planar atmosphere of an O4 V star, with gravity $\log g = 3.6$ (in cm s^{-2}) en $T_{\text{eff}} = 45\,000 \text{ K}$. The run of the NLTE departure coefficients b_i (see eq. 6.29) of the first four levels of hydrogen is

The fluorescence mechanism causing the strong [Ni II] $\lambda 7379 \text{ Å}$ is schematically drawn in figure 14.3. Multiple channels are possible, but here we focus on the channel shown by the arrows. Continuum photons with a wavelength of 1742 Å from the star P Cygni ($T_{\text{eff}} = 20\,000 \text{ K}$, $R_* = 89.2 R_\odot$, $L_* = 1.15 \times 10^6 L_\odot$), at a distance of 0.08 pc from the nebulae (i.e. the shell), pump electrons from the $a^2D_{5/2}$ ground level (level 1 in the figure) to the $z^2D_{5/2}^0$ level (level 3). A

given in figure 14.4 as a function of Rosseland optical depth τ_R (see section 10.3). Deep in the atmosphere, where densities are high and the contribution of scatterings to the total source function is small, such that $\epsilon_\nu = \kappa_\nu / (\kappa_\nu + \epsilon_\nu) \rightarrow 1$ (zie vgl. 13.1), the gas is in LTE. For all four levels $b_i = 1$.

Moving in the outward direction, i.e. the direction of decreasing τ_R , we first reach the layer in which the continuum is formed. At $\tau_R \sim 0.1$ the radiation processes dominate the ionization. At about this optical depth this is the case for ionization energies of at least a few eV in almost all stellar atmospheres, even for the sun⁴. In order to understand the behavior of b_i we therefore consider the ratio of the local radiation field to the local Planck function. Applying approximation eq. (14.2) we may write

$$\frac{J_\nu(r)}{B_\nu(r)} = W(r) \frac{e^{h\nu/kT(r)} - 1}{e^{h\nu/kT_R} - 1} = W(r) \frac{e^x - 1}{e^{x_R} - 1}, \quad (14.12)$$

for which hold the following limiting cases

$$\frac{J_\nu(r)}{B_\nu(r)} = \begin{cases} W(r)e^{(x-x_R)} & x \gg 1 \\ W(r)(T_R/T) & x \ll 1 \end{cases} \quad (14.13)$$

The value $x = 11604.8 \Delta E/T$ for the Lyman continuum is $x = 157825/T$; for the Balmer continuum $x = 39456/T$. We estimate the temperature at $\tau = 0.1$ to be 39 200 K from eq. (10.13). The radiation temperature at this position is about 52 000 K due to scatterings. For the limiting frequency of the Lyman continuum (912 Å) we find, using $x = 4.03$ and $x_R = 3.04$, that $J_\nu/B_\nu = 2.78 \times W(r) > 1$, adopting $W(r) \sim 1/2$. For the limiting frequency of the Balmer continuum (3645 Å) it follows, using $x = 1.01$ and $x_R = 0.76$, that $J_\nu/B_\nu = 1.53 \times W(r) < 1$, adopting $W(r) \sim 1/2$. The choice $W(r) \sim 1/2$ implies that we consider $\tau_R \sim 0.1$ as ‘far from the surface’, but that the atmosphere as a whole is compact, i.e. $H/R_* \ll 1$ (see section 3.3). For the Paschen continuum ($n_3 \rightarrow \infty$) and the Brackett continuum ($n_4 \rightarrow \infty$) J_ν/B_ν will drop below unity even slightly further. Because the radiation field in the Lyman continuum is stronger than the local Planck radiation field electrons will be pumped from the ground level more efficiently compared to the LTE situation, i.e. the population n_1 will drop below the LTE value, therefore $b_1 < 1$. For the Balmer continuum the situation is reversed. Here the radiation field is weaker compared to LTE, which leads to a (very weak) overpopulation of n_2 , i.e. $b_2 > 1$. For n_3 and n_4 this overpopulation is more prominent.

There is a second reason as to why the departure coefficient b_2 does not reach as high a values as that of the two higher levels: the Lyman lines are still optically thick at $\tau_R \sim 0.1$ and in particular the levels 1 and 2 are relatively strongly coupled to each other, the oscillator strength

⁴Actually, in the sun the radiative processes are often more important relative to the case of a typical O star as hydrogen is almost completely neutral in our star, therefore the electron density is much less than the ion density, whereas in O stars n_e and N_N are comparable.

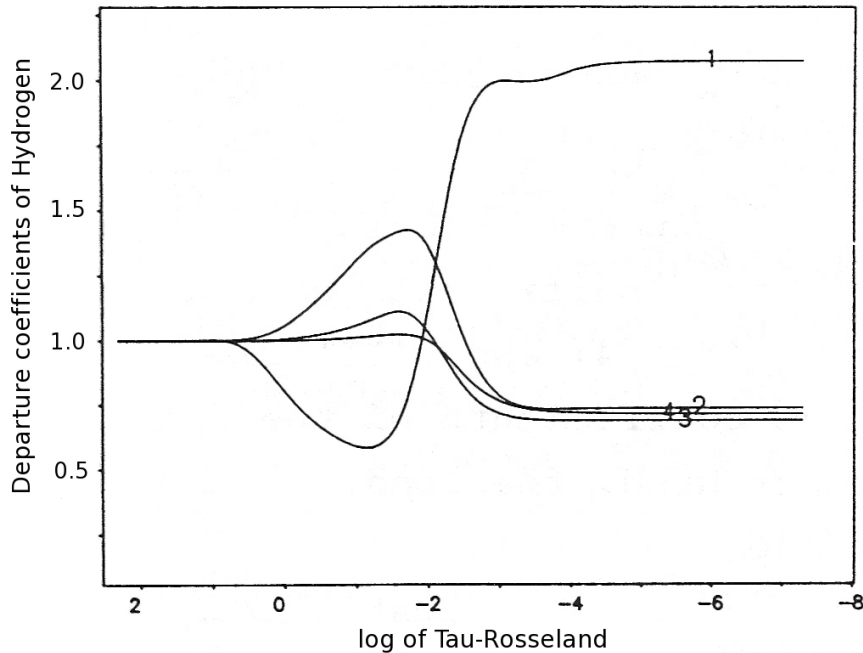


Figure 14.4: The NLTE departure coefficients of the first four levels of hydrogen as a function of Rosseland optical depth for an O star with effective temperature $T_{\text{eff}} = 45\,000\text{ K}$ and gravity $\log g = 3.6$. Source: Kudritzki, The atmospheres of hot stars: modern theory and observation, 1988.

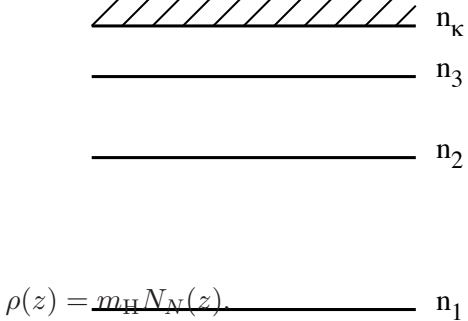
f_{12} being large compared to f_{13} and f_{14} (see table 7.1). Because of this the n_1 level has the tendency to impose its departure coefficient on n_2 . If this coupling would be complete – one would then state that the Ly α is in *detailed balance* – the value of b_2 would even follow that of b_1 . The latter is not the case in figure 14.4, but there is some degree of coupling. This explains why b_2 does not rise as high as b_3 , which in turn does not rise as high as b_4 .

Proceeding further in the outward direction one will reach the regime where the Lyman lines become optically thin. This happens at $\tau_R \sim 0.01$. High levels are now no longer (significantly) populated by means of photoexcitations from the ground level. The main channel through which these high levels attain electrons is by photoionisation from the ground level followed by recombination and cascading to lower levels. The processes governing these layers therefore are similar to those of the photoionisation equilibrium discussed in section 14.2. The upper levels will rain down in the ground level, causing $b_1 > 1$ en $b_i < 1 \forall i > 1$.

Statistical equilibrium, an example

The simple hydrogen model of the O4 V star lends itself well for a general discussion of the solution of the equations of statistical equilibrium 9.15. To keep a clear view of the situation

(and to make sure that the formulae fit on one page) we reduce the number of bound levels of hydrogen to three. For the principle of things this does not matter. Figure 14.5 provides the Grotrian diagram of our model atom. As always the index κ represents the continuum level, in this case ionized hydrogen. In the general sense n_κ is the ground level of the ion that forms if the ion under consideration is ionized. It therefore could have been the ground level of Fe XX if we were to consider the model for Fe XIX.



We assume that the local temperature $T(z)$, the local density $\rho(z)$ and the local radiation field $J_\nu(z)$ are known. As in the LTE model (see sections 11.1 and 11.2) the construction of a NLTE model requires an iteration process. The word ‘known’ in the one but last sentence therefore implies: to use the current values of the named parameters. For the hydrogen model the density can be easily coupled to the number density of nuclei through

Figure 14.5: A simple model of an H-atom consisting of three bound levels and a continuum level.

For our four level atom we may write the following four statistical equilibrium equations:

$$\begin{aligned} -n_1(P_{12} + P_{13} + P_{1\kappa}) + n_2P_{21} + n_3P_{31} + n_\kappa P_{\kappa 1} &= 0 \\ -n_2(P_{21} + P_{23} + P_{2\kappa}) + n_1P_{12} + n_3P_{32} + n_\kappa P_{\kappa 2} &= 0 \\ -n_3(P_{31} + P_{32} + P_{3\kappa}) + n_1P_{13} + n_2P_{23} + n_\kappa P_{\kappa 3} &= 0 \\ -n_\kappa(P_{\kappa 1} + P_{\kappa 2} + P_{\kappa 3}) + n_1P_{1\kappa} + n_2P_{2\kappa} + n_3P_{3\kappa} &= 0 \end{aligned} \tag{14.14}$$

where

$$P_{ij}(z) = R_{ij}(z) + C_{ij}(z). \tag{14.15}$$

The coefficients R_{ij} are given by equations (7.1), (7.4), (8.8) en (8.10) for $i > j$ and by (7.3) and (8.1) for $i < j$. The coefficients C_{ij} are given by (7.8) and (8.15) for $i > j$ and by (7.5) and (8.12) for $i < j$.

This system of four equations is however redundant (the determinant equals zero) as one may always reconstruct one of the equations from the remaining three. This is not the only problem, we also still have to fulfill the requirement of particle conservation eq. (6.32). Both problems can be resolved by, for instance, replacing the last equation by

$$n_1 + n_2 + n_3 + n_\kappa = A_k N_N \tag{14.16}$$

where A_k is the number abundance of element k and N_N is the nucleon density of nuclei. The system of equations may be written in matrix format

$$\begin{pmatrix} -P_{12} - P_{13} - P_{1\kappa} & +P_{21} & +P_{31} & +P_{\kappa 1} \\ +P_{12} & -P_{21} - P_{23} - P_{2\kappa} & +P_{32} & +P_{\kappa 2} \\ +P_{13} & +P_{23} & -P_{31} - P_{32} - P_{3\kappa} & +P_{\kappa 3} \\ 1 & 1 & 1 & 1 \end{pmatrix} \begin{pmatrix} n_1 \\ n_2 \\ n_3 \\ n_\kappa \end{pmatrix} = \begin{pmatrix} 0 \\ 0 \\ 0 \\ A_k N_N \end{pmatrix}$$

or

$$\mathbf{A} \vec{n} = \mathbf{B} \quad (14.17)$$

where \mathbf{A} is the transition probability matrix or *rate matrix* with dimension 4×4 ; $\vec{n} = (n_1, n_2, n_3, n_\kappa)$ is the population vector, and $\mathbf{B} = (0, 0, 0, A_k N_N)$ is a vector for which all elements equal zero save one. The last element of this vector provides the number density of element k . In our hydrogen model the number abundance $A_k = A_1 = 1$. The values for the populations follow from

$$\vec{n} = \mathbf{A}^{-1} \mathbf{B}. \quad (14.18)$$

Inversion of the matrix \mathbf{A} can for instance be done using a LU decomposition technique.

This shows the technique to solve the general set of statistical equilibrium equations.

15

The sun

15.1 Introduction

The study of the solar atmosphere is fundamental for multiple reasons: *i*) First, the properties of the sun are vital to everything that happens in our solar system. The climate of planetary atmospheres, for instance, is determined by the precise shape of the solar spectral energy distribution. Realize too that our eyes have evolved to be sensitive to the part of the solar spectrum reaching the earth surface in which the most flux is emitted. *ii*) Second, obviously, to learn more about the sun itself. For instance, to learn about its temperature and pressure stratification; chemical composition, magnetic fields, and time dependent spatial structures and velocity fields present at its surface. The basic solar properties are essential for determining its current evolutionary stage. This is done through a confrontation of these properties with models of stellar evolution, which also allows to study the history of our star as well as its future. *iii*) Third, because the sun is by far the brightest star in the sky. It offers the opportunity to study a plethora of processes that also occur in other stars, but at a much higher spatial resolution, a higher signal-to-noise ratio – and related to this a much higher spectral resolution – and a much higher time resolution. *iv*) Fourth, because the solar spectrum is the most stable calibration source of spectral properties of atoms and molecules. Moreover, it provides such information at temperatures that can not be (easily) achieved in laboratory experiments.

One can think of other reasons why the sun is so important – it is for instance the only star for which the equilibrium neutrino luminosity can be measured – however, the above listed reasons should be sufficient.

15.2 General information about the sun

In order to determine the fundamental parameters of the sun it is essential that its distance is known. The mean distance, or *astronomical unit*, is $149\,597\,870 \pm 2$ km. This value is the

mass	M_{\odot}	1.9889 ± 0.0003	$\times 10^{33}$	gr
radius	R_{\odot}	6.957 ± 0.001	$\times 10^{10}$	cm
luminosity	L_{\odot}	3.844 ± 0.010	$\times 10^{33}$	erg sec $^{-1}$
effective temperature	T_{eff}	5770 ± 4		K
age		4.57 ± 0.05	$\times 10^9$	year
bottom convection zone	r_{cv}	0.713 ± 0.003		R_{\odot}
mass fraction at surface				
– hydrogen	X_s	0.739 ± 0.005		
– helium	Y_s	0.248 ± 0.005		
– other elements	Z_s	0.012 ± 0.002		

Table 15.1: Basic solar parameters.

mean distance between the centers of the sun and the earth. The “mean” is over the eccentric anomaly, i.e. the angle between the sun-earth line and the direction to the perihelion of the elliptical orbit of the earth around the sun.

Basic parameters

Fundamental or *basic parameters* of the sun are given in table 15.1. Here, the solar radius is defined as the point in the atmosphere where the visual optical depth in the radial direction $\tau_V = 2/3$. What is actually measured is the angular diameter between the inflection points, at both sides of the solar disk, of the visual specific intensity profile across the solar disk. Model computations show that this is about 300 km above the layer where $\tau_V = 2/3$, for which the radius is corrected. The earth atmosphere absorbs and reflects a sizable fraction of the solar light. For this reason the solar luminosity needs to be measured from space. Balloon, rocket, and satellite observations show both short and long term variations in the bolometric luminosity. Most pronounced is an 11 year cycle in which the maximum of the irradiance corresponds to the number of sunspots. The peak-to-peak amplitude of this variation is about 0.09 percent. The mean luminosity and radius imply an effective temperature of 5770 K. The mass and radius imply a gravity in cm sec $^{-2}$ at the solar surface of $\log g = 4.438$. The age of the sun follows from radioactive decay of long living isotopes, such as U 238 , in meteorites. The depth of the convection zone is determined from helioseismic measurements.

Abundances

Knowledge of the chemical composition of the sun is essential for the modeling of its atmosphere and internal structure. The sun, though being the best studied star, is considered an ordinary star. This makes it very suited to serve as a reference in abundance studies of other stars. It is also very interesting to compare the chemical composition of other objects in our solar system – such as planets, comets and meteorites – with those of the sun, as this may give insight in the formation and evolution of the solar system as a whole. Other reasons for

studying the solar abundance pattern in great detail is its importance for theories of nucleosynthesis, as well as for models of the chemical evolution of galaxies, our Milky Way in particular, and of the universe itself. The first to perform a “quantitative” analysis of abundances in the solar atmosphere was Henry Norris Russell, who in 1929 on the basis of by-eye estimates determined the abundances of 56 elements.

The signature of 65 of the 83 stable elements is present in the photospheric absorption line spectrum, that is observed at high signal-to-noise ratio from ultraviolet to far infrared wavelengths using high spectral resolution instruments. The remaining elements are actually also present in the sun, but their lines are too weak to measure in the mentioned spectral range. Surprisingly, helium is in the list of non-observable elements. Spectral analysis of the elemental lines can be done well using LTE model atmospheres because in the solar photosphere collisional processes dominate over radiative processes. The derived abundances are usually expressed in logarithm of the number abundance normalized to 10^{12} particles of hydrogen, i.e.

$$A_{\text{el}} = \log(N_{\text{el}}/N_{\text{H}}) + 12.0 \quad (15.1)$$

Table 15.2 lists these abundances for the most important elements. It is to be noted that the above definition differs from that of A_k in eq. (6.32). The normalization relative to $10^{12} N_{\text{H}}$ was originally adopted in order to avoid negative numbers for the least abundant elements. Alas, it later turned out that tantalum ($A_{\text{Ta}} = -0.13$) and uranium ($A_{\text{U}} = -0.52$) are so rare that they do not fulfill this rule.

Nowadays, extremely sophisticated models of the solar atmosphere are used to derive the abundances. In 2005 Asplund and co-workers reported A_{el} values based on a 3-dimensional, time-dependent, hydrodynamical solar model atmosphere (see table 15.2). Compared to earlier work, significantly lower C, N, and O abundances were found. These low C, N, and O abundances agree much better with the corresponding abundances in the local interstellar medium and nearby B stars as well as the values measured in the solar corona/wind. A major challenge for these revised solar abundances, however, is that the excellent agreement achieved until now with helioseismology using standard solar evolution modeling is destroyed. The solution to this problem has not yet been identified.

It is common to use square brackets to denote that a stellar abundance is given relative to the solar value. The definition is

$$[X] \equiv \log X_{\text{star}} - \log X_{\text{Sun}} \quad (15.2)$$

In particular this is done for iron, where

$$[\text{Fe}/\text{H}] = \log (N_{\text{Fe}}/N_{\text{H}})_{\text{star}} - \log (N_{\text{Fe}}/N_{\text{H}})_{\text{Sun}} \quad (15.3)$$

is sometimes referred to as the *metal abundance* of the star. Do not get confused with $Z = 1 - X - Y$, i.e. the mass fraction of all elements except hydrogen (X) and helium (Y), which is commonly referred to as the *metallicity*. Relatively young stars in the plane of the Milky Way have about solar abundances (therefore $[\text{Fe}/\text{H}] \sim 0$). “Metal poor” stars have $[\text{Fe}/\text{H}] \sim -1$ to

	Element	Symbol	Atomic mass	Photosphere A_k	Mass fraction	Mass Z_s	Meteorites A_k	Phot - Meteor
1	Hydrogen	H	1.0079	12.00	0.735		8.25 ± 0.05	3.75
2	Helium	He	4.0026	$10.93 \pm 0.01^*$	0.248		—	—
3	Lithium	Li	6.941	1.05 ± 0.10	5.68(-11)	—	3.25 ± 0.06	-2.20
4	Beryllium	Be	9.0122	1.38 ± 0.09	1.57(-10)	—	1.38 ± 0.08	0.00
5	Boron	B	10.811	2.70 ± 0.20	3.96(-9)	—	2.75 ± 0.04	-0.05
6	Carbon	C	12.011	8.39 ± 0.05	2.15(-3)	126.76	7.40 ± 0.06	+0.99
7	Nitrogen	N	14.007	7.78 ± 0.06	6.15(-4)	36.28	6.25 ± 0.07	+1.53
8	Oxygen	O	15.999	8.66 ± 0.05	5.33(-3)	314.53	8.39 ± 0.02	+0.27
9	Fluorine	F	18.998	4.56 ± 0.30	5.03(-7)	0.03	4.43 ± 0.06	+0.13
10	Neon	Ne	20.180	7.84 ± 0.06	1.02(-3)	60.11	—	—
11	Sodium	Na	22.990	6.17 ± 0.04	2.48(-5)	1.46	6.27 ± 0.03	-0.10
12	Magnesium	Mg	24.305	7.53 ± 0.09	6.01(-4)	35.43	7.53 ± 0.03	0.00
13	Aluminium	Al	26.982	6.37 ± 0.06	4.61(-5)	2.72	6.43 ± 0.02	-0.06
14	Silicon	Si	28.086	7.51 ± 0.04	6.62(-4)	39.06	7.51 ± 0.02	0.00
15	Phosphorus	P	30.974	5.36 ± 0.04	5.17(-6)	0.31	5.40 ± 0.04	-0.04
16	Sulphur	S	32.066	7.14 ± 0.05	3.23(-4)	19.04	7.16 ± 0.04	-0.02
17	Chlorine	Cl	35.453	5.50 ± 0.30	8.17(-6)	0.48	5.23 ± 0.06	-0.03
18	Argon	Ar	39.948	6.18 ± 0.08	4.40(-5)	2.59	—	—
19	Potassium	K	39.098	5.08 ± 0.07	3.43(-6)	0.20	5.06 ± 0.05	+0.02
20	Calcium	Ca	40.078	6.31 ± 0.04	5.96(-5)	3.52	6.29 ± 0.03	+0.02
21	Scandium	Sc	44.956	3.05 ± 0.08	3.68(-8)	—	3.04 ± 0.04	+0.01
22	Titanium	Ti	47.88	4.90 ± 0.06	2.79(-6)	0.17	4.89 ± 0.03	+0.01
23	Vanadium	V	50.942	4.00 ± 0.02	3.71(-7)	0.02	3.97 ± 0.03	+0.03
24	Chromium	Cr	51.996	5.64 ± 0.10	1.59(-5)	0.94	5.63 ± 0.05	+0.01
25	Manganese	Mn	54.938	5.39 ± 0.03	9.83(-6)	0.58	5.47 ± 0.03	-0.08
26	Iron	Fe	55.847	7.45 ± 0.05	1.15(-3)	67.68	7.45 ± 0.03	0.00
27	Cobalt	Co	58.933	4.92 ± 0.08	3.57(-6)	0.21	4.86 ± 0.03	+0.04
28	Nickel	Ni	58.693	6.23 ± 0.04	7.27(-5)	4.29	6.19 ± 0.03	+0.04
29	Copper	Cu	63.546	4.21 ± 0.04	7.51(-7)	0.04	4.23 ± 0.06	-0.02
30	Zinc	Zn	65.39	4.60 ± 0.03	1.90(-6)	0.11	4.61 ± 0.04	-0.01
31	Gallium	Ga	69.723	2.88 ± 0.10	3.86(-8)	—	3.07 ± 0.06	-0.19
32	Germanium	Ge	72.61	3.58 ± 0.05	2.01(-7)	0.01	3.59 ± 0.05	-0.01
33	Arsenic	As	74.922	—	1.28(-8)	—	2.29 ± 0.05	—
34	Selenium	Se	78.96	—	1.48(-7)	0.01	3.33 ± 0.04	—
35	Bromine	Br	79.904	—	2.48(-8)	—	2.56 ± 0.09	—
36	Krypton	Kr	83.80	3.28 ± 0.08	1.16(-7)	0.01	—	—
37	Rubidium	Rb	85.468	2.60 ± 0.15	2.48(-8)	—	2.33 ± 0.06	+0.27
38	Strontium	Sr	87.62	2.92 ± 0.05	5.31(-8)	—	2.88 ± 0.04	+0.04
39	Yttrium	Y	88.906	2.21 ± 0.02	1.05(-8)	—	2.17 ± 0.04	+0.04
40	Zirconium	Zr	91.224	2.59 ± 0.04	2.59(-8)	—	2.57 ± 0.02	-0.02
56	Barium	Ba	137.33	2.17 ± 0.07	1.48(-8)	—	2.16 ± 0.03	+0.01
63	Europium	Eu	151.96	0.52 ± 0.06	3.66(-10)	—	0.49 ± 0.04	+0.03
90	Thorium	Th	232.04	—	2.08(-10)	—	0.06 ± 0.04	—
92	Uranium	U	238.03	<-0.47	5.49(-11)	—	-0.52 ± 0.04	—

Table 15.2: Elemental abundances as determined from the solar photosphere and meteorites given in number ratio relative to hydrogen: $A_{\text{em}} = \log N_{\text{el}}/N_{\text{H}} + 12$. * The helium abundance is the current value, and corresponds to $Y_s = 0.248$ (see also table 15.1). For the initial value, i.e. at the time of formation of the sun, $A_{\text{He}} = 10.99 \pm 0.02$, which corresponds to $Y_s = 0.275$ and $X_s = 0.708$. From: Asplund et al. 2005, ASP Conf. Ser. 336, 25.

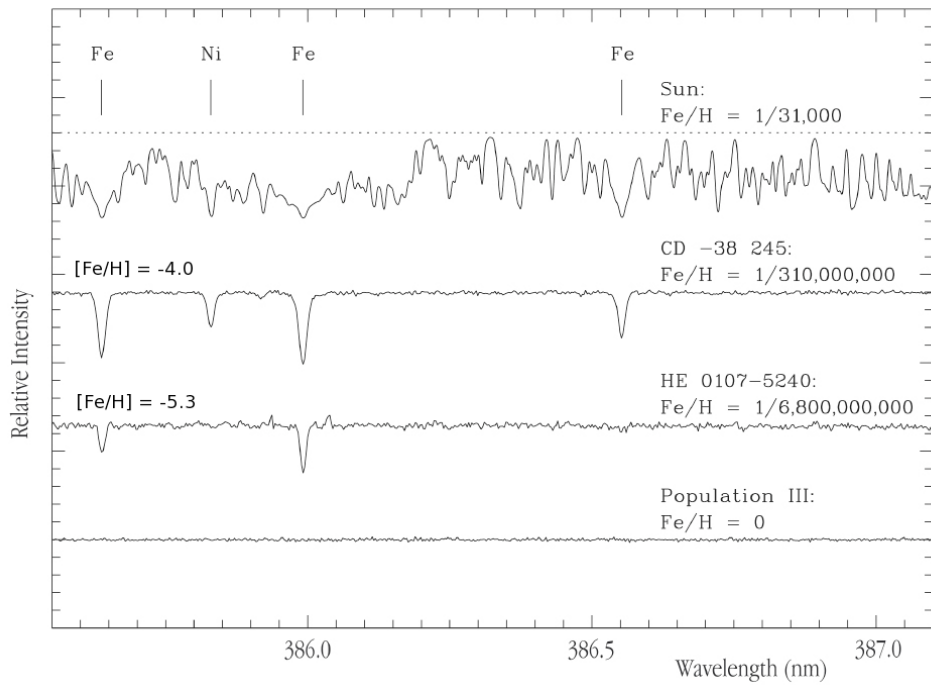


Figure 15.1: Optical spectra of the sun and the hyper metal poor stars CD -38 245 ($[Fe/H] = -4.0$) and HE 0107-5240 ($[Fe/H] = -5.3$). The latter object is so far the most metal poor star known. Clearly visible is that strength of metal lines decreases with decreasing metal abundance. In comparison to CD -38 245 the iron lines in the spectrum of HE 0107-5240 are weaker (or absent) and nitrogen is not visible at all. The bottom spectrum is for a hypothetical Population III star with a chemical abundance pattern as produced in the Big Bang, i.e. H, He and traces of Li.

–2. Population II halo dwarf stars have formed relatively early in the history of the Galaxy and are “extremely metal poor”, showing $[Fe/H] \sim -3$. Astronomers are vigorously searching for stars with even less metals because these must have formed in the very early history of the Milky Way. The abundance pattern of such hyper metal poor stars can tell us about the properties of the first generations of stars in our galaxy, that must have been responsible for the metals in these hyper metal poor objects. In addition it is very interesting to determine the masses of these hyper metal poor stars as theory predicts that the first stars to ever form in our universe (so called Population III stars) must have been very massive. The star that so far has the lowest iron abundance is HE 0107-5240, having $[Fe/H] = -5.3$ (see figure 15.1). Just as a side note, the mass of HE 0107-5240 is only $0.8 M_{\odot}$.

Although most of the matter of the solar system is concentrated in the sun, very useful information concerning the chemical composition of the initial solar nebula can be obtained from the study of other bodies of the solar system. A complicating factor in the study of such objects is that they may have suffered chemical fractionation, which is the sinking towards the center of relatively heavy elements at times when such bodies were partly or fully melted.

Objects that experienced chemical fractionation include the terrestrial planets and (the parent bodies of) meteorites. For this reason, earth is not suited for doing a representative abundance analysis. The most suited objects turn out to be meteorites of the type *CI carbonaceous chondrites*. These are formed early on in the formation of the solar system and appear to have preserved the bulk composition of the nebula from which they condensed, except for the highly volatile elements (H, C, N, O, and the rare gases) which partly escaped. Meteoritic chemical composition can be measured with such high accuracy that it is better known than the sun's photospheric abundance pattern (of which the abundance of some elements suffer from poorly known oscillator strengths). Meteoritic abundances are also given in table 15.2.

The abundance determination of helium warrants extra attention. In 1868, a new element was discovered in the solar coronal spectrum obtained during an eclipse. The name of the sun was given to this unknown element: helium. It was only discovered on earth in 1895. The reason why helium is not present in the photosphere is because in a medium with a typical temperature around 6000 K, no lines of helium (neutral or once-ionized) fall within the visual spectral range. Until recently the He abundance was derived from coronal observations. Now A_{He} is being determined from stellar structure calculations. This yields $N_{\text{He}}/N_{\text{H}} = 9.8 \pm 0.4\%$ for the initial composition of the sun and the proto-solar nebula. Inversion of helioseismic observations leads to a more accurate, albeit lower abundance $N_{\text{He}}/N_{\text{H}} = 8.5 \pm 0.07\%$. The latter number (corresponding to $A_{\text{He}} = 10.93$) is the present day solar abundance of helium in the outer convection zone. The difference between these two values is explained by slow element diffusion at the base of the convection zone during the solar lifetime.

Finally, the current solar abundance of lithium is about 160 times lower than is derived from meteoritic data. This is a direct consequence of the low nuclear binding energy of Li, causing the destruction of lithium at temperatures of only a few million kelvins by (in a thermonuclear sense: warm) proton collisions. The low A_{Li} implies that gas is transported between the surface and deeper, hotter layers. This probably occurs in convective motions, though possibly mixing through internal (differential) rotation may also play a role. Li- as well as Be-depletion is observed in F- and G-type stars. Also B can become depleted through thermonuclear burning in layers that are connected with the surface. The behavior of the boron depletion is, however, less well understood as its only potentially useful spectral line in the optical spectral range is in the violet (Be II $\lambda 3130$), where detectors are not very sensitive.

Structure of the atmosphere

The solar atmosphere can be divided in several zones (see figure 15.2). From inside out these are: (1) the photosphere, from which the visual spectrum originates and where the temperature decreases with height; (2) a zone around the temperature minimum at about 4 400 to 4 500 K; (3) an extended *chromosphere* in which the temperature is increasing up to values sufficiently high to cause (partial) hydrogen ionization; (4) a small *transition region* separating the chromosphere from the corona, with a very steep temperature gradient. This gradient is relatively large just above the chromosphere but flattens in higher regions; (5) a hot *corona* ($T > 10^6$ K) where hydrogen is fully ionized.

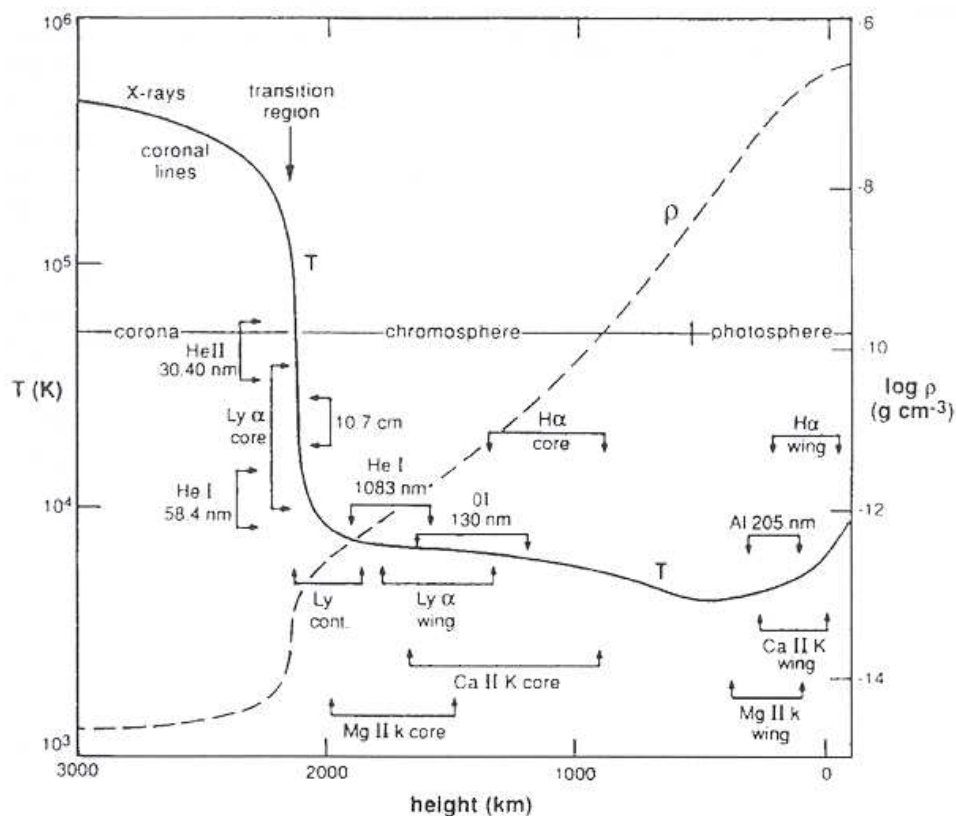


Figure 15.2: Temperature and density as a function of height for a model of the quiet sun. The zones from which several continua and important spectral lines originate are indicated.

Suppose, we secure the spectrum of a quiet spot on the solar surface. As the extinction is wavelength dependent, we can, by observing from X-ray through radio, probe different heights in the solar atmosphere. For a wavelength at which the extinction is small we probe radiation originating from a deep layer. Likewise, for a wavelength at which the extinction is large we see a layer that is higher up. At $1.6 \mu\text{m}$, i.e. the wavelength at which the H^- extinction has a local minimum (see § 8.3 and the upper panel of figure 8.4) we can see deepest into the sun. At the center of the solar disk the brightness temperature of this layer is 6 800 K. The disk averaged T_b at $1.6 \mu\text{m}$ is about 500 K lower due to limb darkening. At larger (infrared) wavelengths the extinction increases implying that the radiation that we observe originates from cooler layers. The brightness temperature reaches a minimum of about 4 500 K at $\lambda = 150 \mu\text{m}$. Beyond this wavelength the extinction still increases, but the observed T_b increases due to the increasing chromospheric temperature. At wavelengths shorter than $1.6 \mu\text{m}$ we see a decrease in the brightness temperature because of an increasing extinction. In the ultraviolet at about 1600\AA T_b reaches a minimum of 4 400 K. The extinction continues to increase for even shorter wavelengths, but the brightness temperature runs up due to the chromospheric

temperature increase.

Spectral lines also contain information on the temperature structure in the solar atmosphere as the extinction at line center is much larger than it is in the wings or in the continuum next the line. For instance, the strong Ca II resonance lines at $\lambda 3934$ (Fraunhofer's K line) and $\lambda 3968 \text{ \AA}$ (H line) have two small emission peaks at both sides of line center because of the temperature increase in the chromosphere (see figure 15.3). These peaks are observed to vary in strength as a function of time and spatial position on the solar disk and are sensitive to local velocity fields.

The temperature rise in the upper layers of the chromosphere and in the transition region between chromosphere and corona is the result of a competition between two effects: a mechanical heating and a strong cooling by resonance lines of hydrogen and helium. This competition results in a flattening of the temperature in the uppermost layers of the chromosphere at about 8 000 K, such that hydrogen is only partly ionized. In even higher, more rarefied layers hydrogen gets fully ionized (see eq. 6.26 and realize that n_e is decreasing further) and the line cooling mechanism becomes inefficient. Consequently, the temperature shows a steep rise. The amount of energy needed to let the temperature increase with distance is modest: only $\sim 10^{-4}$ of the total luminosity of the sun is needed to heat the chromosphere. The energy that is needed to heat the corona – which is even less dense – is extremely modest. It is an order of magnitude less than that needed for the chromosphere, and the largest part of it is transported back to the upper part of the transition region by means of thermal conduction, where it is radiated away by H en He resonance lines.

Heating of chromosphere and corona

What mechanism heats the chromosphere and corona? Though solar physicists have been investigating this seemingly simple question for several decades the answer is still poorly known. Concerning the chromospheric heating some consensus appears to have been reached: acoustic waves originating in turbulent convective layers below the photosphere could at least heat the lower regions of the chromosphere. When these waves propagate outward through the atmosphere, to regions of lower density, the pressure fluctuations grow and shock waves develop. These shocks can heat the gas locally. In the sun, however, the dissipation of these shock waves is so strong that they can not reach the upper regions of the chromosphere. In other stars, notably in M dwarfs, circumstances can be significantly better and acoustic waves may "survive" into the upper chromosphere. In M dwarfs acoustic waves (of the longest wavelengths) may even heat part of the lower coronal regions. Though our knowledge of coronal heating is still limited, it seems logical to expect that magnetic processes play a dominant role. A possible mechanism may be waves propagating outward along magnetic field lines.

Exercise 15.1

Determine the mass of the sun from Newton's gravitation law and the centrifugal force.
Use the Earth as a test particle and assume that the Earth orbit is circular and the Earth

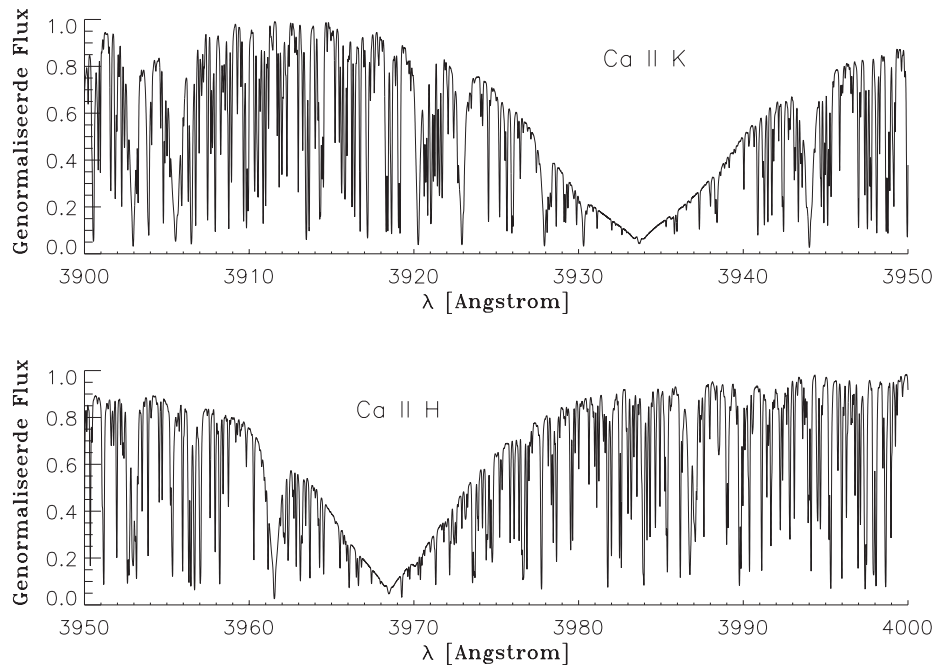


Figure 15.3: The Ca II K in the solar spectrum. This resonance transition, by Fraunhofer referred to as the “K” line, is the strongest line in the visual part of the solar spectrum. Many weak spectral lines are superposed on the broad wings of the line (so called blends); most are from neutral metals such as Fe I. In its line core the K line shows two minuscule peaks. The K line is just sufficiently strong for the line source function to feel the onset of the temperature rise towards the chromosphere before other effects start to dominate that cause a decoupling from the local Planck function.

mass to be negligible compared to the solar mass. The gravitational constant is $G = 6.67 \times 10^{-8}$ dyn cm 2 gr $^{-2}$.

Exercise 15.2

The ten most important elements in life on Earth are H, O, C, N, Ca, P, S, Na, K, and Cl (see *An introduction to Astrobiology*, Revised edition 2011, Cambridge University Press). Which percentage do these building blocks of life, save H, represent of the total of elements heavier than helium? Are stars ‘geared’ towards producing the elements necessary for life on Earth or are these elements only a byproduct of stellar nucleosynthesis?

Exercise 15.3

The Ca II K line, at $\lambda 3933$ Å, is the strongest line in the visual spectrum of the sun. At both sides of the line core, within one Angström from line centre, the K line shows two

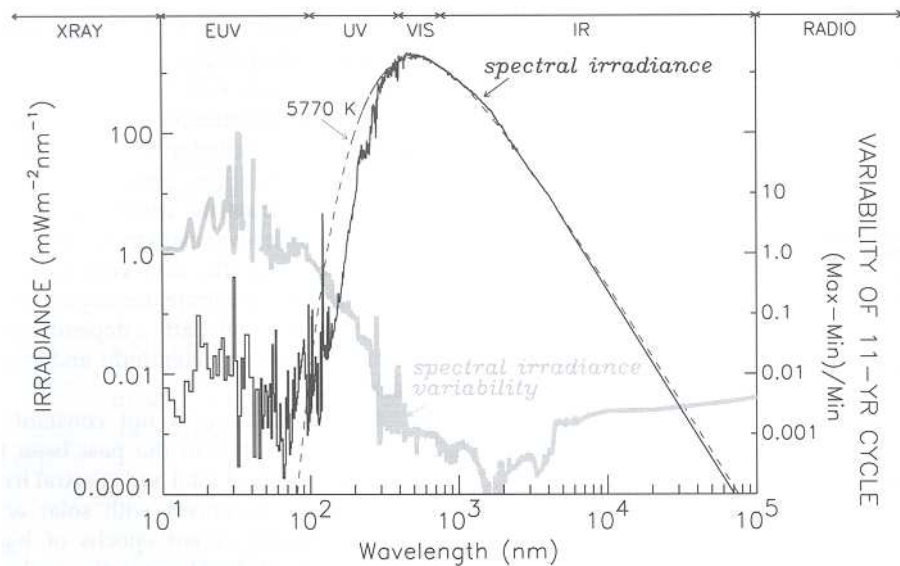


Figure 15.4: The spectrum of the solar irradiance as observed from above the earth atmosphere. The gray curve provides an estimate of the natural variation of the irradiance during a recent 11 year solar cycle. The variation in the total irradiance is at most 0.2 percent. At 1.6 μm (or 1600 nm) one can see deepest into the solar atmosphere; these layers are the most stable, hence fluctuations in R_ν are the smallest. The EUV emission ($\lambda < 912 \text{ \AA}$) is due to non-thermal processes in the chromosphere and corona; at these wavelengths the irradiance shows the largest variations.

minuscule peaks (see figure 15.3) that have been discussed extensively in the literature. Can you draw four panels as in figure 4.5 that explain these minuscule peaks? Assume that the profile shape of the K line has the standard “clock” shape.

15.3 Solar spectrum

Irradiance at the top of the earth atmosphere

The mean total solar irradiance $\mathcal{R} = (1.365 \pm 0.002) 10^6 \text{ erg cm}^{-2} \text{ sec}^{-1}$ or $1365 \pm 2 \text{ W m}^{-2}$. This number used to be called the solar constant, however, as we now know that \mathcal{R} is not constant the term *total irradiance* is preferred. The mean spectral energy distribution of this light, i.e. the *irradiance* (see § 3.4), is shown in figure 15.4.

For different reasons the total and spectral irradiance fluctuate. Obviously there is a variation as a result of the elliptical path of the earth around the sun causing the distance earth-sun to vary between 1.0167 and 0.9833 AU. This effect, causing a 3% fluctuation on \mathcal{R} , is not intrinsic but geometric in nature and officially is not included in the variation of \mathcal{R} or \mathcal{R}_ν .

Precise measurements of the (total) irradiance show that fluctuations occur that reach 0.2% on timescales of days to weeks, mainly due to changes in the number of dark spots and bright faculae on the part of the solar surface that we observe. These variations of 0.2% are recorded in visual and near-infrared light, i.e. at the wavelengths where the sun emits most of its energy; for *x-ray* and radio emission such short period variations can lead to fluctuations exceeding a factor of two. During recent epochs of relatively high solar activity, near maxima in the 11 year solar cycle, the mean level of the total irradiance was about 0.1 to 0.15% higher than during cycle minima. A comparison of these relatively recent data to historical observations of the sun (for instance of sunspots), geomagnetic activity and cosmogenic isotopes (e.g. from ^{13}Be in ice-cores and ^{14}C in growth rings of trees) shows that the total irradiance has increased by a few tenth of a percent (between 0.2 and 0.5%, depending on the method used) relative to an epoch of anomalously low solar activity in the seventeenth century, named the *Maunder minimum*. This epoch of exceptional low solar activity is possibly the most recent one in a series of comparable periods the sun has experienced in previous millennia. The Maunder minimum caused a noticeable change in the earth climate. For a thorough understanding of anthropogenic (originating in human activity) effects on our climate it is essential to correct for this type of natural variation.

Irradiance at the earth surface

Figure 15.5 compares the irradiance at the top of the atmosphere (light grey / yellow) and that of direct sunlight at sea level (dark grey / red). The spectrum at sea level is significantly attenuated by absorption by the constituents of the earth atmosphere, primarily molecular bands due to water, oxygen and ozone. Water vapor in the atmosphere absorbs much of the radiation past $1\ \mu\text{m}$ via molecular transitions in H_2O . However, water also allows a considerable amount of solar radiation to be transmitted through the atmosphere in certain ‘windows’ where it has inefficient absorption. Compare these windows to Fig. 2.10, showing the transmission of the earth atmosphere at the summit of Mount Mauna Kea, Hawaii, and identify the location of the *J*, *H* and *K* bands.

Another interesting feature is the difference in radiation above and below the atmosphere on the UV-blue side, where the Wien part of the spectrum starts. This is a combination of the *ozone effect*, as O_3 prevents the life-threatening UV radiation from reaching the surface of our planet, and Rayleigh scattering (see section 8.4). Figure 15.5 also shows a fit to the peak of the solar spectrum at the earth surface. Notice that the temperature of this fit (5 523 K) is lower than 5 770 K.

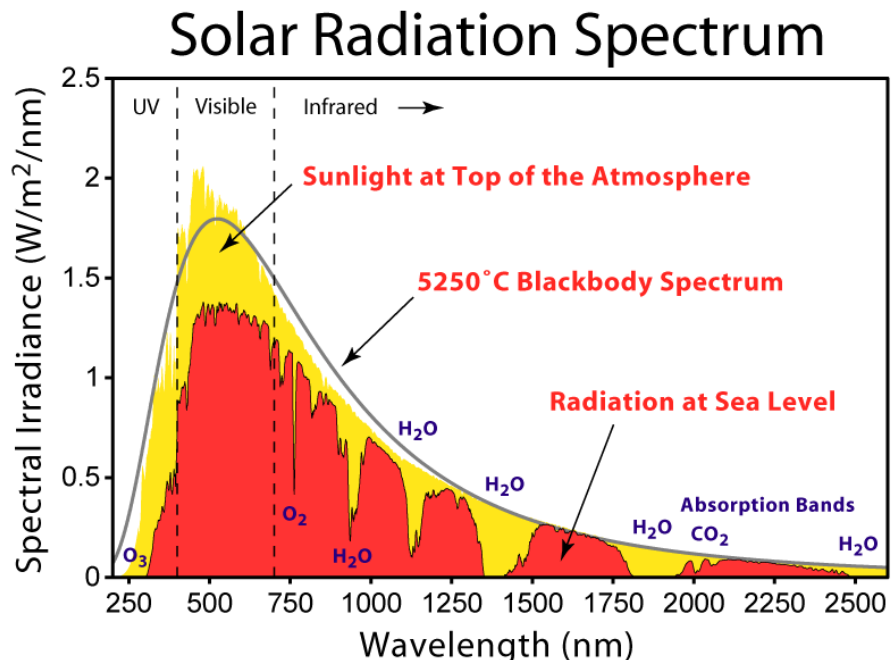


Figure 15.5: Sunlight as received at the top of the Earth atmosphere and at sea level after attenuation by atmospheric constituents, primarily ozone, oxygen, water and carbon dioxide. The radiation measured at sea level is that of direct sunlight (so not that of diffuse sunlight). Figure from Robert A. Rhode, http://globalwarmingart.com/wiki/Image:Solar_Spectrum.png.

Active regions

At almost every moment the part of the solar surface that can be observed from earth shows a number of *active regions*. Near the minimum of the 11 year solar cycle there are only very few, sometimes even none; in the solar maximum there can be as much as five to ten. The structure of these active regions is extremely complex, and we suffice by providing only a general description. Active regions form when the top part of loops of magnetic flux in the solar interior reach into and above the solar atmosphere, where they (thus) can be observed. The shape of such a loop is somewhat similar to the Greek letter Ω . It is thought that the magnetic loops are generated by the solar dynamo, deep in the solar interior.

The shape and appearance of an active region depends sensitively on the observed wavelength and the angle at which it is seen. To give an example: in an active regions near the solar rim, seen against the dark sky background, the loop shaped structure of the magnetic fields can be seen clearly in x-ray line emission of highly ionized gas streaming along the field lines. These loops of intensely heated gas are referred to as *coronal arcs* or *coronal loops* (see figure 15.6). High resolution x-ray imaging of active regions near the center of the solar disk show a fine-structured pattern of magnetic strings connecting the point where the beam of magnetic flux

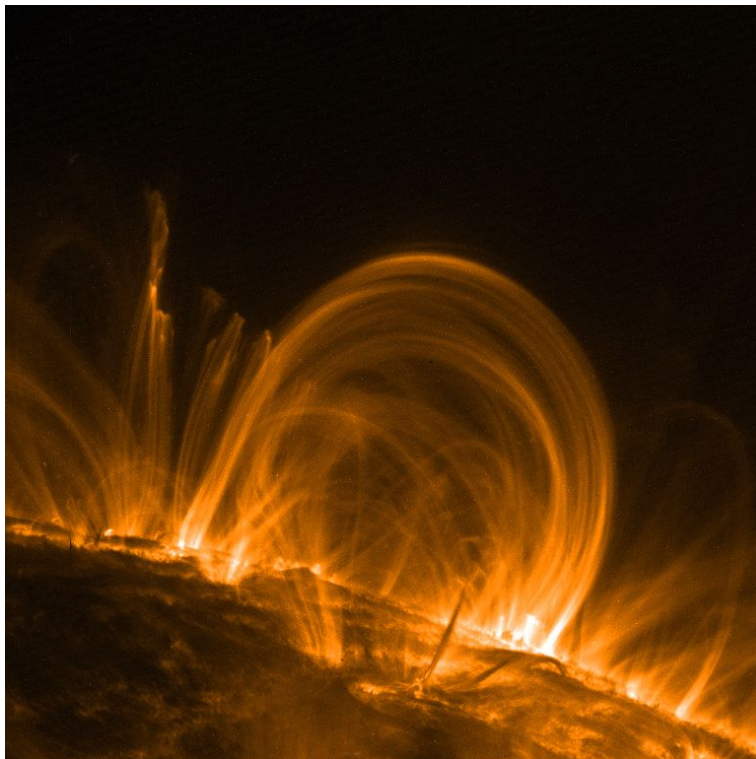


Figure 15.6: An active region at the edge of the solar disk, observed in a spectral line of highly ionized iron. The temperature of the emitting gas is about 1.5 MK. Foto © NASA TRACE satellite.

breaks through the photosphere and chromosphere (the north pole) to the point where the field again enters the sun (the south pole). These points are called the *footpoints* and each active region consists of a collection of such bi-polar footpoints, connected by coronal loops. The high density of magnetic field lines in footpoints is what sets active regions apart from quiet regions on the solar surface. The effect of these field lines on the (local) temperature and density structure depends on *a*) the strength of the magnetic field, *b*) the fraction of magnetized relative to unmagnetized gas in the footpoints, and *c*) the topology of the area, i.e. the way in which each point (inside a footpoint) is connected to another point. Regions in which the magnetic field has a 10 to 100 times larger density compared to the surrounding quiescent regions are referred to as *plage* (see figure 15.7). In H α we see the chromospheric emission from this plage (at temperatures of about 10 000 K) as bright regions, provided that one does not observe it at a too high spatial resolution, as in that case individual chromospheric arcs can be seen. In *sunspots* the field lines are so closely packed that there are (almost) no unmagnetized regions left. This inhibits energy transport through convection, explaining why sunspots appear cooler and darker than their surroundings. Figure 15.7 also shows irregular dark strings or *filaments*. These filaments mark regions of opposite polarity on the solar surface. At a considerable height (in the corona) the field lines will arc over these filaments, creating a sort of tunnel. In this tunnel, along the dividing line of magnetic polarity, referred to

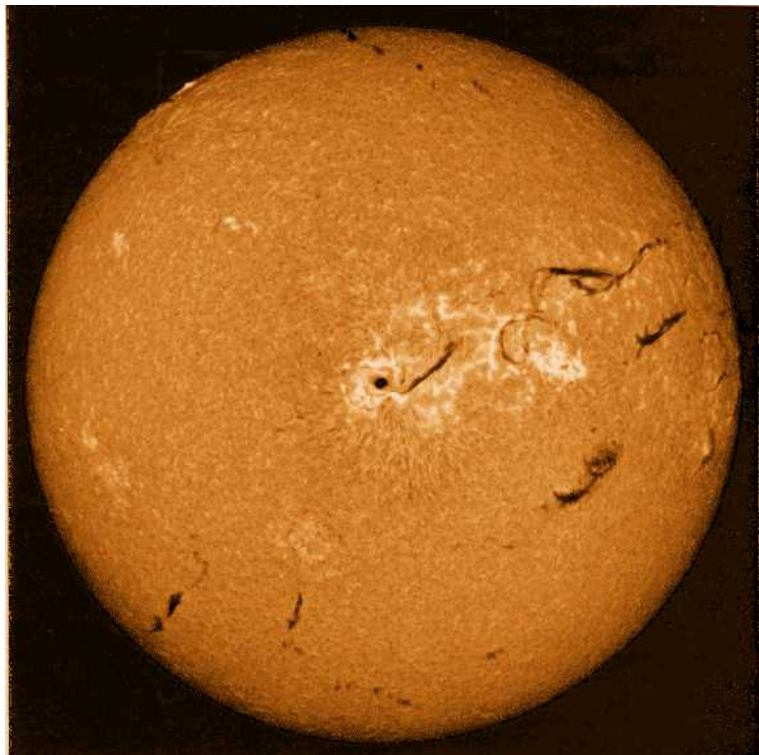


Figure 15.7: An image of the solar disk in $H\alpha$, identifying gas at a temperature of about 10 000 K. An extended active region is visible somewhat to the right of the center of the disk, with sunspots, plage, and filaments. Photograph © the National Solar Observatory.

as the *filament channel*, magnetic field lines cross the channel allowing clouds of ionized gas to be captured above the photosphere. These clouds emit in continuum light, but not in $H\alpha$ or Ca II. Filaments that are seen in profile at the edge of the solar disk are called *prominences*. Prominences are somewhat similar to coronal loops, but do not show a clear arc structure (they are clouds).

Active regions come and go, with a characteristic lifetime that depends on their size. There is no preferential size for an active region, but they do show a continuous distribution in their sizes. The smallest can barely be resolved with a telescope (and probably this implies that smaller regions exist that we can not detect with the current arsenal of instruments); the largest ones occupy 1–2 % (or 50 000 to 100 000 Mkm^2) of the total solar surface. It is typically these large regions where sunspots and solar flares are seen. The lifetime of the large regions is roughly two months, i.e. one to two rotation periods. The smaller regions have shorter lifetimes.

Solar flares and coronal mass ejections

Like most dynamic phenomena on the sun, the occurrence of solar flares is closely related to the presence and evolution of solar magnetic fields. As a simple introduction (which is all we will do here), we compare flares with earthquakes. The occurrence of earthquakes involves two steps: energy build-up and energy release. The stress and energy are build up by relative motions of two tectonic plates along fault lines. When the stress reaches a critical point, two plates cannot slide further, the equilibrium brakes down and a section of the fault line is restored to its original position of minimum energy. The excess energy is released in the form of kinetic energy and is propagated away from the epicenter as seismic waves.

A flare can be described by a very similar scenario. We start with two magnetic regions of opposite polarities, such as for instance is marked by filament structure. The line dividing two polarities is called the neutral line. In the starting- or *potential configuration* the field lines run perpendicular to the magnetic neutral line. If, for some reason, magnetic regions slide, the field lines will start to move away from perpendicular to the neutral line. This is called the sheared configuration. In an extremely sheared configuration, the magnetic field lines are nearly parallel to the neutral line. A sheared magnetic field has more magnetic energy than the corresponding potential field configuration and the extra energy is called the *free magnetic energy*. When the fields are extremely sheared, an instability may occur. Fields tend to be restored to the potential configuration and the extra energy is released by the process of *magnetic reconnection*. The free magnetic energy is converted to thermal and non-thermal energy. This causes a solar flare, in which thermal radiation is emitted and non-thermal particle are accelerated.

Solar flares are wonderfully complex phenomena and are observed across the electromagnetic spectrum as well as via energetic particles in space. They are classified according to their size, duration, morphology or magnetic topology and the composition of their associated energetic particles. Despite the seemingly infinite variety in solar flare characteristics, one may identify two basic types – impulsive and gradual. *Impulsive flares* have time scales of the order of a few minutes or less while gradual flare durations range from tens of minutes to several hours. These two basic types are combined in fully developed flares in which an impulsive phase is followed by a gradual main phase. Long-duration gradual flares are also characterized by *coronal mass ejections*.

A coronal mass ejection can carry 10^{15} to 10^{16} gram of plasma into space. The source region within the sun's atmosphere can be hundreds of thousands of km across and the resulting ejection can expand into space at many hundreds of km sec^{-1} . The rate of coronal mass ejections varies with the solar cycle; one may expect of the order of 0.1 event per day during solar minimum, upto more than one a day during maximum. They represent a very significant disturbance of the solar wind. Given their size and mass, combined with the fact that the expanding clouds carry a frozen-in magnetic field, such events can engulf the Earth system and their arrival at the Earth can generate significant geomagnetic storms.

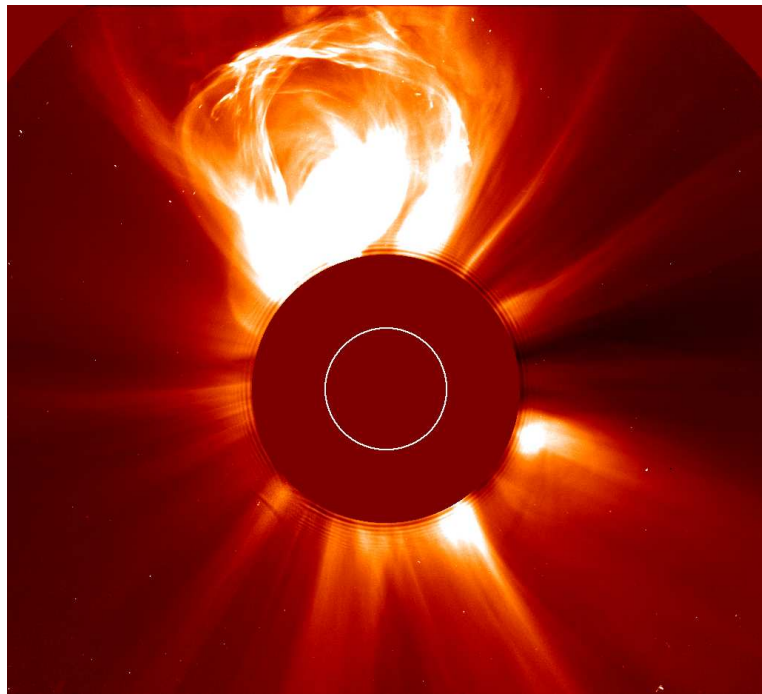


Figure 15.8: *Coronal mass ejection observed by the SOlar and Heliosphere Observatory (SOHO) on March 9 2004. Direct sun light is blocked; the position of the solar disk is given by the half circle. Foto © SOHO satellite.*

Solar cycle and sunspot cycle

Important properties of active regions vary with the 22 year *solar cycle* or the 11-year *sunspot cycle*. Only few active regions, together with the sunspots they contain, are visible during the solar minimum – sometimes (for a few weeks) none are seen at all. During a sunspot maximum typically five and sometimes \sim ten active regions are seen from earth and the mean level of the irradiance is found to be about 0.1 to 0.15% higher than during cycle minima.

At the start of a sunspot cycle spots appear at about 30° (sometimes even 40°) north and south of the equator. The sunspots slowly migrate towards the equator. During maxima, about 4 to 5 years later, spots appear in a strip with an average latitude of about 15° . Near the end of the cycle, close to minimum, the strip has narrowed and is centered around 8° and new sunspots start to appear at $\sim 30^\circ$. In every bi-polar pair of sunspots the one that is in front – in the sense of the rotation direction of the sun – is called the *leader*, and its trailing companion the *follower*. During an entire cycle, from minimum to mimimum, all leaders on the northern hemisphere have equal polarity (say +) as do all leaders on the southern hemisphere, though the polarity of these southern leaders will be opposite to that of the leaders on the northern hemisphere (in this case -). At the end of each cycle the pattern of polarity is reversed (so + to - on the northern hemisphere and - to + on the southern hemisphere). A complete

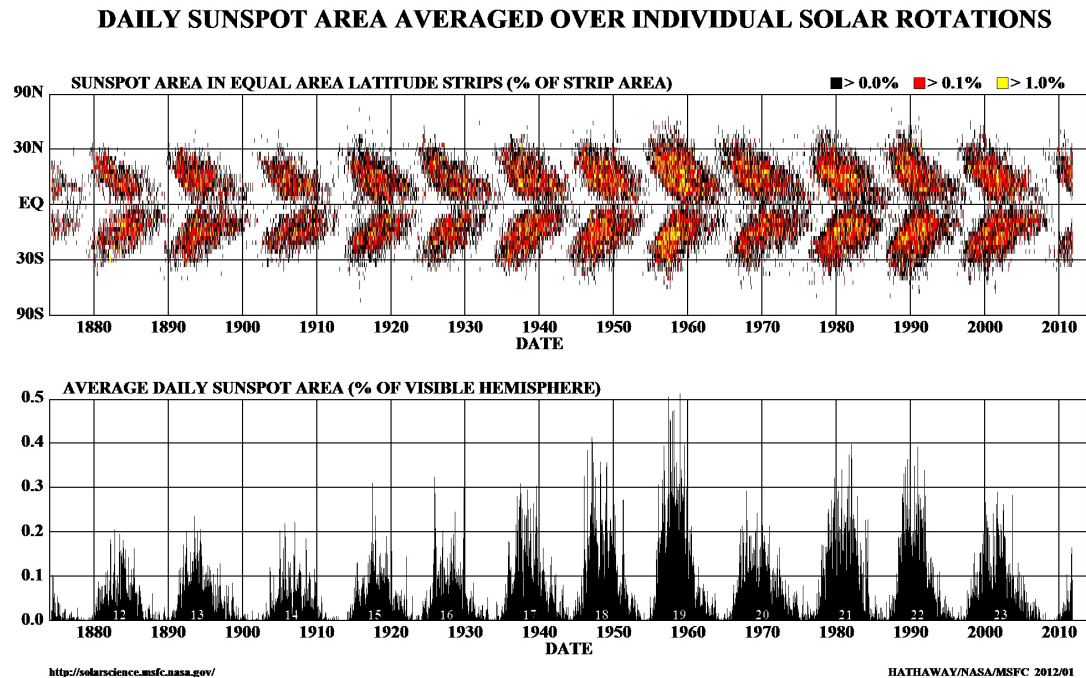


Figure 15.9: Top: the latitude of sunspots as a function of time. At the start of the 11 year cycle sunspot appear at the circles of latitude at $+30^\circ$ and -30° distance from the equator. At maximum solar activity, about 4 to 5 years later, sunspots also emerge at the equator. After 11 years the last sunspots of the cycle form near the equator while new ones again appear at 30° , starting a new cycle. The distribution of spots appears symmetrical around the equator and is known as the butterfly diagram. Bottom: the average percentage of the visible solar surface that is covered by sunspots as a function of time. Notice that the current cycle (cycle 24) appears not to develop itself as prominently as previous cycles. Source: NASA, NSSTC, Hataway.

magnetic cycle thus consists of two solar cycles of 11 years, and lasts 22 years.

The sunspot cycle is part of a larger wider-ranging cycle in which all aspects of the solar activity, including sunspots, plages, prominences, solar flares and coronal mass ejections, as well as the shape, size and structure of the chromosphere and corona, show a cyclic variability with a period of 11 years. The number and the dimensions and energies of prominences, flares and coronal mass ejections reflect the increase and decrease of the number of sunspots, the corona being brighter, more extended and more symmetric during minimum activity.

Solar wind

The solar wind is a continuous, about spherical outward flow of charged particles from the sun into interplanetary space. The outflow “blows” past the planets at speeds that fluctuate between 200 and 900 km sec $^{-1}$, and cause the sun to lose about $2 \times 10^{-14} M_\odot$ of mass per

year. At a distance of 1 AU from the sun, the mean density of the solar wind is about 5 particles per cm^3 and its temperature is about 10^5 K. Close to the plane of the ecliptic, the average wind speed is about 400 km sec^{-1} . The particles that comprise this relatively slow wind emerge predominantly from streamer-like structures in the solar corona that tend to be located relatively close to the solar equator. A relatively fast wind, with a mean speed of about 750 km sec^{-1} , flows out of coronal holes that are centered permanently on the solar poles. When coronal holes (temporarily) extend down to, or across, the solar equator, high-speed streams flow out past the Earth and planets (such that the wind speed shows a period modulation with the solar rotation period). This explains the fluctuation in the solar wind speed.

The solar wind carries with it lines of magnetic force, which spread out to form the weak interplanetary field. The sun's rotation, combined with the radial outward flow of the solar wind, caused the interplanetary field lines to take up a spiral form. The solar wind outflow is eventually stopped when the pressure of the solar wind equals that of the interplanetary medium. This boundary is at about 100 AU and is referred to as the *heliopause*; the enclosed region is the *heliosphere*. The radius of the heliosphere is expected to vary with the solar cycle.

Stellar winds

A stellar wind is a continuous outflow of matter from a star. This outflow plays an important role in the life cycle of gas and dust in the interstellar medium and in the evolution of stars.

After a short introduction we discuss the most characteristic signature of mass loss in a stellar wind, i.e. the P Cygni profile. From these profile one can easily determine the terminal velocity of the stellar wind. Next, we focus on several methods to determine the rate of mass loss from stellar winds from spectroscopic and/or photometric observations. For hot stars there are three such approaches that use, respectively: *i*) non saturated P Cygni profiles *ii*) emission lines, and *iii*) infrared and radio excess.

The most sensitive diagnostics of stellar winds are the P Cygni profiles of resonance lines in the ultraviolet part of the spectrum. Saturated profiles of these lines only yield lower limits to \dot{M} . Intrinsically strong resonance lines of stars with mass loss can already display a P Cygni shape if $\dot{M} \sim 10^{-9} M_{\odot}\text{yr}^{-1}$. If the line is not saturated one can derive the number density of absorbing particles n_{ijk} as a function of distance from a comparison of the observed profile with model predictions, and by that the mass loss rate. For resonance lines it holds that $n_{0jk} \simeq N_{jk}$. To accurately derive the mass loss it is therefore necessary that the ionisation properties $q_{jk}(r)$ are known. Sometimes, if it is safe to assume that the relevant ion is dominant throughout the entire wind, i.e. $q_{jk}(r) \simeq 1$, the required computations are relatively simple and a reliable mass loss is found. In most cases the ion responsible for the P Cygni profile being studied is not the dominant ion. Sometimes it is even far from it. In that case there is no other option than to do a proper computation of the state of the gas in the stellar wind. These computations are extremely complex as both NLTE effects, stellar wind, non-thermal radiation as a result of instabilities in the stellar wind (read: shocks), and the line blanketing effect need to be included in a self-consistent way. This is such a complicated and extensive problem that it is at (or even beyond) what we are currently capable of. The uncertainties in the wind ionisation therefore make the P Cygni method a relatively unreliable one.

The emission line method for mass loss determinations usually employs the wind emission in the H α profile (though for very hot stars also He II $\lambda 4686$ may be a useful diagnostic) and yields reasonably reliable results. The most reliable way to derive \dot{M} is that based on radio flux measurements. In §§ 16.3 and 16.4 we will discuss the principles of these latter two methods.

For completeness, in the case of cool stars the diagnostics of mass loss and terminal velocity are: *iv)* molecular emission lines, and *v)* infrared and (sub-)millimeter continuum radiation by dust that condenses in the stellar wind outflow. These methods will not be discussed in these lecture notes.

16.1 Historical introduction

The P Cygni profiles that are so characteristic for stars with a stellar wind were, you never guess, first seen in the star P Cygni. This star – to provide a nice trivia – was discovered as a “new star” in the summer of 1600 by the Dutch chartographer Blaeu. The discovery of the characteristic profiles and insight in their meaning followed only much later.

Beals (1929) noticed that both the spectra of Wolf-Rayet stars (see § 2.2) and of novae showed P Cygni profiles. Photographic plates of novae, first that of Nova Aurigae in 1891, showed that these events were associated with the formation of shells of gas centered around the star that experienced the outburst. Continued observations of these shells, over periods of years, showed that the diameters of the shells increased, associating P Cygni profiles with the outward expansion of gaseous envelopes. An important difference between Wolf-Rayet stars and novae was that the P Cygni profiles in the WR-stars do not change over time. This led Beals to propose that a continuous outflow occurs from Wolf-Rayet stars. This was confirmed by Chandrasekhar (1934), who developed a solid footing for interpreting P Cygni profiles as arising in expanding atmospheres (see § 16.2). Korisev (1934) used the diagnostics developed by Chandrasekhar to estimate the mass loss and maximum outflow velocity of a Wolf-Rayet star and found, respectively, $\sim 10^{-5} M_{\odot}\text{yr}^{-1}$ and $\sim 1000 \text{ km sec}^{-1}$.

In the case of cool stars, it was more difficult to find evidence for mass loss. The crucial evidence was presented by Deutsch (1956), who showed that the M5 giant in the binary system α Hercules loses mass at a rate of $\sim 10^{-7} M_{\odot}\text{yr}^{-1}$ and at a maximum flow speed that reached $\sim 10 \text{ km sec}^{-1}$. Deutsch noticed that the spectrum of the accompanying G5 star contained a set of shifted lines that are also present in that of the M star. He realized that the orbit of the G-dwarf is embedded in the expanding envelope of the M giant, making the G-dwarf serves a “probe” of the velocity and density in the remoter parts the M giant outflow. As the measured velocity in these remote parts of the M giant atmosphere was in excess of the local escape speed he concluded that the gas would escape from the M giant.

In addition to spectroscopic evidence, Wilson (1960) realized from stellar structure considerations that stellar mass loss must occur. For stars with initial masses in excess of the Chandrasekhar limit of $1.4 M_{\odot}$, it was necessary that mass was lost in order for these objects to evolve to the white dwarf phase.

Research into the properties and nature of stellar winds expanded dramatically in the 1960s. In 1962 the existence of a solar wind was observationally confirmed by the *Mariner 2* inter-

planetary probe. In 1967, Morton, using a balloon experiment, secured UV spectra of several O and B supergiant. These showed P Cygni profiles, a telltale signature of stellar winds. Since that time many observations, ground based as well as from rockets, balloons and satellites, have conclusively shown that stellar winds occur in many different types of stars. The evidence is found in almost all wavelength domains, from X-ray to extreme-UV, UV, optical, infrared, sub-millimeter to the radio regime. Space observatories that have contributed very significantly to these studies include the *Copernicus* satellite, the *International Ultraviolet Explorer* (IUE), the *Einstein* röntgen observatory, the Dutch-American *Infrared Astronomy Satellite* (IRAS), *Extreme Ultraviolet Explorer* (EUVE), *Hubble Space Telescope* (HST), and the partly Dutch *Infrared Space Observatory* (ISO).

16.2 P Cygni profiles

In general one can easily distinguish spectral lines that are formed in a stellar wind from those that originate in the photosphere. The wind lines have a much larger width, a result of the acceleration of the outflowing gas, compared to the photospheric lines that are formed in the (more or less) hydrostatic parts of the atmosphere and which are only affected by thermal and turbulent broadening. The wind lines have either absorption or emission profiles, or a combination of these two: the so called P Cygni profile.

P Cygni profiles usually occur if the line forms through the process of *resonance scattering*. This occurs if the transition is between the groundlevel (or a meta-stable level) and an excited level. Often, the upper level is the first level excited level, however this is not strictly required. In a scattering the extinction of a photon in a photo excitation is followed by the spontaneous emission of a photon of (virtually) equal frequency. The photon is therefore not lost, but has only changed direction. Examples of resonance lines are N V $\lambda\lambda 1239, 1243$, C IV $\lambda\lambda 1548, 1551$, and Si IV $\lambda\lambda 1394, 1403$ in the spectra of O and early B-type stars; C II $\lambda\lambda 1335, 1336$ in late B- and A-type stars, and Mg II $\lambda\lambda 2796, 2803$ in late B- to M-type stars. Notice that these are all lines of relatively abundant elements.

Schematic explanation of the formation of a P Cygni profile

Figure 16.1 provides a schematic representation of the formation of a P Cygni profile. We assume a spherically symmetric outflow in which the velocity of the gas increases monotonically, reaching a *maximum outflow velocity* or *terminal velocity* v_∞ . A distant observer can identify four regions that each contribute in a specific way to the line profile.

- a) The photosphere of the star, emitting the continuum “on top of which” the line is formed. In almost all cases the photosphere is formed in a layer that has an outflow velocity that is very low compared to the local thermal Doppler velocity, i.e. $v \ll \xi_D$.

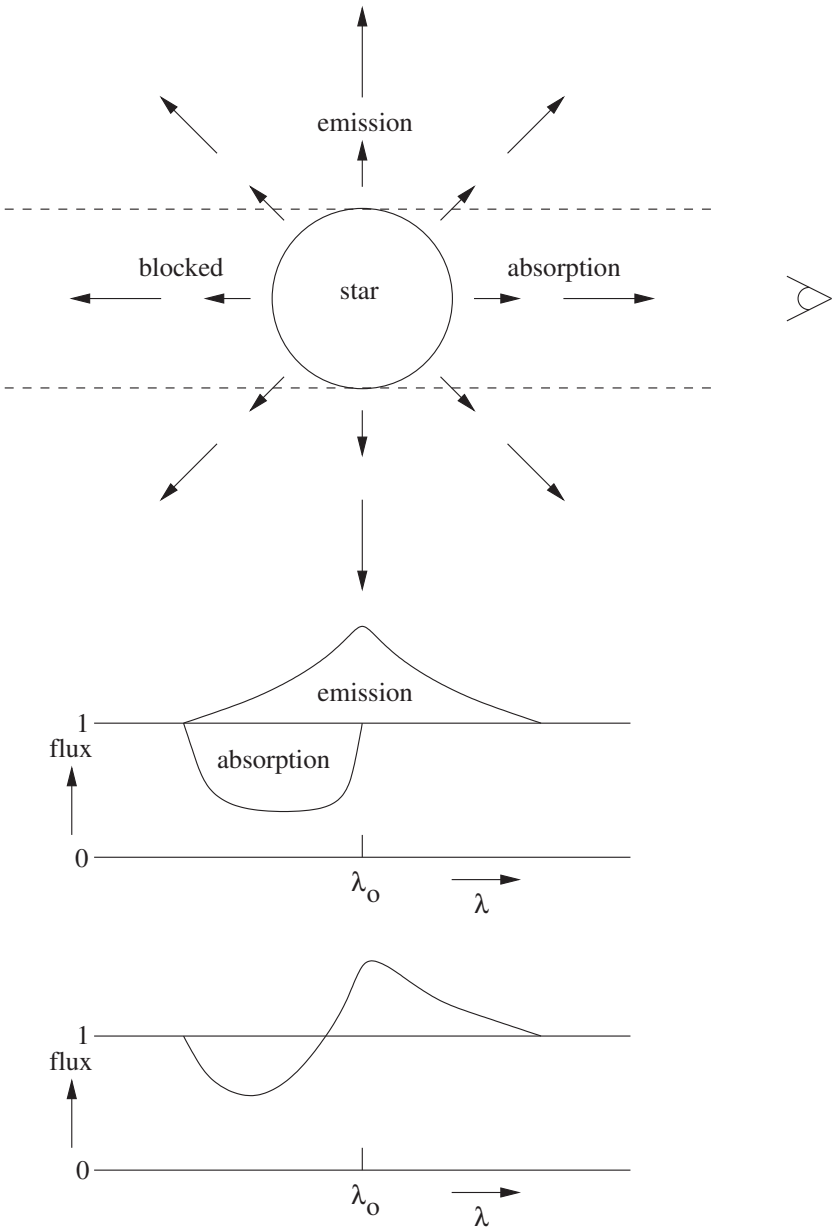


Figure 16.1: Schematic representation of the formation of a P Cygni profile. The observer can identify four regions: a) the photosphere of the star, from where the continuum originates; b) the ‘tube’ in front of the stellar disk, where blue shifted absorption occurs; c) the ‘tube’ behind the stellar disk, which can not be observed, and d) the halo surrounding the stellar disk from which the symmetrical emission profile originates. In a fully developed P Cygni line the contributions from the regions b and d dominate the profile. In first order, the P Cygni profile is the sum of a, b, and d.

Therefore, a “normal” absorption profile will form at the rest wavelength λ_{lu} of the line. This absorption profile may not be visible as such because the more outward stellar wind may “deform” the profile.

- b) A tube like or cylindrical region in front of the stellar disk, where gas is moving in the direction of the observer with velocities that range between $v \simeq 0$ and the maximum outflow velocity $+v_\infty$. In this tube, continuum photons at the blue side of λ_{lu} , i.e. photons with shorter wavelength, will be scattered out of the line of sight towards the observer. If $v_\infty \gg \xi_D$ a broad blueshifted absorption profile will form.
- c) A tube like or cylindrical region behind the stellar disk, where gas is moving away from the observer. As the stellar disk is occulting this tube, radiation emitted in this region can not be observed. It implies that, at least in principle, the maximum redshift of line photons, i.e. those corresponding to the velocity $v = -v_\infty$, can never be seen. In practice, however, this effect is so small that it can not be identified.
- d) The region next to the stellar disk that the observer would see as a halo surrounding the stellar disk if one would be able to spatially resolve the wind outflow. The gas in this halo can have both positive (i.e. blue shifted) as well as negative (i.e. red shifted) velocities relative to the observer and causes a symmetric emission profile with Doppler-shifted velocities between $-v_\infty$ and $+v_\infty$.

In shaping the observed profile the contributions of regions *b* and *d* are dominant, *proviso* the stellar wind is not very weak (in which case *a* will dominate). The net effect of all four contributions – which in a simplistic way of thinking one might view as the sum of four independent profiles – yields the P Cygni profile (see figure 16.1).

The determination of the terminal flow velocity

The maximum outflow velocity can easily be determined from P Cygni profiles that have a strongly saturated blue shifted absorption. To give an example of such saturated P Cygni profiles we show in figure 16.2 a number of UV resonance lines of the O4 If star ζ Puppis. This star at a distance of 450 parsec is the closest early-O supergiant.

If we neglect the thermal velocity ξ_D (see eq. 12.18), gas that is approaching us with the terminal velocity will cause the most blue shifted absorption in the line profile. The wavelength of this maximum Doppler shift is, using eq. (12.15)

$$\lambda_{\text{edge}} = \lambda_{lu} (1 - v_\infty/c) \quad (16.1)$$

If the line is so strong that even at (read: very close to) the terminal velocity all stellar light is extinguished there will be no flux at the long wavelength side of λ_{edge} , i.e. the line is saturated, while suddenly at the short wavelength side the stellar continuum will be visible again. By simply measuring the wavelength at this abrupt transfer from no flux to the full continuum flux, the terminal velocity is found using eq. (16.1).

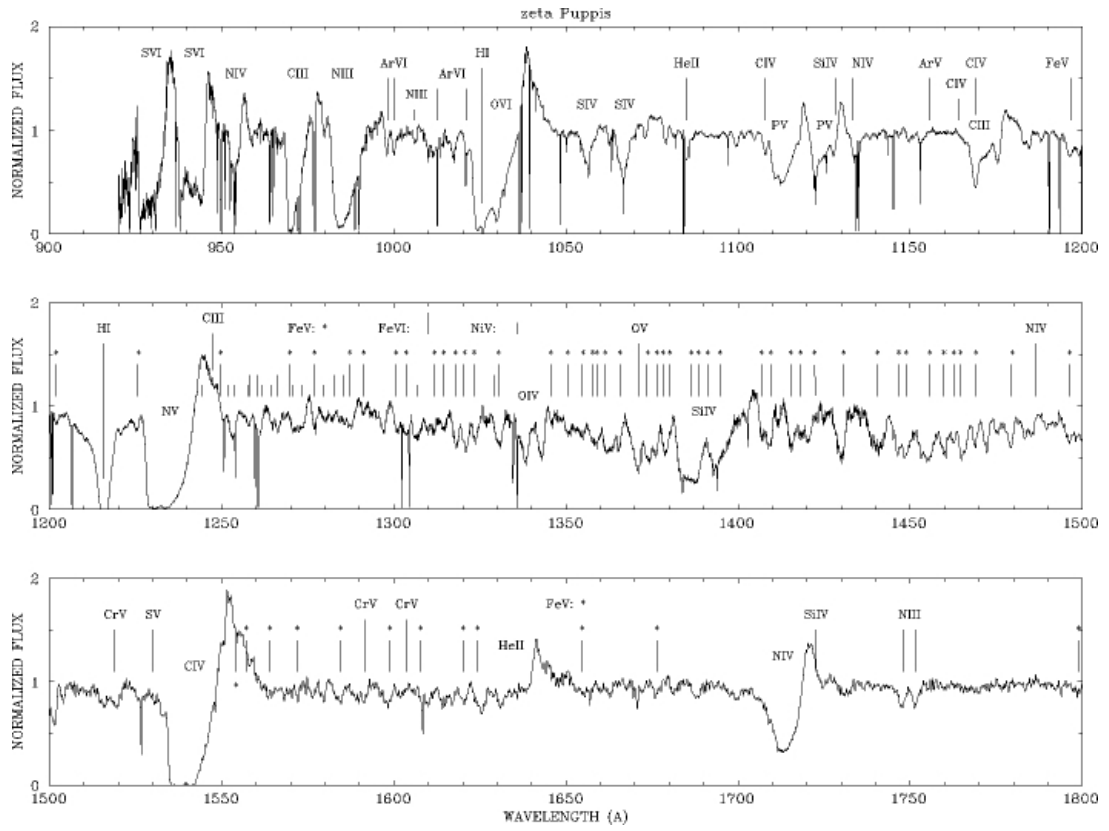


Figure 16.2: *Merged spectrum of Copernicus and IUE ultraviolet high-resolution observations of the O4(f) supergiant ζ -Puppis. The most important wind lines of the light elements are identified and marked. Also marked are the large number of lines from iron group elements (e.g. Fe V) which are especially present between 1250 and 1500 Å. Most of these iron-group lines are formed in the photosphere and in lower part of the outflow. The resonance PCygni profiles of O VI, N V and C IV are saturated and can be used to measure the terminal velocity.* Figure from Pauldrach et al. 1994, Space Science Reviews 66, 105.

Though the above is a trivial procedure, there are a number of effects that can complicate the determination of v_∞ . These are: *a)* The P-Cygni profile is not saturated. In this case the bluest wavelength showing line extinction no longer corresponds to that of the terminal velocity, and only a lower limit for v_∞ can be measured; *b)* The ionisation of the ion responsible for the P Cygni profile may at some point in the outflow suddenly decrease. If this happens, the same scenario as in case *a* applies, i.e. one measures a lower limit for the terminal velocity; *c)* The stellar wind is turbulent. Both observations and theory point to the presence of strong turbulent motions in stellar winds. At the radial distance where $v \sim v_\infty$ these motions can reach an amplitude $\xi_{\text{micro}} \sim 0.05 - 0.15 v_\infty$. If this turbulence is not taken into account the terminal velocity will be overestimated by roughly 10 to 30 percent; *d)* At the blue side of the P-Cygni profile, just past the wavelength corresponding to v_∞ , some absorption lines of other elements may be present. If one would not be aware of the presence of such lines, one would

overestimate the terminal velocity.

Velocity law

Observations and theory of stellar winds both show that the behaviour of the outflow speed can be approximated by a *β -type velocity law*, first introduced by Castor and Lamers

$$v(r) = v_\circ + (v_\infty - v_\circ) \left(1 - \frac{R_\star}{r}\right)^\beta \quad (16.2)$$

This law describes a monotonic increase of the outflow velocity with distance from v_\circ at the photosphere ($r = R_\star$) to a maximum velocity v_∞ at large distance. For O- and B-type stars the starting velocity is subsonic, whereas the terminal velocity v_∞ is highly supersonic. It actually holds that $v_\circ \ll v_\infty$. The parameter β is a measure of the velocity gradient or “steepness” of the velocity law. For early-type stars $\beta \simeq 1$, so that 80 percent of the terminal velocity is reached at $5 R_\star$, i.e. $4 R_\star$ above the surface. For increasing β , the velocity gradient in the wind becomes smaller. An alternative way of describing the velocity law is

$$v(r) = v_\infty \left(1 - \frac{r_\circ}{r}\right)^\beta \quad (16.3)$$

where

$$r_\circ = R_\star \left[1 - \left(\frac{v_\circ}{v_\infty}\right)^{1/\beta}\right] \quad (16.4)$$

This representation is often preferred as it is easier to handle in analytical considerations. Sometimes, for practical reasons, the velocity law is normalised to the terminal velocity, i.e.

$$w(x) \equiv v(r)/v_\infty \quad (16.5)$$

where the distance measure $x \equiv r/R_\star$ is in units of the stellar radius.

Exercise 16.1

Measure the terminal velocity of the wind of ζ Puppis, using the spectrum displayed in Fig. 16.2, from the saturated C IV $\lambda\lambda 1448, 1551$ doublet resonance line. Use the pdf version of these lecture notes to zoom in on the profile to enlarge the region around the C IV profile to improve the accuracy of your measurement.

Exercise 16.2

Sketch the profile of an inflow sensitive line, formed through resonance scattering, of a star that is accreting material through spherical infall. In this process, the gas accelerates from a negligibly small infall velocity $v \sim 0$ far away from the star to a maximum infall velocity v_∞ at the stellar surface. Assume that the radius of the star is much smaller than the volume surrounding the star from which the emission originates.

Exercise 16.3

Let us consider a spectral line that is formed in an extended stellar wind. The line formation volume is so large that the star may be considered a point source. The line is formed through pure scattering and shows a P Cygni profile.

- a) Is the emission equivalent width of this line (i.e. the part of the profile surface above the stellar continuum larger/equal/smaller to the absorption equivalent width (i.e. the part of the profile surface that is below the stellar continuum? Explain your choice.

Let us now consider a case where the line formation volume is small compared to the dimension of the star.

- b) Is the emission equivalent width larger/equal/smaller than the absorption equivalent width? Explain your choice.

Exercise 16.4

In this exercise we aim to determine the velocity law for a stationary, i.e. time-independent, radial stellar wind that is driven *solely* by the force due to the gradient of the radiation pressure (see eq. 9.36). We assume that the extinction can be expressed using the flux-weighted mean extinction (see eq. 10.20). This implies that we focus on continuum driven winds as it is not allowed to express the radiation pressure on spectral lines using a grey extinction. At the stellar radius, the flow has velocity $v(R_\star) = v_\circ$. The equation of motion is given by Eq. 9.26, i.e.,

$$\rho \frac{d\mathbf{v}}{dt} = \rho \left[\frac{\partial \mathbf{v}}{\partial t} + (\mathbf{v} \cdot \nabla) \mathbf{v} \right] = -\nabla p + \mathbf{f}, \quad (16.6)$$

where d/dt is the fluid-frame time derivative (see Eqs. 9.10 and 9.25) and $\partial/\partial t$ the partial time derivative at a fixed point in space. For a time-independant radial flow this implies

$$\frac{d\mathbf{v}}{dt} = \frac{\partial \mathbf{v}}{\partial t} + \mathbf{v} \frac{\partial}{\partial r} = \mathbf{v} \frac{dv}{dr}, \quad (16.7)$$

where we have switched to total derivative notation (d/dt) in the last equality as changes in velocity are only traced in one direction.

- a) Give an expression for the ratio, Γ , between the acceleration due to radiation pressure and gravity

- b) Show that the equation of motion of our problem is given by

$$v \frac{dv}{dr} = -\frac{GM_\star(1-\Gamma)}{r^2} \quad (16.8)$$

- c) Solve the equation of motion.

- d) Take $v_\circ = 0$. (Why is this not physical?). Give the solution $v(r)$ in terms of the escape velocity, v_{esc} , at the stellar radius. Which value of β describes the steepness of the velocity law?

- e) Give an expression for the terminal flow velocity in terms of Γ and v_{esc} . Which values of Γ assure a physical solution?

16.3 The determination of mass loss from H α

We assume that we may consider the star and the stellar wind as two separate entities. This is called the *core-halo approximation*. In reality, there obviously will be a fluent transition from photosphere to stellar wind. The star has a stellar radius R_* and emits a spectrum that is given by $\mathcal{F}_\nu(R_*)$. We may expect the photospheric profile of H α to be an absorption line. A spherically symmetric stellar outflow will either partly, fully, or more than fully fill in this profile by H α line emission. We assume that the H α transition in the wind is optically thin such that all photons emitted in the spectral line will escape, save for those that happen to be emitted in the direction of the stellar disk. The latter photons will be absorbed by the star. Given the above assumptions the luminosity of the wind in H α is given by (see eq. 7.15)

$$L(\text{H}\alpha) = \int_{R_*}^{\infty} [1 - W(r)] h\nu_{lu} n_u(r) A_{ul} 4\pi r^2 dr \quad (16.9)$$

where $u=3$ and $l=2$ and ν_{lu} is 6563 Å. In this equation $W(r)$ is the geometrical dilution (eq 3.10), which corrects the volume integral for the fraction of total solid angle in which photons can not escape (as they will find the star on their way). The term $h\nu_{lu} n_u A_{ul}$ is the total energy that is emitted by the transition, in all directions and for all line frequencies, in $\text{cm}^{-3} \text{ sec}^{-1}$ (see § 7.3). The number density of particles in level $n=3$ can be written in terms of the electron density n_e and the proton density n_p , using Saha-Boltzmann equation (6.28) and the NLTE departure coefficient of the upper level b_u (see eq. 6.29). Manipulating a number of equations presented in § 6.5 we find (see eq. 6.34)

$$n_e = \sum_k \sum_{j=1}^{J_k} j N_{jk} = N_N \sum_k A_k \sum_{j=1}^{J_K} j q_{jk} \equiv N_N \gamma \quad (16.10)$$

We further assume that the wind consists of a fully ionised hydrogen gas, such that $\gamma = 1$. The proton density is the product of the hydrogen ionisation fraction, the hydrogen number abundance and the number density of nuclei, i.e. $n_p = N_{11} = N_{jk} = q_{jk} A_k N_N$ (see § 6.5). In our case $n_p = N_N$. This results in

$$L(\text{H}\alpha) = 4\pi h\nu_{lu} A_{ul} \int_{R_*}^{\infty} [1 - W(r)] b_u \Phi_u(T) N_N^2 r^2 dr \quad (16.11)$$

where b_u is the departure coefficient of the upper level of the line (see eq. 6.28 and 6.29). The relation between the density of nuclei and the mass loss rate is described by eq. (9.13). If we also assume that the wind is isothermal and that the NLTE departure coefficient is constant throughout the wind, equation eq. (16.11) simplifies to

$$L(\text{H}\alpha) = \frac{h\nu_{lu} A_{ul}}{4\pi m_{\text{amu}}^2} b_u \Phi_u(T) \frac{\dot{M}^2}{\mu_a^2} \int_{R_*}^{\infty} \frac{[1 - W(r)]}{r^2 v^2(r)} dr \quad (16.12)$$

In assuming a pure hydrogen gas we have fixed the mean atomic weight to $\mu_a = 1$. If we normalize the velocity law to the terminal velocity (eq. 16.5) and switch to a dimensionless

distance $x \equiv r/R_\star$, it follows, after substitution of constants, that

$$L(\text{H}\alpha) = 35.57 b_u T^{-3/2} \exp(17538/T) \frac{\dot{M}^2}{R_\star v_\infty^2} \int_1^\infty \frac{[1 - W(x)]}{x^2 w^2(x)} dx \quad L_\odot \quad (16.13)$$

where \dot{M} is in $M_\odot \text{yr}^{-1}$; R_\star in R_\odot , and v_∞ in km sec^{-1} . The integral at the right side of this equation can easily be computed and is only a modest function of the free parameters $w_o \equiv v_o/v_\infty$ and β in the normalized velocity law (see eq. 16.2). For the wind temperature T we adopt a certain fraction of the effective temperature. Typically, it holds that $T/T_{\text{eff}} \sim 0.5$ to 1. To be fair, a constant value for b_3 throughout the wind is a poor approximation, but, as we have chosen to go down this road, let us assume $b_3 \sim 1.3$. For O-type stars this is a fair compromise.

One can "measure" the quantity $L(\text{H}\alpha)$ with relative ease: From the relations given in § 12.1 it follows that the luminosity in $\text{H}\alpha$ produced by wind emission is given by

$$L(\text{H}\alpha) = 4\pi d^2 \mathcal{F}_{\text{H}\alpha}^c [W^{\text{phot}}(\text{H}\alpha) - W(\text{H}\alpha)] = 4\pi d^2 \mathcal{F}_{\text{H}\alpha}^c W^{\text{net}} \quad (16.14)$$

where $\mathcal{F}_{\text{H}\alpha}^c$ is the continuum flux at the wavelength 6563 Å; W^{phot} is the absorption equivalent width of the photospheric $\text{H}\alpha$ profile, and W is the measured equivalent width. The net equivalent width, W^{net} , i.e. the difference between the photospheric and measured equivalent width, provides a measure of the filling in of the spectral line by wind emission. If the effective temperature and gravity of the star are known we may obtain, for instance from Kurucz models, values for $\mathcal{F}_{\text{H}\alpha}^c$ and W^{phot} . The stellar radius follows from the distance d . The terminal velocity may be determined from P Cygni profiles (see § 16.2).

Let us make a rough estimate of the photospheric flux in order to establish the way in which the net equivalent width depends on basic stellar parameters. For hot stars the $\text{H}\alpha$ line is more or less in the Rayleigh-Jeans part of the spectrum. In that case we may use as a first order approximation of the photospheric flux

$$\mathcal{F}_\lambda^c \sim 4\pi R_\star^2 \pi B_\lambda(T_{\text{eff}}) \propto R_\star^2 T_{\text{eff}} \quad (16.15)$$

If we assume the wind temperature to be a constant fraction of the effective temperature and that for hot O- and B-type stars the exponential term in eq. (16.13) is about unity, it follows that

$$W^{\text{net}} \propto \left(\frac{\dot{M}}{R_\star^{3/2} v_\infty T_{\text{eff}}^{5/4}} \right)^2 \quad (16.16)$$

For an optically thin wind line the equivalent width is thus proportional to the square of the mass loss rate. The essence of the derived proportionality can easily be grasped by realizing that the assumptions imply that $\text{H}\alpha$ is formed by recombination processes, and that therefore the column density will be proportional to $\sim \bar{\rho}^2 R_\star$. Applying continuity equation (9.10) the derived dependence is explained (save for the T_{eff} part).

16.4 The determination of mass loss from radio measurements

In 1975 Panagia & Felli and Wright & Barlow almost simultaneously pointed out that the mass loss from hot stars should also be measurable in infrared- and radio light. If a hot star has a stellar wind, it must be surrounded by an ionized plasma that can absorb and emit through bound-free and free-free transitions. The emission of the wind medium will cause the spectral energy distribution (SED) in the IR and radio to be flatter than the $\mathcal{F}_\nu \propto \nu^2$ one expects for a star without a wind (see eq. 6.9). In this section we concentrate on the radio as for this wavelength regime the observed flux can easily (read: analytically) be related to the mass loss.

For radio frequencies one may apply the Rayleigh-Jeans approximation ($h\nu/kT \ll 1$). Moreover, free-free processes are dominant. For a gas mixture the free-free extinction coefficient per cm is given by (see eq. 8.19)

$$\chi_\nu^{\text{ff}} = 1.772 \times 10^{-2} \bar{g}_{\text{III}}(\nu, T) \frac{Z^2 \gamma}{T^{3/2} \nu^2} N_N^2 \quad (16.17)$$

$$\equiv K(\nu, T) N_N^2 \quad (16.18)$$

where we used eq. (16.10) to describe the electron density and

$$Z^2 \equiv \sum_k A_k \sum_{j=1}^{J_K} Z_{jk}^2 q_{jk} \quad (16.19)$$

for the quadratic mean of the charge of the ions. We also assume that the wind consists of a fully ionized hydrogen gas, such that $Z^2 = 1$ and $\gamma = 1$ (For this reason we have not added Z^2 en γ to the list of dependencies of K).

The optical depth along the line-of-sight at a projected distance $p > R_\star$ to the center of the stellar disk is (see § 3.4)

$$\tau_\nu^{\text{ff}}(p) = K(\nu, T) \int_{-\infty}^{+\infty} N_N^2(p, z) dz \quad (16.20)$$

Using eq. (9.13) we get for the density of nuclei

$$N_N(r) = \frac{\dot{M}}{4\pi m_{\text{amu}} \mu_a r^2 v(r)} \simeq \frac{\dot{M}}{4\pi m_{\text{amu}} \mu_a r^2 v_\infty} \equiv \frac{A}{r^2} \quad (16.21)$$

For our hydrogen gas $\mu_a = 1$. In our case the almost equal sign in the above equation is justified because the bulk of the radio radiation will be emitted at large distances from the star. The optical depth further simplifies to

$$\tau_\nu^{\text{ff}}(p) = K(\nu, T) A^2 \int_{-\infty}^{+\infty} \frac{dz}{r^4} = K(\nu, T) A^2 \int_{-\infty}^{+\infty} \frac{dz}{(p^2 + z^2)^2} = K(\nu, T) A^2 \frac{c_2}{p^3} \quad (16.22)$$

In the last equality $c_2 = \pi/2$, which follows from

$$\int \frac{dz}{(p^2 + z^2)^2} = \frac{1}{2} \frac{z}{p^2(p^2 + z^2)} + \frac{1}{2} \frac{\arctan(z/p)}{p^3} \quad (16.23)$$

To obtain the emerging specific intensity along a beam specified by impact parameter $p > R_\star$ we assume that the wind is isothermal. In that case (see eq. 4.43)

$$I_\nu(p) = B_\nu(T) \left[1 - e^{-\tau_\nu^{\text{ff}}(p)} \right] \quad (16.24)$$

The flux at distance d is given by (see eq. 3.24)

$$\begin{aligned} \mathcal{F}_\nu(d) &= \frac{2\pi}{d^2} \int_0^\infty I_\nu(p) p dp \\ &\simeq \frac{2\pi}{d^2} B_\nu(T) (K(\nu, T) A^2 c_2)^{+2/3} \int_0^\infty \left[1 - e^{-1/y^3} \right] y dy \end{aligned} \quad (16.25)$$

where

$$y \equiv p (K(\nu, T) A^2 c_2)^{-1/3} \quad (16.26)$$

The the last term in eq. (16.25) is not identical to the previous term because the optical depth along lines of sight intercepted by the star, i.e. for $p \leq R_\star$, are strictly speaking, not given by eq. (16.22) (in this case the integration should run from $\sqrt{R_\star^2 - p^2}$ to $+\infty$), and $I_\nu(p)$ should not be represented by eq. (16.24); see eq. 4.43). However, as the radio radiation is produced in a large volume around the star this introduces a negligible error. The y -integral can be solved numerically, from which results $C_2 = 1.339$. For the radio regime ($h\nu/kT \ll 1$) we obtain

$$\mathcal{F}_\nu(d) = 23.454 \frac{\nu^{2/3}}{(d/\text{kpc})^2} \left(\frac{\bar{g}_{\text{III}}(\nu, T) \gamma Z^2}{\mu_a^2} \right)^{2/3} \left(\frac{\dot{M}/M_\odot \text{yr}^{-1}}{v_\infty/\text{km sec}^{-1}} \right)^{4/3} \text{Jy} \quad (16.27)$$

The flux is given in jansky. Notice that in our isothermal wind \mathcal{F}_ν , save for a weak dependence which enters through the Gaunt factor, is independent of the temperature of the gas. This is important in view of uncertainties in the temperature structure of stellar winds. If we also neglect the modest frequency dependence of \bar{g}_{III} we find for *spectral slope* or *spectral index* $n \equiv \partial \log \mathcal{F}_\nu / \partial \log \nu = 2/3$, i.e.

$$\mathcal{F}_\nu \propto \nu^{2/3} \quad (16.28)$$

A good approximation for the Gaunt factor in the radio domain is provided by

$$\bar{g}_{\text{III}} = 9.77 \left(1 + 0.13 \log[T^{3/2}/\nu Z] \right) \quad (16.29)$$

Corrected for this behaviour we obtain $\mathcal{F}_\nu \propto \nu^{0.6}$. In the infrared \bar{g}_{III} is almost independent of frequency and the spectral slope remains as implied by eq. (16.28). Inversion of eq. (16.27) yields for the mass loss

$$\dot{M} = 0.094 \frac{(d/\text{kpc})^{3/2}}{\nu^{1/2}} \frac{\mu_a}{(\gamma \bar{g}_{\text{III}})^{1/2} Z} (v_\infty/\text{km sec}^{-1}) (\mathcal{F}_\nu/\text{Jy})^{3/4} M_\odot \text{yr}^{-1} \quad (16.30)$$

The insensitivity of the radio flux for the temperature of the wind and the stellar radius make that mass loss rates derived from radio measurements are among the most reliable. Unfortunately, the number of stars for which we can use the radio method is small as the fluxes are low, therefore difficult to measure. For a star at a distance of 1 kpc, having $\dot{M} = 10^{-6} M_{\odot}\text{yr}^{-1}$ and $v_{\infty} = 2000 \text{ km sec}^{-1}$, the flux at 6 cm is $\mathcal{F}_{\nu} \simeq 0.3 \text{ mJy}$. The detection limit of large radio telescopes is near 0.1 mJy. The radio method can therefore only be applied for relatively nearby stars ($d \lesssim 1 \text{ kpc}$) with relatively high mass loss ($\dot{M} \gtrsim 10^{-6} M_{\odot}\text{yr}^{-1}$).

Effective radius at radio wavelengths

Based on the measured ratio \dot{M}/v_{∞} we can assign to a star an effective radius at radio wavelengths. The value for the radius is a function of wavelength at which it is measured and depends on the exact definition of r_{ν}^{ff} .

The optical depth at the effective radius r_{ν}^{ff} is (compare to eq. 16.22)

$$\tau_{\nu}^{\text{ff}}(r_{\nu}^{\text{ff}}) = K(\nu, T) A^2 \int_{r_{\nu}^{\text{ff}}}^{\infty} \frac{dr}{r^4} = \frac{KA^2}{3(r_{\nu}^{\text{ff}})^3} \quad (16.31)$$

We discuss two possible definitions of the effective radius. In the first case we focus our attention to the medium above the radio surface of the star and assume that this radiating medium is optically thin; in the second case we require the emission to come from an optically thick radiating sphere.

If we require the observed flux to be equal to the total emission in the wind above a certain effective radius r_{ν}^{ff} , i.e.

$$L_{\nu} = 4\pi d^2 \mathcal{F}_{\nu}(d) = 4\pi \left(r_{\nu}^{\text{ff}}\right)^2 \mathcal{F}_{\nu}(r_{\nu}^{\text{ff}}) = \int_{r_{\nu}^{\text{ff}}}^{\infty} 4\pi \eta_{\nu}^{\text{ff}} 4\pi r^2 dr \quad (16.32)$$

we find using $\eta_{\nu}^{\text{ff}} = \chi_{\nu}^{\text{ff}} B_{\nu}(T)$, substitution of eq. (16.31) and equating with eq. (16.25), that the effective radius should be measured at $\tau_{\nu}^{\text{ff}} = 0.247$. Notice that in this definition we have implicitly assumed that the radiating medium is optically thin. Substitution of constants and inversion of eq. (16.31) leads to

$$r_{\nu}^{\text{ff}} = 3.633 \times 10^{17} \frac{1}{(\tau_{\nu}^{\text{ff}})^{1/3}} \frac{1}{\nu^{2/3} T^{1/2}} \left(\frac{\bar{g}_{\text{III}}(\nu, T) \gamma Z^2}{\mu_a^2} \right)^{1/3} \left(\frac{\dot{M} / M_{\odot}\text{yr}^{-1}}{v_{\infty} / \text{km sec}^{-1}} \right)^{2/3} R_{\odot} \quad (16.33)$$

If we again take $\dot{M} = 10^{-6} M_{\odot}\text{yr}^{-1}$ en $v_{\infty} = 2000 \text{ km sec}^{-1}$ and assume that the temperature of the wind $T = 30000 \text{ K}$ we find at the wavelength of 6 cm an effective radius $r_{\nu}^{\text{ff}} = 1308 R_{\odot}$. The typical stellar radius of an O star (measured at optical wavelengths) is about $15 R_{\odot}$ (see table A.1) which shows that the radio radius $r_{\nu}^{\text{ff}} \gg R_{\star}$.

We may also define the effective radius at radio wavelengths by equating the measured radio flux with the total amount of radiation emitted by a spherical surface of radius r_{ν}^{ff} , i.e. (see

vgl. 3.21)

$$\mathcal{F}_\nu(d) = \pi B_\nu(T) \left(\frac{r_\nu^{\text{ff}}}{d} \right)^2 \quad (16.34)$$

After substitution of eq. (16.31) and equating to eq. (16.25) it follows that the effective radius should be measured at $\tau_\nu^{\text{ff}} = 0.0484$. Note that in this definition the emission is thought to originate from an optically thick surface. The reason why the “optically thick” effective radius is larger than the “optically thin” one has to do with the fact that the latter requires an integration over a large volume.

H II regions

In this chapter we move away from the stellar surface into the ambient interstellar medium of O- and early B-type stars. As we have seen in chapter 2 these massive stars are both extremely luminous ($L_\star \gtrsim 10^4 L_\odot$) and extremely hot, with surface temperatures $T_{\text{eff}} \gtrsim 20\,000$ K. The extreme ultraviolet radiation that is the result of these stellar properties causes ionization of the surrounding gas. As the ionized gas is predominantly hydrogen these regions are known as H II regions. The balance between photo-ionization and radiative recombination determines the degree of ionization. The kinetic energy of the photo-electrons (those kicked out of the atom or ion during ionization) is quickly shared with other free electrons in the nebula, establishing a Maxwellian energy distribution. Electrons from the thermal pool can excite low-lying levels of metals, such as O III, and downward radiative transitions cool the nebula. This energy balance sets the temperature of the gas.

The processes setting the ionization and temperature structure of nebulae represent extreme NLTE conditions; studying these conditions provides important insight in NLTE physics and for this region this topic is part of these lecture notes. We first give a brief historical introduction. This is followed by a discussion of what sets the size of an H II-region. We continue with a discussion on hydrogen line radiation and hydrogen free-free radio continuum emission. Finally, we discuss emission from metal lines.

17.1 Historical introduction

In the 19th century an animated debate ensued on the question whether the diffuse objects seen through telescopes, loosely termed ‘nebulae’, were in fact unresolved stellar associations or gas clouds. The answer came when these objects were studied using spectroscopy. The small ‘white nebulae’, those located primarily outside of the plane of the Milky Way, featured spectra typical for that of stars. These are stellar associations or star clusters. Other nebulae showed a pronounced line spectrum, sometimes accompanied by an underlying continuum that did not appear to be of stellar origin. These are the gas clouds, including planetary

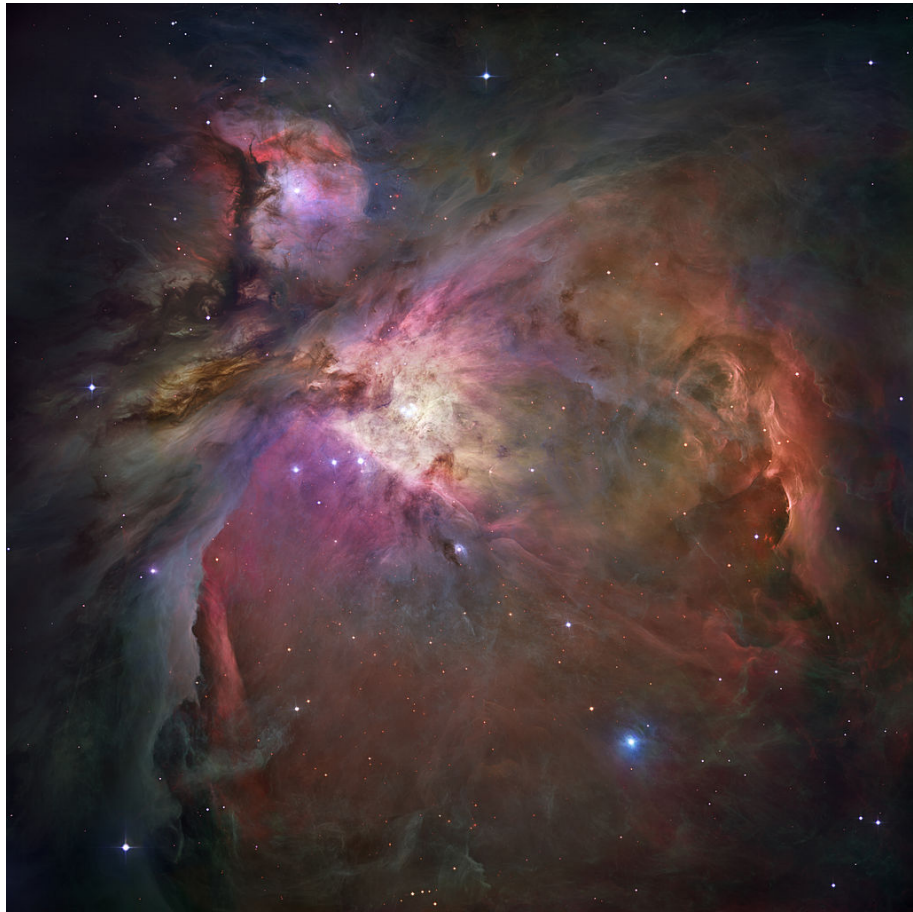


Figure 17.1: The Orion Nebula (also known as Messier 42, M42, or NGC 1976) at a distance of ~ 400 pc is the closest region of massive star formation to Earth. The dimensions of this image are 65×60 arcmins, corresponding to a physical scale of 7.5×7.0 pc. The open cluster of stars in the heart of the Orion Nebula contains several O-type stars of which the O6pe V star θ^1 Orionis C is the most massive. The optical light we see is the result from line emission of hydrogen (Balmer lines) and reflection of star light on dust grains.

nebulae, H II regions, and supernova remnants.

The spectrum of the brightest of these nebulae, the Orion nebula (see Fig. 17.1), was observed in 1863 by William Huggins. Soon after, Balmer lines were recognized in this and other nebulae. Quite some time later also lines from the Paschen series, and, when infrared instruments became available, also those of the Brackett series were identified. After it was discovered in the Sun, also helium was found. Surprisingly enough, the identification of the by far strongest lines in many nebular spectra – in green light at 4959 and 5007 Å – and those of other strong transitions, turned out to be an enormous challenge. Some even speculated these unidentified lines to be produced by a new and hypothetical element ‘nebulium’. Due to progress in the

understanding of atomic structure these lines were eventually identified as forbidden transitions of O III and other strong nebular lines with similar transitions in known elements such as nitrogen, neon, sulfur and argon.

17.2 The primary radiation mechanism in nebulae

The first thing to realize when identifying the relevant physical processes in a gaseous nebula is the large distance of the nebula to the hot star (or stars) that irradiates (or irradiate) the gas. This causes the radiation field, though very ‘hot’, to be very diluted.

Atomic processes that depend on radiation, such as photoexcitation and photoionization, thus proceed at a rate that is a factor W (see eq. 3.10, or for a more practical version eq. 14.3) slower than in thermodynamic equilibrium. However, the rate of recombinations is independent of W as it is controlled by local properties only, that is, the electron and ion densities and the temperature of the medium (see vgl. 8.8). To give an example, a hydrogen atom in an excited state will almost certainly experience a spontaneous de-excitation to a lower level before it can absorb a photon that could bring it in a higher excited state, or cause ionization. The result is that almost all the neutral hydrogen will be in the ground state. All H ionizations by photons having $\lambda < 912 \text{ \AA}$ will thus arise from the ground level, whilst recombinations may happen to any level. When the capture of a free electron leads to a recombination to the ground level, a Lyman continuum photon will be emitted. When recombination to $n = 2$ takes place, a Balmer continuum photon will be released ($\lambda < 3646 \text{ \AA}$), followed by a Ly α photon when the atom returns to the ground state. An electron captured in level $n = 3$ will discharge a Paschen continuum photon ($\lambda < 8204 \text{ \AA}$). There are now two possibilities. Either the atom de-excites to $n = 2$ by emitting a H α photon and subsequently to $n = 1$ by releasing a Ly α photon, or it cascades directly to the ground level by emitting a Ly β photon. Scenarios for recombinations to $n = 4$ or higher levels can easily be worked out (see figure 6.4).

17.3 Ionization equilibrium and the Strömgren sphere

The ionization equilibrium of the elements, at each position in the nebula, is determined by the balance between photoionizations and recombinations of electrons with ions. Let us assume that the nebula is composed of hydrogen only. What then is the ionization condition of H? Using Eq. (8.1), (8.3) and (8.8), we may write (see Eq. 14.4)

$$n_0 4\pi \int_{\nu_o}^{\infty} \alpha_{\nu}^{\text{bf}} \frac{J_{\nu}}{h\nu} d\nu = N^+ n_e \alpha_A(T) \quad (17.1)$$

where ν_o corresponds to 912 \AA , and α_A denotes the total recombination coefficient of hydrogen to all levels (see Table 17.1). As discussed, we may safely assume that all the neutral

hydrogen is in the ground state, i.e. $n_0 = N^0$. If $q^0 = N^0/N$ is the fraction of neutral hydrogen, it then follows that $N^+ = n_e = (1 - q)$. We further assume that the radiation field in the nebula is completely controlled by a star at a large distance. If we adopt the star to be a isotropically radiating sphere, it follow from Eq. (3.9) and (3.21) that

$$J_\nu(r) = \frac{1}{4\pi} \mathcal{F}_\nu(r) = \frac{1}{4\pi} \frac{L_\nu}{4\pi r^2} \quad (17.2)$$

Writing for the total number of Lyman continuum photons leaving the star each second

$$Q_0 \equiv \int_{\nu_0}^{\infty} \frac{L_\nu}{h\nu} d\nu \quad (17.3)$$

and approximating the extinction coefficient of photoionization with a constant (frequency independent) value $\bar{\alpha}_\nu^{\text{bf}}$, we obtain for the fraction of neutral hydrogen

$$\frac{q}{(1 - q)^2} = \frac{4\pi r^2 \alpha_A N}{\bar{\alpha}_\nu^{\text{bf}} Q_0}. \quad (17.4)$$

Let us consider a point in the nebula with a typical particle density $N = 10 \text{ cm}^{-3}$, at a distance of 5 pc from an O7V star having $\log Q_0 = 48.7$. We then find – using $\bar{\alpha}_\nu^{\text{bf}} \sim 6 \times 10^{-18}$ (see Eq. 8.3) and $\alpha_A \sim 4 \times 10^{-13}$ (see Table 17.1) – for the fraction of neutral hydrogen $q \sim 4 \times 10^{-4}$. Phrased differently: hydrogen is almost completely ionized.

The recombination time of nebular gas

The recombination time of the nebular gas is given by

$$t_{\text{rec}} = \frac{1}{n_e \alpha_A} \quad (17.5)$$

For $n_e = 10 \text{ cm}^{-3}$ (assuming nearly completely ionized H) the recombination time is $\sim 3 \times 10^{11} \text{ sec}$ or $\sim 10^4 \text{ yr}$. Thus, in such a region, if a neutral hydrogen atom is photoionized, it stays ionized for a long time before recombining. Once it recombines, it is relatively quickly ionized again, and so the instantaneous neutral fraction in this region should be very small.

— — —

A source that is producing a finite number of ionizing photons can of course not ionize an infinitely large volume. Therefore, if the star is located in a sufficiently large gas cloud, there must be a boundary to the H II region. Somewhere there will be a zone in which hydrogen is recombining and outside of which there is an H I region. The thickness of the transition zone will be small because when hydrogen starts to recombine the optical depth in the Lyman continuum rapidly increases, effectively preventing ionizing radiation to penetrate deeper into the medium. Hence we may estimate the thickness of the recombination zone by equating it

Table 17.1: Recombination coefficients of hydrogen as a function of temperature in $\text{cm}^3 \text{ sec}^{-1}$: $\alpha_A \equiv \sum_{i=0}^{\infty} \alpha_{i,H}^{RR}$ gives the total number of recombinations to all levels; $\alpha_B \equiv \sum_{i=1}^{\infty} \alpha_{i,H}^{RR}$ gives the total number of recombinations to all levels above the ground level.

T	$\alpha_A / 10^{-13}$	$\alpha_B / 10^{-13}$
3 000	9.74	6.74
5 000	6.83	4.53
10 000	4.17	2.59
15 000	3.11	1.84
20 000	2.51	1.43
30 000	1.84	0.991
T	$\sim 4.15 (T/10\,000 \text{ K})^{-0.72}$	$\sim 2.60 (T/10\,000 \text{ K})^{-0.80}$

to the mean free path at the point where half of the hydrogen is recombined, i.e. at $q = 0.5$. We find (see Eq. 4.26)

$$\Delta r \sim \frac{1}{\bar{\alpha}_{\nu}^{\text{bf}} N^0} = \frac{1}{\bar{\alpha}_{\nu}^{\text{bf}} q N} \sim 0.01 \text{ pc.} \quad (17.6)$$

This is much smaller than the typical radius of an H II region. Classical H II regions thus have a sharp boundary. Inside of the boundary hydrogen is almost completely ionized; outside of the boundary hydrogen is almost completely neutral.

Strömgren sphere

How big is an H II region? We assume a homogeneous spherical cloud of hydrogen gas with a star in the center. We do not assume that the radiation field in the nebula is completely controlled by the central star, but we allow the specific intensity I_{ν} to have a diffuse component as a result of radiation emitted in the nebula. For frequencies in the Lyman continuum the equation of transfer is given by (see Eq. 4.11)

$$\frac{dI_{\nu}}{ds} = \eta_{\nu} - \chi_{\nu} I_{\nu} \quad (17.7)$$

where η_{ν} is the local volume emission coefficient for radiation with frequencies $\nu \geq \nu_0$. The only source of this type of photons in the nebula are recombinations to the ground level. Therefore

$$4\pi \int_{\nu_0}^{\infty} \frac{\eta_{\nu}}{h\nu} d\nu = N^+ n_e \alpha_{1,H}^{RR}(T), \quad (17.8)$$

where $\alpha_{1,H}^{RR}$ is the recombination coefficient to the ground level of hydrogen. Suppose the nebula is optically thick for Lyman radiation, such that no Lyman continuum photons can escape. Each and every Lyman photon produced by the diffuse radiation field will be absorbed elsewhere in the nebula. For the mean intensity of the diffuse component of the radiation field, J_{ν}^d , we find

$$N_0 4\pi \int_{\text{nebula}} \alpha_{\nu}^{\text{bf}} \frac{J_{\nu}^d}{h\nu} dV = 4\pi \int_{\text{nebula}} \frac{\eta_{\nu}}{h\nu} dV \quad (17.9)$$

where the integration is over the entire volume of the nebula. If the mean free path of the photons is small, that is, if the photons are absorbed close to where they are created, one may even write

$$J_\nu^d = \frac{\eta_\nu}{N_0 \alpha_\nu^{bf}}. \quad (17.10)$$

This is referred to as the *on-the-spot* approximation. For nebulae having particles densities that are not too small this is a reasonable assumption.

As a result of absorptions (read: photoionizations) Lyman continuum radiation that originates directly from the star gets weakened. To within very large accuracy it holds that $I_\nu^s(r) = I_\nu^s(R_\star) \exp[-\tau_\nu(r)]$, where τ_ν is the radial optical depth

$$\tau_\nu(r) = \int_0^r N_0 \alpha_\nu^{bf} dr t. \quad (17.11)$$

In a formal sense, the integration of course needs to start at R_\star in stead of at the origin. However, as we will show below, things work out more elegantly if we accept this minute error. For the mean intensity of the stellar component of the radiation field we may write

$$J_\nu^s(r) = \frac{1}{4\pi} \frac{L_\nu}{4\pi r^2} e^{-\tau_\nu} \quad (17.12)$$

We represent the radiation field in the nebula as the sum of the stellar and diffuse component, i.e. $J_\nu = J_\nu^s + J_\nu^d$. Substituting Eq. (17.10) and (17.12) in ionization equilibrium (17.1) then yields

$$N_0 \int_{\nu_o}^{\infty} \frac{L_\nu}{h\nu} \frac{e^{-\tau_\nu}}{4\pi r^2} d\nu = N^+ n_e [\alpha_A(T) - \alpha_{1,H}^{RR}(T)] = N^+ n_e \alpha_B(T), \quad (17.13)$$

where we have used Eq. (17.8). We have introduced the recombination coefficient α_B to represent the total number of recombinations to all levels above the ground level (see Table 17.1). The physical meaning of the above equation is that in an optically thick nebula ionizations caused by the stellar radiation field are in equilibrium with recombinations to excited levels of hydrogen. Recombinations to the ground level produce Lyman continuum photons that (in the on-the-spot approximation) are almost on-the-spot reabsorbed and thus have no effect on the ionization equilibrium.

To determine the radius of the ionized region we use that $d\tau_\nu/dr = N_0 \alpha_\nu^{bf}$ (see Eq. 17.11) and integrate over distance. This yields

$$\int_{\nu_o}^{\infty} \frac{L_\nu}{h\nu} \left[\int_0^\infty e^{-\tau_\nu} d\tau_\nu \right] d\nu = \int_{\nu_o}^{\infty} \frac{L_\nu}{h\nu} d\nu = \int_0^{\infty} N^+ n_e \alpha_B(T) 4\pi r^2 dr \quad (17.14)$$

By letting the optical depth run from zero to infinity we have assured that all Lyman continuum photons are ‘used up’. To find a simple expression for the size of the ionized region we assume that the gas is fully ionized up to a distance R_S , and that the gas outside of this region is neutral.

As we have seen, we expect a classical H II region to have a sharp boundary implying that our assumption is quite reasonable. Using Eq. (17.3) it follows that

$$Q_0 = \frac{4\pi}{3} R_S^3 N^2 \alpha_B(T) \quad (17.15)$$

The meaning of this result is that the total number of ionizing photons emitted by the star (per second) is exactly balanced by the total number of recombinations to excited states of all hydrogen atom within a sphere of volume $4\pi R_S^3/3$. This volume, in honor of the pioneer of this field, is referred to as the *Strömgren sphere*, and R_S as the *Strömgren radius*.

The two assumptions that we have made to estimate the size R_S of the H II region are the on-the-spot approximation and that the medium is either fully ionized or fully neutral. In this we could avert having to solve the equation of transfer explicitly.

Ionization bounded and density bounded

Note that we have assumed that the ionizing star is in a sufficiently large gas cloud, that is, that the edge of the Strömgren sphere is determined by the region where hydrogen recombines. This is referred to as *ionization bounded*. It is however possible that the nebula contains insufficient hydrogen for all Lyman continuum photons to ‘be used’. In that case we refer to the H II region as *density bounded*.

Case A and Case B recombination

While we are in the process of defining things: in case the nebula is optically thin in all recombination lines, i.e. all radiation produced by recombination processes in the nebula is able to escape freely, one speaks of *Case A*. H II regions that fulfill the Case A requirement can only contain a relatively small amount of gas. So little gas, as a matter of fact, that they will be hard to observe.

Nebulae containing appreciable amounts of gas will rapidly develop large optical depths in the hydrogen Lyman lines. We can easily estimate this. The ratio between the extinction coefficients per particle in the ground state for line- and continuum radiation follows from Eq. (7.20) and (8.3). Comparison of the collisional cross section at line center, assuming a Doppler profile for ϕ_ν a, with the continuum cross section at the ionization boundary yields, after substitution of constants

$$\frac{\tau(\text{Ly}n)}{\tau(\text{Ly-edge})} = 14.68 \frac{\lambda_{1n} [\text{\AA}] f_{1n}}{g_{\text{II}}(\nu_\circ, n) (T/10\,000)^{1/2}}. \quad (17.16)$$

For a characteristic temperature $T = 10\,000$ K and $g_{\text{II}} \sim 1$ we find that Ly α has about a 10^4 times larger optical depth than the continuum at the Lyman ionization boundary (see Table 7.1). For an ionization bounded nebula with $\tau(\text{Ly-edge}) \sim 1$ one thus obtains $\tau(\text{Ly}\alpha) \sim 10^4$, $\tau(\text{Ly}\beta) \sim 10^3$, $\tau(\text{Ly}8) \sim 10^2$, and $\tau(\text{Ly}18) \sim 10$. For a typical nebula a better

approximation than Case A therefore is the opposite assumption, i.e. that it is optically thick in all Lyman lines. This assumption formally implies that all Lyman lines are in detailed balance (see § 6.1) and is called *Case B*.

The above two limiting cases have been described in 1938 by Menzel and Baker and are therefore often called Menzel & Baker Case A and Case B. It should not be forgotten that the realistic situation in a nebula is likely in between these two limits. For fairly low lying transitions in the Lyman series Case B will hold, while for the higher transitions, i.e. $n \rightarrow \infty$ and $\tau(\text{Lyn}) \rightarrow 1$, the situation will be more similar to Case A.

Exercise 17.1

Show that if one may neglect diffuse radiation in the nebula, the radius of the Strömgren sphere is given by

$$Q_0 = \frac{4\pi}{3} R_S^3 N^2 \alpha_A(T) \quad (17.17)$$

17.4 The emission measure as a density diagnostic

Let us assume that the fraction of all recombinations which leads through the transition $j \rightarrow i$ is $f_{ji}(T)$, then the volume emission coefficient for the line $j \rightarrow i$ is (see also Eq. 7.15)

$$\eta_\nu^\ell = \frac{h\nu}{4\pi} f_{ji}(T) \alpha_A n_p n_e \psi_\nu = \eta_\circ^\ell \psi_\nu \quad (17.18)$$

where we have replaced N^+ with n_p , the number of free protons, for the case of hydrogen. ψ_ν is the profile function for spontaneous emission. Though to determine $f_{ji}(T)$ requires a general approach (see Sect. 17.5), it is found that $f_{H\alpha} \sim 0.3$, i.e. only about 30 percent of hydrogen recombinations produce a H α photon. Similarly, $f_{H\beta} \sim 0.1$, so only about 10 percent of hydrogen recombinations produce an H β photon.

If we look at an H II region on a line-of-sight where there is negligible background specific intensity, and if the emission from the H II region is optically thin, then (see Sect. 4.6), we have

$$I_\nu^{\text{obs}} \sim \int S_\nu(\tau_\nu) d\tau_\nu = \int \eta_\nu(s) ds, \quad (17.19)$$

where I_ν^{obs} is the observed specific intensity and s is the spatial coordinate along the line-of-sight. It follows that the specific intensity integrated over the line profile is

$$I^{\text{obs}} = \int I_\nu d\nu = \int \left[\int \eta_\nu^\ell ds \right] \psi_\nu d\nu = \int \eta_\circ^\ell ds = \frac{h\nu}{4\pi} f_{ji}(T_\circ) \alpha_A(T_\circ) \int n_p n_e ds, \quad (17.20)$$

assuming the emitting medium has uniform temperature $T = T_{\circ}$. The integral in the last equation is called the *emission measure* of the line-of-sight, \mathcal{EM}_H , where

$$\mathcal{EM}_H = \int n_p(s) n_e(s) ds. \quad (17.21)$$

If the emitting medium has uniform density, then $\mathcal{EM}_H = n_p n_e L$, where L is the length of the intercept which the line-of-sight makes with the emitting medium.

Thus a measurement of the total line specific intensity Eq. 17.20 enables us to estimate the emission measure of the emitting medium. Suppose, we also have an independent estimate of the linear size L of the emitting region, say from its distance d and its angular size α , via $L = d \alpha$, assuming spherical symmetry, which is often a good approximation (see also exercise 4.6). Then we can combine this with the emission measure to obtain $\langle n_p n_e \rangle = \mathcal{EM}_H / L$. Typically in an H II region, we have $n_p \sim n_e$, and so the hydrogen emission measure obtained from a hydrogen recombination line gives

$$\langle n_e^2 \rangle \sim \langle n_p n_e \rangle = \frac{\mathcal{EM}_H}{L}. \quad (17.22)$$

We see that, from the study of hydrogen recombination lines, we can estimate the density of gas in an H II region.

17.5 The equation of state of nebular hydrogen gas

The nebular line spectrum of hydrogen is caused by the capture of free electrons into excited levels that cascade or ‘rain down’ to the ground level. In Case A theory, i.e. in the limit of very low particle densities, one only needs to consider spontaneous photo-recombinations and spontaneous radiative de-excitations. In this case, the statistical equilibrium equation (9.15) reduces to

$$N^+ n_e \alpha_i^{RR}(T) + \sum_{u=i+1}^{\infty} n_u A_{ui} = n_i \sum_{l=1}^{i-1} A_{il} \quad (17.23)$$

in which the recombination coefficient into level i is given by α_i^{RR} , and where u denotes levels that are higher up than i and l levels that are lower than i .

If we describe the level populations in terms of the NLTE departure coefficients b_i (Eq. 6.29), such that

$$n_i = b_i N^+ n_e \Phi_i(T), \quad (17.24)$$

we obtain

$$\alpha_i^{RR}(T) + \sum_{u=i+1}^{\infty} b_u \Phi_u(T) = \Phi_i(T) b_i \sum_{l=1}^{i-1} A_{il}. \quad (17.25)$$

This result shows that if photo-recombinations and spontaneous radiative de-excitations are the only relevant processes, the dimensionless b_i will be independent of the density of the medium.

Note that if the departure coefficients above a certain value $i > i_K$ are known, equation (17.25) can be used in a systematic procedure – starting with level i , subsequently $i - 1$, et cetera – to determine all b_i . This yields the state of the gas.

Cascade matrix

An alternative way to determine the nebular state of the gas is, one that is considered very elegant, is in terms of the *cascade matrix*. The cascade matrix \mathcal{C}_{ul} gives the probability that an upper level u , through all possible cascade routes, ends up in lower level i . This matrix can be constructed in a straightforward way from all downward rates P_{ul} providing the fractional probability that an upper level u returns directly to a lower level l through spontaneous radiative de-excitation. This probability is

$$P_{ul} = \frac{A_{ul}}{\sum_{\ell=1}^{u-1} A_{u\ell}} \quad (17.26)$$

Using this definition one obtains for the first few coefficients of the cascade matrix

$$\begin{aligned} \mathcal{C}_{i,i-1} &= P_{i,i-1} \\ \mathcal{C}_{i,i-2} &= P_{i,i-2} + \mathcal{C}_{i,i-1} P_{i-1,i-2} \\ \mathcal{C}_{i,i-3} &= P_{i,i-3} + \mathcal{C}_{i,i-1} P_{i-1,i-3} + \mathcal{C}_{i,i-2} P_{i-2,i-3} \end{aligned}$$

and therefore for the general form

$$\mathcal{C}_{ul} = \sum_{i=l+1}^u \mathcal{C}_{ui} P_{il} \quad (17.27)$$

where it is agreed that $\mathcal{C}_{ii} \equiv 1$. The cascade matrix only depends on atomic properties and needs to be computed only once. The statistical equilibrium solution (17.23) can now be re-written in terms of \mathcal{C}_{ul} realizing that the population of level i is given by the balance between on the one hand all recombinations to levels $u > i$ that after cascade end up in i , and on the other hand all spontaneous radiative de-excitations away from level i . This yields

$$N^+ n_e \sum_{u=i+1}^{\infty} \alpha_u^{RR}(T) \mathcal{C}_{ui} = n_i \sum_{l=1}^{i-1} A_{il} \quad (17.28)$$

or, in terms of NLTE departure coefficients

$$b_i = \frac{\sum_{u=i+1}^{\infty} \alpha_u^{RR}(T) \mathcal{C}_{ui}}{\Phi_i(T) \sum_{l=1}^{i-1} A_{il}} \quad (17.29)$$

To arrive at the solution the behavior of α_u^{RR} en C_{ui} needs to be extrapolated to infinity, such that the series $u \rightarrow \infty$ can be determined. This can be done for α_u^{RR} by means of eq. (8.3) and for C_{ui} using Kramers's formula eq. (7.22). This than completes the determination of the state of the gas.

It is practical (besides elegant) to determine the state of nebular gas in this way as it allows to account for collisional processes without having to change the structural setup of the solution in a fundamental way. However, we will not discuss this further here.

— — —

The above discussed method to derive the state of the gas is, as said, valid for Case A recombination. If one is in a situation of Case B each emitted Lyman photon $\nu(u, 1)$ will immediately be absorbed by the nebular gas, and excite (a nearby) hydrogen atom into level u . This process therefore has no real effect and it is thus trivial to describe Case B recombination by starting the summations in equations (17.23), (17.25), (17.26), (17.28), and (17.29) at level $l = 2$ rather than at the ground level $l = 1$.

— — —

Now that the level populations are known it is trivial to compute the line emission coefficients for each transition. These are (see Eq. 7.15)

$$\eta_\nu(u, l) = \frac{h\nu(u, l)}{4\pi} n_u A_{ul} \psi_\nu \quad (17.30)$$

where we have divided by the total solid angle 4π because the emission coefficient is defined per unit solid angle (see Eq. 4.7). The total line emission coefficient is

$$\eta(u, l) = \frac{h\nu(u, l)}{4\pi} n_u A_{ul} \quad (17.31)$$

The ratio between the total emission coefficients of two lines $\eta(u, l)/\eta(u', l')$ is proportional to the luminosities of these lines $L(u, l)/L(u', l')$, assuming that the two lines are formed in the same volume of gas. These ratios are easily measured in the spectrum as they are equal to the ratio $\mathcal{F}_{\nu(u,l)}^c W(u, l)/\mathcal{F}_{\nu(u',l')}^c W(u', l')$, where \mathcal{F}_ν^c is the continuum flux at the line frequency and W is the emission equivalent width of the line. By comparing the measured value with predictions the temperature of the radiating medium can be derived. Table 17.2 lists the theoretical values $\eta(u, l)/\eta(4, 2) = \eta(u, l)/\eta(\text{H}\beta)$ for a number of hydrogen lines as a function of temperature.

17.6 Free-free radio continuum emission as a temperature diagnostic

How does the continuum spectrum from an H II region look like? As the part of the continuum spectrum that is typically observed is at long wavelengths and the region is almost completely

Table 17.2: *Balmer line intensities related to those of H β , for both Case A and Case B recombination. Using these ratios the temperature of a nebula can be estimated. The Case A values are independent of the electron density; the Case B values assume $n_e = 10^4 \text{ cm}^{-3}$. From Osterbrock, "Astrophysics of Gaseous Nebulae and Active Galactic Nebulae."*

Case A recombination $\eta(\text{line})/\eta(\text{H}\beta)$	2 500 K	5 000 K	10 000 K	20 000 K
H α	3.42	3.10	2.86	2.69
H γ	0.439	0.458	0.470	0.485
H δ	0.237	0.250	0.262	0.271
H ϵ	0.143	0.153	0.159	0.167
H8	0.0957	0.102	0.107	0.112
H9	0.0671	0.0717	0.0748	0.0785
H10	0.0488	0.0522	0.0544	0.0571
H15	0.0144	0.0155	0.0161	0.0169
H20	0.0061	0.0065	0.0068	0.0071
Case B recombination $\eta(\text{line})/\eta(\text{H}\beta)$	2 500 K	5 000 K	10 000 K	20 000 K
H α	3.00	2.85	2.74	
H γ	0.460	0.469	0.476	
H δ	0.253	0.260	0.264	
H ϵ	0.155	0.159	0.163	
H8	0.102	0.105	0.107	
H9	0.0714	0.0734	0.0746	
H10	0.0520	0.0533	0.0541	
H15	0.0163	0.0162	0.0161	
H20	0.0082	0.0075	0.0072	

ionized, the extinction is dominated by free-free processes. Therefore, if we look at an H II region with uniform temperature T and the background intensity is negligible, we should observe free-free radiation with intensity given by (see Eq. 4.43)

$$I_\nu^{\text{obs}} = S_\nu [1 - e^{-\tau_\nu}] = B_\nu(T) [1 - e^{-\tau_\nu}]. \quad (17.32)$$

Typical H II regions have temperatures $T \sim 10^4 \text{ K}$ and almost always have $7000 \text{ K} \lesssim T \lesssim 14000 \text{ K}$. Assuming the medium consists of fully ionized hydrogen only, the free-free optical depth integrated over the H II region is (see Eq. 8.19)

$$\begin{aligned} \tau_\nu &= 1.772 \times 10^{-2} \bar{g}_{\text{III}}(\nu, T) T^{-3/2} \nu^{-2} \int n_p n_e ds \\ &= 1.772 \times 10^{-2} \bar{g}_{\text{III}}(\nu, T) T^{-3/2} \nu^{-2} \mathcal{EM}_H \end{aligned} \quad (17.33)$$

in the Rayleigh-Jeans limit. Recall that in the Rayleigh limit the Planck function reduces to Eq 6.9.

We can identify a critical frequency ν_{turnover} , such that the spectrum of free-free radiation has different asymptotic forms for $\nu \ll \nu_{\text{turnover}}$ and $\nu \gg \nu_{\text{turnover}}$. Here ν_{turnover} is the frequency at which the optical depth equals unity.

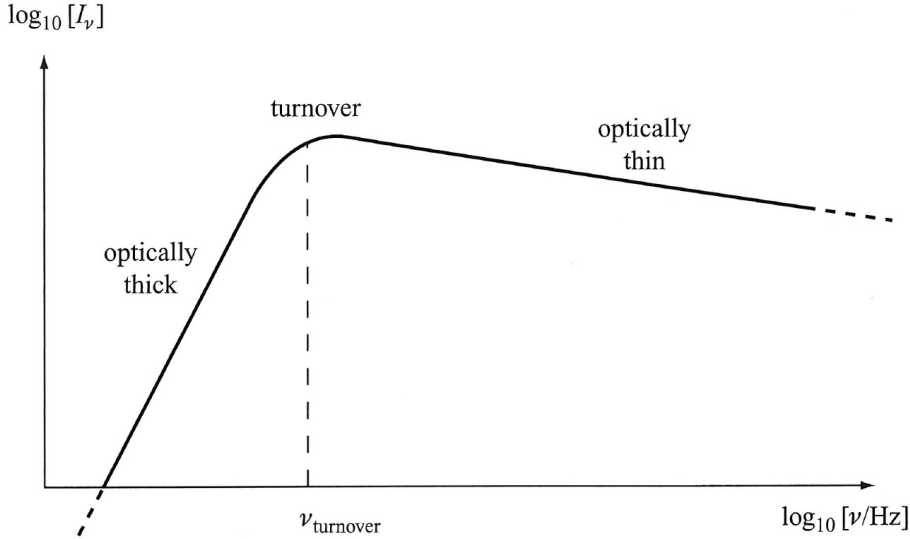


Figure 17.2: The free-free continuum spectrum from an H II region, showing the transition from optically thick at $\nu \ll \nu_{\text{turnover}}$ to optically thin at $\nu \gg \nu_{\text{turnover}}$. Figure: An introduction to Star Formation, D. Ward-Thompson & A.P. Whitworth.

At high frequencies, the emission is optically thin, so we can write, for $\nu \gg \nu_{\text{turnover}}$ and $\tau_\nu \ll 1$

$$I_\nu^{\text{obs}} \simeq B_\nu(T) \tau_\nu \propto \bar{g}_{\text{III}}(\nu, T) T^{-1/2} \mathcal{EM}_H, \quad (17.34)$$

where the Gaunt factor for free-free processes at long wavelengths is given by Eq. 16.29, scaling approximately as $\bar{g}_{\text{III}} \propto \nu^{-0.1}$.

Conversely, at (relatively) low frequencies the emission is optically thick, so we can write, for $\nu \ll \nu_{\text{turnover}}$ and $\tau_\nu \gg 1$

$$I_\nu^{\text{obs}} \simeq B_\nu(T) \simeq \frac{2kT\nu^2}{c^2}. \quad (17.35)$$

Figure 17.2 illustrates a typical free-free continuum spectrum from an H II region. One can clearly identify the two asymptotic forms, and the turnover frequency ν_{turnover} .

From the intensity at low frequencies, where the emission is optically thick, we can obtain an estimate of the gas kinetic temperature (see Eq. 6.48)

$$T \simeq \frac{c^2}{2k\nu^2} I_\nu^{\text{obs}}, \quad (17.36)$$

for $\nu \ll \nu_{\text{turnover}}$.

We can also obtain an estimate of the emission measure from the turnover frequency. The optical depth at the turnover frequency is unity. Hence

$$\mathcal{EM}_H \simeq \frac{56.43}{\bar{g}_{\text{III}}(T, \nu_{\text{turnover}})} T^{3/2} \nu_{\text{turnover}}^2 \quad (17.37)$$

Applying Eq. 17.22 we once again have an estimate of the gas density. Remember that these estimates of n_p and n_e are strictly speaking root-mean-square values averaged along the line-of-sight.

17.7 Collisional excitation of meta-stable levels and forbidden line emission

The strongest lines in the optical spectrum of many H II regions and planetary nebulae are the *forbidden transitions* in the ground $2p^2$ configuration of O III (see figure 14.1 and 17.3). The transition of the excited 1D_2 level to two terms of the ground level, 3P_1 and 3P_2 , produce the eye-catching lines at, respectively, 4959 and 5007 Å. The excitation-potential of the 1D_2 level is only 2.51 eV. The highest term of this configuration is 1S at 5.35 eV above the ground level. Other levels of O III have considerably higher excitation potentials. Transitions between levels in the same configuration are called ‘forbidden’ because they break *Laporte’s parity rule* and are denoted by straight brackets, e.g. $[O\text{ III}]\lambda 5007$. Forbidden transitions usually have small Einstein coefficients A_{ul} . For $[O\text{ III}]\lambda 4949$ en $\lambda 5007$ for instance these are 0.007 and 0.014 sec^{-1} . This implies that the average lifetime of the 1D_2 level of O III is $\langle t \rangle = 1/0.021 = 36$ sec (zie vgl. 7.11). This is extremely long, therefore these excited levels are referred to as *meta-stable*. Similar conditions as for O III occur for other ions, sometimes with even lower transition probabilities.

Why are the forbidden lines in nebulae so strong compared to allowed transitions? To answer this question we must first consider the formation mechanism of these lines. These lines will certainly not be formed by recombination followed by cascade, as in that case one would have expected both lines from high and low levels. However, save for the O III lines that are caused by the Bowen fluorescence mechanism (see section 14.4), all O III lines involving higher levels are extremely weak or absent. Note that the meta-stable levels are only a few eV above the ground level, while all other levels that may cause optical transitions need a high excitation energy. The typical energy of a free electron in the plasma is of the order of an electron volt. The Maxwellian velocity distribution (see figure 6.3) shows that in that case there will still be ample numbers of electrons that have energies of a few electron volts, and even some that will have 5 to 7 eV, though energies of say 20 eV will be extremely rare. Phrased differently, there is a reservoir of free electrons that is capable of exciting ions to meta-stable levels. Once excited these ions can fall back through collisional de-excitation or through forbidden line emission.

Now it may be clear why forbidden lines in the optical spectrum of nebulae dominate. It is because the occupation of the meta-stable levels is relatively high. So high even, that it is only a few orders of magnitude below the TE value – given by Boltzmann equation (6.23). The allowed transitions can not use this collisional excitation mechanism as the relevant excitation potentials are too high (typically 10 to 50 eV). These lines can thus only be formed by means of the ionization/recombination/cascade mechanism. However, this process depends on the strongly diluted stellar radiation field (and not exclusively on local conditions as does the

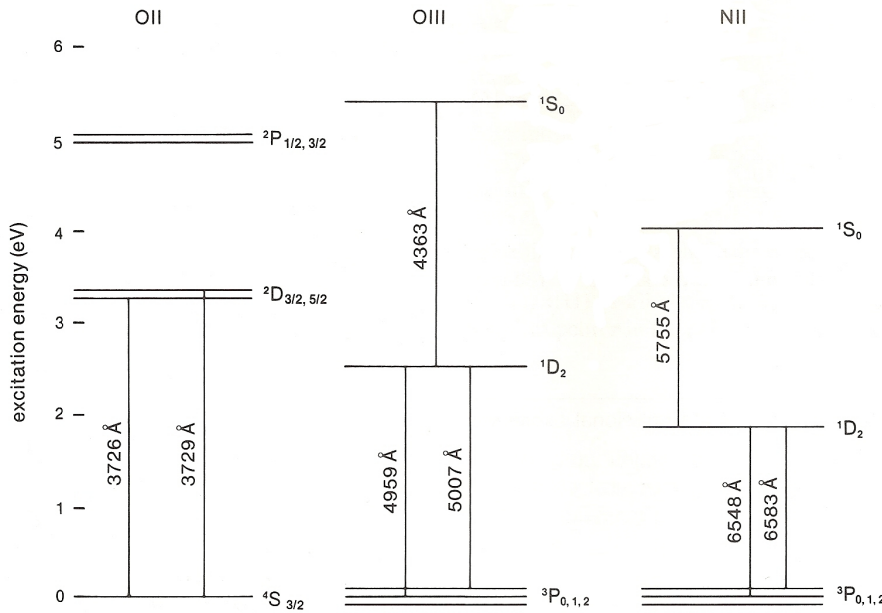


Figure 17.3: The low-lying energy levels of O II, O III and N II. Excitation energies are relative to the ground level of the ion and are given in electron volt. Figure from Bowers & Deeming, Astrophysics II: Interstellar matter and galaxies, 1984.

collisional process). The number of recombinations (or ionizations) per second is thus many order of magnitude lower than in TE; roughly a factor of W . This difference is so large that even though there are thousands of times as many H II ions than O III ions, the Balmer lines are not capable of dominating the [O III] lines. No, observations show that the green [O III] lines in nebular spectra can even be ten to twenty times as strong as H β .

Nebular emission lines as a temperature diagnostic

The forbidden emission lines of O III at $\lambda 4363$, 4959 and 5007 \AA (see figure 14.1 and 17.3) turn out to be very suited for constraining the temperature of the nebular gas. We assume that the electron density of the gas is much less than the critical density (see section 14.3), such that collisional excitations are negligible.

To keep a clear view of the situation we refer to the ground state $^3P_{0,1,2}$ as level 1, the first excited level 1D_2 as level 2, and the second excited level 1S_0 as level 3. This notation ignores that there are two¹ possible transitions from level 2 to 1, namely $^3P_1 - ^1D_2$ ($\lambda 5007\text{ \AA}$) and $^3P_2 - ^1D_2$ ($\lambda 4959\text{ \AA}$), however, we will repair that later. The statistical equilibrium equa-

¹There is a third possibility, namely $^3P_0 - ^1D_2$ ($\lambda 4931\text{ \AA}$), that can only occur by means of a quadrupole transition, but that is so weak that it can be ignored altogether.

tion (9.15) for level 2 is

$$\begin{aligned} n_2 A_{21} &= n_1 C_{12} + n_3 A_{32} \\ &\simeq n_1 C_{12}. \end{aligned} \quad (17.38)$$

This reflects that the n_2 level can be populated either by collisional excitations from the ground level ($n_1 C_{12}$) or by spontaneous radiative de-excitations from level 3 ($n_3 A_{32}$). Note that the second process is negligible relative to the first and can be safely ignored, simplifying the derivation. For level 3 it follows that

$$n_3 (A_{31} + A_{32}) = n_1 C_{13}. \quad (17.39)$$

This level can be populated by collisional excitations from the ground level ($n_1 C_{13}$) or be de-populated by cascade to level 2 ($n_3 A_{32}$) or level 1 ($n_3 A_{31}$). Note that in this case we do not ignore the process $n_3 A_{32}$ as here it contributes significantly to the depopulation of level 3. The ratio of the populations of levels 2 and 3 is now given by

$$\frac{n_2}{n_3} = \frac{(A_{31} + A_{32})}{A_{21}} \frac{C_{12}}{C_{13}} = \frac{(A_{31} + A_{32})}{A_{21}} \frac{\Upsilon_{12} e^{-E_{12}/kT}}{\Upsilon_{13} e^{-E_{13}/kT}} = \frac{(A_{31} + A_{32})}{A_{21}} \frac{\Upsilon_{12}}{\Upsilon_{13}} e^{+E_{23}/kT}, \quad (17.40)$$

where we have used the Maxwellian averaged collisional strength $\Upsilon_{lu}(T)$ (see section 7.1) to describe C_{lu} .

In our spectrum we measure the total line flux (eq. 12.6) of each of the three lines. If we assume that each of the lines is optically thin (such that we do not have to solve the equation of transfer and the situation is similar to, for example, that discussed in section 16.3 for the case of H α emission in stellar winds) the observed line profile integrated flux is given by (see also eq. 7.15)

$$\mathcal{F}_{lu} = \frac{1}{4\pi d^2} \int_V \eta_{lu} dV = \frac{1}{4\pi d^2} \int_V \frac{h\nu_{lu}}{4\pi} n_u A_{ul} dV, \quad (17.41)$$

where d is the distance to the nebula. Because η_{lu} is the line emission coefficient per cm³ we need to integrate over the entire volume V of the nebular gas. We assume the gas has a constant temperature T . Should this not be the case, this assumption will still provide a typical value. A constant temperature assures that the ratio of the line strengths 21 and 32 is the same in each cubic centimeter of the nebula and if we focus on this ratio we thus need not integrate over the whole volume. In this way we obtain for the ratio

$$\begin{aligned} \frac{\eta_{4959} + \eta_{5007}}{\eta_{4363}} &= \frac{h\nu_{4959} A_{4959} + h\nu_{5007} A_{5007}}{h\nu_{4363} A_{4363}} \frac{n_2}{n_3} \\ &= \frac{A_{2321} + A_{4363}}{A_{4959} + A_{5007}} \frac{\nu_{4959} A_{4959} + \nu_{5007} A_{5007}}{\nu_{4363} A_{4363}} \frac{\Upsilon_{12}}{\Upsilon_{13}} e^{+E_{23}/kT} \\ &= \frac{A_{2321} + A_{4363}}{A_{4363}} \frac{\bar{\nu}}{\nu_{4363}} \frac{\Upsilon_{12}}{\Upsilon_{13}} e^{+E_{23}/kT}, \end{aligned} \quad (17.42)$$

where $\bar{\nu}$ is the Einstein A averaged frequency of the 21 transition. Notice that we have again split up the 21 transition in the lines ${}^3P_1 - {}^1D_2$ ($\lambda 5007 \text{ \AA}$) and ${}^3P_2 - {}^1D_2$ ($\lambda 4959 \text{ \AA}$).

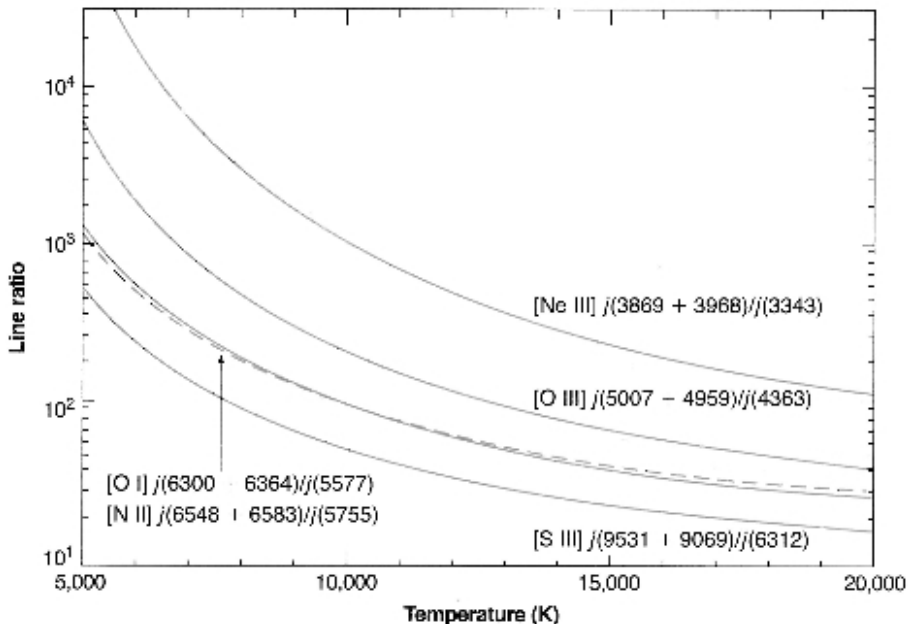


Figure 17.4: Five temperature sensitive forbidden line ratios as function of the electron temperature. The [O I] (solid line) and [N II] (dashed line) are almost superimposed, partly because they have very similar excitation potentials. All ratios shown are in the limit $n_e \ll n_e^{\text{crit}}$ ($n_e = 1 \text{ cm}^{-3}$). Figure from Osterbrock & Ferland, Astrophysics of Gaseous Nebulae and Active Galactic Nuclei, 2006.

This diagnostic is useful for temperatures ranging from 5 000 – 20 000 K (or $\sim 0.5 – 2 \text{ eV}$; see eq. 14.7) and earns this sensitivity to the fact that the energy levels 2 and 3 are some distance apart. If indeed the distance between these levels would have been small, $\exp(E_{23}/kT) \sim 1$ and consequently the line flux ratios would have been insensitive to temperature. There are other ions that have a similar favorable positioning of energy levels and that can be used in a similar fashion to constrain the temperature of warm gaseous nebulae, for instance [N II], [O I], [Ne III], [S III]. Figure 17.4 provides an overview of the relevant lines and shows the sensitivity of these diagnostics in the limit of low electron densities.

Equation 17.42 is a good approximation up to $n_e \sim 10^5 \text{ cm}^{-3}$. At higher electron densities collisional de-excitations start to play a role (see also the discussion on the critical density in section 14.3). The ${}^1\text{D}$ term has a considerably longer lifetime than ${}^1\text{S}$, and therefore will be de-populated at a lower n_e by collisional de-excitations, causing a weakening of the $\lambda 4959$ and $\lambda 5007$ lines. What starts to play a role at electron densities above the value given previously are collisional excitations from ${}^1\text{D}$ to ${}^1\text{S}$. This strengthens the emission from $\lambda 4363$. A proper description of this problem requires the solution of the statistical equilibrium equation (9.15), however, an analytical solution that is correct to within first order in $\exp(-\Delta E_{23}/kT)$ is

$$\frac{\eta_{4959} + \eta_{5007}}{\eta_{4363}} = \frac{7.90 \exp(3.29 \times 10^4/T)}{1 + 4.5 \times 10^{-4} n_e/T^{1/2}} \quad (17.43)$$

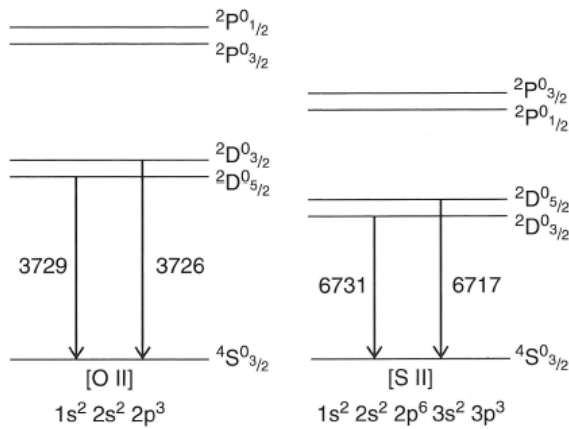


Figure 17.5: Energy-level diagram of the $2p^3$ ground configuration of $O\text{ II}$ and $3p^3$ ground configuration of $S\text{ II}$, relevant for the formation of forbidden $[O\text{ II}]$ and $[S\text{ II}]$ lines. Note that the fine-structure levels $^2D^o_{3/2,5/2}$ and $^2P^o_{1/2,3/2}$ (the energy separation of the different J -levels is exaggerated for clarity) are switched around in these two ions.

In the second edition of Osterbrock & Ferland similar approximations are given for $[N\text{ III}]$, $[Ne\text{ III}]$, en $[S\text{ III}]$. Note that the correction term for the electron density is very small. Even if only a rough estimate of n_e is used, very reasonable estimates for T can be made. Giving eq. (17.43) some thought one must admit that it is a fascinating result: the temperature of the nebular gas can be derived without any knowledge of the local radiation field, the distance to the nebula, and (often) the local electron density.

Nebular emission lines as a density diagnostic

An estimate of the electron density n_e in the rarefied nebular gas can be made by determining the ratio of the line strengths of forbidden transitions in the ground configuration of ions with very comparable excitation energy (contrary to what is required for a good T -diagnostic, see the discussion about $[O\text{ III}]$). The two best examples of such a situation are $[O\text{ II}] \lambda 3729 / \lambda 3726$ en $[S\text{ II}] \lambda 6716 / \lambda 6731$ ².

We again take oxygen as an example. To keep a clear view of the situation we refer to the ground level $^4S^o_{3/2}$ as level 1, the first excited level $^2D^o_{5/2}$ as level 2, and the second excited level $^2D^o_{3/2}$ as level 3. The two highest terms in the ground level configuration, $^2P^o_{1/2,3/2}$, need not be considered. In formulating the relevant statistical equilibrium equations (9.15) we consider collisional excitations, collisional de-excitations and spontaneous de-excitations. Note that we ignore the (forbidden) transition $^2D^o_{3/2} - ^2D^o_{5/2}$. Though this is a good approximation for the radiative transition between these two fine structure levels it is not so for the collisional coupling. However, in the two limiting situations $n_e \rightarrow 0$ and $n_e \rightarrow \infty$ this is not a

²Notice that for the oxygen line the line ratio is longest wavelength / shortest wavelength of the doublet while this is reversed in case of sulphur. This is because in these ions the $^2D^o_{3/2,5/2}$ are interchanged, see figure 17.5.

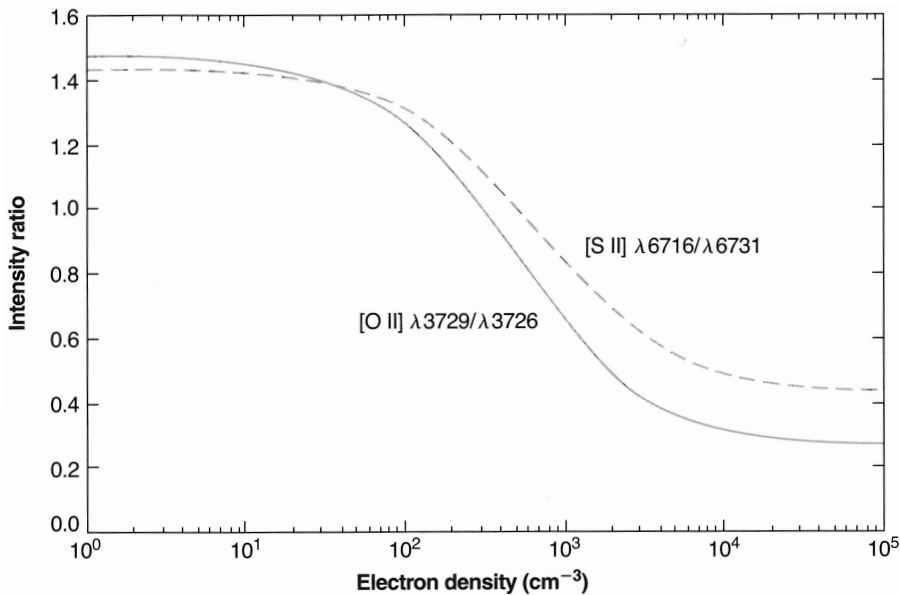


Figure 17.6: Statistical equilibrium calculation of line ratios for $[O\text{ II}]$ (solid line) and $[S\text{ II}]$ (dashed line) as a function of n_e for a temperature $T = 10\,000\text{ K}$. At other temperatures the relations shown are nearly correct if one assumes the horizontal scale represents $n_e(10^4/T)^{1/2}$.

problem: in the first instance these collisions are indeed negligible; in the second instance the two levels (2 and 3) will be in LTE relative to each other. This is automatically taken care of by considering the collisional transitions between 1–2 and 1–3. SE calculations of arbitrary n_e , however, do require a consideration of the ${}^2\text{D}_{3/2}^\circ - {}^2\text{D}_{5/2}^\circ$ coupling.

In this case the statistical equilibrium equation for level 2 is

$$n_2(A_{21} + C_{21}) = n_1 C_{12}. \quad (17.44)$$

That for level 3 is

$$n_3(A_{31} + C_{31}) = n_1 C_{13}. \quad (17.45)$$

For the ratio between the line strengths 21 and 31 it follows that

$$\begin{aligned} \frac{\eta_{21}}{\eta_{31}} &= \frac{\eta_{3729}}{\eta_{3726}} = \frac{n_2 A_{21} h\nu_{21}}{n_3 A_{31} h\nu_{31}} \simeq \frac{A_{21}}{A_{31}} \frac{C_{12}}{C_{13}} \frac{(A_{31} + C_{31})}{(A_{21} + C_{21})} = \frac{A_{21}}{A_{31}} \frac{C_{12}}{C_{13}} \frac{C_{31}}{C_{21}} \frac{(A_{31}/C_{31} + 1)}{(A_{21}/C_{21} + 1)} \\ &\simeq \frac{A_{21}}{A_{31}} \frac{g_2}{g_3} \frac{(A_{31}/C_{31} + 1)}{(A_{21}/C_{21} + 1)}. \end{aligned} \quad (17.46)$$

The approximately equal sign denotes that $\nu_{21} \simeq \nu_{31}$. For the last equality we have used eq. (7.7) and realized that $E_{12} \simeq E_{13}$.

We first consider the limiting situation $n_e \rightarrow 0$, in which case each collisional excitation is followed by the emission of a photon. One obtains $\eta_{3729}/\eta_{3726} = C_{12}/C_{13} = \Upsilon_{12}/\Upsilon_{13} =$

$\Omega_{12}/\Omega_{13} = 6/4$, where Ω_{lu} is the energy specific collisional strength³. The energy specific collisional strength *de facto* scales with the statistical weight of the upper level⁴. In the high density limit, that for $^2D_{5/2}^\circ$ is reached at $n_e^{\text{crit}} \sim 3 \times 10^3 \text{ cm}^{-3}$ and for $^2D_{3/2}$ at $n_e^{\text{crit}} \sim 1.6 \times 10^4 \text{ cm}^{-3}$, it follows that $\eta_{3729}/\eta_{3726} = A_{21} g_2/A_{31} g_3 = 0.34$.

Figure 17.6 shows the behavior of η_{3729}/η_{3726} as function of n_e for the exact solution of the SE equations, also accounting for collisional excitations to the $^2P_{1/2,3/2}^\circ$ levels.

³ Ω_{lu} is related to the collisional cross section through $\sigma_{lu}(v) = (\pi \hbar^2 / m_e^2 v^2) \Omega_{lu} / g_l$; see section 7.1.

⁴It holds that $g_J = 2J + 1$.

18

ISM and IGM

The medium in-between the stars of our Milky Way is filled with interstellar matter. About 99 percent of the mass of this material is due to gas and about 1 percent due to solid state particles. The gas may be in an atomic, ionized, or (ionized) molecular state. The typical sizes of interstellar solid state particles are 0.01 to 0.1 μm , although grains up to a few micron in diameter may be present as well. Though only responsible for a very small fraction of the mass of interstellar matter, it is the extinction properties of these dust particles that most affect the stellar light traveling through interstellar space. We briefly discuss the impact of interstellar gas on the appearance of the spectra of stars. Most of the chapter, however, concentrates on the effect that interstellar dust can have on the stellar energy distribution. We will not care much about the origin and nature of this dust, nor the processes that shape its properties.

18.1 Introduction

Interstellar absorption lines

Stellar spectra may contain lines that originate from material in the interstellar medium. These *interstellar absorption lines* become stronger in more distant stars as the result of superpositioning of an increasing number of interstellar clouds. When the spectral resolution and signal-to-noise are high enough to resolve these multiple structures one often finds differences among lines of different elements, demonstrating that there are differences between clouds.

The interstellar lines originate from ground-level (resonance) transitions. Examples of well known interstellar lines are C IV $\lambda\lambda 1548, 1551$, Mg II $\lambda\lambda 2796, 2803$ in the ultraviolet part of the spectrum, and Ca I $\lambda 4227$, Mg I $\lambda 4571$, and Na I $\lambda\lambda 5890, 5896$ in the optical. Interstellar lines may also be due to molecules, such as, in the optical, NH, CH, CH⁺, CN and C₂.

It is not always trivial to distinguish interstellar lines from the, often, plentiful stellar lines. Hints that point to lines originating in the interstellar medium, rather than in the stellar atmosphere or in a strictly circumstellar region are:

- Certain absorption lines are seen in the spectra of distant stars, but are not seen in the spectra of otherwise very similar nearby stars.
- Certain absorption lines seen in stellar spectra are due to species which are not anticipated to be present in the atmosphere of the background star. Usually they are species expected to be in a lower or higher stage of ionization or to be dissociated at the temperatures and densities of the background source.
- Certain absorption lines seen in stellar spectra are too narrow to have been produced in a stellar atmosphere. The thermal width of a spectral line is given by Eq. 12.21. The typical temperatures in stellar atmospheres are much higher than those of the bulk of the interstellar medium, that is rather cold. Additional broadening may cause the stellar lines to be even wider. Perhaps the easiest way to separate the interstellar lines from the stellar lines is to observe stars that are rotating rapidly enough to make their lines wash out (see Sect. 12.3).
- The central frequency of an absorption line may indicate that the absorbing gas has a different radial velocity from the background star. The existence of interstellar gas was first unambiguously confirmed from observations of a spectroscopic binary. The central frequencies of the absorption lines produced in the stellar atmosphere shifted with a regular period, as the star orbited its companion. The central frequencies of the absorption lines produced in the intervening interstellar medium were constant.
- Often close groups of absorption lines are observed, with all the lines in a group being attributable to the same transition in the same species. The inference is that the absorbing particles are not distributed uniformly along the line of sight to the background star, but are concentrated in discrete clouds having different bulk radial velocities. The number of lines in a group tends to be larger for more distant stars as, on average, the number of intervening clouds increases with the distance to the background star.

Discrete Interstellar Bands

In the optical part of the spectrum there are over a hundred rather weak absorption bands. Though these bands are already known since the 1930s, their carriers are still not identified. The bands are known as the *Diffuse Interstellar Bands* or DIBs. The wavelengths of the DIBs range from the blue (for instance the strongest one at 4428 Å) to the far red (e.g. the one at 8650 Å). There are indications for different sets of bands. This may imply that not all bands are caused by the same material. In many cases the strength of the diffuse bands are correlated with the amount of interstellar absorption by dust. This suggests that the material that is responsible for the interstellar absorption is also responsible for the diffuse bands, or that the material that caused the DIBs is well mixed with the interstellar dust. Surprisingly enough, there is no evidence for the presence of DIBs in *circumstellar dust*, i.e. dust in the direct surroundings of a star, or in comets. Apparently the diffuse bands are a purely interstellar phenomenon.

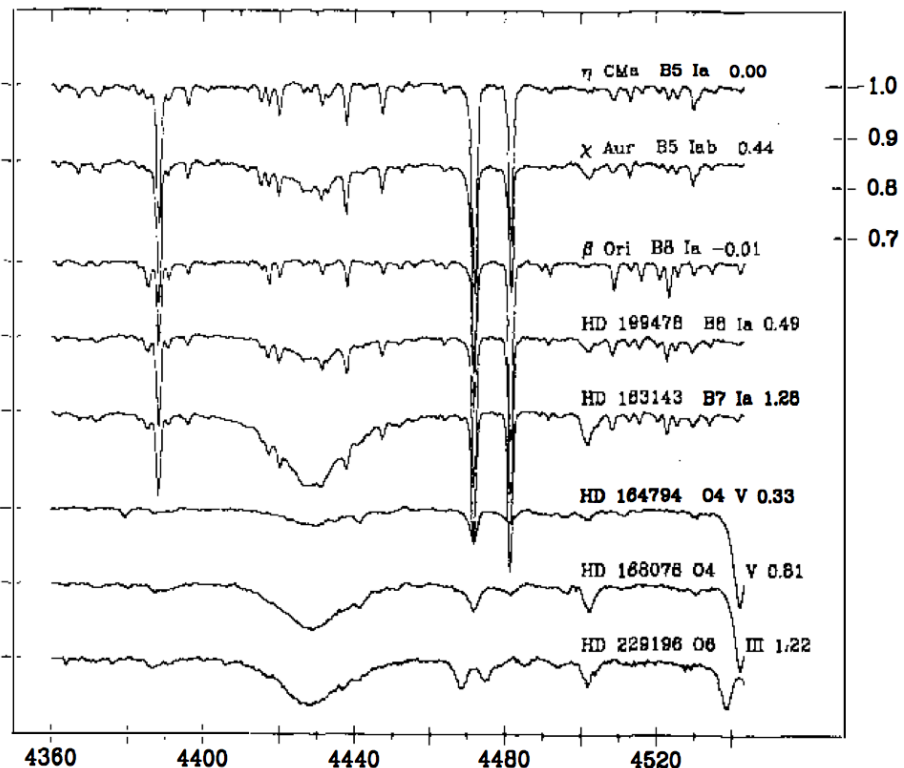


Figure 18.1: The spectral region containing the diffuse band at $\lambda 4428 \text{ \AA}$ in both weakly and strongly reddened stars. Spectral types and $E(B-V)$ values appear on the right. All spectra have been shifted in wavelength so that their stellar lines coincide. For similar spectral type and luminosity class unreddened and reddened spectra have been included. The broad $\lambda 4428$ feature is more apparent in the reddened stars, as is the DIB at $\lambda 4501$, although the latter is blended with stellar Ti II lines in the B stars. The lowermost star, HD 229196, is a double-line spectroscopic binary with a line splitting of about 400 km sec^{-1} . From: Herbig, G.H., 1995, ARA&A 33, 19.

The prevailing suspicion at the moment is that the carriers are complex, carbon-based (i.e. "organic") molecular structures, possibly Poly-Aromatic Hydrocarbons (PAHs); they are probably ionized and perhaps protonated. Strangely enough, PAHs features *are* seen in spectra of circumstellar envelopes and cometary tails, where DIB features are conspicuously absent.

Interstellar dust

The existence of solid state material between the stars was first proposed by Wilhelm Struve in 1847 based on the analysis of star counts which suggested that the number of stars per unit volume decreased with increasing distance from the sun. Struve proposed that the starlight was experiencing absorption proportional to distance. It was not until 1909 that Kapteyn realized the full significance of this interstellar extinction. Shortly thereafter Barnard documented

the irregular variations in the distribution of the absorbing matter. The identification of small solid state particles as the source of this extinction was finally accepted in the 1930s through the work of Trumpler and Stebbins, Huffer, and Whitford.

The properties of the interstellar particles can be studied through their emission, scattering, and absorption properties. The most abundant dust particles are composed of either amorphous silicates or carbon. The latter probably is in the form of graphite. The silicates have a chemical composition that is about that of olivine ($Mg_xFe_{2-x}SiO_4$ where $0 \leq x \leq 1$) and can be spectroscopically identified by emission or absorption bands at ~ 9.7 and $18 \mu\text{m}$, though these grains absorb quite effectively over a wavelength interval that extends from the ultraviolet to the far-infrared. The graphite grains too show this broad continuum absorption and are likely responsible for an absorption band at 2175 \AA . In regions where the interstellar particle density is relatively high, i.e. in molecular clouds, water ice may freeze on the dust particles, causing an absorption at $\sim 3.08 \mu\text{m}$. Absorption by solid carbon monoxide at $\sim 4.08 \mu\text{m}$ is often observed in molecular clouds.

18.2 Continuum extinction by interstellar dust

We consider the line of sight towards a star that emits an intensity I_λ^* . If the optical depth in the ISM inbetween us and the star is τ_λ , the observed intensity will be given by

$$I_\lambda(0) = I_\lambda^* e^{-\tau_\lambda} \quad (18.1)$$

The amount of extinction of starlight is often expressed in magnitudes. If we introduce

$$A_\lambda \equiv m - m_\circ \quad (18.2)$$

where m_\circ is the intrinsic magnitude of the stellar light, we find for the relation between extinction and optical depth

$$A_\lambda = -2.5 \log \left[\frac{I_\lambda(0)}{I_\lambda^*} \right] = 1.086 \tau_\lambda \quad (18.3)$$

This equation shows that the extinction of starlight by dust expressed in magnitudes is almost equal to the optical depth (at the chosen wavelength).

Interstellar extinction law

The wavelength dependence of the interstellar extinction in the direction of three stars is shown in figure 18.2, where A_λ/A_V is the interstellar extinction normalized to the photometric V band. The functional behaviour of this quantity is referred to as the *interstellar extinction law*. It only depends on the (mean) intrinsic properties of dust particles in the beam towards the

star, and not on the length of the beam. The use of A_V , the extinction in the V band (see § 6.6) to normalize the extinction law is arbitrary and one could argue that it is more meaningful to use, for instance, the extinction in the I or J filter (centered around ~ 0.9 and $1.25\ \mu\text{m}$ respectively) as for these wavelengths the extinction is almost independent of the direction in which we look. Detailed analysis of the extinction law in many directions shows that the behaviour of A_λ/A_V can well be described with only one free parameter, the *total-to-selective extinction*

$$R_V \equiv \frac{A_V}{A_B - A_V} = \frac{A_V}{E(B-V)} \quad (18.4)$$

The *selective extinction* is formally defined as $E(\lambda_1 - \lambda_2) \equiv A_{\lambda_1} - A_{\lambda_2}$ (see also eq. 18.6). Observed values of R_V are in between ~ 2.75 and 5.5 . As this number is always positive, it implies that the extinction in the B band is always larger than that in the V band. This can also be seen in figure 18.2. We will return to this below. For dust particles in the diffuse (read: typical) interstellar medium one typically derives $R_V \sim 3.1$. Larger values of R_V are found in lines of sight towards dense molecular clouds. A larger value for R_V implies a decrease of A_B/A_V . This is equivalent to an increase of the “greyness” of the extinction. A grey(er) extinction is characteristic for relatively large dust grains, and the tendency to find relatively large values of R_V in directions in which the interstellar medium has a larger density therefore strongly suggests that the dust particles in these clouds are relatively large. How large is relatively large? The behaviour of the extinction of light on solid state particles is dependent on the value $2\pi a/\lambda$, where a is the radius of the grain. For $2\pi a/\lambda \gg 1$ the extinction is grey as the cross section of the particle reaches its geometrical surface πa^2 ; for $2\pi a/\lambda \lesssim 1$ the extinction properties are complex, however usually they are proportional to λ^{-2} to λ^{-1} ; only for $2\pi a/\lambda \ll 1$ the wavelength dependence becomes that of Rayleigh scattering, i.e. λ^{-4} . Relatively large therefore implies $a \sim 1\text{--}2\ \mu\text{m}$. The “growth” of dust particles occurs through coagulation, i.e. the sticking of grains in collisions.

The strongest spectroscopic feature in the extinction curve is a conspicuous “bump” at $2175\ \text{\AA}$ or $4.6\ \mu\text{m}^{-1}$. This feature is visible for all values of R_V . Its origin is not well understood. In view of the prominent nature of the bump it must be formed by an abundant material. Graphite, an ordered and stable form of carbon, has a strong resonance at $2175\ \text{\AA}$ with about the correct width and strength to explain the bump. While identification of the $2175\ \text{\AA}$ bump is still not certain, many ascribe it to graphite or perhaps a somewhat less ordered form of carbon.

One might think that the large differences in the ultraviolet and optical part of the extinction curve are also present in the near infrared (from ~ 1 to $3\ \mu\text{m}$). This is not the case. Measurements in the Johnson J ($1.25\ \mu\text{m}$), H ($1.66\ \mu\text{m}$), and K ($2.2\ \mu\text{m}$) filters show that ratio of the selective extinctions $E(J-H)/E(H-K) \sim 1.6$, irrespective of the chosen line of sight. It is further found that the extinction in the near-IR can well be described by a power law

$$\frac{A_\lambda}{A_J} = \left(\frac{\lambda}{1.25\ \mu\text{m}} \right)^{-\alpha} \quad (18.5)$$

From the measured ratio of the selective extinctions it follows that $\alpha = 1.7 \pm 0.1$. The universal nature of the extinction law in the near-IR implies that the size distribution of the

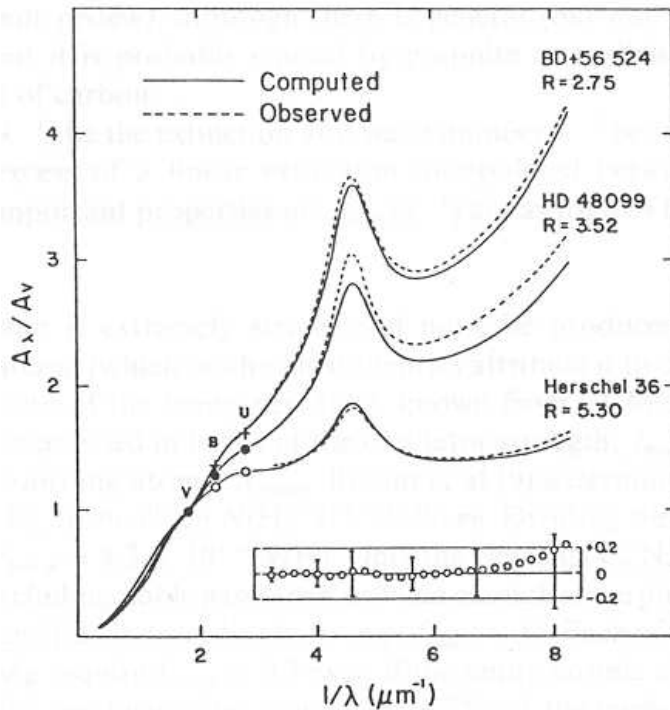


Figure 18.2: The measured wavelength dependence of the interstellar extinction for three directions into the ISM (dashed lines). The extinction is normalized to the value in the V band (5500 \AA). The extinction in the direction of Herschel 36 – the ionizing star in the $H\text{ II}$ region M8 – is considered “peculiar”. The full lines are fits to the measured A_λ/A_V .

largest grains is similar in all directions. For wavelengths larger than $\sim 5 \mu\text{m}$ the extinction is not well known. Beyond a wavelength of $20 \mu\text{m}$ the uncertainty in the extinction is probably a factor of two. Realize that this far into the infrared the extinction is often negligible anyway.

Interstellar reddening

We saw that at wavelengths larger than 2175 \AA the extinction decreases with increasing wavelength. Blue starlight therefore suffers more from dust in the ISM than does red starlight, causing a *reddening* of the spectral energy distribution emitted by the star. The amount of reddening is often expressed in terms of the visual selective extinction or *color excess*

$$E(B-V) = A_B - A_V = (B-V)_{\text{obs}} - (B-V)_0 \quad (18.6)$$

where $(B-V)_{\text{obs}}$ is the measured and $(B-V)_0$ the intrinsic color of the star. In our Milky Way the interstellar dust is concentrated in the galactic plane, with an effective scaleheight of about 100 pc. The mean reddening in the plane is about $0.61 \text{ magn kpc}^{-1}$. If we take $R_V = 3.1$ we get an $A_V = 1.9 \text{ magn kpc}^{-1}$. Beware that in reality the distribution of dust is very

patchy, i.e. concentrated in small and large interstellar clouds, and that there are directions in which the reddening deviates a factor of 5 to 10 from the mean. Measurements of the correlation between the column density of gas and the interstellar reddening yield an average gas-to-color-excess ratio $N(\text{H I} + \text{H}_2)/E(B-V) = 5.8 \cdot 10^{21}$ atoms cm⁻² magn⁻¹, where $N(\text{H I} + \text{H}_2) = N(\text{H I}) + 2N(\text{H}_2)$. For atomic hydrogen only the mean value is $N(\text{H I})/E(B-V) = 4.8 \cdot 10^{21}$ atoms cm⁻² magn⁻¹.

In view of the distribution of dust in our Milky Way interstellar reddening is particularly problematic for stars located in the galactic plane, i.e. population I stars, and that are at reasonably large distances. However, also (young) stars in star forming regions can suffer from a large extinction due to dust grains in the molecular clouds from which these stars have recently (up to a few million years ago) formed. Part of the extinction of starlight in star forming regions can be caused by *circumstellar dust*, i.e. dust in the direct surroundings of a young star. The extinction curve of this circumstellar dust can deviate strongly from that of ISM dust. The reason for this is that the proximity of the central star and the potential high density of the circumstellar material can lead to chemical alteration, crystallization or coagulation of the grains. This affects the extinction properties. A different category of stars that may suffer strongly from circumstellar extinction are red giants and supergiants. In the stellar winds of these cool stars dust may actually condense. The (super)giants with extremely strong stellar winds ($\dot{M} \sim 10^{-4} \text{ à } 10^{-3} M_{\odot} \text{yr}^{-1}$) can form such large amounts of circumstellar dust that they can no longer be observed in the optical – though they can still be observed in the infrared. One may expect that the extinction curves of these so-called OH/IR stars differ strongly from that of ISM dust.

Reddening in the color-color diagram

For the typical interstellar medium, which has $R_V = 3.1$ magn, the color excess $E(U-B)$ scales linearly with $E(B-V)$, following

$$E(U-B) = 0.72 E(B-V) \quad (18.7)$$

Consequently the quantity

$$Q = (U-B) - 0.72(B-V) \quad (18.8)$$

for any star is independent of the reddening in the direction of the star, provided the star suffers no additional circumstellar extinction.

Affection of the spectrum by interstellar reddening

The effect of interstellar reddening on the color indices $U-B$ and $B-V$ is shown in figure 18.3. As an example we show the effect that corresponds to a visual extinction $A_V = 1$. The open symbols denote the intrinsic colors; filled symbols are for reddened colors. If, say, the only thing we have available for a star are photometric measurements in UBV , and if we would assume that interstellar extinction is negligible, we would, for instance, wrongly

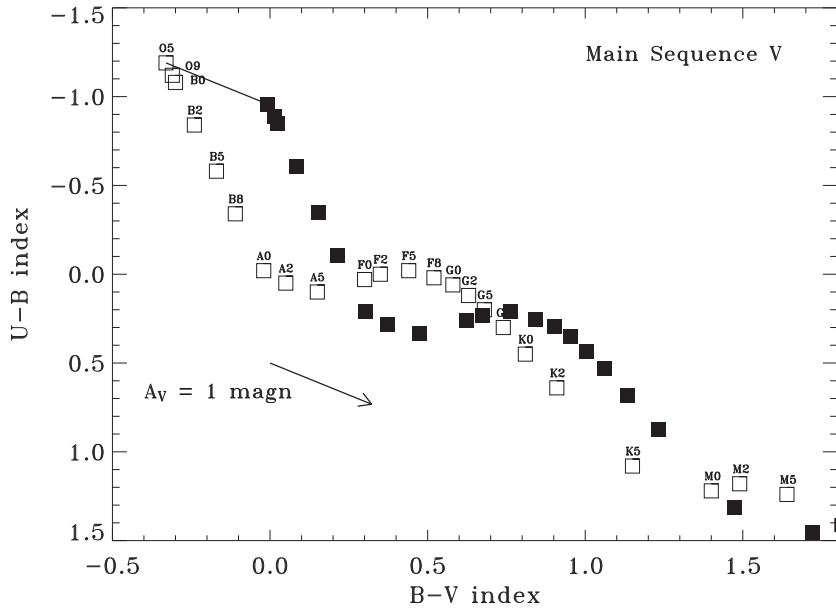


Figure 18.3: Relation between the color indices $U-B$ and $B-V$ for dwarf stars (luminosity class V). The open symbols denote the intrinsic colors; the filled symbols are the observed colors for an interstellar extinction $A_V = 1$ magn. To a certain extent, one could say that interstellar reddening simulates a lower T_{eff} .

classify an F2 V star as a G5 V star if in reality $A_V = 1$ magn. Phrased differently, if one erroneously neglects interstellar reddening one will underestimate the effective temperature of the star.

Figure 18.4 shows the effect of interstellar reddening on the spectrum of a G5 V star. In the top panel the flux is plotted on a linear scale, such that it is clearly visible that for $A_V = 1$ magn the observed optical flux at 5500 Å (i.e. in the V band) is only $\exp(-1/1.086) \sim 0.4$ times the intrinsic value, i.e. the starlight at this wavelength is weakened by a factor 2.5. The lower panel (in which the flux is given on a logarithmic scale) again shows that due to a more efficient extinction at short wavelengths the stellar spectrum will be reddened, and that if the extinction is very large only stellar light at infrared or even longer wavelengths can be observed.

There are different ways to measure the amount of interstellar extinction towards a star. In all cases it is important that the optical spectrum of the star is available, such that its spectral type, and, ideally, its luminosity class can be determined.

- If the spectral type and luminosity class are known, the intrinsic $(B-V)_0$ can be obtained from table A.1. Measurement of $B-V$ then yields $E(B-V)$ (see eq. 18.6). This

method does not constrain the value of R_V .

- A Kurucz or other model, or an observed spectrum of a nearby non-reddened star that is characteristic of the spectral energy distribution of the star of interest (to be determined from the known spectral type & luminosity class), is artificially reddened and fitted to the measured UBVRI broadband photometry. The interstellar extinction can e.g. be described by the fit formula given by Cardelli et al. (1989, ApJ 345, p245). In principle, this method can provide some information on the value of R_V .
- A measured spectrum, from the UV to the near-IR, is divided by a representative intrinsic spectrum (observed or predicted – see previous method). This provides detailed information on the interstellar extinction curve in the line of sight towards the target star (see eq. 18.3).

18.3 Dust in and in-between galaxies

Dust not only resides in the interstellar medium of our Milky Way, but is a property of galaxies in general. Just as the dust in our galaxy betrays its presence by causing dark silhouette structures (by blocking the light from stars located behind these structures), dust in other galaxies also produces such silhouettes (see figure 18.5). If we observe individual stars in other galaxies, and we correct for dust in our Milky Way, we also see the wavelength dependent extinction that is so characteristic for small solid state particles. A third way to prove the presence of interstellar dust in other galaxies is to focus on the thermal emission that this material produces. Heated by the stars in the galaxy, or by non-thermal radiation from the central parts of the system, dust will emit at infrared wavelengths. This last detection method of dust in other galaxies has shown itself to be especially successful in the study of distant galaxies, that can not be resolved spatially.

The study of the dust extinction laws in the Magellanic Clouds is especially intriguing as the interstellar gas in both these satellite galaxies has elemental abundances that are different from those in our Galaxy. For instance, the abundance of oxygen in the Large Magellanic Cloud is about a factor of two lower than in our Milky Way, while that in the Small Magellanic Cloud is even lower by about a factor of five. Such differences in the chemical abundance pattern of the interstellar gas may hint to possible differences in the interstellar dust population, and hence in the extinction laws of our two satellites. It is found that the shape of the extinction law is strongly dependent on the line of sight that is probed (even within the LMC or SMC). For the Large Magellanic Cloud some lines of sight show a similar extinction curve as derived for our galaxy. But there are also directions within the LMC for which the bump in the extinction around 2175 Å is weaker and the rise in extinction to the far ultraviolet is steeper. In the case of the SMC the extinction law lacks the 2175 Å bump. For this system the extinction law in the near infrared, optical, and ultraviolet is reasonably well represented by a single power law.

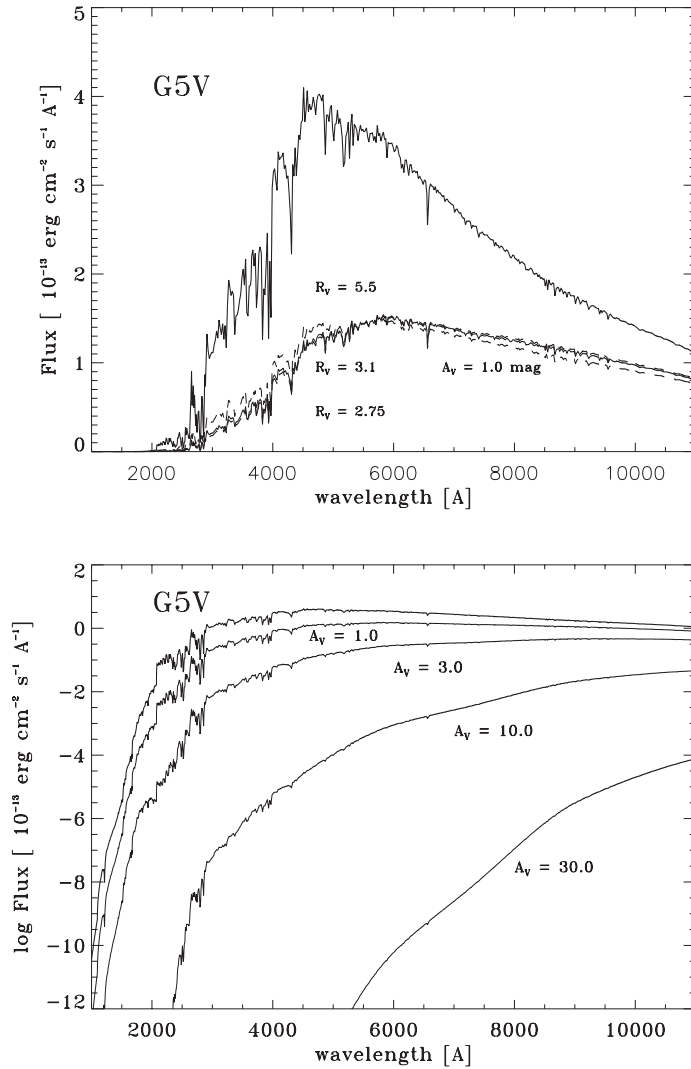


Figure 18.4: Examples of the effect of interstellar reddening on the energy distribution of a G5 V star. The top panel shows the flux on a linear scale; the bottom panel on a logarithmic scale. To describe the extinction curve we adopted the fit formula by Cardelli et al. (1989; ApJ 345, p245) using $R_V = 3.1$.

Is there *intergalactic dust*, i.e. are there solid state particles residing in the space between galaxies? The existence of such dust could have severe consequences for, for instance, the cosmological distance scale, and potentially be an important source of dark matter. So far, however, it has not been found. The search for any intergalactic dust can – as in the case of dust in the ISM – be conducted in three ways: by looking at effects of extinction, obscuration, or infrared emission. There might be dust grains between galaxies that are part of a cluster of galaxies. It would be relatively easy to look for this *intracluster dust* (that following our

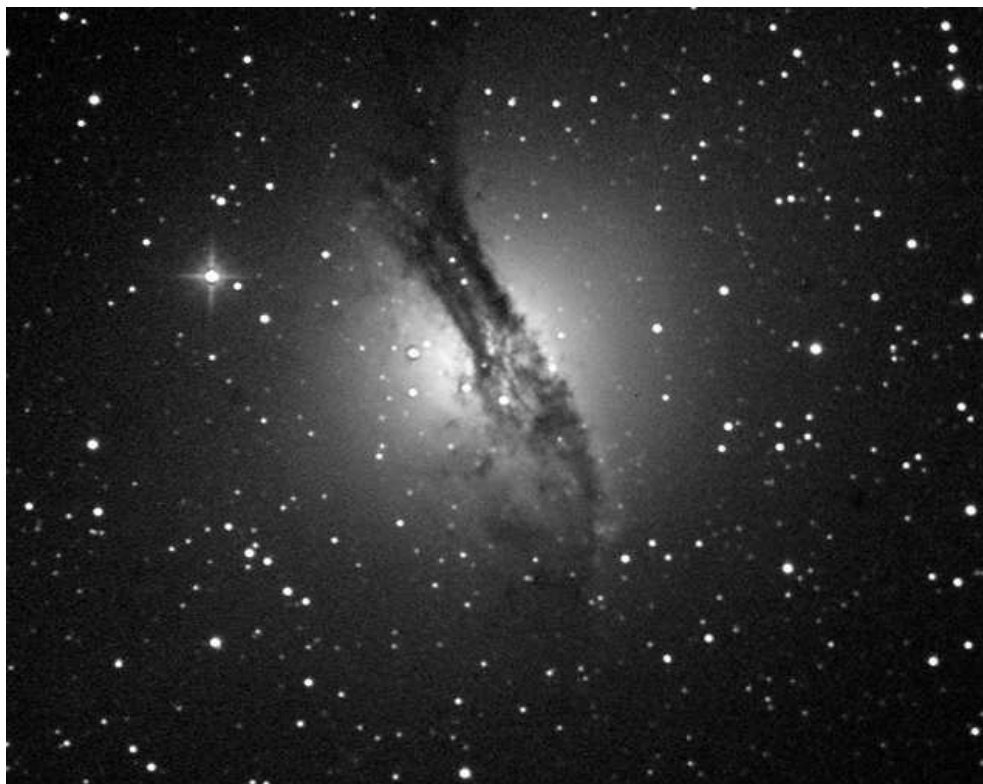


Figure 18.5: The irregular galaxy NGC 518 (Centaurus A), at a distance of 4.6 Mpc, shows a dark band that is the result of the absorption of starlight by interstellar dust grains present in the system. The dust lane is possibly the remnant of the merging of this system with a smaller spiral galaxy, a few billion years ago. The collision also caused an explosive increase in the star forming activity (a so-called starburst).

definition should also be classified as intergalactic dust) if only for the fact that one knows where to look for it. One possibility is to investigate whether distant galaxies seen through a nearby cluster seem fainter and/or redder compared to distant galaxies in lines of sight that do not cross the cluster. Alternatively, one could use the idea that extinction by intracluster gas may render distant background galaxies so faint that they are no longer visible. If so, one would detect a deficiency of faint galaxies in the direction of nearby clusters.

If intergalactic dust truly exist, it may lead to a relation between intrinsic brightness and/or color of galaxies as a function of distance. For example, do quasars of higher redshift appear redder than those of lower redshift? A complicating problem in detecting dust grains in intergalactic space is disentangling the effects of such IGM dust from evolutionary effects in the systems used as probes. After all, changes in the colors of galaxies on very long timescales (billions of years) may also be caused by changes in, for instance, the stellar population and/or amount of interstellar dust in these systems. An alternative method to detect IGM dust would be to use the scattering properties of dust grains at röntgen (*X-ray*) wavelengths. Quasars,

for instance, are very bright in X-rays and should possess detectable X-ray halo's if the intergalactic medium contains a sizeable amount of grains. Such haloes have yet to be searched for. One might also study the distribution of galaxies on the sky: are there "holes" in this distribution (akin to those originally found by Herschel in the distribution of stars). The distribution of nearby galaxies do indeed show such gaps. However, if these gaps are due to clouds of intergalactic dust one ought to find that they are also devoid of more distant galaxies. This is not the case, which is contrary to what one would expect if the gaps were due to clouds of intergalactic dust. One problem with the above described method to search for IGM dust is that on very large scales the three-dimensional distribution of clusters of galaxies is far from uniform and consists of large so-called *voids* with clusters draped around these voids. Clearly this means of searching for intergalactic dust is not likely to be fruitful.

Appendix

List of Tables

- A.1 Calibration of the MK spectral type including their color indices.
- A.2 Temperature calibration of the MK spectral types for different luminosity classes.
- A.3 Luminosity calibration of the MK spectral types for different luminosity classes.
- A.4 Limb darkening coefficients for Kurucz model atmospheres for solar-type stars.
- A.5 Kurucz-model atmospheres for solar composition stars
- A.6 The most important Fraunhofer lines from the Sun

Sp	M_V	$B-V$	$U-B$	$V-R$	$R-I$	$V-K$	$J-H$	$H-K$	$K-L$	T_{eff}	BC	$\log L$
MAIN SEQUENCE, V												
O5	-5.7	-0.33	-1.19	-0.15	-0.32					42 000	-4.40	5.940
O9	-4.5	-0.31	-1.12	-0.15	-0.32	-0.87	-0.14	-0.04	-0.06	34 000	-3.33	5.032
B0	-4.0	-0.30	-1.08	-0.13	-0.29	-0.83	-0.12	-0.04	-0.06	30 000	-3.16	4.764
B2	-2.45	-0.24	-0.84	-0.10	-0.22	-0.66	-0.09	-0.03	-0.05	20 900	-2.35	3.820
B5	-1.2	-0.17	-0.58	-0.06	-0.16	-0.42	-0.06	-0.01	-0.04	15 200	-1.46	2.964
B8	-0.25	-0.11	-0.34	-0.02	-0.10	-0.24	-0.03	0.00	-0.04	11 400	-0.80	2.320
A0	+0.65	-0.02	-0.02	0.02	-0.02	0.00	0.00	0.00	0.00	9 790	-0.30	1.760
A2	+1.3	+0.05	+0.05	0.08	0.01	0.14	0.02	0.01	0.01	9 000	-0.20	1.460
A5	+1.95	+0.15	+0.10	0.16	0.06	0.38	0.06	0.02	0.02	8 180	-0.15	1.180
F0	+2.7	+0.30	+0.03	0.30	0.17	0.70	0.13	0.03	0.03	7 300	-0.09	0.856
F2	+3.6	+0.35	+0.00	0.35	0.20	0.82	0.17	0.04	0.03	7 000	-0.11	0.504
F5	+3.5	+0.44	-0.02	0.40	0.24	1.10	0.23	0.04	0.04	6 650	-0.14	0.556
F8	+4.0	+0.52	+0.02	0.47	0.29			0.05		6 250	-0.16	0.364
G0	+4.4	+0.58	+0.06	0.50	0.31	1.41	0.31	0.05	0.05	5 940	-0.18	0.212
G2	+4.7	+0.63	+0.12	0.53	0.33	1.46	0.32	0.05	0.05	5 790	-0.20	0.100
G5	+5.1	+0.68	+0.20	0.54	0.35			0.06	0.05	5 560	-0.21	-0.056
G8	+5.5	+0.74	+0.30	0.58	0.38					5 310	-0.40	-0.140
K0	+5.9	+0.81	+0.45	0.64	0.42	1.96	0.45	0.08	0.06	5 150	-0.31	-0.336
K2	+6.4	+0.91	+0.64	0.74	0.48	2.22	0.50	0.09	0.07	4 830	-0.42	-0.492
K5	+7.35	+1.15	+1.08	0.99	0.63	2.85	0.61	0.11	0.10	4 410	-0.72	-0.752
M0	+8.8	+1.40	+1.22	1.28	0.91	3.65	0.67	0.17	0.14	3 840	-1.38	-1.068
M2	+9.9	+1.49	+1.18	1.50	1.19	4.11	0.66	0.20	0.16	3 520	-1.89	-1.304
M5	+12.3	+1.64	+1.24	1.80	1.67	6.17	0.62	0.33	0.29	3 170	-2.73	-1.928
GIANTS, III												
G5	+0.9	+0.86	+0.56	0.69	0.48					5 050	-0.34	1.676
G8	+0.8	+0.94	+0.70	0.70	0.48	2.16	0.50	0.09	0.06	4 800	-0.42	1.748
K0	+0.7	+1.00	+0.84	0.77	0.53	2.31	0.54	0.10	0.07	4 660	-0.50	1.820
K2	+0.5	+1.16	+1.16	0.84	0.58	2.70	0.63	0.12	0.09	4 390	-0.61	1.944
K5	-0.2	+1.50	+1.81	1.20	0.90	3.60	0.79	0.17	0.12	4 050	-1.02	2.388
M0	-0.4	+1.56	+1.87	1.23	0.94	3.85	0.83	0.19	0.12	3 690	-1.25	2.560
M2	-0.6	+1.60	+1.89	1.34	1.10	4.30	0.87	0.22	0.15	3 540	-1.62	2.788
M5	-0.3	+1.63	+1.58	2.18	1.96	5.96	0.95	0.29	0.20	3 380	-2.48	3.012
SUPERGIANTS, I												
O9	-6.5	-0.27	-1.13	-0.15	-0.32	-0.82	-0.05	-0.13	-0.08	32 000	-3.18	5.772
B2	-6.4	-0.17	-0.93	-0.05	-0.15	-0.40	-0.04	0.00	-0.07	17 600	-1.58	5.092
B5	-6.2	-0.10	-0.72	0.02	-0.07	-0.13	0.01	0.00	0.02	13 600	-0.95	4.760
B8	-6.2	-0.03	-0.55	0.02	0.00	0.07	0.07	-0.02	0.05	11 100	-0.66	4.644
A0	-6.3	-0.01	-0.38	0.03	0.05	0.19	0.09	-0.02	0.07	9 980	-0.41	4.584
A2	-6.5	+0.03	-0.25	0.07	0.07	0.32	0.12	-0.01	0.08	9 380	-0.28	4.612
A5	-6.6	+0.09	-0.08	0.12	0.13	0.48	0.13	0.02	0.07	8 610	-0.13	4.592
F0	-6.6	+0.17	+0.15	0.21	0.20	0.64	0.15	0.04	0.06	7 460	-0.01	4.544
F2	-6.6	+0.23	+0.18	0.26	0.21	0.75	0.18	0.05	0.06	7 030	-0.00	4.540
F5	-6.6	+0.32	+0.27	0.35	0.23	0.93	0.22	0.06	0.07	6 370	-0.03	4.552
F8	-6.5	+0.56	+0.41	0.45	0.27	1.21	0.28	0.07	0.07	5 750	-0.09	4.536
G0	-6.4	+0.76	+0.52	0.51	0.33	1.44	0.33	0.08	0.08	5 370	-0.15	4.520
G2	-6.3	+0.87	+0.63	0.58	0.40				0.08	5 190	-0.21	4.504
G5	-6.2	+1.02	+0.83	0.67	0.44					4 930	-0.33	4.512
G8	-6.1	+1.14	+1.07	0.69	0.46	1.99	0.43	0.11	0.09	4 700	-0.42	4.508
K0	-6.0	+1.25	+1.17	0.76	0.48	2.15	0.46	0.12	0.10	4 550	-0.50	4.500
K2	-5.9	+1.36	+1.32	0.85	0.55	2.43	0.52	0.13	0.12	4 310	-0.61	4.504
K5	-5.8	+1.60	+1.80	1.20	0.90	3.50	0.67	0.14	0.18	3 990	-1.01	4.624
M0	-5.6	+1.67	+1.90	1.23	0.94	3.80	0.73	0.18	0.20	3 620	-1.29	4.656
M2	-5.6	+1.71	+1.95	1.34	1.10	4.10	0.73	0.22	0.24	3 370	-1.62	4.788
M5	-5.6	+1.80	+1.60:	2.18	1.96					2 880	-3.47	5.528

Table A.1: Calibration of the MK spectral type including their color indices. The colors are for the Johnson-Glass system, as described by Bessell & Brett (1988, PASP 100, p1134). Luminosity class is in L_\odot ; temperature is in K. For K5-M supergiants we have adopted a luminosity class Iab. Source: Allen's Astrophysical Quantities, 4th edition, p. 388–389.

Sp	Ia ⁺	Ia	Iab	Ib	II	III	IV	V
O3	4.642	4.650	4.667	4.673	4.660	4.639	4.618	4.699
O4	4.624	4.626	4.639	4.643	4.631	4.616	4.596	4.656
O4.5	4.614	4.614	4.626	4.629	4.617	4.606	4.588	4.638
O5	4.604	4.602	4.612	4.615	4.604	4.596	4.580	4.623
O5.5	4.593	4.590	4.599	4.601	4.592	4.587	4.574	4.609
O6	4.582	4.578	4.586	4.588	4.579	4.578	4.567	4.596
O6.5	4.570	4.565	4.573	4.574	4.567	4.570	4.562	4.585
O7	4.557	4.553	4.559	4.561	4.555	4.562	4.556	4.574
O7.5	4.544	4.540	4.546	4.548	4.543	4.553	4.550	4.564
O8	4.531	4.527	4.532	4.534	4.531	4.544	4.545	4.554
O8.5	4.517	4.513	4.519	4.521	4.518	4.536	4.539	4.545
O9	4.503	4.500	4.505	4.507	4.506	4.527	4.533	4.536
O9.5	4.457	4.457	4.462	4.465	4.467	4.497	4.511	4.508
O9.7	4.439	4.440	4.445	4.448	4.452	4.485	4.502	4.496
B0	4.410	4.414	4.419	4.422	4.427	4.465	4.486	4.477
B0.5	4.361	4.370	4.374	4.378	4.386	4.429	4.455	4.443
B1	4.312	4.326	4.330	4.334	4.343	4.389	4.420	4.405
B1.5	4.265	4.282	4.287	4.290	4.300	4.348	4.381	4.364
B2	4.219	4.241	4.245	4.247	4.257	4.305	4.339	4.320
B2.5	4.197	4.221	4.224	4.227	4.236	4.284	4.318	4.297
B3	4.175	4.201	4.204	4.207	4.216	4.262	4.296	4.274
B4	4.135	4.165	4.167	4.168	4.176	4.220	4.252	4.228
B5	4.098	4.131	4.132	4.132	4.139	4.179	4.208	4.182
B6	4.064	4.100	4.100	4.099	4.104	4.140	4.166	4.138
B7	4.033	4.072	4.071	4.068	4.072	4.103	4.125	4.096
B8	4.005	4.047	4.045	4.041	4.042	4.069	4.088	4.058
B9	3.980	4.024	4.021	4.016	4.016	4.038	4.053	4.023
A0	3.958	4.003	3.999	3.993	3.991	4.010	4.022	3.991
A1	3.944	3.990	3.985	3.978	3.976	3.992	4.002	3.973
A2	3.930	3.978	3.972	3.965	3.962	3.976	3.984	3.955
A4	3.905	3.954	3.947	3.939	3.936	3.946	3.952	3.926
A5	3.893	3.943	3.935	3.927	3.924	3.932	3.937	3.913
A6	3.880	3.931	3.923	3.915	3.912	3.919	3.924	3.901
A8	3.856	3.908	3.898	3.890	3.888	3.894	3.898	3.881
F0	3.831	3.883	3.873	3.865	3.864	3.869	3.875	3.864
F2	3.805	3.858	3.847	3.839	3.839	3.845	3.852	3.848
F4	3.779	3.831	3.819	3.811	3.813	3.820	3.828	3.832
F5	3.765	3.817	3.804	3.797	3.800	3.807	3.816	3.823
F6	3.751	3.802	3.790	3.782	3.786	3.794	3.804	3.815
F8	3.722	3.773	3.760	3.753	3.759	3.766	3.778	3.796
G0	3.694	3.744	3.730	3.723	3.730	3.738	3.751	3.774
G2	3.680	3.730	3.715	3.708	3.716	3.724	3.737	3.763
G4	3.666	3.715	3.700	3.694	3.702	3.710	3.723	3.751
G8	3.638	3.688	3.672	3.666	3.675	3.681	3.694	3.725
K0	3.625	3.675	3.658	3.652	3.663	3.668	3.679	3.712
K1	3.612	3.663	3.646	3.640	3.650	3.654	3.665	3.698
K3	3.586	3.639	3.622	3.617	3.628	3.629	3.637	3.671
K4	3.574	3.628	3.612	3.606	3.618	3.618	3.624	3.657
K5	3.561	3.618	3.601	3.597	3.609	3.607	3.611	3.644
K7	3.536	3.598	3.583	3.580	3.594	3.588	3.588	3.618
K9	3.509	3.579	3.567	3.566	3.582	3.573	3.568	3.595
M0	3.494	3.569	3.559	3.560	3.577	3.567	3.560	3.584
M1	3.461	3.549	3.543	3.548	3.569	3.556	3.545	3.564
M1.5	3.442	3.538	3.535	3.542	3.565	3.552	3.539	3.555
M2	3.422	3.526	3.527	3.536	3.561	3.549	3.533	3.547
M3	3.376	3.499	3.507	3.523	3.554	3.542	3.524	3.532
M4	3.322	3.467	3.485	3.507	3.546	3.536	3.516	3.517
M5	3.262	3.432	3.459	3.490	3.536	3.529	3.508	3.501
M6	3.200	3.395	3.433	3.471	3.526	3.522	3.498	3.482
M6.5	3.170	3.378	3.421	3.463	3.521	3.518	3.493	3.470
M7	3.143	3.363	3.411	3.456	3.517	3.514	3.487	3.457
M8	3.106	3.348	3.403	3.452	3.517	3.510	3.475	3.426
M9	3.109	3.365	3.422	3.472	3.534	3.515	3.465	3.388

Table A.2: Temperature calibration of the MK spectral types for different luminosity classes. The logarithm of T_{eff} is given in Kelvin. Source: de Jager & Nieuwenhuijzen (1987, A&A 177, 217). In the article a fit-formula is given that provides the temperature as a function of a numerical spectral type and luminosity class. This formula (based on a 20th order Chebychev polynomial) is not used to generate the tables provided here and in the original paper (that are based on a 40th order Chebychev polynomial).

Sp	Ia ⁺	Ia	Iab	Ib	II	III	IV	V
O3	5.751	6.016	6.179	6.281	6.313	6.252	6.009	6.137
O4	5.822	5.997	6.114	6.177	6.159	6.047	5.807	5.904
O4.5	5.852	5.987	6.084	6.129	6.090	5.955	5.717	5.798
O5	5.880	5.977	6.055	6.084	6.025	5.870	5.635	5.698
O5.5	5.905	5.966	6.027	6.041	5.964	5.791	5.558	5.602
O6	5.927	5.955	5.999	6.000	5.905	5.715	5.485	5.510
O6.5	5.946	5.942	5.971	5.959	5.849	5.643	5.417	5.421
O7	5.962	5.929	5.943	5.919	5.794	5.574	5.351	5.335
O7.5	5.976	5.914	5.914	5.879	5.741	5.507	5.287	5.251
O8	5.987	5.898	5.886	5.840	5.689	5.442	5.225	5.168
O9.5	6.010	5.802	5.732	5.640	5.429	5.124	4.920	4.749
O9.7	6.009	5.775	5.693	5.590	5.366	5.046	4.845	4.661
B0	6.004	5.733	5.632	5.513	5.269	4.928	4.729	4.512
B0.5	5.986	5.658	5.526	5.381	5.103	4.723	4.527	4.258
B1	5.962	5.579	5.417	5.245	4.930	4.508	4.311	3.998
B1.5	5.934	5.499	5.306	5.106	4.752	4.282	4.081	3.733
B2	5.906	5.422	5.197	4.966	4.570	4.047	3.840	3.465
B2.5	5.892	5.384	5.144	4.897	4.479	3.927	3.716	3.332
B3	5.879	5.348	5.091	4.829	4.387	3.806	3.590	3.199
B4	5.854	5.280	4.991	4.696	4.206	3.562	3.335	2.936
B5	5.833	5.220	4.898	4.569	4.030	3.319	3.078	2.681
B6	5.815	5.167	4.814	4.451	3.860	3.080	2.824	2.436
B7	5.802	5.123	4.739	4.342	3.700	2.849	2.576	2.203
B8	5.791	5.087	4.674	4.244	3.550	2.628	2.337	1.985
B9	5.782	5.060	4.619	4.158	3.414	2.420	2.110	1.783
A0	5.773	5.039	4.574	4.083	3.291	2.228	1.898	1.596
A1	5.768	5.029	4.549	4.039	3.216	2.109	1.766	1.481
A2	5.761	5.021	4.528	4.000	3.149	1.999	1.641	1.373
A4	5.745	5.012	4.496	3.937	3.033	1.803	1.416	1.177
A5	5.735	5.009	4.484	3.911	2.984	1.718	1.316	1.089
A6	5.724	5.008	4.475	3.890	2.942	1.642	1.224	1.005
A8	5.695	5.007	4.464	3.859	2.876	1.517	1.067	0.853
F0	5.658	5.007	4.459	3.841	2.832	1.428	0.943	0.717
F2	5.613	5.007	4.458	3.833	2.809	1.373	0.852	0.590
F4	5.564	5.006	4.461	3.834	2.805	1.350	0.791	0.469
F5	5.539	5.005	4.464	3.837	2.809	1.350	0.771	0.409
F6	5.513	5.004	4.466	3.841	2.817	1.358	0.758	0.349
F8	5.465	5.003	4.473	3.854	2.842	1.395	0.750	0.226
G0	5.424	5.005	4.482	3.872	2.880	1.456	0.766	0.098
G2	5.408	5.007	4.488	3.882	2.903	1.496	0.782	0.031
G4	5.395	5.011	4.494	3.894	2.928	1.541	0.802	-0.038
G8	5.385	5.025	4.510	3.919	2.985	1.645	0.857	-0.183
K0	5.388	5.035	4.520	3.933	3.016	1.703	0.890	-0.258
K1	5.397	5.048	4.531	3.948	3.048	1.766	0.926	-0.336
K3	5.435	5.083	4.558	3.980	3.116	1.899	1.007	-0.497
K4	5.465	5.106	4.574	3.998	3.151	1.969	1.050	-0.580
K5	5.501	5.133	4.593	4.017	3.187	2.041	1.095	-0.665
K7	5.595	5.196	4.635	4.057	3.260	2.188	1.188	-0.839
K9	5.715	5.275	4.686	4.100	3.334	2.336	1.281	-1.019
M0	5.784	5.320	4.715	4.124	3.370	2.409	1.325	-1.111
M1	5.933	5.421	4.780	4.176	3.444	2.550	1.407	-1.299
M2	6.092	5.536	4.858	4.236	3.520	2.684	1.475	-1.492
M3	6.251	5.666	4.952	4.309	3.601	2.808	1.523	-1.692
M4	6.401	5.812	5.068	4.405	3.697	2.925	1.548	-1.901
M5	6.531	5.981	5.218	4.537	3.820	3.040	1.547	-2.122
M6	6.635	6.185	5.422	4.727	3.993	3.166	1.520	-2.356
M7	6.710	6.445	5.707	5.009	4.247	3.321	1.473	-2.604

Table A.3: Luminosity calibration of the MK spectral types for different luminosity classes. The logarithm of L is given in L_{\odot} . Source: de Jager & Nieuwenhuijzen (1987, A&A 177, 217). In the article a fit-formula is given that provides the luminosity as a function of a numerical spectral type and luminosity class. This formula (based on a 20th order Chebychev polynomial) is not used to generate the tables provided here and in the original paper (that are based on a 40th order Chebychev polynomial).

T_{eff}	$\log g$	U	B	V	R	I	J	H	K
3500	3.50	0.8051	0.8536	0.8265	0.7515	0.6551	0.4581	0.4371	0.3618
	4.00	0.7690	0.7941	0.7736	0.7198	0.6242	0.3979	0.3409	0.2836
	4.50	0.7440	0.7573	0.7380	0.6956	0.6014	0.3664	0.2887	0.2428
	5.00	0.7252	0.7358	0.7130	0.6781	0.5853	0.3522	0.2693	0.2268
4000	3.50	0.8538	0.9011	0.8348	0.7786	0.6690	0.5307	0.4812	0.4083
	4.00	0.8194	0.8728	0.8117	0.7618	0.6549	0.5136	0.4688	0.3961
	4.50	0.7767	0.8131	0.7555	0.7132	0.6137	0.4628	0.4251	0.3545
	5.00	0.7411	0.7525	0.6947	0.6565	0.5655	0.4048	0.3554	0.2962
4500	3.50	0.9213	0.8988	0.8078	0.7272	0.6263	0.5092	0.4439	0.3793
	4.00	0.8987	0.8927	0.8040	0.7266	0.6258	0.5087	0.4443	0.3803
	4.50	0.8704	0.8837	0.7990	0.7259	0.6255	0.5078	0.4439	0.3802
	5.00	0.8359	0.8650	0.7846	0.7162	0.6178	0.4984	0.4359	0.3724
5000	3.50	0.9154	0.8588	0.7599	0.6803	0.5890	0.4676	0.3999	0.3439
	4.00	0.9045	0.8567	0.7611	0.6817	0.5898	0.4700	0.4028	0.3466
	4.50	0.8882	0.8536	0.7615	0.6830	0.5905	0.4721	0.4055	0.3491
	5.00	0.8670	0.8485	0.7605	0.6834	0.5910	0.4732	0.4064	0.3501
5500	3.50	0.8767	0.8133	0.7067	0.6297	0.5453	0.4251	0.3574	0.3108
	4.00	0.8779	0.8135	0.7097	0.6329	0.5483	0.4287	0.3622	0.3145
	4.50	0.8745	0.8122	0.7117	0.6353	0.5507	0.4315	0.3659	0.3171
	5.00	0.8658	0.8097	0.7132	0.6375	0.5531	0.4340	0.3687	0.3190
6000	3.50	0.8107	0.7687	0.6581	0.5819	0.5003	0.3851	0.3172	0.2765
	4.00	0.8192	0.7682	0.6608	0.5857	0.5051	0.3899	0.3236	0.2818
	4.50	0.8250	0.7673	0.6630	0.5887	0.5090	0.3937	0.3292	0.2860
	5.00	0.8267	0.7653	0.6640	0.5904	0.5117	0.3959	0.3327	0.2883
6500	3.50	0.7410	0.7330	0.6236	0.5459	0.4642	0.3529	0.2850	0.2502
	4.00	0.7497	0.7292	0.6233	0.5478	0.4682	0.3572	0.2913	0.2551
	4.50	0.7586	0.7263	0.6233	0.5494	0.4719	0.3609	0.2973	0.2593
	5.00	0.7661	0.7226	0.6222	0.5496	0.4742	0.3631	0.3021	0.2622
7000	3.50	0.6849	0.7070	0.6016	0.5207	0.4364	0.3275	0.2610	0.2319
	4.00	0.6894	0.7003	0.5997	0.5215	0.4403	0.3315	0.2661	0.2358
	4.50	0.6959	0.6942	0.5974	0.5216	0.4435	0.3346	0.2715	0.2393
	5.00	0.7051	0.6894	0.5957	0.5221	0.4472	0.3383	0.2777	0.2430
7500	3.50	0.6487	0.7111	0.6067	0.5157	0.4214	0.3147	0.2490	0.2204
	4.00	0.6397	0.6761	0.5793	0.4969	0.4131	0.3073	0.2448	0.2192
	4.50	0.6471	0.6690	0.5790	0.5003	0.4204	0.3132	0.2517	0.2242
	5.00	0.6541	0.6621	0.5765	0.5004	0.4244	0.3168	0.2573	0.2275

Table A.4: Limb darkening coefficients for Kurucz model atmospheres for solar-type stars. The limb darkening is described by a linear law: $I_m(\mu)/I_m(1) = 1 - u(1 - \mu)$, where m is the label for the photometric passband. The models have a solar chemical composition and are for a micro-turbulent velocity of 2 km sec^{-1} (Claret 2000, A&A 363, 1081).

Table A.5: Kurucz-model atmospheres for solar composition stars

T_{eff}									
$\log g$	$\log \tau$	$\log z$	T	$\log p_{\text{G}}$	$\log n_{\text{e}}$	$\log N_N$	$\log \rho$	$\log p_{\text{R}}$	F_{conv}/F
5 500	-3.0	6.79	4 282	3.23	11.35	15.47	-8.19	0.09	0.00
	-2.0	7.65	4 487	3.84	11.91	16.05	-7.61	0.10	0.00
	-1.0	7.92	4 846	4.41	12.49	16.59	-7.07	0.17	0.00
	0.0	8.08	6 130	4.92	13.50	16.99	-6.66	0.54	0.01
	1.0	8.14	8 176	5.10	14.94	17.04	-6.62	1.05	0.85
5 500	-3.0	10.65	4 104	1.28	9.53	13.52	-10.13	0.09	0.00
	-2.0	10.98	4 444	2.09	10.35	14.30	-9.36	0.10	0.00
	-1.0	11.14	4 846	2.73	11.08	14.91	-8.75	0.17	0.00
	0.0	11.22	6 145	3.13	12.55	15.20	-8.46	0.56	0.00
	1.0	11.24	8 431	3.18	14.06	15.07	-8.58	1.10	0.91
6 000	-3.0	7.60	4 667	3.29	11.48	15.49	-8.17	0.24	0.00
	-2.0	7.90	4 891	3.87	12.04	16.04	-7.61	0.25	0.00
	-1.0	8.08	5 293	4.42	12.62	16.55	-7.10	0.32	0.00
	0.0	8.18	6 789	4.82	13.94	16.85	-6.81	0.70	0.05
	1.0	8.22	8 709	4.95	15.12	16.86	-6.79	1.16	0.88
6 000	-3.0	10.75	4 489	1.26	9.72	13.47	-10.19	0.24	0.00
	-2.0	11.03	4 869	2.02	10.62	14.19	-9.47	0.25	0.00
	-1.0	11.17	5 318	2.59	11.44	14.72	-8.94	0.33	0.00
	0.0	11.24	6 861	2.89	13.01	14.90	-8.75	0.75	0.00
	1.0	11.25	8 981	2.92	14.11	14.73	-8.93	1.21	0.91
7 000	-3.0	7.63	5 458	3.10	11.87	15.22	-8.44	0.51	0.00
	-2.0	7.95	5 726	3.67	12.45	15.77	-7.89	0.52	0.00
	-1.0	8.12	6 190	4.17	13.13	16.23	-7.42	0.60	0.00
	0.0	8.20	8 217	4.45	14.63	16.39	-7.26	1.02	0.20
	1.0	8.24	9 911	4.55	15.37	16.37	-7.28	1.38	0.92
10 000	-3.0	8.34	7 586	1.71	12.84	13.63	-10.03	1.13	0.00
	-2.0	8.48	8 030	2.36	13.42	14.36	-9.40	1.15	0.00
	-1.0	8.58	8 982	2.86	14.08	14.67	-8.99	1.28	0.00
	0.0	8.65	11 655	3.17	14.62	14.71	-8.95	1.68	0.00
	1.0	8.83	16 287	3.75	15.08	15.12	-8.54	2.25	0.00
20 000	-3.0	8.70	13 060	1.38	12.81	12.84	-10.82	2.34	0.00
	-2.0	8.90	14 067	2.09	13.49	13.52	-10.14	2.35	0.00
	-1.0	9.02	15 560	2.71	14.07	14.08	-9.57	2.40	0.00
	0.0	9.15	19 521	3.33	14.60	14.60	-9.05	2.63	0.00
	1.0	9.28	27 451	4.03	15.15	15.15	-8.50	3.15	0.00
40 000	-3.0	9.48	28 059	1.19	12.31	12.29	-11.37	3.54	0.00
	-2.0	9.66	31 336	2.16	13.24	13.21	-10.45	3.55	0.00
	-1.0	9.77	34 855	2.93	13.96	13.93	-9.72	3.62	0.00
	0.0	9.87	40 920	3.55	14.52	14.48	-9.18	3.85	0.00
	1.0	9.97	53 682	4.21	15.06	15.02	-8.64	4.32	0.00

τ = continuum optical depth at $\lambda 5000 \text{ \AA}$; z = geometrical depth in cm; T = temperature in K; p_{G} = gas pressure; n_{e} = electron density in cm^{-3} ; N_N = nucleon density in cm^{-3} ; ρ = density in gr cm^{-3} ; p_{R} = radiation pressure; F_{conv}/F = fraction of the flux that is transported by convection. All units in cgs. From: Allen's Astrophysical Quantities, 4th edition, section 15.4.1., p. 393.

λ Å	W_λ mÅ	Elem. & Ion	Fr. id	λ Å	W_λ mÅ	Elem. & Ion	Fr. id	λ Å	W_λ mÅ	Elem. & Ion	Fr. id
2795.4		Mg II		3709.256	573	Fe I ¹		4077.724	428	Sr II ¹	
2802.3		Mg II		3719.947	1664	Fe I		4101.748	3133	H δ	h
2851.6		Mg		3734.874	3027	Fe I	M	4132.067	404	Fe I ¹	
2881.1		Si		3737.141	1071	Fe I		4143.878	466	Fe I	
3067.262	663	Fe I ¹		3745.574	1202	Fe I ¹		4167.277	200	Mg I	
3134.116	414	Ni I ¹		3748.271	497	Fe I		4202.040	326	Fe I	
3242.007	270	Ti II		3749.495	1907	Fe I		4226.740	1476	Ca I	g
3247.569	246	Cu I		3758.245	1647	Fe I		4235.949	385	Fe I ¹	
3336.689	416	Mg I		3759.299	334	Ti II		4250.130	342	Fe I ¹	
3414.779	816	Ni I		3763.803	829	Fe I		4250.797	400	Fe I ¹	
3433.579	492	Ni I ¹		3767.204	820	Fe I		4254.346	393	Cr I ¹	
3440.626	1243	Fe I		3787.891	512	Fe I		4260.486	595	Fe I	
3441.019	634	Fe I		3795.012	547	Fe I ¹		4271.774	756	Fe I	
3443.884	655	Fe I		3806.718	209	Fe I ¹		4325.775	793	Fe I ¹	
3446.271	470	Ni I		3815.851	1272	Fe I		4340.475	2855	H γ	f
3458.467	656	Ni I		3820.436	1712	Fe I	L	4383.557	1008	Fe I	e
3461.667	758	Ni I		3825.891	1519	Fe I		4404.761	898	Fe I	
3475.457	622	Fe I		3827.832	897	Fe I		4415.135	417	Fe I ¹	
3476.712	465	Fe I ¹		3829.365	874	Mg I		4528.627	275	Fe I ¹	
3490.594	830	Fe I		3832.310	1685	Mg I		4554.036	159	Ba II	
3492.975	826	Ni I		3834.233	624	Fe I		4703.003	326	Mg I	
3497.843	726	Fe I		3838.302	1920	Mg I		4861.342	3680	H β	F
3510.327	489	Ni I		3840.447	567	Fe I		4891.502	312	Fe I	
3515.066	718	Ni I		3841.058	517	Fe I ¹		4920.514	471	Fe I ¹	
3521.270	381	Fe I		3849.977	608	Fe I		4957.613	696	Fe I ¹	c
3524.536	1271	Ni I		3856.381	648	Fe I		5167.327	935	Mg I ¹	b ₄
3554.937	404	Fe I		3859.922	1554	Fe I		5172.698	1259	Mg I	b ₂
3558.532	485	Fe I ¹		3878.027	555	Fe I		5183.619	1584	Mg I	b ₁
3565.396	990	Fe I		3886.294	920	Fe I		5250.216	62	Fe I ¹	
3566.383	458	Ni I		3899.719	436	Fe I		5269.550	478	Fe I ¹	E
3570.134	1380	Fe I		3902.956	530	Fe I ¹		5328.051	375	Fe I	
3578.693	488	Cr I		3905.532	816	Si I		5528.418	293	Mg I	
3581.209	2144	Fe I	N	3920.269	341	Fe I		5889.973	752	Na I ¹	D ₂
3586.990	532	Fe I		3922.923	414	Fe I ¹		5895.940	564	Na I	D ₁
3593.495	436	Cr I		3927.933	187	Fe I		6102.727	135	Ca I	
3608.869	1046	Fe I		3930.308	108	Fe I		6122.226	222	Ca I	
3618.777	1410	Fe I		3933.682	20253	Ca II ¹	K	6162.180	222	Ca I	
3619.400	568	Ni I		3944.016	488	Al I		6302.499	83	Fe I ¹	
3631.475	1364	Fe I		3961.535	621	Al I		6562.808	4020	H α	C
3647.851	970	Fe I		3968.492	15467	Ca II ¹	H	8498.062	1470	Ca II	
3679.923	448	Fe I		4045.825	1174	Fe I		8542.144	3670	Ca II	
3685.196	275	Ti II		4063.605	787	Fe I ¹		8662.170	2600	Ca II	
3705.577	562	Fe I		4071.749	723	Fe I		10830		He I	

Table A.6: The most important Fraunhofer lines from the Sun after Moore, Minnaert, and Houtgast (1966). ¹ Blended line. Adapted from: *Astrophysical Formulae*, Kenneth R. Lang, 2nd edition, page 175. The column labeled Fr provides the letter designation given originally by Fraunhofer to the most prominent absorption features. From: Gray, *The observation and analysis of stellar photospheres*, 3rd edition, page 521.

Index

- Abundance
 - number, 92
- Abundantie
 - getals-, 218
- Adams W.S., 13
- Angular diameter
 - definition, 44
- Binaries
 - Cataclysmic variables, 24
 - Low-mass X-ray binaries, 25
- Blackbody radiation, *see* Planck function
- Boltzmann excitation equation, 87
- Cannon A.J., 13
- Collisional cross section
 - electron, 105
- Column mass
 - definition, 131
- Complete redistribution, 104, 110
- Conservation
 - of charge, 92
 - of particles, 92
- Coordinate systems
 - axial symmetry, 35
 - conventions, 35
 - plane parallel layers, 35
 - spherical shells, 36
- De-excitation processes
 - collisional, 106
 - induced, 104
 - spontaneous, 103
- Diffusion approximation, 70
- Draper H., 11, 13
- Earth atmosphere
 - transmission, 29, 33
- Eddington approximation, 143
- Eddington benadering, 191
- Eddington factor
 - limits, 49
- Eddington factors
 - definition, 46
 - limits, 68
- Eddington-Barbier approximation, 74
- Eddington-Barbier approximation, 64
- Einstein relations, 107
- Einstein coefficient
 - extinction, 104, 108
 - spontaneous emission, 103
 - stimulated emission, 104
- Electron volt, 89
- Emission coefficient
 - definition, 53
 - line, 107
 - mass, 53
 - total, 53
 - volume, 53
- Energy density
 - definition, 40
 - total, 41
- Excitation
 - energy, 88
 - potential, 89
- Excitation processes

- collisional, 105
- Excitation processes
 - radiative, 103
- Extinctiecoëfficiënt
 - dwarsdoorsnede, 108
- Extinction coefficient, 110
 - absorption, 53
 - cross section, 53
 - definition, 52
 - line, 108
 - linear, 52
 - mass, 53
 - Rosseland mean, 70
 - scattering, 53
 - total, 53
 - volume, 52
- Feautrier method, 72
 - elimination scheme, 78
- Finite difference method, 77
- Flux
 - r^{-2} dependence, 43
 - astrophysical, 42
 - definition, 41
 - Eddington, 42
 - observed, 43
 - outward & inward, 42
 - ray-by-ray description, 43
 - total, 43
- Fotonweglengte
 - gemiddelde optische, 192
- Fraunhofer J. von, 11
- Free path, *see* Mean-free-path
- Gaunt factor
 - bound-bound, 109
- Geometrical dilution, 40
- Herschel F.W., 25
- Hertzsprung E., 12
- Huggins W., 26
- Ideal gas, 91
- Impact parameter
 - definition, 44
- Intensity, mean
 - definition, 39
 - total, 39
- Intensity, specific
 - definition, 37
 - invariance, 37
 - moment
 - first order, 42
 - second order, 45
 - zero-order, 39
 - total, 37
- Irradiance, *see* Flux, observed
- Jansky
 - definition, 42
- Kayser, 89
- Kinetic equilibrium, 86
- Kirchhoff, 81
- Kirchhoff's law, 82
- Kirchhoff-Planck relation, 82
- Line profile
 - Lorentz, 108
 - P Cygni, 21, 22
- Linear perturbation, 93
- Local thermodynamic equilibrium, 99
- Luminosity
 - definition, 43
 - monochromatic, 43
- Magnitude
 - apparent, 29
 - color index, 29
 - filter transmission, 29
 - response function, 30
 - UBV system, 29
- Mean-free-path
 - definition, 57
- Nebulae
 - around massive stars, 26
 - Planetary-, 25
- Newton-Raphson method, *see* Linear perturbation

- Non local thermodynamic equilibrium
 departure coefficient, 90
- Optical depth
 definition, 56
 interval, *see* Optical depth interval
 mean optical path, 57
 thick & thin, 57
- Optical depth interval
 along a beam of light, 56
 definition, 56
 planar layers, 59
- Oscillator strength, 108
 Kramers formula, 109
- Oscillatorsterkte, 98
- Pannekoek, A., 90
- Partition function, 89
- Photo excitation, *see* Excitation processes
- Photons
 conversion, 51
 thermal, 50
- Pickering E.C., 11
- Planck function, 81
- Planck, M., 81
- Planck-functie, 83
- Planets
 Jupiter-like-, 23
- Profile function, 103
- Radiation pressure
 definition, 45
 total, 46
- Radiative conductivity, 70
 effective, 71
- Rate, 103
- Rayleigh-Jeans approximation, 84
- Resolving power
 definition, 169
- Saha ionization equation, 89
- Saha-Boltzmann equation, 90
- Secchi A., 11
- Short characteristics method, 73
- Solid angle
- definition, 39
 total, 39
- Source function
 definition, 58
 line, 110
 proto-typical, 59
 total, 59
- Spectral classification
 luminosity class, 13
 spectral type
 MK classification, 12
 WR classification, 21
- Spectral line formation
 principle, 62, 65
- Spectral resolution
 definition, 169
- Spectrum
 continuum
 Balmer jump, 29
 color index, 28
 UBV filters, 28
 spectral type
 MK classification, 13
- Spontaneous emission
 see De-excitation processes, 103
- Stars
 Am- and Ap-, 23
 Be, 15
 Brown dwarfs, 23
 Carbon-, 22
 Luminous Blue Variable, 22, 27
 Wolf-Rayet, 21
- Statistical weight, 88
- Stefan-Boltzmann's law, 85
- Stimulated emission, *see* De-excitation processes
- Supernovae, 26
 classification scheme, 27
 spectra, 32
 Type Ia, 26
 Type II, Ib and Ic, 27
 Type IIn, 27
- Surface brightness, *see* Intensity, specific

Taylor-McLaurin expansion, 68

Temperature

brightness, 95

color, 96

effective, 43, 98

electron, 86

excitation, 98

ionization, 98

kinetic, 86

Thermodynamic equilibrium, 81

Transfer equation

finite slab, 62

first order planar form, 61

first order spherical form, 61

for a beam of light, 54

formal solution, 59

general form, 54, 55

planar layers, 55

semi-infinite medium, 64

spherical shells, 56

zero order planar form, 60

zero order spherical form, 61

Velocity

most probable, 86

root-mean-square, 86

Velocity distribution

Maxwellian, 86

Wien's approximation, 85

Wien's displacement law, 83

Wollaston W., 11